Pertanika Journal of

SCIENCE & TECHNOLOGY

JST

VOL. 24 (1) JAN. 2016

PERTANIKA JOURNALS

A scientific journal published by Universiti Putra Malaysia Press

Journal of Science & Technology
Journal of Science & Technology

Journal of Social Sciences & Humanities

About the Journal

Overview

Pertanika Journal of Science & Technology (JST) is the official journal of Universiti Putra Malaysia published by UPM Press. It is an open-access online scientific journal which is free of charge. It publishes the scientific outputs. It neither accepts nor commissions third party content.

Recognized internationally as the leading peer-reviewed interdisciplinary journal devoted to the publication of original papers, it serves as a forum for practical approaches to improving quality in issues pertaining to science and engineering and its related fields.

JST is a **biannual** (January and July) periodical that considers for publication original articles as per its scope. The journal publishes in **English** and it is open to authors around the world regardless of the nationality.

The Journal is available world-wide.

Aims and scope

Pertanika Journal of Science and Technology aims to provide a forum for high quality research related to science and engineering research. Areas relevant to the scope of the journal include: bioinformatics, bioscience, biotechnology and bio-molecular sciences, chemistry, computer science, ecology, engineering, engineering design, environmental control and management, mathematics and statistics, medicine and health sciences, nanotechnology, physics, safety and emergency management, and related fields of study.

History

Pertanika was founded in 1978. A decision was made in 1992 to streamline Pertanika into three journals as Journal of Tropical Agricultural Science, Journal of Science & Technology, and Journal of Social Sciences & Humanities to meet the need for specialised journals in areas of study aligned with the interdisciplinary strengths of the university.

After almost 25 years, as an interdisciplinary Journal of Science & Technology, the revamped journal now focuses on research in science and engineering and its related fields.

Goal of *Pertanika*

Our goal is to bring the highest quality research to the widest possible audience.

Quality

We aim for excellence, sustained by a responsible and professional approach to journal publishing. Submissions are guaranteed to receive a decision within 14 weeks. The elapsed time from submission to publication for the articles averages 5-6 months.

Abstracting and indexing of *Pertanika*

Pertanika is almost 40 years old; this accumulated knowledge has resulted in Pertanika JST being abstracted and indexed in SCOPUS (Elsevier), Thomson (ISI) Web of Knowledge [BIOSIS & CAB Abstracts], EBSCO & EBSCOhost, DOAJ, ERA, Cabell's Directories, Google Scholar, MyAIS, ISC & Rubriq (Journal Guide).

Future vision

We are continuously improving access to our journal archives, content, and research services. We have the drive to realise exciting new horizons that will benefit not only the academic community, but society itself.

Citing journal articles

The abbreviation for Pertanika Journal of Science & Technology is *Pertanika J. Sci. Technol.*

Publication policy

Pertanika policy prohibits an author from submitting the same manuscript for concurrent consideration by two or more publications. It prohibits as well publication of any manuscript that has already been published either in whole or substantial part elsewhere. It also does not permit publication of manuscript that has been published in full in Proceedings.

Code of Ethics

The Pertanika Journals and Universiti Putra Malaysia takes seriously the responsibility of all of its journal publications to reflect the highest in publication ethics. Thus all journals and journal editors are expected to abide by the Journal's codes of ethics. Refer to Pertanika's **Code of Ethics** for full details, or visit the Journal's web link at http://www.pertanika.upm.edu.my/code_of_ethics.php

International Standard Serial Number (ISSN)

An ISSN is an 8-digit code used to identify periodicals such as journals of all kinds and on all media–print and electronic. All Pertanika journals have ISSN as well as an e-ISSN.

Journal of Science & Technology: ISSN 0128-7680 (*Print*); ISSN 2231-8526 (*Online*).

Lag time

A decision on acceptance or rejection of a manuscript is reached in 3 to 4 months (average 14 weeks). The elapsed time from submission to publication for the articles averages 5-6 months.

Authorship

Authors are not permitted to add or remove any names from the authorship provided at the time of initial submission without the consent of the Journal's Chief Executive Editor.

Manuscript preparation

Refer to Pertanika's **INSTRUCTIONS TO AUTHORS** at the back of this journal.

Most scientific papers are prepared according to a format called IMRAD. The term represents the first letters of the words **I**ntroduction, **M**aterials and Methods, **R**esults, **A**nd, **D**iscussion. IMRAD is simply a more 'defined' version of the "IBC" [Introduction, Body, Conclusion] format used for all academic writing. IMRAD indicates a pattern or format rather than a complete list of headings or components of research papers; the missing parts of a paper are: *Title, Authors, Keywords, Abstract, Conclusions*, and *References*. Additionally, some papers include Acknowledgments and Appendices.

The *Introduction* explains the scope and objective of the study in the light of current knowledge on the subject; the *Materials and Methods* describes how the study was conducted; the *Results* section reports what was found in the study; and the *Discussion* section explains meaning and significance of the results and provides suggestions for future directions of research. The manuscript must be prepared according to the Journal's **INSTRUCTIONS TO AUTHORS**.

Editorial process

Authors are notified with an acknowledgement containing a *Manuscript ID* on receipt of a manuscript, and upon the editorial decision regarding publication.

Journal of Science & Technology
Journal of Science & Technology

Pertanika follows a **double-blind peer-review** process. Manuscripts deemed suitable for publication are usually sent to reviewers. Authors are encouraged to suggest names of at least three potential reviewers at the time of submission of their manuscript to Pertanika, but the editors will make the final choice. The editors are not, however, bound by these suggestions.

Notification of the editorial decision is usually provided within ten to fourteen weeks from the receipt of manuscript. Publication of solicited manuscripts is not guaranteed. In most cases, manuscripts are accepted conditionally, pending an author's revision of the material.

As articles are double-blind reviewed, material that might identify authorship of the paper should be placed only on page 2 as described in the first-4 page format in Pertanika's **INSTRUCTIONS TO AUTHORS** given at the back of this journal.

The Journal's peer-review

In the peer-review process, three referees independently evaluate the scientific quality of the submitted manuscripts.

Peer reviewers are experts chosen by journal editors to provide written assessment of the **strengths** and **weaknesses** of written research, with the aim of improving the reporting of research and identifying the most appropriate and highest quality material for the journal.

Operating and review process

What happens to a manuscript once it is submitted to *Pertanika*? Typically, there are seven steps to the editorial review process:

1. The Journal's chief executive editor and the editorial board examine the paper to determine whether it is appropriate for the journal and should be reviewed. If not appropriate, the manuscript is rejected outright and the author is informed.

2. The chief executive editor sends the article-identifying information having been removed, to three reviewers. Typically, one of these is from the Journal's editorial board. Others are specialists in the subject matter represented by the article. The chief executive editor asks them to complete the review in three weeks.

   Comments to authors are about the appropriateness and adequacy of the theoretical or conceptual framework, literature review, method, results and discussion, and conclusions. Reviewers often include suggestions for strengthening of the manuscript. Comments to the editor are in the nature of the significance of the work and its potential contribution to the literature.

3. The chief executive editor, in consultation with the editor-in-chief, examines the reviews and decides whether to reject the manuscript, invite the author(s) to revise and resubmit the manuscript, or seek additional reviews. Final acceptance or rejection rests with the Edito-in-Chief, who reserves the right to refuse any material for publication. In rare instances, the manuscript is accepted with almost no revision. Almost without exception, reviewers' comments (to the author) are forwarded to the author. If a revision is indicated, the editor provides guidelines for attending to the reviewers' suggestions and perhaps additional advice about revising the manuscript.

4. The authors decide whether and how to address the reviewers' comments and criticisms and the editor's concerns. The authors return a revised version of the paper to the chief executive editor along with specific information describing how they have answered' the concerns of the reviewers and the editor, usually in a tabular form. The author(s) may also submit a rebuttal if there is a need especially when the author disagrees with certain comments provided by reviewer(s).

5. The chief executive editor sends the revised paper out for re-review. Typically, at least one of the original reviewers will be asked to examine the article.

6. When the reviewers have completed their work, the chief executive editor in consultation with the editorial board and the editor-in-chief examine their comments and decide whether the paper is ready to be published, needs another round of revisions, or should be rejected.

7. If the decision is to accept, an acceptance letter is sent to all the author(s), the paper is sent to the Press. The article should appear in print in approximately three months.

   The Publisher ensures that the paper adheres to the correct style (in-text citations, the reference list, and tables are typical areas of concern, clarity, and grammar). The authors are asked to respond to any minor queries by the Publisher. Following these corrections, page proofs are mailed to the corresponding authors for their final approval. At this point, **only essential changes are accepted**. Finally, the article appears in the pages of the Journal and is posted on-line.

JST
Journal of Science & Technology
AN INTERNATIONAL PEER-REVIEWED JOURNAL

EDITORIAL OFFICE
JOURNAL DIVISION
Office of the Deputy Vice Chancellor (R&I)
1st Floor, IDEA Tower II
UPM-MTDC Technology Centre
Universiti Putra Malaysia
43400 Serdang, Selangor Malaysia.
Gen Enq.: +603 8947 1622 | 1619 | 1616
E-mail: executive_editor.pertanika@upm.my
URL: www.journals-jd.upm.edu.my

PUBLISHER
Kamariah Mohd Saidin
UPM Press
Universiti Putra Malaysia
43400 UPM, Serdang, Selangor, Malaysia.
Tel: +603 8946 8855, 8946 8854
Fax: +603 8941 6172
E-mail: penerbit@putra.upm.edu.my
URL: http://penerbit.upm.edu.my

ABSTRACTING/INDEXING
Pertanika is now over 35 years old; this accumulated knowledge has resulted the journals being indexed in SCOPUS (Elsevier), Thomson (ISI) Web of Knowledge [BIOSIS & CAB Abstracts], EBSCO, DOAJ, Google Scholar, AGRICOLA, ISC, Citefactor, Rubriq and MyAIS. JST is also indexed in ERA.

Pertanika Journal of Science & Technology
Vol. 24 (1) Jan. 2016

Contents

Foreword

Welcome to the **First Issue 2016** of the Journal of Science and Technology (JST)!

JST is an open-access journal for studies in science and technology published by Universiti Putra Malaysia Press. It is independently owned and managed by the university and is run on a non-profit basis for the benefit of the world-wide science community.

In this issue, **15 articles** are published, **three** are review articles, **eleven** are regular articles and **one** is a case study. The authors of these articles vary in country of origin, coming from **Malaysia**, **Indonesia**, **Iran**, **Australia**, **Italy**, **Bangladesh**, **Pakistan**, **Egypt**, **USA** and **Nigeria**.

The first review article in this issue discusses the Theory Inventive of Problem Solving (TRIZ) or Design for Manufacture and Assembly (DFMA) combination with Quality Function Deployment (QFD) as product design methodology (*Rosnani Ginting and Amir Yazid Ali*). The second review article discusses simulation methods for the structure of cementitious material hydrates at different length scales (*Tarighat, A., Zehtab, B. and Tavakoli, D.*) and the third review article describes the potential of 3'-Fluoro-3' Deoxythymidine as a cellular proliferation marker in PET oncology examination (*Hishar, H., R. Price, Fathinul Fikri, A. S., Eddie Lau, W. F., Assunta, C. and A. J. Nordin*).

The first regular article in this issue is on scaling group transformation for MHD double-diffusive flow past a stretching sheet with variable transport properties, taking into account velocity slip and thermal slip boundary conditions (*Uddin, M. J., Khan, W. A. and Ismail, A. I. M.*). The following articles look at: morphological and physico-chemical characteristics of soils in the Tasik Chini catchment in Pahang, Malaysia (*Sujaul, I. M., Ismail, B. S., Tayeb M. A., Muhammad Barzani, G. and Sahibin, A. R.*); development of an integrated catalytic membrane-based unit for biofuel production (*El-Zanati, E., Ritchie, S. M. C. and Abdallah, H.*); going beyond barebones cloud infrastructure services in dealing with competitiveness during an economic turbulence (*JosephNg, P. S. and Kang, C. M.*); optimisation of combined acid and enzymatic hydrolysis of cocoyam starch to produce a fermentable hydrolysate (*Amenaghawon, N. A., Osagie, E. I. and Ogbeide, S. E.*); simulation of a bioreactor with an improved fermentation kinetics – fluid flow model (*Emily Liew Wan Teng and Law Ming Chiat*); expression of C5a and its receptor in canine spontaneous tumours, which is a preliminary finding (*Norhaifa, G., Nashreq, K. N., Kamarudin, N. H., Bachek, N. F., Ajat, M. M., Hafandi, A., Selvarajah, G. T. and Hezmee, M. N. M.*); a comparative study of group runs and side sensitive group run control charts (*Yew, S. Y., Khoo, M. B. C., Teoh, W. L., Teh, S. Y. and Yeong, W. C.*); analysis of bit-plane images using principal component imaging from a face and palmprint database (*Therry Z. Lee and David B. L. Bong*); classification using the General Bayesian Network (*Sau Loong Ang, Hong Choon Ong and Heng Chin Low*); and potential impacts of climate change

on precipitation and temperature at Jor dam lake (*Aida Tayebiyan, Thamer Ahmad Mohammad, Abdul Halim Ghazali, M. A. Malek and Syamsiah Mashohor*).

I conclude this issue with a case study that reports on parotid oncocytoma in Birt-Hogg-Dubé syndrome, which considers a new pitfall in 18F-Fluorodeoxyglucose Positron Emission Tomography/Computed tomography imaging (*Sethu Thakachy Subha, Abdul Jalil Nordin, Norhafizah Mohtarrudin and Fathinul Fikri Ahmad Saad*).

I anticipate that you will find the evidence presented in this issue to be intriguing, thought-provoking, and, hopefully, useful in setting up new milestones. Please recommend the journal to your colleagues and students to make this endeavour meaningful.

I would also like to express my gratitude to all the contributors, namely, the authors, reviewers and editors for their professional contribution towards making this issue feasible. Last but not least, the editorial assistance of the journal division staff is fully appreciated.

JST is currently accepting manuscripts for upcoming issues based on original qualitative or quantitative research that opens new areas of inquiry and investigation.

Chief Executive Editor
Nayan Deep S. KANWAL, FRSA, ABIM, AMIS, Ph.D.
nayan@upm.my

Pertanika J. Sci. & Technol. 24 (1): 1 - 25 (2016)

PERTANIKA JOURNALS

SCIENCE & TECHNOLOGY

Journal homepage: http://www.pertanika.upm.edu.my/

Review Article

TRIZ or DFMA Combined With QFD as Product Design Methodology: A Review

Rosnani Ginting[1*] and Amir Yazid Ali[2]

[1]*Department of Industrial Engineering, Universitas Sumatera Utara, Medan 20155, Indonesia*

[2]*School of Mechanical Engineering, Universiti Sains Malaysia, 14300 Nibong Tebal, Pulau Pinang, Malaysia*

ABSTRACT

Quality Function Deployment (QFD) is a structured methodology that uses customer and technical requirements for designers and manufacturers to provide better products. Many researchers combine or integrate the technique of QFD with other methodologies such as Theory Inventive of Problem Solving (TRIZ) or Design for Manufacture and Assembly (DFMA) to optimise product design innovation and improvement. The combined methodologies are even used to solve process problems. Initial literature review of the application of stand-alone QFD poised several problems. Combining QFD with other techniques, such as TRIZ and DFMA, has helped to address these issues and forms the basis of future research. The integrated methods can solve main contradictory problems more precisely from product demand analysis to product design, production and application. Review work of the literature, specifically that on research and development of QFD, TRIZ and DFMA, showed that the said methodologies have been widely and successfully implemented in several practical applications such as resolving conflicts between customer and technical/engineering requirements and reducing production cost. This review work provides an in-depth analysis of identifying and finding issues of strengths, weaknesses and outcomes of the QFD when combined with TRIZ and also of QFD integrated with DFMA.

Keywords: Product design, QFD TRIZ, DFMA.

INTRODUCTION

Many companies have tried various new approaches in product design to stay competitive. With globalisation, enterprises have to compete with both local and international companies. Many of them are adopting quality as a source of competitive

Article history:
Received: 8 January 2015
Accepted: 13 April 2015

E-mail addresses:
rosnani_usu@yahoo.co.id (Rosnani Ginting),
meamir@usm.my (Amir Yazid Ali)
*Corresponding author

ISSN: 0128-7680

advantage so as to achieve a greater number of satisfied customers (Lai *et al*., 2007). Therefore, having products which continuously meet customers' or users' needs is top priority in the product development process. Every stage of product design and manufacturing is meticulously done to ensure that the products meet users' needs (Luo *et al*., 2012). According to Sakao (2013), several design guidelines have actually been developed, while a large number of individual design methods and tools have been generated, of which some were implemented as a standard part of design activities.

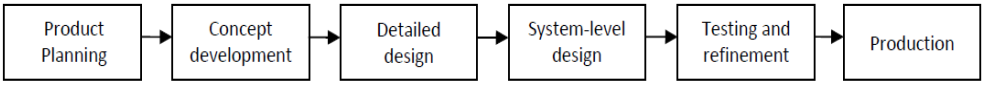

Fig.1: Product development process (Ulrich & Eppinger, 2008).

Fig.1 shows a generic model of the product development process consisting of a few linear steps (Ulrich & Eppinger, 2008). In actuality, the process is more complicated as different properties of the product (technical, economic, ergonomic and environmental) need to be considered simultaneously and this requires involvement of experts from various disciplines and departments. Most of the products consist of a variety of parts and subsystems and for this reason, different levels of product design need to be combined (e.g. components, parts and complete product).

Quality Function Deployment (QFD) is one of the widely used approaches today. It can drive a product development process from conception to manufacturing. It is a well-structured methodology and technique tool that combines customers' requirements with technical requirements that aid designers and manufacturers to produce better products, enhance their competitiveness in the marketplace and increase customer satisfaction (Prasad, 1998; Chan & Wu, 2002a; Mendoza *et al*., 2003; Lai *et al*., 2012; Farsi & Hakiminezhad, 2012).Van de Poel (2007) stressed that the main goal of QFD was to translate customers' demands into target values for the engineering characteristics of a product. By systematically and quantitatively employing the relationship between customers' demands and engineering characteristics, those engineering characteristics that are most promising for improving customer satisfaction can be selected, while target values can be set (Lai *et al*., 2012). Initial in-depth review of articles is to categorise problems pertaining to using QFD in product design. The categories of the QFD problem are depicted in Table 1.

These problems or drawbacks prompt the need for other approaches to be added when applying the QFD method. There are many different methods for generating new ideas and selecting the ideas in order to create a new design or to improve existing ones. In general, researchers tend to focus only on one aspect of the design process, that is, either on the concept generation method or on the concept selection method (Claudio, 2010). Combining QFD with other techniques helps to address these drawbacks and can form the basis of future research. The integrated innovation method, which combines QFD with other technique tools, can precisely solve main contradictory problems in the process from the stage of product demand analysis to that of product design, production and application. However, there is a need to establish the conditions under which the given combinations of particular methods are useful.

TABLE 1 Literature Survey of QFD Problems

QFD Problems	References
Customers' needs may be confused with technical responses, conflicts between technical measures and the House of Quality (HoQ) may be too large and confusing with excessive detail.	Chan & Wu (2002a)
Problems associated with 'working in teams', maintaining a commitment to the methodology and an unsuitable 'organizational culture'	Martins & Aspinwall (2001)
Problems related to organisational conditions such as project definition and project management, as well as team selection and building.	Govers (1996)
Complex and very time consuming	Büyüközkan et al. (2007); Mak (1999)
Size of the matrices may be too big and complex.	Franceschini & Rossetto (1998); Temponi et al. (1999)
Often difficult to reach agreement on conflicting technical requirements	Balthazar & Gargeya (1995); Lai & Chang (1999)
Difficult to meet the needs of different customer groups or segments	Kim et al. (1998); Partovi & Corredoira (2002)
Customers' needs, correlation among technical requirements and the relationship between customers' needs and technical requirements are often expressed informally in subjective and vague terms and linguistic variables	Zhou (1998); Kim et al. (2000); Fung et al. (2005)
The voice of the customer (VOC) is dynamic in nature and listening to the current VOC is insufficient	Fung et al. (2005)
Manual input of customer survey into the House of Quality (HOQ) is time-consuming and difficult	Bouchereau & Rowlands (2013); Karanjekar (2013)

This paper focuses specifically on the following areas:

- Analysis and identification of (investigates, analyses and reviews) the finding issues, particularly when QFD is combined with TRIZ and QFD is integrated with DFMA.
- Advancement of theory and practices directed to the combination/integration of the QFD method with TRIZ and DFMA approach are discussed and identified.
- Provision of a high-level overview of the current model of the combined QFD methodology in product design, as well as identifying current strengths, weaknesses and outcomes.

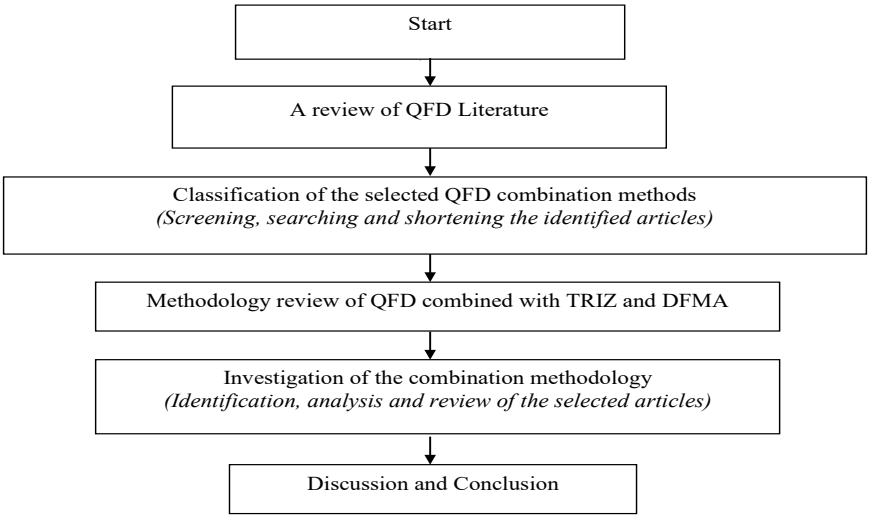

Fig.2: Flowchart of the methodology.

RESEARCH METHODOLOGY

The initial step of the process is to define the context of the literature survey based on the combination of the QFD methodology with TRIZ and DFMA. Fig.2 shows a flowchart of the methodology used to provide the literature review of the study. The work was divided into six sections. The parameters taken into consideration included:

- Product planning and development methods,
- Method of use and time boundaries (year of publication).

A table was used to record and classify the articles being reviewed. It is important to note that this paper focuses on and considers only journal articles whose goal was to either develop theoretical-conceptual work or reviews of the literature or a case study or theoretical modelling (keywords in the title, abstract, introduction were analysed). Even though the above identification methods were used during the searching process, the number of published articles is quite large; hence, it was not possible to analyse all the articles. In order to reduce the possibility of missing the latest developments, the emphasis of the analysis was on the literature published mainly within the last 20 years (1993 to 2014).

A screening process was needed to restrict the articles pertaining to combined QFD with TRIZ and/or DFMA approaches. As a result, a total 28 articles (out of 80) were selected from the following 13 journals, reviewed and further analysed: Production Research Journal, Institute of Electrical and Electronics Engineers Journal, Journal of Applied Operational Research, Science and Business Journal, Science and Agriculture Journal, Industrial Management Journal, International Journal of Operations and Production Management, Computers and Industrial Engineering Journal, International Journal of Ergonomic, Management and Development Journal, Journal of Engineering Education, International Journal of Collaborative Enterprise and Advances in Environmental Biology Journal.

The first and second sections present the Introduction and Research Methodology. Section 3 gives an overview of the QFD methodology and its applications. Section 4 and 5 discuss the combined methods of QFD with TRIZ and QFD with DFMA, as well as finding issues in depth-analysis of the combined methodology. Finally, discussion and conclusions are presented in Section 6.

Overview of Quality Function Deployment Methodology and Its Applications

Quality Function Deployment (QFD) is recognised as an effective method for integrated product and process development (Yang *et al*., 2012). It was developed by Yoji Akao, who described QFD as a "method to transform user demands into design quality, to deploy the functions forming quality, and to deploy methods for achieving the design quality into subsystems and component parts, and ultimately to specific elements of the manufacturing process." In other words, QFD is a tool for transforming the 'Voice of Customer (VOC)' to product design (Felice, 2010). QFD is a general concept that provides a method for translating customers' requirements into suitable technical requirements in each stage of product development and production (Shih & Chen, 2013). Fig.3 shows the translation between both requirements.

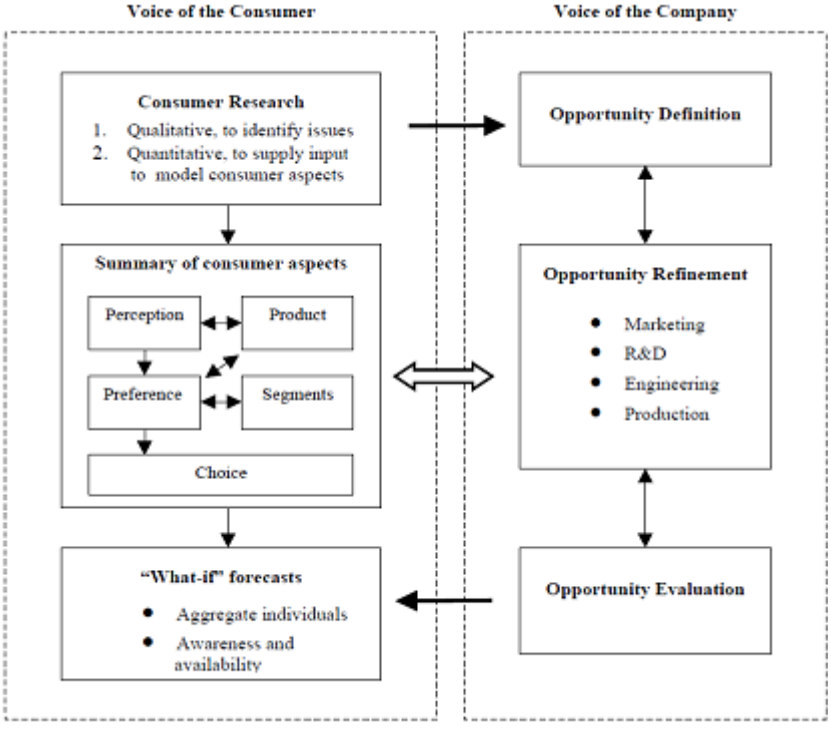

Fig.3: Phases of customer-orientated product design (Urban & Hauser, 1993).

House of Quality (HOQ) is a structure with interrelated matrices that can convert every customer's requirements into several technical requirements at all levels (Kao *et al*., 2002; Hung *et al*., 2007; Kao *et al*., 2010; Lai *et al*., 2012). Fig.4 illustrates a generic HoQ.

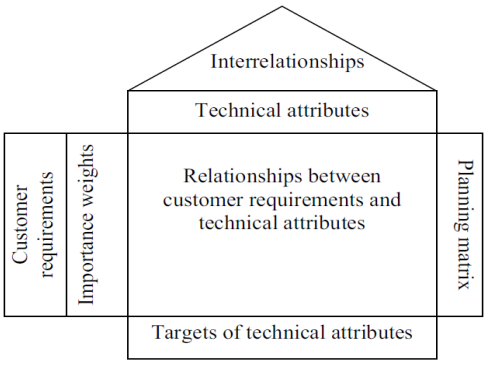

Fig.4: Matrix of HOQ (Cohen, 1995).

QFD also uses some principles from Concurrent Engineering (CE) because cross-functional teams are involved in all phases of product development (Cohen, 1995; Jaiswal, 2012). The QFD process involves four phases, as follows:

- Product planning: house of quality;
- Product design: parts deployment;
- Process planning;
- Process control (quality control charts).

A chart (matrix) represents each phase of the QFD process. The complete QFD process requires at least four houses to be built that extend throughout the entire system's development life-cycle (see Fig.5). Each of the four phases in a QFD process uses a matrix to translate customers' requirements from initial planning stages through production control. Bouchereau and Rowland (2000) stated that the starting point of any QFD project is the customers' requirement, which is often referred to as non-measurable. These requirements are then converted into technical specifications, referred to as the engineering characteristics or measurable. Each phase or matrix can represent more specific aspects of the product's requirements. Relationships between the elements were evaluated for each phase; however, only the most important aspects were deployed into the next matrix.

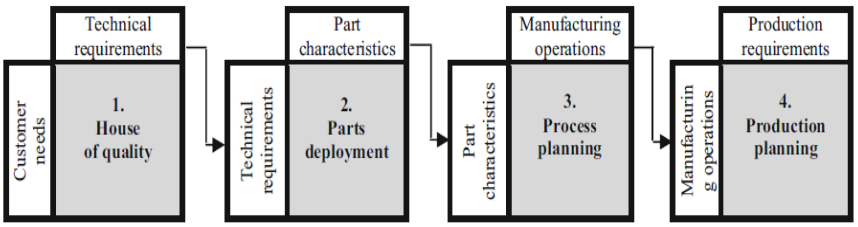

Fig.5: The QFD matrix phases (Hauser & Clausing, 1998, as cited in Kazemzadeh *et al*., 2009).

QFD with TRIZ and/or DFMA

Several optimisation approaches have been applied in QFD analysis in recent years. Due to the complexity of deployment, various quantitative methods have been suggested to improve the reliability and objectiveness of QFD (Chan & Wu, 1998). Benchmarking is also used to

determine an objective set of technical attributes in QFD (Shen & Tan, 1998). Meanwhile, Kazemzadeh and Behzadian (2009) analysed 650 articles on QFD and grouped them according to their content and came up with four broad categories, which are, general introduction, functional field, industrial application and theoretical development. They also discussed some benefits and common implementation problems. Their findings indicated that a particular weakness of QFD is that it is only suitable for specific applications.

The performance of QFD can be improved by combining it with product design tools. Fig.6 demonstrates how QFD can be used as a framework for product development processes (Sasananan, 2008). The most common method to improve QFD performance to prioritise customers' requirements is to link it with TRIZ and DFMA approaches. The combination of QFD with TRIZ is the most commonly used technique when dealing with incomplete and imprecise information pertaining to customers' requirements (Owlia & Aspinwall, 1998; Ngai & Chow, 1999; Pelt & Hey, 2010; Farsijani *et al*., 2013a). The combination of QFD-DFMA, on the other hand, can be used to improve the design quality of products during the product concept stage (Bahill & Chapman, 1993; Bergquist & Aberysekera, 1996; Bush & Robotham, 1999).

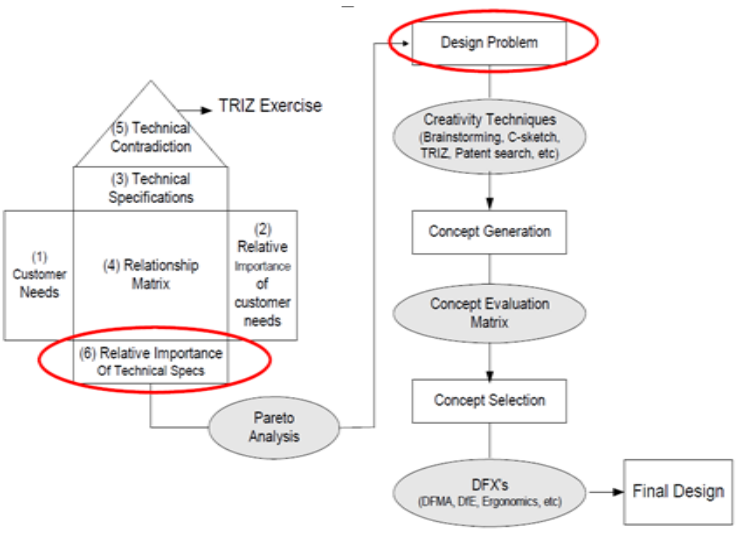

Fig.6: A conceptual model of how QFD is integrated with other methods for product design (Sasananan, 2008).

The findings showed that only two journal articles summarised the topic of QFD combination. Other topics that are commonly focused on in the literature are investigation and analysis of the application of QFD with TRIZ combination and application of QFD with DFMA combination. The common sectors where the combinations are applied include higher education, both large and medium-sized manufacturing, logistics, ergonomics, eco-design and product service. Meanwhile, the common product biased application areas are on product design, product design process, redesigning process, product development, redesigning product, product design cost, analysis cost and product cycle time. Table 2 lists some relevant literature on sector and applications in relation to the type of combinations.

TABLE 2 : Selected Literature Survey of QFD Combined with TRIZ

References	QFD combined	Method Applied in
Clarke (2000)	TRIZ	New product design development
Green & Bonollo (2002)	DFMA	Innovative conceptual idea
Yamashina et al. (2002)	TRIZ	Innovative product development
Suk & Kyeong (2003)	TRIZ	Product design
Mendoza et al. (2003)	DFMA	Product design
Marsot et al. (2004)	TRIZ	Product design
Estorilio & Marcelo (2006)	DFMA	Product design
Chuan & Chun Yu (2007)	DFMA	Product design
Bohm et al. (2008)	TRIZ	New product process and development
Su & Lin (2008)	TRIZ	Product development
Horak & Timar (2008)	DFMA	Product design process
Shang Liu et al. (2009)	TRIZ	Product design
Boppana & Azizi (2009)	DFMA	Product planning, conceptual design
George et al. (2009)	DFMA	New product development
Tseng et al. (2010)	TRIZ	Redesigning process
Claudio et al. (2010)	TRIZ	Redesigning product
Butdee & Trakunsaranakom (2010)	TRIZ	QFD (E), TRIZ
Yeh et al. (2011)	TRIZ	Innovative product design
Johangir & Noraddin (2012)	DFMA	Developing new service
Rau & Tse Fang (2012)	TRIZ	Design Improvement
Sojung & Byungun (2012)	TRIZ	Product and service components
Melgozaa et al. (2012)	TRIZ	Product Design
Yihong et al. (2012)	TRIZ	New Product Design
Farsijani et al. (2013)	TRIZ	Product designation processes
Sakao (2013)	TRIZ	Product planning
Shih & Chen (2013)	TRIZ	Product Design
Mayda & Borklu (2014)	TRIZ	Product Design
Vinodh et al. (2014)	TRIZ	Product Design and Development

Combination of QFD and TRIZ

QFD should not only address product functions but also quality requirement. This can be met by considering generated contradicting effects and evaluating improvement options. Tools on quality requirement in QFD alone are rather weak. The TRIZ methodology can better support designers to find such improvement solutions; hence, it is deployed together with QFD. This is because the tools and techniques of TRIZ, based on the integrated innovation methods, can be organised in many ways. The flowchart in Fig.7 illustrates the TRIZ systemic innovation knowledge. It is useful for the understanding of the integrated innovation methods (see Fig.7), particularly the tools and how they are related (Yihong *et al*., 2012). The synergy attained between the four phases of QFDs and TRIZ is a powerful tool to enable development

of breakthrough in products because it emphasises on error prevention practices (Yeh *et al*., 2011). The attained synergy can detect problems such as quality characteristic conflicts in target specifications and also negative interactions between product structures, materials, manufacturing processes and shop floor control requirements.

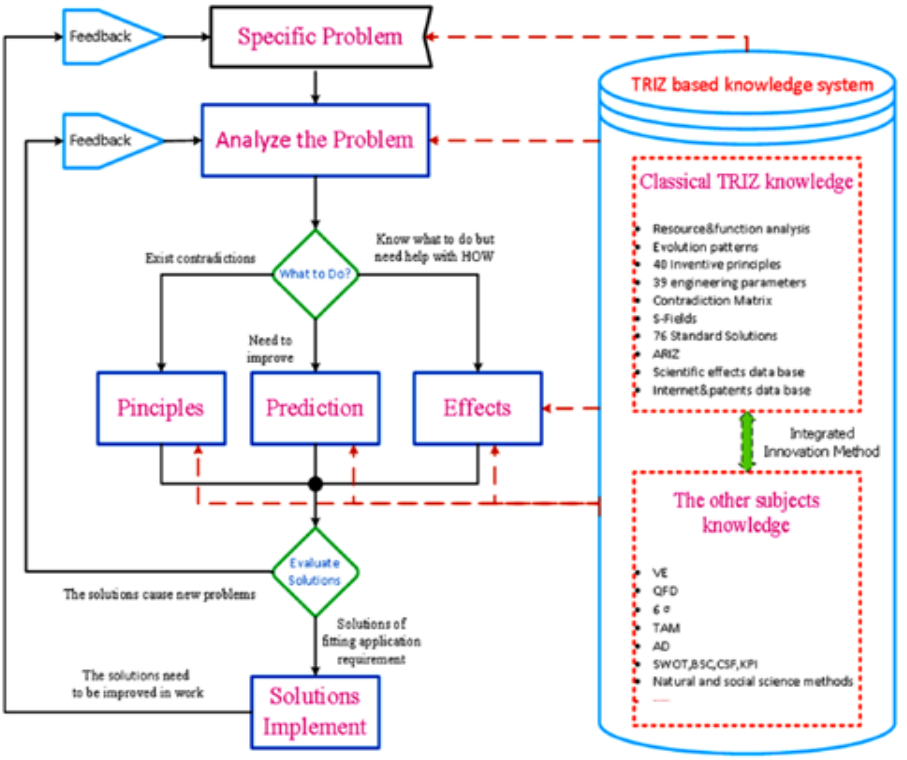

Fig.7: TRIZ problem solving flow chart with integrated innovations tools.

TABLE 3: Some Identified Literature Reviews on Combination of QFD and TRIZ

References	**Selected Variables**	**Identified Outcomes**
Clarke (2000)	Engineering characteristics	TRIZ and QFD has synergies that can be used for a wide range of innovative problem solving
Hajime et al. (2002)	Customers requirement and quality characteristic	Product development process carried out systematically with the integration of QFD and TRIZ
Hong Suk & Kyeong (2003)	Eliminating stool, bowl flushing, odour prevention, rinsing reduces sound	Flexible rubber and operation using TRIZ, which is applied to dipper in toilet, thus reducing water consumption in buildings (from 13 to 3 litres).
Marsot et al. (2004)	Voice of customer and engineering characteristic	Integration of FA, QFD and TRIZ can be used to create ergonomic products

TABLE 3: (Continued)

References	Selected Variables	Identified Outcomes
Liu et al. (2009)	Voice of customer, engineering characteristic	The Integration of QFD and TRIZ and non-linear programming can produce simulation design products that meet consumers' satisfaction with cost minimisation and elimination of contradicting technical characteristics.
Tseng et al. (2010)	Priority technical characteristics in product design	The combined QFD-TRIZ can be applied to determine sequence of technical characteristics and correlations between them.
Yeh et al. (2011)	Customer and environmental requirements, technical product characteristics, QFD contradictions	QFD supported TRIZ to translate Notebook's customers' needs into required design attributes, components/modules, process operations and production, concurrent with the desire to realise high applicability and innovation in products.
Rau & Fang (2012)	Packaging weight, size, prices, resilience, handling costs, resistance of moisture, vibration, pounding, pressure and durability wrapping	The proposed QFD was combined with the TRIZ approach to survey design requirements and attributes and their weights in terms of importance for notebook computer packaging design; a fuzzy QFD matrix was constructed, and it was found that the results were highly practical, extensible and applicable.
Yihong et al. (2012)	External variables, motivation (perceived usefulness, consumers' taste perception, behaviour, habits) and actual system used	With the integrated innovation method of QFD, TAM and TRIZ combined, the company's new wall material products are designed, and green, environmental, economic series wall material products have been designed and marketed in China
Sakao (2013)	Customer and environmental requirements; Technical attributes	The methodology supporting the effective planning in term of product cost and environment

TABLE 3: (Continued)

References	Selected Variables	Identified Outcomes
Mayda & Borklu (2014)	Capacity, weight, simple design, ergonomics, human effort, safety, durability, and dimensions	The applicability of the proposed model is demonstrated through a case study. The case study shows that the proposed model allows designers to find easily innovative and customer-centred solutions. Based on Altshuller's levels of innovation, the effectiveness of the proposed model was evaluated, and high innovative solutions were obtained.
Vinodh et al. (2014)	Durable, easy to operate and cost effective.	The results of this study highlight the practical feasibility of the integrated model of QFD combined with TRIZ, which includes a VOC translation mechanism, an innovative design tool, and an MCDM framework for innovative and sustainable product development.

Table 3 lists the works pertaining to the combination of QFD with TRIZ in the literature in chronological order. It shows the variables or sector that are being applied and the identified outcome of each work.

Many researchers have worked on the QFD and TRIZ combination and deployed TRIZ to address QFD problems and shortcomings. For example, Wang *et al*. (2005) identified contradictions within TRIZ by defining rules based on HOQ (House of Quality) in QFD. Several main parameters can be extracted and used to resolve conflicts and contradiction in QFD (Lu *et al*., 2006). Regazzoni *et al*. (2010) pointed out that taking an innovative, active and prospective approach is much more effective than showing passive reactions in preventing product collapse during its initial designation stages. TRIZ instrument was implemented to resolve these conflicts by translating the technical requirements into 39 designation parameters.

In the contradiction matrix, ameliorating parameters in rows and deteriorating parameters are arranged in columns. As QFD reveals the “what’s” of required operations, TRIZ instrument determines the “how’s” of the required operations (Hassan Farsijani *et al*., 2013). Sakao (2013) presented TRIZ as a set of technology trends related closely to quality control. The purpose is to help designers to become more efficient in making improvements to their designs. Designers need only to focus on more influential components to improve the quality of a product. This is because QFD reveals the “what” of the required operations, while the TRIZ instrument determines the “how” of the required operations. Farsijani *et al*. (2013) addressed the combination of QFD and TRIZ as seen in Fig.8.

Many researchers have also developed models or algorithms based on the QFD and TRIZ combinations. For example, Su and Lin (2008) developed a model based on the TRIZ

methodology to generate creative solutions using Fuzzy QFD to improve service quality by examining the service quality determinant and analysing the correlation between imprecise customer requirements and service quality determinants. Meanwhile, Yeh *et al*. (2011) proposed and developed using the four phases of QFD to translate customers' needs into required design attributes, components/modules, process operations and production into TRIZ inventive principles and a contradiction matrix. The purpose was to achieve green-design solutions. The software of the TRIZ matrix was developed based on the algorithm. Kim and Yoon (2012) implemented the TRIZ and QFD instrument to resolve the conflicts between production and consumption requirements in 500 automobile factories in the world.

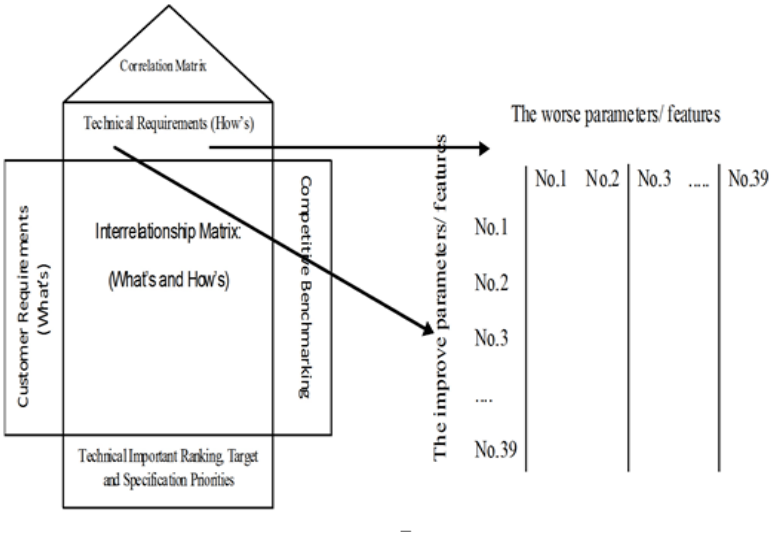

Fig.8: A conceptual model of how QFD was integrated with other methods (Hassan Farsijani et al., 2013).

Analysis of the QFD Combined TRIZ

This section reviews the analysis of the case studies applying the combined QFD-TRIZ. Fifteen case studies were selected for analysis in this section (see Table 3). Cases 1 to 7 are categorised as development and improvement of the combined QFD-TRIZ, cases 8 to 18 are categorised as application, and cases 19 and 20 are the fuzzy version of the combined QFD-TRIZ.

Case 1. Clarke (2000). A new combined QFD-TRIZ approach was used to employ elements from the existing customer assessment from concept generation methods to concept selection methods. The TRIZ method was used to transfer the ideas generated through brainstorming into concepts and solutions. The result was to obtain and develop ideas in designing a product that is actually needed by customers. Unfortunately, the amount of ideas generated was insufficient to completely fulfil all customers' requirements.

Case 2. Yamashina et al. (2002). A new combined QFD-TRIZ approach was developed and named Innovative Product Development Process (IPDP). It systematically integrates QFD with TRIZ and enables effective and systematic technical innovation for new products. The IPDP was developed to assist engineers in finding innovative solutions during the technical

product development process. However, the work does not show the effectiveness of QFD and TRIZ integration as it lacks the concentration of an in-depth method. Other in-depth analyses in other literature also indicate that there are no other methods that can effectively show the integration of QFD and TRIZ.

Case 3. Su & Lin (2008). Their combined approach was used to identify critical determinants that pertain to customer satisfaction by analysing the correlation between imprecise requirements obtained from customers and determinants of service quality. The approach can be used to overcome both technical and non-technical problems. However, the applicability of the method is rather complex.

Case 4. Bohm et al. (2008). Their combined QFD-TRIZ approach covers the conceptual development of new products. The methodology was structured into several specific steps and used an IT tool. It provides the transition from isolated support tools to information management along all the phases of the conceptual development in an innovation process. The integration of KNOW-IT, HoQ and TRIZ can improve the overall process of new product development concepts and link it to integrated management information. The communication of each department in developing the product must be transparent when applying the methodology.

Case 5. Liu et al. (2009). Their integrated approach emphasises the contradictions between engineering characteristics rather than compromising trade-off during the early stage of product development. They suggested utilising TRIZ to solve contradictions as the first step. The second step is to amend the correlation matrix of engineering characteristics. The next step is to validate; this is followed by planning and executing IFR (ideal final result). However, they did not describe cost calculation optimisation in detail. MatLab was used for non-linear programming.

Case 6. Claudio et al. (2010). They proposed using the combined QFD-TRIZ approach to create a new design, right from the customer needs assessment to the final design. The methodology was created while a variable message-sign mounting device was designed. The methodology utilises elements from existing customer assessment tools, concept generation methods and concept selection methods.

Case 7. Tseng et al. (2010). They developed a new combined QFD-TRIZ model in terms of Prioritisation of Product Design Tasks. TRIZ was used to generate conflict problems arising from HoQ. DSM and the importance of ECs are applied to overcome the conflicting problems. The methodology of combined QFD, TRIZ and DSM provides ease in determining absolute priority importance in HoQ. However, its application is rather complicated for problem solving whenever simultaneous resource constraints exist.

Case 8. Lee & Won (2003). They used the combined QFD-TRIZ approach to find innovative conceptual ideas to develop a super water-saving toilet system. The physical contradiction in TRIZ with QFD was defined for the fixed ceramic S type trap for saving water while preventing a bad smell from the septic tank at the same time. The concept of using a flexible tube to save water was obtained by using the separation principle to resolve physical contradictions. The aim was to make the innovative concepts more structured so that the physical contradiction of every customer need can be eliminated. Unfortunately, identifying what customers desire using the approach is very difficult to do, and it is even more challenging to use it to generate creative ideas.

Case 9. Marsot et al. (2004). The QFD-TRIZ approach was used to design and produce an ergonomic boning knife. However, the advantages of the newly-designed product compared to the others were not mentioned to prove the effectiveness of their methodology.

Case 10. Tomohiko Sakao (2007). The combined QFD-TRIZ approach was utilised to support the product planning and conceptual design stages effectively. The author provided the concept of innovative product design and eco-friendly design. Nonetheless, it is difficult to quantify the environmental attributes into QFD using this particular concept.

Case 11. Butdee & Trakunsaranakom (2010). The combined QFD-TRIZ approach was used to support redesigning of the High Temperature Machine (HTM). Key TRIZ contradictions for HTM include power duration of action, quantity of substance in the water, as well as temperature and weight of major objects. This combination was used to design eco-friendly products. However, their paper does not describe the validation steps in TRIZ.

Case 12. Yeh et al. (2011). Their combined approach utilises a methodology that integrates TRIZ inventive principles and contradiction matrix to achieve green-design solutions for major contradictions. TRIZ was used to propose innovative methods to resolve problems. This helps designers to anticipate the end results of product development process, a result that is innovative and enhances the chances of product success. However, it is difficult to solve problems when there are simultaneous resource constraints.

Case 13. Kim & Yoon (2012). The combined QFD-TRIZ approach was applied to create product-service system (PSS) concepts by resolving contradictions between product and service components. They applied TRIZ's 40 inventive principles to PSS cases. QFD was adopted to identify critical features of products and services. Characteristics of good products and services were identified using QFD so that the resulting product could be appropriately generated. However, using a tool that is only used to reduce losses due to the product will not be able to prove or show the service quality of existing products.

Case 14. Melgozaa et al. (2012). The methodology they used is based on the synergy between several methods such as attribute listing, QFD and TRIZ to solve physical contradictions related to geometry and material used. Through the combination of QFD and TRIZ, physical contradictions related to geometry and material can be solved. This resulted in a form of stent that is approved by doctors. Although the device has been adjusted, the design techniques do not allow feature geometry to be detailed at this level.

Case 15. Yihong et al. (2012). Through the QFD combined TRIZ and TAM, a design of new building wall materials was achieved. Technical contradictions and physical contradictions at various stages of product design and production were resolved from the perspectives of a user survey, R & D design, manufacturing and marketing. On the other hand, some researchers claimed that TAM might be easy to use and a quick study it is less representative of the real problems of technology acceptance.

Case 16. Shih & Chen (2013). They proposed the combined QFD, ANP and TRIZ to design a mobile healthcare device in the healthcare industry. The proposed process for designing a future mobile healthcare device points out some important features, meets the needs of customers and could be a future direction for the development of the healthcare industry. The concept of innovative ideas has become more structured. Therefore, physical contradiction of each customer's needs can be eliminated.

Case 17. Mayda & Borklu (2014). The proposed combination of QFD and TRIZ into Pahl and Beitz's conceptual design approach was used to design a punch according to two different design models: classical conceptual design process and TRIZ and QFD-assisted conceptual design. This was done to see the results of these designs.

Case 18. Vinodh et al. (2014). They applied fuzzy in their combined Fuzzy QFD-TRIZ approach to redesign the product packaging system. Requirements derived through fuzzy QFD were used to identify design attributes using the TRIZ method. This approach can eliminate the contradictions between material and technical features. However, determination of technical characteristics is still subjective. A combination of QFD and TRIZ can boost innovative thinking in the designing process. Moreover, the total time taken by QFD and TRIZ in assisting the designing process is significantly shorter compared to the classical design process. However, in this paper, QFD did not consider product life cycle but focused on what to do instead. The answer to the question of how to do it is not given, while the process of converting customers' desires into a characteristic technique cannot be defined as well.

Case 19. Rau & Fang (2012). They applied fuzzy in their combined Fuzzy QFD-TRIZ approach to redesign product packaging system. Requirement derived through the fuzzy QFD was used to identify design attributes by using the TRIZ method. This approach can eliminate the contradictions between material and technical features. However, determination of technical characteristics relationship is still subjective. QFD and TRIZ in synergy can save about 40% of time. In terms of cost, on the other hand, the negative effects can cause noise. There is an increase in the coss incurred, while operational complexity is also increased.

Case 20. Farsijani et al. (2013). The combined Fuzzy QFD-TRIZ approach was used to increase product designation efficiency. The researchers implemented the Fuzzy Analytic Hierarchical Process (FAHP) to weigh customers' requirements. Meanwhile, an advanced decision-making software was used to calculate adaption coefficients. The TRIZ instrument was used to resolve the conflicts between technical requirements in a short time based on priorities of customers' requirements. Data from consumers were collected indirectly. However, researchers did not focus on and make comparisons between competitors' products.

The QFD-DFMA Combination Methodology

Design for Manufacture and Assembly (DFMA) focused on operation issues during product design. According to Rajagopalan (2011), this can be critical even though design costs are just a small part of a product's total cost because wastage of raw materials or duplicating efforts could substantially cause negative impacts on any business's profitability. Silva *et al*. (2009) identified QFD as having a concept similar to that of the Design for Manufacturing (DFM) because it also attempts to integrate the relationship between product engineering, quality, marketing and customers. The systematic evaluation approach by DFMA tools provides critical insight into the strengths and weaknesses of the existing product design during its production life phase.

Designers will be led to focus on searching for new product concepts after using this evaluation method in combination with QFD's needs analysis and benchmarking exercises. The inadequacies highlighted by the QFD and DFMA evaluation will be resolved into a solution. It will form the basis of new product concepts with an improved design quality. This technique

also reduces total project time. Gupta and Okudan (2012) described QFD as a popular DFM tool that is used at the conceptual design stage to convert customers' demands into quality characteristics. Design for Assembly (DFA) is closely linked to DFM as it also attempts to reduce the total number of parts and also the total cost incurred. Ideally, DFA must be applied at the conceptual design stage to attain maximum effects. Thus, QFD and DFM promote integration between engineering, manufacturing and marketing by reducing the total cycle time of product development and implementing product quality to be in full compliance with customers' desires (Bush & Robotham, 1999). Table 4 shows the list of some literature related to the combined QFD-DFMA approach and the identified variables and outcomes.

TABLE 4 : Some Literature Reviews Related to QFD Combined DFMA

References	**Identified Variables**	**Identified Outcomes**
Green & Elivio (2002)	Conceptual and detail design	Provides solutions on the study guide to other researchers in product design
Mendoza *et al.* (2003)	Voice of customers, quality characteristic, cost, cycle time	This study shows the methodology used is more suitable for products in the early stages of product cycle.
Estorilio & Simiao (2006)	Cost, detail design	Application of QFD, DFMA and FMEA can be used to show the critical subsystems identified by using cost.
Chiu & Lin (2007)	Product design costs, analysis costs, product design stages	Integration of QFD-DFMA to streamline the design of the product by reducing cost and time in order to improve the quality
Horak & Timar (2008)	Estimating manufacturing costs, cost of assembling product	The application of DFMA has led to quantum leaps in productivity that are reflected in saving programme timing reductions of >50%, assembly time reductions of >63%, assembly defect reductions of >68%, separate part reductions of >50%.
Chowdary & Harris (2009)	Customers' needs, material selection, material assembly time	Product design concepts allow designs to be produced at lower costs and lower environmental impacts, thus enabling organisations employing these principles to become more profitable.
George & Vosniakos. (2009)	Product manufacturing, system simulation, parametric design	Combination of QFD-TRIZ allowed the designer a better control over the intermediate results, enhancing the ability to simulate and test more variations with built-in computerised decision making tools.
Farsi & Noraddin (2012)	Customers' needs and requirements	The technique of QFD, DFMA and VE in the design of product/service or production process is the selection of suitable alternatives that lead to increased value for the customers but does not increase product/service cost. In other words, improved product/service costs lead to greater customer satisfaction.

Analysis of the Combined QFD-DFMA

Eight works were studied for the combined QFD-DFMA approach. Cases 1 and 2 involved new developments and improvement to the combined approach while cases 3 to 8 were on the application of the combined approach.

Case 1. Green & Bonollo (2002). They proposed collaboration between QFD-DFMA and the Value Analysis (VA) approach as a means to improve both outcomes and quality of product design solutions. They explained and described in detail the knowledge and stages involved in the design methodology and also clarified the relationship design process stage. However, their explanation of the integration of product design development method with other methods is not detailed.

Case 2. Chowdary & Harris (2009). They presented an integrated DFMA and DFE with the QFD method. In this regard, QFD aided DFMA and DFE in determining the limits of any design. The study also showed the connections between customers' needs and the metrics used to satisfy them. It also illustrated what the development team should focus on to produce quality products. Once a final concept is selected, two concept variants should be developed. The first variant is without the use of DFE and DFMA methodologies, while the second variant uses DFE and DFMA. However, their proposed combination methodology is only useful for reducing the time required for product design.

Case 3. Mendoza et al. (2003). They applied the combined QFD-DFMA and VE approach in five case studies, and showed that DFMA eased evaluation efforts in terms of information that was generated during the QFD/VE process. Through this combination, DFMA could be used to optimise design proposals. Information from the QFD/VE processes could then be used to evaluate the would-be impacts due to modifications suggested by the DFMA analysis of the product's performance. However, the results of the QFD process are not necessarily balanced because requests focusing on improving the performance of specific features may not be relevant to specific populations. Customers appeared to make assumptions about the products that were not immediately evident from their requests.

Case 4. Estorilio & Simiao (2006). They utilised the integrated QFD-DFMA approach to reduce assembly costs in a diesel engine model, thus making the engine economically feasible. They presented a detailed description of how the most critical engine subsystem was a delimiter by considering the cost and applying DFMA guidelines to the subsystem. Hence, it was concluded that QFD, DFMA and FMEA could be used to reduce the number of components when developing product design.

Case 5. Chiu & Lin (2007). The integrated concept of QFD and DFMA was used to produce low-cost products with high quality in a shorter lead time. Their concept could be used to reduce materials and energy usage, while reducing emissions. However, this integration has a major constraint in the form of the complexity of organising and analysing large-scale matrix relationships.

Case 6. Horak & Timar (2008). They applied the combined QFD-DFMA approach with FMEA to reduce assembly time, assembly defects and separate parts of the door-lock system of tractors in a DFMA laboratory. The combination of QFD, DFMA and FMEA could be used to reduce the number of components used in developing a product design. DFMA also aided DFE to reduce costs, develop future products and minimise the number of design errors.

Case 7. George & Vosniakos (2009). They applied the combined QFD-DFMA approach to examine the path of preliminary products and process development to detailed product design to manufacturing system design focusing on performance prediction. Emphasis was given to analysis-based configuration issues. Their methodology attempted to integrate several different tools within the context of concurrent product and manufacturing system development. Each tool has certain advantages and disadvantages. Holistically from an integration perspective, there are several areas that need attention. One area of interest is the methodology's sequential nature. The difference between the three phases is rather obvious even though there are instances of change in the feedback given and used for decision making.

Case 8. Farsi & Hakiminezhad (2012). They applied the combined QFD-DFMA approach with VE to reduce service/product costs without lowering its quality or performance. Their approach showed that the tools could be used to maintain the team's focus during the design process. They explained the stages involved in identifying processes that facilitated the designer to make inferences. Integration of the three methods simultaneously led to cost reduction and quick or instant improvement of the performance of services or products. However, the method has been presented as too complex to be integrated with other methods.

DISCUSSION AND CONCLUSION

The main objective of this work was to analyse and review several works in the literature on QFD methodology in combination with other techniques that were aimed to improve product design and perform designing tasks as quickly as possible during the product development process. The analysis focused on the combined use of three established methodologies of Quality Function Deployment (QFD), Theory of Inventive Problem Solving (TRIZ) and Design for Manufacturing and Assembly (DFMA).

For this work, journal articles pertaining to the combined QFD approaches from 1993 to 2014 were reviewed and analysed. The articles were distributed over 13 different journals. For this purpose, the initial screening process of relevant journal articles was done whereby 28 combination methods were identified. The combined methods were categorised and presented in two groups: one was based on their type and the other on their methodological characteristics. The categorisation was done for both the approaches of combined QFD-TRIZ and the combined QFD-DFMA.

The strengths and weaknesses of the combined methods and their application in the specific cases were also highlighted. The combined techniques were also analysed separately. This paper also elaborates on details of the combination methodology, specifically details related to both QFD combined with TRIZ and QFD combined with DFMA.

It was found that the QFD combination methodology could provide relevant guidelines and information pertaining to designers on matters to be considered during product design and development processes. The combined QFD-TRIZ and QFD-FMA approaches were the most commonly used techniques to deal with incomplete and imprecise information related to customers' and technical requirements. However, their shortcomings have also been encountered. Among these shortcomings were that many of the combination methods were classified under only one type; the combination methodologies were discussed separately and

compared with no integration; and systematic framework in combining the methods was not described in detail. DFMA could be used to optimise design proposals, while information from the QFD/VE processes could be used to evaluate the impacts the modifications might have on the product's performance, as suggested by the DFMA analysis.

This paper also reviewed the important benefits of the combined QFD-TRIZ and QFD-DFMA approach. Some of the benefits of the combined QFD approach obtained from the literature reviewed are listed below:

- The integration of with TRIZ improves the overall process of new product development, from concepts to integrated management information.
- Completion of the technical characteristics on the relationship in QFD's house of quality (HoQ) using TRIZ contradiction can result in cost optimisation.
- The combined QFD-TRIZ method easily determined absolute priority importance in HoQ.
- Contradictions in the requirements and technical features can be eliminated.
- With the QFD, customer's needs could be determined and attribute needs could be arranged systematically, while TRIZ resolved any contradictions that occurred.
- The combination of TRIZ and QFD can reduce flaws in product design.
- The combined QFD-DFMA can determine the limits of a design and relate customers' needs to the metrics used to satisfy them.
- QFD-DFMA could be used to reduce the components used during the product design development stage.
- QFD-DFMA with FMEA can reduce assembly time and assembly defects and also separate parts of products.

REFERENCES

Abastante, F., & Lami, I. M. (2012). Quality function deployment (QFD) and analytic network process (ANP): an application to analyze a cohousing intervention. *Journal of Applied Operational Research, 4*(1), 14-27.

Bahill, A. T., & Chapman, W. L. (1993). A tutorial on quality function deployment. *Engineering Management Journal, 5*(3), 24-35.

Balthazar, P. A., & Gargeya, V. B. (1995). Reinforcing QFD with group support systems: Computer-supported collaboration for quality in design. *International Journal Quality Reliability Management, 12*(6), 43-62.

Bergquist, K., & Abeysekera, J. (1996). Quality function deployment (QFD) – A means for developing usable products. *International Journal of Industrial Ergonomics, 18*(4), 269-275.

Boppana, V. C., & Azizi Harris. (2009, June). Integration of DFMA and DFE for development of a product concept: A case study. *Seventh LACCEI Latin American and Caribbean Conference for Engineering and Technology* (LACCEI'2009). 2009, June 2-5, San Cristóbal, Venezuela, pp.1-8.

Bouchereau, V., & Hefin, R. (2000). Methods and techniques to help quality function deployment (QFD), benchmarking. *An International Journal, 7*(1), 8-19. MCB University Press, pp. 1463-5771.

Bras, B. (1997). Incorporating environmental issues in product design and realization. *Journal of Industry and Environment, 20*(1-2), 7-13.

Bush, S. A. & Robotham, A. J. (1999). Improving conceptual design quality by use of QFD & DFMA processes. *International Conference On Engineering Design ICED*, 99 Munich, August 24-26.

Butdee, S. T. (2010). QFDE combined with TRIZ framework to formulate and respond to functional design for a high temperature machine (HTM). *Asian International Journal of Science and Technology in Production and Manufacturing Engineering, 3*(4), 77-84.

Büyüközkan, G., Fiyzioglu, O., & Rual, D. (2007). Fuzzy group decision-making to multiple preference formats in quality function deployment. *Computer Industry, 58*(5), 392-402.

Chan, L. K. & Wu, M. L. (1998). Prioritizing the technical measures in quality function deployment. *Quality Engineering Journal, 10*(3), 467-469.

Chan, L. K., & Wu, M. L. (2002). Quality function deployment: A literature review. *European Journal Operation Research, 143*, 463-497.

Chang-Lin Yang., Rong-Hwa Huang, & Wei-Ling Wei. (2012). A modified TRIZ for new product development management. *Business and Information* (Sapporo, July 3-5), 323-334.

Chao-Ton Su, & Chin-Sen Lin. (2008). A case study on the application of fuzzy QFD in TRIZ for service quality improvement. *Journal Quality & Quantity, 42(*5), 563-578.

Chien-Jung, L., Chih-Hung Hsu, & Fang Ou-Yang. (2012). A hybrid mining and predicting system based on quadratic exponential smoothing model and grey relational analysis for green supply chain. *Academic Journal, 11*(8), 336-348.

Chiu, M. C., & Kremer, G. E. O. (2011). Investigation of the applicability of Design for X tools during design concept evolution: a literature review. *International Journal of Product Development, 13*(2), 132-167.

Chougule Mahadeo Annappa & Kallurkar Shrikant Panditrao. (2013). *International Journal of Innovative Technology and Exploring Engineering* (IJITEE), *2*(6), 45 – 52.

Clarke, D. W. (2000). Leveraging TRIZ to combine ideas into implementable concepts. Transactions from the symposium on quality function deployment. *Quality Function Deployment Symposium;* 12th, 386-396.

Claudio, D., Chen, J., & Gül, O. (2010), A comprehensive methodology to generate and select design ideas. *Proceedings IIE Annual Conference*. IIE Annual Conference.

Cohen, L. (1995). *Quality function deployment – How to make QFD work for you*. Addison Wesley Longman Inc., USA.

De Felice, F. & Petrillo, A. (2010). A multiple choice decision analysis: An integrated QFD – AHP model for the assessment of customer needs. *International Journal of Engineering, Science and Technology, 2*(9), 25-38.

Eshan, S. J. (2012). A case study on quality function deployment (QFD). *IOSR Journal of Mechanical and Civil Engineering (IOSR-JMCE), 3*(6), 27-35.

Estorilio, C., & Simião, M. C. (2006). Cost reduction of a diesel engine using the DFMA method. *Journal of Management & Development, 4*(2), 95-103.

Farsi, J. Y., & Hakiminezhad, N. (2012). The integration of QFD technique, value engineering and design for manufacture and assembly (DFMA) during the product design stage. *Journal of Advances in Environmental Biology, 6*(7), 2096-2104.

Franceschini, F., & Rossetto, S. (1998). Quality function deployment: How to improve its use. *Journal of Total Quality Management, 9*(6), 491-500.

Fung, R. Y. K., Chen, Y. Z., Chen, L., & Tang, J. F. (2005). A fuzzy expected value-based goal programming model for product planning using quality function deployment. *Engineering Optimization, 37*(6), 633-647.

Govers, A., Martins, & Aspinwall, E. M. (2001). Quality function deployment: An empirical study in the UK. *Total Quality Management Journal, 12,* 575-588.

Govers, C. P. M. (1996). What and how about quality function deployment (QFD). International *Journal of Production Economics, 46-47*, 575-585.

Hassan, F., & Mohammad Ali, T. (2013). Improvement of efficiency in product designing by usage of fuzzy QFD & TRIZ: A case study on Transfo Company. J*ournal of Applied Science and Agriculture, 8*(4), 451- 461.

Ho, E. S. S. A., Lai Y. J., & Chang, S. I. (1999). An integrated group decision making approach to quality function deployment. *Institution of Electrical Engineers Transaction, 31*(6), 553-567.

Horák, P., & Timár, I. (2008). Environment friendly DFMA/QFD/FMEA laboratory on the University of Pannonia. *Fascicle of Management and Technological Engineering, VII* (XVII), 1474-1479.

Hundal, G. S., & Kant, S. (2014). Product Design through QFD Approach with Hybrid of AHP and Fuzzy Logics. *International Proceedings of Economics Development and Research, 75*, 112.

Hung, H. F., Kao, H. P., & Juang, Y. S. (2008). An integrated information system for product design planning. *Expert systems with applications, 35*(1), 338-349.

Kao, H. P., Su, E., & Wang, B. (2002). I2QFD: a blackboard-based multiagent system for supporting concurrent engineering projects. International Journal of Production Research, 40(5), 1235-1262.

Kao, H. P., Su, E., & Wang, B. (2002). IQFD: A blackboard-based multi-agent system for supporting concurrent engineering projects. *International Journal of Production Research, 40*(5), 1235-1262.

Kazemzadeh, R. B., Majid Behzadian, Mohammad Aghdasi, Amir Albadvi. (2009). Integration of marketing research techniques into house of quality and product family design. *The International Journal of Advanced Manufacturing Technology, 41*(9-10), 1019-1033.

Kim, B., & Yoon, B. (2012). Developing a process of concept generation for new product-service systems: A QFD and TRIZ-based approach. (pp. 1-26). Korea: Springer.

Kim, J. K., Han, C. H., Choi, S. H & Kim, S. H. (1998), A knowledge-based approach to the quality function deployment. *Computer Industrial Engineering, 35*(1-2), 233-236.

Kim, K. J., Moskowitz, H., Dhingra, A., & Evans, G. (2000). Fuzzy multi-criteria models for quality function deployment. *European Journal Operation Research, 121*(3), 504-518.

Lai, X., Kay-Chuan, T., & Xie, M. (2007). Optimizing product design using quantitative quality function deployment: A case study. *International Journal of Quality and Reliability Engineering, 23*(1), 45-57.

Lai, X., Tan, K. C., & Xie, M. (2007). Optimizing product design using quantitative quality function deployment: a case study. *Quality and reliability engineering international, 23*(1), 45-57.

Lance, N. G., & Bonollo, E. (2002). The development of a suite of design methods appropriate for teaching product design. *Global Journal of Engineering Education, 6*(1), 45-52.

Lu, C., Liao, Z., Jiang, S. H., & Lin, G. (2006). Research on innovative product design system based on QFD and TRIZ. *China Trans Technology Publication,* 1144-1147.

Luo Yihong, Shao Yunfei, & Chen Ting. (2012). Study of new wall materials design based on TRIZ integrated innovation method. *Management Science and Engineering, 6(*4), 15-29.

Mak, K. L. (1999). Web-based collaborative conceptual design. *Journal of Engineering Design, 10*(2), 183-194.

Mansor, M. R., Sapuan, S. M., Zainudin, E. S., Nuraini, A. A., & Hambali, A. (2014). Conceptual design of kenaf fiber polymer composite automotive parking brake lever using integrated TRIZ–Morphological Chart–Analytic Hierarchy Process method. *Materials and Design, 54,* 473-482.

Marsot, J., & Claudon, L. (2004). Design and ergonomics. Methods for integrating ergonomics at hand tool design stage. *International Journal of Occupational Safety and Ergonomics: JOSE (Impact Factor, 10*(1), 13-23.

Melgoza, E. L., Serenó, L., Rosell, A., & Ciurana, J. (2013, December). An integrated parameterized tool for designing a customized tracheal stent. *Computer-Aided Design, 44*(12), 1173-1181.

Mendoza, N., Horacio A., & Molina. A. (2003). Case STUDIES IN THE INTEGRATION of QFD, VE and DFMA during the product design stage. *The Proceedings of the 9th International Conference of Concurrent Enterprising*, Espoo, Finland, 2003, June 16-18.

Murat, M., & Huseyin, R. B. (2014). Development of an innovative conceptual design process by using Pahl and Beitz's systematic design, TRIZ and QFD. *Journal of Advanced Mechanical Design, Systems, and Manufacturing, 83,* 1-12.

Owlia, M. S., & Aspinwall, E. M. (1998). Application of quality function deployment for the improvement of quality in an engineering department. *European Journal of Engineering Education, 23*(1), 105-115.

Partovi, F. Y., & Corredoira, R. A. (2002). Quality function deployment for the good of soccer. *European Journal Operation Research, 137*, 642-656.

Prabhdeep, S. B., & Dalgobind, M. (2013). Concepts, tools and techniques of problem solving through TRIZ: A review. *International Journal of Innovative Research in Science, Engineering and Technology, 2*(7), 3061-3073.

Prasad, B. (1998). Review of QFD and related deployment techniques. *Journal Manufacturing System, 17*(3), 221-234.

Rau, H., & Fang, Y. T. (2009). Conflict resolution of product package design for logistics using the TRIZ method. Machine Learning and Cybernetics, *International Conference, 5*, 2891-2896.

Renganathan, R. (2011). *Strategies for building world class operations.* ICOQM-10 2011, June 28-30.

Russo, D., & Regazzoni, D. (2010). TRIZ tools to enhance risk management. TRIZ Future Conference 2010, *Procedia Engineering, 9,* 40-51.

Saraj Gupta, & Gül E. Okudan. (2012). Computer-aided generation of modularised conceptual designs with assembly and variety considerations. *Journal of Engineering Design, 19*(6), 533-551.

Sasananan, M. (1996). Using quality function deployment as a framework for teaching product design and development. *Veridian E-Journal, Silpakorn University, 1*(1), 1-13.

Shang, L., Dongyan, S., & Ying, Z. (2009). A planning approach of engineering characteristics based on QFD-TRIZ integrated. RIFIP AICT 304. *IFIP International Federation for Information Processing,* 117-126.

Shen, X. X., & Tan, K. C. (1998). Customer satisfaction benchmarking in QFD: Avoiding PIT FALLS. *Proceedings of the 2nd International and 5th National Research Conference on Quality Management*. Monash University: Victoria, Australia, 196-203.

Shih, H. S., & Chen, S. H. (2013). A conceptual design of a mobile healthcare device-an application of three-stage QFD with ANP and TRIZ. *International Journal of Operations Research, 10(*2), 80-91.

Silva, I. B., Batalha, G. F., Stipkovik, M., Filho, F. Z., Ceccarelli, J. B., Anjos, & Fesz, M. (2009). Integrated product and process system with continuous improvement in the auto parts industry. *Journal of Achievements in Material and Manufacturing Engineering, 34(*2), 204-210.

Sojung, K., & Byungun, Y. (2012). Developing a process of concept generation for new product-service systems: A QFD and TRIZ-Based approach. J*ournal Service Business, 6*(3), 323-348.

Somadatta, B. K., Ramesh, R., L., & Vishwas, S. D. (2013). Integration of quality function deployment and value engineering in furniture manufacturing industry for improvement of computer work station. *International Journal of Basic and Advanced Research,* 124-132.

Stevenson, W. J. (2009). *Operations management*. New York: McGraw-Hill.

Su C. T., & Lin, C. S. (2008). A case study on the application of fuzzy QFD in TRIZ for service quality improvement. *International Journal of Quality Quantitative, 42*(5), 563-578.

Temponi, C., Yen, J., & Tiao, W. A. (1999). House of quality: A fuzzy logic-based requirements analysis. *European Journal Operation Research, 117*, 340-354.

Tomohiko, S. (2013). A QFD-centred design methodology for environmentally conscious product design. I*nternational Journal of Production Research, 45*(18-19), 4143-4162.

Tseng, C. C., Torng, C. C., & Lin, S. C. (2010). Prioritization of product design tasks using QFD, TRIZ and DSM. *Industrial Engineering and Engineering Management (IE&EM)*. pp. 871-875. IEEE 17Th International Conference on 2010, Oct. 29-31.

Ulrich, K. T., & Eppinger, S. D. (2008). *Product design and development* (4th ed.). New York: McGraw Hill.

Urban, G. L., & Hauser, J. R. (1993). *Design and marketing of new products* (2nd ed.). Englewood Cliffs NJ: Prentice-Hall.

Van de Poel, I. (2007). Methodological problems in QFD and directions for future development. *Research in Engineering Design, 18*(1), 21-36.

Van Pelt, A., & Hey, J. (2011). Using TRIZ and human-centered design for consumer product development. *Procedia Engineering, 9,* 688-693.

Vinodh, S., Kamala, V., & Jayakrishna, K. (2014). Integration of ECQFD, TRIZ, and AHP for innovative and sustainable product development. *Applied Mathematical Modelling, 38*(11), 2758-2770.

Vosniakos, G. C., Gogouvitis, X. V., & Stathatos, E. E. (2009). Coupling product and manufacturing system design. *International Journal of Collaborative Enterprise, 1*(1), 83-102.

Wang, H., Chen, G., Lin, Z., & Wang, H. (2005). Algorithm of integrating QFD and TRIZ for the innovative design process. *International Journal Computer Application Technology, 23*(1), 41-52.

YamaShina, H., Ito, T., & Kawada, H. (2002). Innovative product development process by integrating QFD with TRIZ. *Journal of the Japan Society for Precision Engineering, 66*(11), 1705-1710.

Yeh, C. H., Jay, C. Y., Huang, & Yu, C. K. (2011). Integration of four-phase QFD and TRIZ in product R&D: A notebook case study. *Research in Engineering Design, 22*(3), 125-141.

Zhou, M. (1998). Fuzzy logic and optimization models for implementing QFD. *Computer Industrial Engineering, 35*(1-2), 237-240.

Pertanika J. Sci. & Technol. 24 (1): 27 - 39 (2016)

PERTANIKA JOURNALS

SCIENCE & TECHNOLOGY

Journal homepage: http://www.pertanika.upm.edu.my/

Review Article

An Introductory Review of Simulation Methods for the Structure of Cementitious Material Hydrates at Different Length Scales

Tarighat, A.*, Zehtab, B. and Tavakoli, D.

Department of Civil Engineering, Shahid Rajaee Teacher Training University, Tehran, Iran

ABSTRACT

Concrete is a very complicated, random, multi-scale and multi-phase material. It is important to know cement paste structure to understand its properties and damage mechanisms that can influence the properties of concrete. Recently, many researchers have focused on the simulation of hydrated cement microstructure to figure out how damage/deterioration might be initiated. Moreover, as the microstructure of hydrated cement is known, we are able to produce greener, stronger and more durable concrete. There is a critical need to survey previous research to direct future study. In recent years due to development of advanced computers, most researchers tend to study the atomistic structure of hydrated cement and to make a bridge between nano and macro scales. Various models have been developed to simulate cement structure. This paper is an introductory review of the most important studies proposed by researchers for simulation of hydrated cement at different scales varying from nano to macro. Impact of the latest advances in simulation methods and their applications for hydrated cement research is investigated. Salient issues are categorised into four main sections including numerical models, microstructural models for cement hydration simulation, atomistic simulations and multi-scale studies.

Keywords: Atomistic simulation, cement, C-S-H, hydration, microstructure, multi-scale

INTRODUCTION

Simulations are useful when the conditions of interest are difficult to achieve in the laboratory. Concrete structure simulation is difficult due to its complex microstructure, which is still not completely understood. A lot of studies have been conducted for cement/concrete materials to know about their structures at different scales. The nature of concrete is random over a broad range of length scales, from nano to macro. Although each length scale presents a random composite, concrete in its engineering uses is considered as a uniform material at the macro scale. Therefore, it is highly necessary

Article history:
Received: 12 March 2015
Accepted: 22 June 2015

E-mail addresses:
tarighat@srttu.edu (Tarighat, A.),
b.zehtab@srttu.edu (Zehtab, B.),
d.tavakoli@srttu.edu (Tavakoli, D.)
*Corresponding author

ISSN: 0128-7680

to study concrete at each length scale to have a better insight into its structure and properties. To simulate multi-scale structures of concrete materials, various sciences including chemistry, materials, physics, strength of materials, heat transfer etc. are needed.

Simulating the hydrated cement microstructure makes it possible to predict different properties and damage/deterioration mechanisms of the hardened cement in relation to time. In this paper, the most major methods that are implemented to simulate hydrated cement microstructure at different nano to macro scales are introduced. In this paper, major methods are introduced and categorised into four methods including:

- numerical models,
- microstructural models for cement hydration simulation,
- atomistic simulations and
- multi-scale studies.

In following section, 'Numerical Models', three basic models used several times as references in later studies are introduced. These models are considered as first research in the field of concrete microstructure simulation. In section 'Microstructural Models for Cement Hydration Simulation', the discussion is provided under five sub-sections for better categorisation. In the sub-section, 'NIST models', there is a brief review of various models proposed by NIST researchers (National Institute of Standards and Technology, USA) that are related to cement microstructure. This sub-section also includes studies proposed by other researchers whose models are based on NIST models. The HYMOSTRUC (van Breugel, 1995a,b), IPKM (Navi & Pignat 1990), μic (Bishnoi, 2008) and De Schutter models (De Schutter & Taerwe, 1995) are introduced in separate sub-sections due to their great importance in the history of hydrated cement microstructure modelling. Colloidal models (CM-I and CM-II) proposed by Jennings (Jennings, 2000, 2008) are introduced in the last sub-section of section. Important concepts used in colloidal models have been used in the development of later models.

In section 'Atomistic Simulations', various research is introduced in three sub-sections depending on the method used for cement microstructure simulation at the atomistic scale. Molecular dynamics, molecular statics and the Monte Carlo method are the three main methods for evaluation of cement properties at the atomistic scale. Each method has specific applications for assessment of different types of cement paste property. Their applications are discussed in section and various research is introduced for each method. In section 'Multi-Scale Studies', research conducted simultaneously in different scales is surveyed. There are two different points of view for multi-scale modelling of cementitious materials: hierarchical and concurrent modelling. Introduction of these methods and their applications are scrutinized in section.

NUMERICAL MODELS

The first attempts to simulate concrete were conducted using the numerical methods. Numerical methods were used to model mechanical properties of concrete. Wittmann *et al*. (1984-85) proposed a method based on the morphological law suggested by Beddow and Meloy (1980), simulating two-dimensional random geometry of natural aggregates to generate realistic

composite structures. They predicted the elasticity modulus and the diffusion coefficient of 'numerical concrete', using the take-and-place algorithm and finite elements method. Using this generated structure the creep and shrinkage of porous composite materials was simulated.

A particle model for brittle aggregate composite materials (concretes, rocks or ceramics) was proposed by Bazant *et al*. (1999). They implemented the take-and-place algorithm for simulation of concrete structure to estimate the propagation of a crack and its location in concrete.

MICROSTRUCTURAL MODELS FOR CEMENT HYDRATION SIMULATION

NIST models

This section introduces important models proposed by NIST (National Institute of Standards and Technology, USA). Jennings and Johnson (1986) introduced a model to describe the hydration processes of C3S in three-dimensional space. In this model cement hydration was considered as nucleation and growth of spherical particles in 3D space. All spheres were shown by the coordinates of their radii and centres. Hydration was simulated as the decrement in the radii of the anhydrous phases and the concentric growth of Calcium Silicate Hydrates (C-S-H) layers on the surface of these particles. Calcium Hydroxide (CH) particles grew as new nuclei formed in the pore-space. Although this model could be used to incorporate some processes relating hydration to microstructural development, it could not be developed further due to limited computational power at the time of development.

Since the Jennings and Johnson model could not calculate mechanical properties of cement paste, NIST researchers, especially Edward J. Garboczi, tried to put the properties issue in context (Garboczi, 2013). Garboczi and Bentz *et al*. (1990) calculated concrete properties and developed a software called 'CEMHYD3D'. This model has two significant capabilities to develop starting 3D microstructures:

1. The embedment of particles of inert fillers, slag, CaCO3 etc. into the particle placement programme, and
2. Simplification of the chemical phase distribution process.

Other features of CEMHYD3D that enhance its capabilities are:

- Addition of the influences of limestone on hydration,
- Incorporation of elementary reactions for slag,
- Prediction of the concentration of the pore solution during hydration and its simultaneous effect on hydration rates,
- The capability to execute hydration under sealed or saturated conditions by specifying a number of cycles after which resaturation of the capillary porosity occurs,
- The ability to precipitate the C-S-H gel in either a random or a "plate" morphology, and
- The addition of a one-pixel dissolution bias that allows for the acceleration or retardation of the hydration rates of the smallest cement particles in the 3D microstructure (Bentz, 2005).

Although CEMHYD3D is still one of the most widely used and well known models in cement hydration, its disadvantage is that there is little kinetic information about the hydration process and requiring resolution, which inherently increases the computation cost of a relatively large volume cement paste (Tan, 2012).

A stochastic simulation model called HydratiCA has been developed for simulating temporal and spatial variations in aqueous mineral systems by Bullard at NIST. In this model nucleation, dissolution, solute transport and precipitation are governed by local probabilistic rules applied on a regular computational lattice. Moreover, the model can simulate ion diffusion in a dilute electrolyte. Consideration for the exponential temperature dependence of the reaction rate constants is shown to provide precise predictions of the effect of temperature on both the equilibrium and kinetics of reactions (Bullard, 2007a,b).

Bentz, Garboczi and Snyder (1999) developed a computer programme for simulating the microstructure of a 3D cubic volume of concrete called the 'HCSS Model' or three-dimensional Hard Core/Soft Shell microstructural model. Using HCSS, Interfacial Transition Zone (ITZ) regions are modelled by a soft gel that surrounds each particle located in a homogeneous matrix.

Recently, NIST researchers have integrated most of their programmes into the Virtual Cement and Concrete Testing Laboratory (VCCTL) that covers the micro to millimeter scales of concrete (Bullard 2011).

HYMOSTRUC model

This model was built by K. van Breugel (1995a,b). In this model, the cement hydration was simulated as a function of the particle size distribution and chemical composition of the cement, the water to cement ratio and the actual reaction temperature. This model was based on the assumption that reaction products were formed close to dissolving cement grains and the density of the reaction product (gel) in case of isothermal curing was constant throughout the hydration process. The model could simulate the development of properties of cement, such as proportional changes in particle size, compressive strength, embedded cement volume changes, porosity in the matrix aggregate ITZ, hydration rate and degree of hydration calculation.

In this model the evolution of hydrating product phases is less focused. This model does not do any calculation of interactions or overlaps between particles; therefore, the microstructural information is not considered in the simulations. Furthermore, the neighbourhood of particles is not considered for the calculation of reaction rates, and localised information at the level of particles, which is extremely important for microstructural properties such as pore connectivity, is lost. Another major criticism of this model is that nucleation of products in the pore-space is not accounted for. Since this model treats the entire microstructure in only a statistical fashion, localised information is lost and cannot be used for further analysis (Bishnoi, 2008).

This model was later modified to account for random parking of particles (Koenders & van Breugel, 1997). In this extended version of the model, the pore-structure constant was determined by analysis of two-dimensional slices from the simulations. The model was extended for calculating autogenous shrinkage of hardening cement paste based on the pore structure using a combination of various empirical equations using pore-parameters calculated from the model (Bishnoi, 2008). Another pixel-based method to analyse pores was later added to the model (Ye *et al*., 2003).

Based on the HYMOSTRUC model, Liu Xian *et al*. made an improvement to take account of the addition of limestone to cement as no-expanding particles and an inert filler without taking part in the hydration process (Tan, 2012).

IPKM Model

The integrated particle kinetics model (IPKM) was developed at EPFL by Navi and Pignat (1990). IPKM simulates 3D model of the evolution of C-S-H microstructure during hydration using the vector approach similar to that used by Jennings and Johnson earlier. This model clearly takes into account the influence of inter-particle contacts and the accessibility of water in pores on the rate of hydration and on microstructure formation.

Unlike the HYMOSTRUC model, it simulates the hydration of every individual particle using kinetics laws that depend not only on the size of the particle, but also on the neighbourhood of each particle. This model also supports the growth and nucleation of new nuclei in the pore space (Bishnoi, 2009). Due to the explicit calculation of all possible interactions, the simulations using IPKM are slow, which leads to the simulations only within relatively small numbers of particles (Tan, 2012).

μic

Like IPKM, a computer programme for modelling the hydration of cements named 'μic' (pronounce Mike) was developed, which preserves the multi-scale nature of the cement microstructure. Support libraries built into the framework enable fast simulation of systems containing millions of particles, allowing every single particle in a system to be modelled and all the interactions to be calculated. It was found that it is possible to explain the hydration kinetics during the first day using a nucleation and growth mechanism when a loosely packed C-S-H with a lower bulk density is assumed to form (Bishnoi, 2008, 2009).

De Schutter Model

G. De Schutter proposed a kinetic hydration model, which carries out adiabatic hydration tests on concrete. It was developed based on the adiabatic and isothermal hydration tests and it is valid both for Portland cement and blast furnace slag cement. This hydration model enables the calculation of the heat production rate as a function of the actual temperature and the degree of hydration. However, the interactions between the cement hydration and the reaction of mineral admixtures are not considered in the model (De Schutter & Taerwe, 1995).

Colloidal Models: CM-I and CM-II

CM-I was introduced by Jennings for the structure of C-S-H as it is formed during the hydration of cement. In this model, the basic building block is a unit of C-S-H that is roughly spherical and flocculates to form larger units. This model describes the structure of the basic units and how they pack to form larger structures and microstructures. CM-I provides a method of the predicting nitrogen accessible gel porosity, density and associated surface area of C-S-H in

cement pastes. The basis for the model is that C-S-H forms as one of two types of cement, high- or low-density C-S-H. (Tennis & Jennings, 2000; Jennings, 2000).

A second-generation model for the C-S-H nanostructure based on the explanation of water absorption isotherms is CM-II. The cornerstone of the model is a description of the globules as small brick-like particles, which consist of solid C-S-H and internal water, and the distribution of water in the small pores between them. Using this model, the properties of C-S-H gel could be estimated; this helps to establish quantitative relationships between the nanostructure and bulk properties (Jennings, 2008).

ATOMISTIC SIMULATIONS

In atomistic simulations, one has essentially infinite control over the specific configuration and geometry of the material. Simulations provide an easier and straighter way to study atomic mechanisms in spite of the advance in resolution of length and time scales in experiments. Observing individual atoms still remains by definition a trivial task in atomistic simulations.

The use of atomistic simulations for cementitious materials is a new field. It is worth noting that molecular modelling studies recently have focused primarily on the structural properties of the cementitious phases rather than the inherent kinetic aspects of cement hydration. However, the precise structural information gained from these atomistic modelling studies may serve as valuable input for the kinetic models (Subramani, 2008).

Two main procedures are used to sample the energy surface and search for the equilibrium configuration of atoms or molecules. Monte Carlo (MC) simulations generate configurations of a system by making 'smart' random movements of the atoms, while Molecular Dynamic (MD) simulations follow the physical time evolution of system by integrating Newton's laws of motion (Selvam *et al*., 2009).

Molecular Dynamics

Molecular dynamics (MD) is a strong simulation technique for studying the chemical and physical properties of solids, liquids, biological molecules and amorphous materials.

Molecular dynamics is used for a better understanding of chemical and physical interaction between atoms and to gain basic properties in the atomistic level. It is good to calculate the time-dependant quantities. In this method the interaction between atoms are approximated and related through empirical interatomic potentials. This approximation provides means to study several nano phenomena using millions of atoms. The interaction between the atoms is governed by Newtonian dynamics. From the time evolution of the atoms and their interactions at specific temperatures, the thermodynamical and mechanical properties and stress-strain relationship can be derived (Gopalakirishan *et al*., 2011).

Manzano *et al*. (2007) performed energy minimisation studies to calculate the key mechanical properties of cement based materials using different crystalline hydro silicates of calcium models. They concluded that the shear (G), bulk (K) and Young's Modulus (E) decreased slightly when calcium to silica ratio of C-S-H increased and when more water molecules entered the composition of C-S-H. In addition, their calculations showed that the mechanical properties of C-S-H structures with dimer or pentamer silicate chains were lower

than the mechanical properties for C-S-H with infinite silicate chains. Subramani (2008) has shown that weak bonds in the Tobermerite structures can be broken to C-S-H blocks by molecular dynamics. The attack of magnesium salt on cement hydrates microstructure using Hamid's (1981) Tobermorite 11 A° crystal structure was also investigated. Murray *et al*. (2010) calculated the stress strain of C-S-H structures by using the molecular dynamics method. Murray *et al*. (2010) and Selvam *et al*. (2009) computed the relationship between stress and strain in C-S-H through the basic block of the C-S-H structure that proposed by Subramani *et al*. (2009). Murray *et al*. (2010) computed the mentioned relationship at nano scale.

Simulation of the structure of C-S-H by MD was investigated by Faucon *et al*. (1996). They studied C-S-H structures with Ca/Si ratios between 0.66 and 0.83. They identified structural instability in the mechanisms causing breaks in the Si-O chains. Dolado *et al*. (2007) studied the formation and the structure of C-S-H by means of molecular dynamics simulation of the polymerisation of Si(OH)2 in the presence of solvated Ca(OH)2,4H2O.

Shahsavari *et al*. (2011) introduced an empirical force field for complex C-S-H layered materials named CSH-FF that was a re-parameterised version of Clay-FF for prediction of C-S-H properties more efficiently and less computationally intensive. Qomi *et al*. (2014) used this force field to optimise the properties of cement hydrates.

Al-Ostaz *et al*. (2010) and Hajilar and Shafei (2015) predicted the mechanical properties of major constituents of cement-based materials using MD. Introducing the COMPASS force field, they investigated the effects of the force field and super-cell size. The results showed that the MD method was capable of providing a good prediction of the mechanical properties of the cement paste.

Molecular Statics

This method uses traditional classical mechanics to model molecular systems. Classical mechanics is used to describe the motion of macroscopic objects according to Newton's second law. In molecular static (MS) modelling, energy minimisations are performed on the atomic structure as explained in Leach (2001). This minimisation will yield an equilibrium structure based on the closest local minima of the initial atomic structure. However, the optimised structure thus obtained may characterise one possible equilibrium or stable structure of the many that could exist. The bulk properties of material like electrical properties, vibrational properties and mechanical properties depend on the curvature of the energy surface.

Subramani *et al*. (2008) showed that molecular statics could be used to determine the energy potential of the crystalline C-S-H structures. They used the computed energy potential to determine key mechanical properties such as Poisson's ratio and Young's modulus of the crystalline C-S-H structure.

GULP code (Gale & Rohl, 2003) was used by many researchers to calculate mechanical properties of C-S-H amorphous structure (Manzanao *et al*., 2007a, Subramani *et al*., 2009) or C-S-H related crystal structure (Gmira *et al*., 2004). This method was also used by Subramani *et al*. (2009) and Manzano *et al*. (2007) to find the possible amorphous atomic structure of C-S-H (Gopalakirishan *et al*., 2011).

Monte Carlo Method

The Monte Carlo (MC) method is a technique to sample the infinite number of available configurations of a material (Binder & Heermann, 2002). In principle, the MD method is one route to obtain such a sample, but there are cases where the MD method is not sufficiently efficient, particularly when sampling configurations that can only evolve dynamically at an extremely slow rate. The Monte Carlo (MC) method is used to model the physical phenomena through probabilities (Leach, 2001). This method does not have time evolution and thus, it is the application of nano science modelling to understand the atomic structure of C-S-H much faster than molecular dynamics. The method is also applied to study film-growth type problems and is called MC for non-equilibrium systems. Similar to MD, this method can also be used to calculate thermodynamical properties. The method can skip high barriers with several local minima faster than MD (Gopalakirishan *et al*., 2011).

A group of researchers (Pellenq *et al*., 1997; Delville & Pellenq, 2000), assuming that C–S–H gel had a layered structure, used atomistic Monte Carlo simulations to gain insight into the electrostatic attraction force between layers.

Gilmer (1976, 1977) used this method successfully to study crystal growth in the 1970s and during the following decade Lasaga and co-workers applied the Monte Carlo method to the study of crystal dissolution (e.g. Wehrli, 1989).

MULTI-SCALE STUDIES

Concrete research topics include complex failure processes. These phenomena are scaled in a bottom-up manner from atomic to continuum scales. Thus, to fully represent cement concrete behaviours, a single-scale modelling method is not suitable as it is difficult to address cross-scale complex behaviour from material scale to structural scale. To look at a problem simultaneously from several different scales and levels of detail is a more mature way of doing modelling (Lu, 2011).

There are two different points of view for multi-scale modelling of cementitious materials: hierarchical modeling (Maekawa *et al*., 1999, Raabe, 2009, Jennings & Bullard, 2011, Sindu *et. al*, 2014) and concurrent modelling (Li *et. al*, 2009a,b, Lloberas-Valls *et al*., 2012 , Ghosh & Chaudhuri, 2013,). In hierarchical methods, results from the lower scale are transmitted to a higher scale, after which single-scale calculations are performed to gain macro scale results (Lu, 2011). Concurrent simulation implements increased resolution of the material scale at certain areas of interest (Lloberas-Valls *et al*., 2012). For instance, the constituents of concrete must be modelled around the fracture process zone while a macroscopic description is used elsewhere. In this method, the whole fine scale region is considered in the computation as opposed to hierarchical methods where the behaviour of a reduced fine scale area is representative for the one at a larger scale (Ghosh & Chaudhuri, 2013).

Hierarchical simulation methods proceed from the smallest scales to the continuum scale. Therefore it named the 'bottom-up' approach (Jennings & Bullard, 2011). In this method, bridging between scales can be done using various methods (Raabe *et al*., 2009).

Maekawa *et al*. (1999) proposed an integrated programme named DUCOM (DUrability COncrete Model), which is a Finite-Element based computational programme to evaluate

various durability properties of concrete. It traces the development of concrete hardening, structure formation and several associated phenomena from casting of concrete to a period of several months or even years. This model can be used to study the effect of ingredient materials and environmental conditions as well as the size and shape of structure on the durability of concrete (Maekawa *et al*., 1999, 2003). However, the DUCOM model did not consider in detail the chemical aspects of the hydration of binary cements.

Recently, a virtual lab called the 'DelftCode', a multi-scale modelling lab, was developed with the aim to line up the models that have been developed for their particular scale-level and to make the results compatible and interchangeable within the modelling framework. The result is a multi-scale simulation tool that covers 10 orders of magnitude and allows including various scale effects to be involved in the calculations. The tool can be used not only for design but also for repair assessments of concrete structures (Koenders *et. al*, 2008, 2012).

FUTURE POSSIBLE RESEARCH

Although good advances have been achieved so far, there are remaining gaps in the simulation results. Some probable studies that might be done to fill these gaps include: realistic quantum mechanical models of clinker phases, effects of impurities on the surfaces of particles, similar studies on the aluminate and ferrite phases, quantification modelling of clinker fracture across multiple levels, studying creep at the mesoscale, finding reasonable relationships between nano, meso and macroscale physical and mechanical properties, evaluation of reversible shrinkage, fracture at the mesoscale, modelling porosity in atomistic scale and determination of the role of water within C-S-H gel nanoparticles (Ulm *et al*., 2014).

Many open questions exist in the mind of researchers that may not be mentioned above. But we can certainly say that all of the future studies would complete the puzzle of cement structure information and more realistic models would be proposed to realise desired economic, environmental and structural needs.

CONCLUSION

This paper is an introductory review of some methods of simulation of cement hydration products. Most of the major methods implemented for simulation of the cement hydration microstructure at various scales from atomistic to macro scales were introduced. Recent studies have shown great potential for improving hydration simulations by providing information on processes occurring at atomic or nanometer length scales. These models will help us to have a better understanding of the behaviour of cement hydration microstructure and will provide more insight into modifying the properties of hardened cement paste at the nano to macro levels.

REFERENCES

Al-Ostaz, A., Wu, W., Cheng, A. H. -D., & Song, C. R. (2010). A molecular dynamics and microporomechanics study on the mechanical properties of major constituents of hydrated cement. *Composites: Part B* 41, 543-549.

Bazant, Z. P., Tabbara, M. R., Kazemi, M. T., & Pijaudier-Cabot, G. (1990). Random particle model for fracture of aggregate or fiber composites. *Journal of Engineering Mechanics, 116*(8), 1686-1705.

Beddow, J. K., & Meloy, T. P. (1980). *Advanced particulate technology.* Boca Raton: CRC.

Bentz, D. P. (2005). CEMHYD3D: *A three-dimensional cement hydration and microstructure development modeling package, version 3.0.* Materials and Construction Research Division National Institute of Standards and Technology Gaithersburg, Maryland, USA.

Bentz, D. P., Garboczi, E. J., & Snyder K. A. (1999). *A hard core/soft shell microstructural model for studying percolation and transport in three-dimensional composite media*. Materials and Construction Research Division National Institute of Standards and Technology Gaithersburg, Maryland, USA.

Binder, K., & Heermann, D. W. (2002). *Monte Carlo simulation in statistical physics,* (4th Ed.). Springer.

Bishnoi, S. (2008). *Vector modelling of hydrating cement microstructure and kinetics.* (Doctoral dissertation). EPFL University, Switzerland.

Bishnoi, S. (2009). Studying nucleation and growth kinetics of alite hydration using μic. *Cement and Concrete Research, 39*(10), 849-860.

Bullard, J. W. (2007a). Approximate rate constants for nonideal diffusion and their application in a stochastic model. *The Journal of Physical Chemistry A, 111*(11), 2084-2092.

Bullard, J. W. (2007b). A three-dimensional microstructural model of reactions and transport in aqueous mineral systems. *Modelling and Simulation in Materials Science and Engineering, 15*(7), 711-738.

Bullard J. W. (2011). *Virtual cement and concrete testing laboratory (VCCTL) user guide.* Materials and Construction Research Division National Institute of Standards and Technology Gaithersburg, Maryland, USA.

De Schutter, G., & Taerwe, L. (1995). General hydration model for portland cement and blast furnace slag cement. *Cement and Concrete Research, 25*(3), 593-604.

Delville, A., & Pellenq, R. J. M. (2000). Electrostatic attraction and/or repulsion between charged colloids: a (NVT) Monte-Carlo study. *Molecular Simulation, 24*, 1-24.

Dolado, J. S., Griebel, M., & Hamaekers, J. (2007). A molecular dynamic study of cementitious calcium silicate hydrate (C-S-H) gel. *Journal of the American Ceramic Society, 90,* 3938-3942.

Faucon, P., Delaye, J. M., & Virlet, J. (1996). Molecular dynamics simulation of the structure of calcium hydrates. *Journal of Solid State Chemistry, 127,* 92-97.

Gale, J. D., & Rohl, A .L. (2003). The general utility lattice program. *Molecular Simulation. 29*(5), 291-341.

Garboczi, E. J. (2013). The computational materials science of concrete: Past, present and future. *American Ceramic Society Bulletin, 92*(4), 40-45.

Ghosh, A., & Chaudhuri, P. (2013). Computational modeling of fracture in concrete using a meshfree meso-macro-multi-scale method. *Computational Materials Science, 69*, 204-215.

Gilmer, G. H. (1976). Growth on imperfect crystal faces: I. Monte-Carlo growth rates. *Journal of Crystal Growth, 36(*1), 15-28.

Gilmer, G. H. (1977). Computer simulations of crystal growth. *Journal of Crystal Growth, 42*, 3-10.

Gmira, A., Zabat, M., Pellenq, R. J. -M., & Van Damme, H. (2004). Microscopic physical basis of the prochemical behavior of cement-based materials. *Materials and structures/Concrete Science and Engineering, 37*, 3–14.

Gopalakerishnan, K, Birgisson, B, Taylor, P., & Attoh-Okine, N. (2011). *Nanotechnology in Civil Infrastructure*. Berlin & Heidelberg: Springer.

Hajilar, S., & Shafei, B. (2015). Nano-scale investigation of elastic properties of hydrated cement paste constituents using molecular dynamics simulations. *Computational Materials Science, 101*, 216-226.

Hamid, S. A. (1981). The crystal structure of the 11 Ä natural tobermorite Ca2. 25 [Si3O7. 5 (OH) 1.5]· 1H2O. *Zeitschrift für Kristallographie-Crystalline Materials, 154*(1-4), 189-198.

Janakiram Subramani, V. (2008). *Potential applications of nanotechnology for improved performance of cement based materials.* (MSCE Thesis). BELL 4190, Department of Civil Engineering, University of Arkansas.

Janakiram Subramani, V., Murray, S., Selvam, R. P., & Hall, K. (2009). Atomic structure of calcium silicate hydrate (C-S-H) using molecular mechanics. In *Proceedings TRB 88th Annual Meeting*, January 11-15, paper no: 09-0200.

Jennings, H. M. (2000). A model for the microstructure of calcium silicate hydrate in cement paste. *Cement and Concrete Research, 30,* 101-116.

Jennings, H. M. (2008). Refinements to colloid model of C-S-H in cement: CM-II. *Cement and Concrete Research, 38*(3), 275-289.

Jennings, H. M., & Bullard, J. W. (2011). From electrons to infrastructure: Engineering concrete from the bottom up. *Cement and Concrete Research, 41*(7), 727-735.

Jennings, H. M., & Johnson, S. K. (1986). Simulation of Microstructure Development during the hydration of a cement compound. *Journal of American ceramic society, 69*(11), 790-795.

Koenders, E. A. B., Dado, E., & Carvalho, D. B. F., (2012). A virtual lab for multi-scale modeling of cementitious materials, concrete repair, rehabilitation and retrofitting III. Alexander *et al*. (Eds.). London: Taylor & Francis Group.

Koenders, E. A. B., Schlangen, E., & van Breugel, K. (2008). *Multi-scale modeling: The Delft Code. International RILEM symposium on concrete modeling*. CONMOD'08, 2008, May 26-28. Delft, the Netherlands.

Koenders, E. A. B., & van Breugel, K. (1997). Numerical modeling of autogenous shrinkage of hardening cement paste. *Cement and Concrete Research, 27*(10), 1489-1499.

Leach, A. R. (2001). *Molecular modeling: Principles and applications* (2nd ed.). Harlow: Pearson Education.

Li, Z. X., Chan, T. H. T., Yu, Y., & Sun, Z. H. (2009). Concurrent multi-scale modeling of civil infrastructures for analyses on structural deterioration-Part I: Modeling methodology and strategy. *Finite Elements in Analysis and Design, 45*(11), 782-794.

Li, Z. X., Chan, T. H. T., Yu, Y., & Sun, Z. H. (2009). Concurrent multi-scale modeling of civil infrastructures for analyses on structural deterioration-Part II: Model updating and verification. *Finite Elements in Analysis and Design, 45*(11), 795-805.

Lloberas-Valls, O., Everdij, F., Rixen, D., Simone, A., & Sluys, B. (2012). Concurrent multi-scale analysis of heterogeneous materials. *European Congress on Computational Methods in Applied Sciences and Engineering* (ECCOMAS 2012), Vienna, Austria, 2012, September 10-14.

Lu, Y. (2011). Multiscale/Multiphysics Modeling of Concrete Structures. *Journal of Civil and Environmental Engineering, 1*, e102.

Maekawa, K., Chaube, R. P., & Kishi, T. (1999). *Modelling of concrete performance,* London: E&FN SPON.

Maekawa, K., Ishida, T., & Kishi, T. (2003). Multi-scale modeling of concrete performance integrated material and structural mechanics. *Journal of Advanced Concrete Technology, 1*(2), 91-126.

Manzano, H., Dolado, J. S., Guerrero, A., & Ayuela, A. (2007). Mechanical properties of crystalline calcium-silicate-hydrates: comparison with cementitious C-S-H gels. *Physica Status Solidi (a), 204*(6), 1775-1780.

Murray, S. J., Jankiram Subramani, V., Selvam, R. P., & Hall, K. D. (2010). Molecular dynamics to understand the mechanical behavior of cement paste. *Transportation Research Record, 2142*, 75-82.

Navi, P., & Pignat, C. (1996). Simulation of cement hydration and the connectivity of the capillary pore space. *Advanced Cement Based Materials, 4*(2), 58-67.

Pellenq, R. M., Caillol, J. M., & Delville, A. (1997). Electrostatic attraction between two charged surfaces: A (N, V, T) Monte Carlo simulation. *The Journal of Physical Chemistry B, 101*(42), 8584-8594.

Qomi, M. A., Krakowiak, K. J., Bauchy, M., Stewart, K. L., Shahsavari, R., Jagannathan, D., & Van Vliet, K. J. (2014). Combinatorial molecular optimization of cement hydrates. *Nature communications, 5.*

Raabe, D., Scheffler, M., Kremer, K., Thiel, W., Neugebauer, J., & Jansen, M. (2009). *Multi-scale modeling in materials science and engineering*. Retrieved from http://www.scribd.com/doc/191094179/Multi-Scale-Modeling-in-Materials-Science-and-Engineering#scribd

Selvam, R. P., Murray, S. J., Jankiram Subramani, V., & Hall, K. D. (2009). *Potential application of nanotechnology on cement based materials*. Report: Mack Blackwell Transportation Center, University of Arkansas, MBTC DOT 2095/3004.

Shahsavari, R., Pellenq, R. J. M., & Ulm, F. J. (2011). Empirical force fields for complex hydrated calcio-silicate layered materials. *Physical Chemistry Chemical Physics, 13(*3), 1002-1011.

Sindu, B. S., Sasmal, S., & Gopinath, S. (2014). A multi-scale approach for evaluating the mechanical characteristics of carbon nanotube incorporated cementitious composites. *Construction and Building Materials, 50*, 317-327.

Tan, Zh. (2012). Review of several existing models simulating the hydration of cementitious materials. *Cement Science*.

Tennis, P. D., & Jennings, H. M. (2000). A model for two types of calcium silicate hydrate in the microstructure of Portland cement pastes. *Cement and Concrete Research, 30(*6), 855-863.

Ulm, F. J., Pellenq, R., Yip, S., Bazant, M., Grossman, Yildiz, B. (2014). *Concrete science platform phase I, summary white paper.* MIT concrete sustainability hub, USA. Retrieved from http://www.rmc-foundation.org/images/MIT%20CSH%20MTLS/CSP-summary-whitepaper-Nov2014.pdf

Van Breugel, K. (1995a). Numerical simulation of hydration and microstructural development in hardening cement-based materials (I) Theory. *Cement and Concrete Research, 25*(2), 319-331.

Van Breugel, K. (1995b). Numerical simulation of hydration and microstructural development in hardening cement-based materials (II) Application. *Cement and Concrete Research, 25*(3), 522-530.

Wehrli, B. (1989). Monte Carlo simulations of surface morphologies during mineral dissolution. *Journal of Colloid and Interface Science, 132*(1), 230-242.

Wittman, F. H., Roelfstra, P. E., & Sadouki, H. (1984-1985). Simulation and analysis of composite structures. *Materials Science and Engineering, 68,* 239-248.

Ye, G., van Breugel, K., & Fraaji, A. L. A. (2003). Three-dimensional microstructure analysis of numerically simulated cementitious materials. *Cement and Concrete Research, 33*(2), 215-222.

Pertanika J. Sci. & Technol. 24 (1): 41 - 52 (2016)

PERTANIKA JOURNALS

SCIENCE & TECHNOLOGY

Journal homepage: http://www.pertanika.upm.edu.my/

Review Article

Potential of 3'-Fluoro-3' Deoxythymidine as a Cellular Proliferation Marker in PET Oncology Examination

Hishar, H.[1*], R. Price[2], Fathinul Fikri, A. S.[1], Eddie Lau, W. F.[3], Assunta, C.[4] and A. J. Nordin[1]

[1]*Centre for Diagnostic Nuclear Imaging, Universiti Putra Malaysia, 43400 Serdang, Selangor, Malaysia*

[2]*Department of Medical Technology & Physics and RAPID PET Technologies, Sir Charles Gairdner Hospital, Western Australia, Australia*

[3]*Centre for Cancer Imaging, Molecular Imaging and Targeted Therapeutics Laboratory the Peter MacCallum Cancer Centre, 12 St. Andrew's Place, East Melbourne, Australia*

[4]*Department of Nuclear Medicine and PET Centre, San Raffaele Hospital, Milan, Italy*

ABSTRACT

Development of the positron emission tomography (PET) diagnostic radiopharmaceutical (^{18}F) fluoro-2-deoxy-D-glucose (^{18}F-FDG) subsequently facilitated the discovery and clinical evaluation of several new tracers as imaging markers for cancer. While ^{18}F-FDG is a widely employed marker for enhanced intracellular glycolysis and metabolic function, one of the newer tracers, (^{18}F)-3'-fluoro-3' deoxythymidine (^{18}F-FLT), has been developed as a biomarker for cell proliferation. In this review, the potential of ^{18}F-FLT as a biomarker for cancer imaging is discussed.

Keywords: ^{18}F-FLT, ^{18}F-FDG, Positron Emission Tomography (PET), cellular proliferation

INTRODUCTION

Positron emission tomography (PET) is a rapidly developing imaging tool, with a clinical role that exceeds 15 years (Fathinul *et al*., 2013). It is a quantitative imaging technique that produces cross-sectional images that are composites of volume elements (NIH, 2006). The signal intensity for images especially in PET, corresponds to the concentration of radionuclide within the target tissue volume. PET is applied mainly in the clinical areas of cardiology, neurology and oncology, with the latter accounting for about 90% of all PET.

Article history:
Received: 12 March 2015
Accepted: 2 June 2015

E-mail addresses:
hishar.hassan@gmail.com (Hishar, H.),
roger.price@uwa.edu.au (R. Price),
ahmadsaadff@gmail.com (Fathinul Fikri, A. S.),
Eddie.Lau@petermac.org (Eddie Lau, W. F.),
assunta.carpinelli@ibfm.cnr.it (Assunta, C.),
drimaging@yahoo.com (A. J. Nordin)
*Corresponding author

ISSN: 0128-7680

The glucose derivative, (^{18}F) fluorodeoxy glucose (^{18}F-FDG), is the ubiquitous PET marker. However, there are numerous other tracers under development and with proven capability in highlighting a broad range of tissue metabolic functions. In a large meta-analysis, PET technique was found to change patients' management to almost 30% (Gambhir *et al*., 2001). Though ^{18}F-FDG is now widely used as a frontier in management of cancer patients, numerous studies have suggested that this marker is not universally selective for tumour imaging. This is because ^{18}F-FDG is a glucose analogue and it is utilised by many cell types, which limits its specificity (Shields *et al*., 1998; Yun *et al*., 2003).

To overcome this limitation, radioisotope-labelled thymidine derivatives have been developed to image cellular proliferation by PET. Radioisotope-labelled thymidine has a long history. Pyrimidine nucleoside was first labelled with radioisotope in 1969 by Langen and his collaborators. In their study, they described the radio-labelled form of pyrimidine nucleoside as a selective inhibitor of DNA synthesis. However, only in 1991, was fluorothymidine (FLT) labelled with ^{18}F successfully introduced as carrier-added ^{18}F-FLT (Wilson *et al*., 1991). Wilson and his collaborators monitored the efficacy of 3'-fluoro-3'-deoxy-thymidine (FDT) in HIV treatment. FDT is a fluorinated analogue of 3'-azido-thymidine (AZT), which was also found to be active against the HIV. However, FDT is more toxic than AZT (Wilson *et al*., 1991). Wilson and his collaborators successfully labelled the 3'-fluoro-3'-deoxy-thymidine (FDT) with the ^{18}F to monitor the drug's distribution and targeting in the body (Grierson *et al*., 1997).

Development of the FLT marker was subsequently continued by Grierson *et al*. in 1997 and it successfully introduced no-carrier-added ^{18}F-FLT. The next year, ^{18}F-FLT was first applied in imaging. The study was carried out to investigate animals and non-small cell lung cancer (NSCLC) patients (Shields *et al*., 1998). From that study, it was found that ^{18}F-FLT was specifically taken up by tissues that actively proliferate, including bone marrow (Barthel *et al*., 2003). Although ^{18}F-FLT appears to be a most promising marker, the major hurdle for its routine use is its low radiochemical yield during production. Nevertheless, it provides greater advantages to the clinicians in management of cancer patients.

THE BASIS OF ^{18}F-FLT AS A PROLIFERATION MARKER

The ^{18}F-FLT marker is administered to the patient by intravenous injection. It is taken up in the cell via both passive diffusion and also by Na+-dependent carriers. The ^{18}F-FLT marker, which is trapped in the cell, will undergo the phosphorylation process by thymidine kinase (TK1) and be converted into ^{18}F-FLT-monophosphate (Been *et al*., 2004). Intracellular trapping and accumulation of ^{18}F makes it possible to be detected by PET camera, which in turn gives a measure of the TK1 activity.

In the physiological pathway, both thymidine and ^{18}F-FLT encounter the same initial fate (Fig.1). Both of them will be phosphorylated by TK1 for DNA synthesis. However, for the ^{18}F-FLT marker, the DNA replication is inhibited due to the lack of the hydroxyl (-OH) group attached at the carbon number 3'-position on the sugar ring. Hence, the ^{18}F-FLT marker will be trapped inside the proliferating cells, and its radioactive signature will continue to accumulate there.

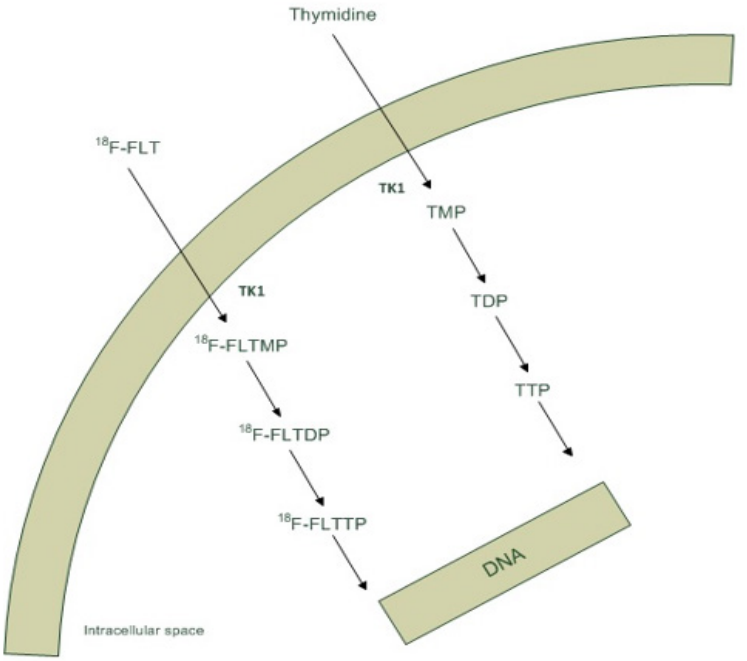

Fig.1: Uptake mechanism of thymidine and ^{18}F-FLT.

The uptake of ^{18}F-FLT by cells is correlated with TK1 activity (Barthel *et al*., 2003; Chen *et al*., 2005). TK1 activity in proliferating cells is noted to be 3 to 4 times higher in malignant cells compared to benign cells (Been *et al*., 2004). The enzymatic activity of TK1 reaches maximum level in the late G1 phase and S phase of the cell proliferative cycle. Therefore, monitoring of TK1 activity should give an early indication as to whether a cell population is in proliferative malignant state, or in benign state.

POTENTIALS OF ^{18}F-FLT IN ONCOLOGY

^{18}F-FDG marker is known for its relative non-specificity. Hence, there are many active inflammatory diseases and some aggressive benign tumours that inevitably give high ^{18}F-FDG uptake in cells. Furthermore, some disease processes healed by fibrosis leave a significant residual mass, thereby limiting categorisation of a complete response to ^{18}F-FDG.

In comparison, the FLT marker has the ability to demonstrate an increased rate of cellular proliferation and is potentially helpful in the setting of therapeutic monitoring as it has less affinity to inflammatory conditions. ^{18}F-FLT is potentially a more specific marker than ^{18}F-FDG with a high positive predictive value for malignancy. ^{18}F-FLT marker is also potentially useful in the evaluation of cerebral malignancy due to the lack of background cerebral uptake, unlike the high cerebral activity normally seen in ^{18}F-FDG.

In addition, there is good evidence that ^{18}F-FLT uptake is closely correlated with cellular proliferation with correlation between the intensity of uptake in lung cancer as measured by SUV with proliferation indices such as Ki-67 staining in a resected specimen (Hofman *et al*.,

2012). The ability of ^{18}F-FLT to identify tissue with a high proliferative rate has potential applications in the assessment of haemopoietic tissue and high grade disease transformation in haematological malignancy. The assessment of bone marrow reserve is important in considering patients for chemotherapy or radionuclide therapy, which is potentially myelotoxic. ^{18}F-FLT has the ability to document the extent and distribution of haemopoietic tissue, including the presence of extramedullary haemopoiesis, which can guide subsequent treatment choice. There are occasions when bone marrow sampling does not provide a representative picture of the true haemopoietic status due to sampling error and heterogeneous distribution of haemopoietic tissue (Fig.2).

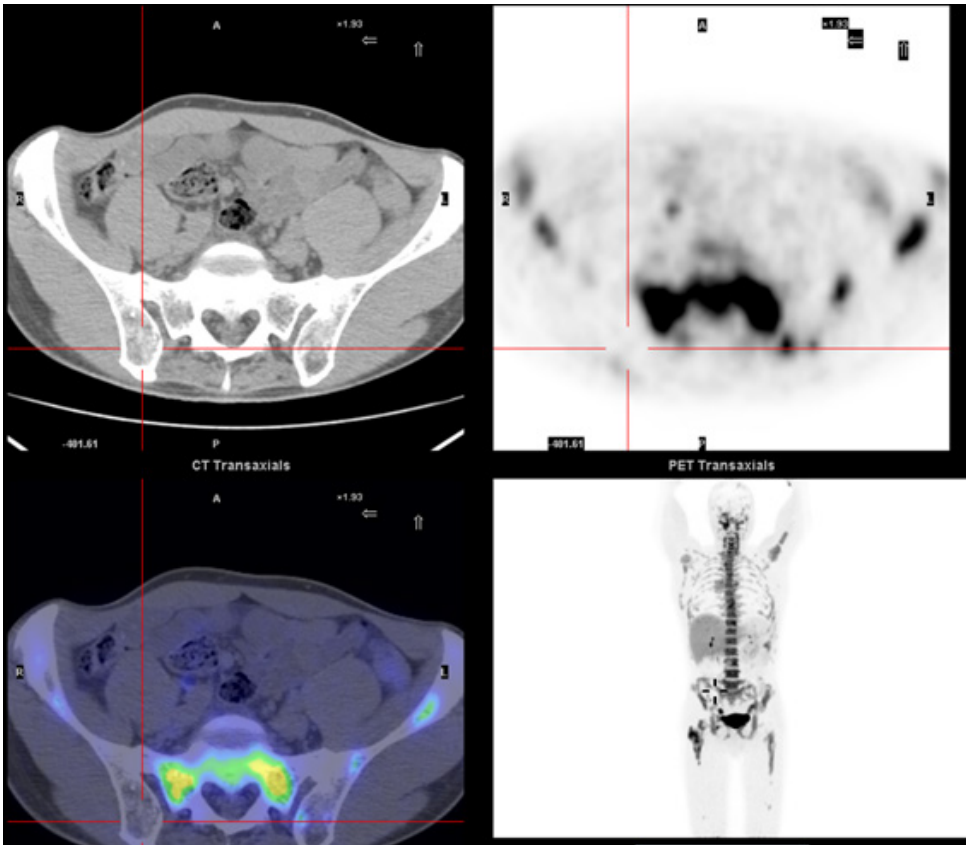

Fig.2: A 55-year-old man with stage IV diffuse large B cell lymphoma with nodal and multifocal bony disease and the pre-treatment bone marrow biopsy from the right posterior ilium showing hypocellular marrow and aplasia, in the presence of normal peripheral blood counts. 18F-FLT PET/CT was performed, which demonstrated absence of proliferative tissue in the right posterior ilium but fairly normal distribution of hyperproliferative bone marrow elsewhere with no evidence of extramedullary haemopoiesis in the spleen or elsewhere. The 18F-FLT PET/CT findings suggested that the initial bone marrow biopsy result was non-representative of his true bone marrow status and the patient went on to undergo systemic chemotherapy treatment without any myelotoxicity problem (Image courtesy of The Peter Mac Callum Centre).

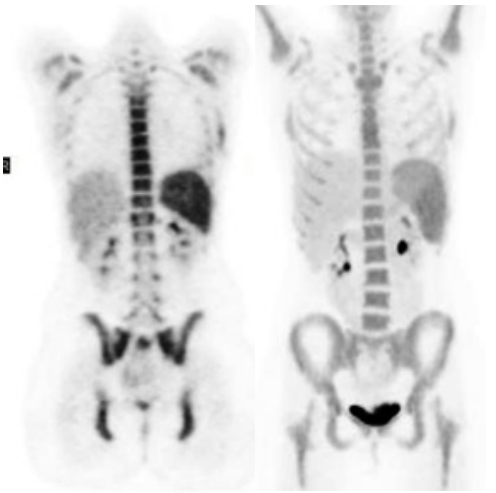

Fig.3: Coronal MIP-PET images using ^{18}F-FLT in the assessment of skeletal sarcoma before (left) and after treatment (right). The images show an increased ^{18}F-FLT intensity in the left lateral chest wall (marked), which appears less proliferative after treatment (right). (Image courtesy of The Peter Mac Callum Centre).

DIAGNOSIS EVALUATION: ^{18}F-FLT VERSUS ^{18}F-FDG

Pancreatic Cancer

^{18}F-FLT has been used in imaging pancreatic-cancer-specific cell lines, SW-979 and BxPc-3. The study was performed by Seitz *et al*. (2002) to prove that ^{18}F-FLT has greater specificity than ^{18}F-FDG. In that study, the ^{18}F-FLT uptake was 18.4% and 5.2%, respectively. In comparison, ^{18}F-FDG was also administered to the same cell lines. It was observed that the ^{18}F-FDG uptake was only 0.6% and 0.3% for the corresponding cells. Evidence such as no increased ^{18}F-FLT uptake was observed in normal pancreatic lobules in comparison with large ^{18}F-FDG uptake detected in normal pancreatic lobules confirmed that ^{18}F-FLT has higher specificity for pancreatic cancer.

The previous work by Seitz was supported by the Herrmann group's findings in 2008. In the study consisting of 21 patients diagnosed with malignant pancreatic tumours, 15 patients had an increased ^{18}F-FLT uptake. Herrmann and his colleagues were able to demonstrate that ^{18}F-FLT was a specific marker for pancreatic cancer (Herrmann *et al*., 2008). They also suggested that ^{18}F-FLT may be used to differentiate pancreatic cancer from pancreatic pseudotumors that were subjected to arise from chronic pancreatitis (Herrmann *et al*., 2008). As any other studies, Herrmann acknowledged that although the ^{18}F-FLT showed high specificity for pancreatic cancer, it turned out that the sensitivity was reduced for malignant lesions (Herrmann *et al*., 2008).

Contrary to the Seitz *et al*. (2002) and Herrmann *et al*. (2008) studies, initial evaluation of ^{18}F-FLT for primary pancreatic study led by Quon *et al*. (2007) demonstrated the opposite. In a pilot study consisting of five patients who were newly diagnosed with unresectable pancreatic

cancer, the visual interpretation of the primary site was assessed using ^{18}F-FLT PET/CT and ^{18}F-FDG PET/CT. In ^{18}F-FLT PET/CT, the primary lesion was detectable in only two of the five patients, while all five showed lesions in the ^{18}F-FDG PET/CT imaging (Quon *et al*., 2007). Throughout the study, ^{18}F-FLT showed poor lesion detectability and low levels of uptake in the primary tumour compared to ^{18}F-FDG. Hence, it was suggested that the use of ^{18}F-FLT was not promising for characterisation of pancreatic cancer and it offerred no benefit in monitoring therapy due to poor baseline scan (Quon *et al*., 2007).

Pulmonary Nodes and Lung Cancer

In pulmonary nodes and lung cancer, one expected difficulty in differentiating malignant from benign solitary pulmonary nodes (Been *et al*., 2004). Although ^{18}F-FDG has proved to be a helpful and accurate diagnostic tool, with excellent sensitivity of 96.8% and good specificity of 77.8%, reports of false-positives still originate, mainly from granulomatous and inflammatory disease. Thus, a more specific tracer that does not show uptake in inflammatory tissues would be useful. In the non-small cell lung cancer (NSCLC) patient, image with low background activity was acquired with the administration of ^{18}F-FLT on patients (Been *et al*., 2004). Buck *et al*. (2003) further investigated 30 patients diagnosed with solitary pulmonary nodes (SPN) and deployed ^{18}F-FLT as a marker. They reported 86% ^{18}F-FLT uptake by the malignant lesions, whereas no ^{18}F-FLT uptake was observed in benign lesions. This demonstrated that in distinguishing the malignant SPN, ^{18}F-FLT had higher specificity than ^{18}F-FDG.

Breast Cancer

On the contrary, in breast cancer cases, although multiple studies have been carried out by many groups using ^{18}F-FLT, the results have not been consistent. In an early investigation in patients diagnosed with breast cancer, it was observed that ^{18}F-FLT was taken up in breast cancer cells (Been *et al*., 2004). In another study by Silverman and his colleagues in 2002, there was a 1.3 to 2.3 times higher ^{18}F-FLT uptake reported in primary breast cancers as compared to ^{18}F-FDG uptake. However, in 2004, Smyczek-Gargya and his colleagues, investigated 12 patients with breast cancer with ^{18}F-FLT and compared it to ^{18}F-FDG, concluding that ^{18}F-FDG uptake was higher than ^{18}F-FLT. Scientists agree that it is still unclear what will be the role for ^{18}F-FLT in patients with breast cancer as inconsistent findings from multiple studies have led to uncertainty in the role of ^{18}F-FLT in breast cancer management. Interestingly, the study of Been and his colleagues showed that ^{18}F-FLT uptake predicted tumour marker response to chemotherapy better than ^{18}F-FDG (Been *et al*., 2004). The latter work was supported by Pio and his colleagues in 2006 and also Kenny *et al*. (2007). Pio and his colleagues had evaluated the treatment response with ^{18}F-FLT PET in patients diagnosed with breast cancer over ^{18}F-FDG PET. Scans were done prior to chemotherapy treatment or anti-hormonal therapy two weeks after completion of the first treatment cycle and after the end of treatment or over a year if the treatment had not yet been completed. In the study, they found that changes in levels of the serum marker, CA27.29, were more strongly correlated with tumour ^{18}F-FLT uptake than with ^{18}F-FDG (Pio *et al*., 2006). Meanwhile, Kenny and his colleagues reported a significant association between tumour ^{18}F-FLT uptakes with the Ki-67 labelling index (Kenny *et al*.,

2007). Hence, it was proposed that measuring the early response to chemotherapy for locally advanced breast cancer is probably the most interesting research question for ^{18}F-FLT studies in patients with breast cancer (Been *et al*., 2004; Pio *et al*., 2006; Kumar, 2007; Kenny *et al*., 2007).

Brain Cancer

In the management of brain tumours, PET provides information on the tumour grade and also assists in assessing the optimal site for biopsy. Several PET radiopharmaceutical markers have been used for brain cancer imaging. These include ^{18}F-FDG, ^{18}F-FLT, and 11C-Met (L-methyl-[11C] methionine). Chen and his colleagues systematically compared ^{18}F-FLT with ^{18}F-FDG in human gliomas, in relation to sensitivity, in the evaluation of recurrent high-grade glioma (Chen *et al*., 2005). They discovered that uptake of ^{18}F-FLT in glioma was relatively rapid. ^{18}F-FLT typically showed a similar uptake as for ^{18}F-FDG. However, an interesting finding was that the ^{18}F-FLT background uptake in normal brain tissue was low, and this could be due to a slow proliferation rate. This feature significantly showed that ^{18}F-FLT has potential to derive a better mean standardised uptake value (SUV) in PET imaging of a tumour, as compared with ^{18}F-FDG.

Although ^{18}F-FDG has been used extensively in brain tumour imaging, one of the several major drawbacks of ^{18}F-FDG in this context is its difficulty in characterising tumours in the brain. This is due to the high basal glucose metabolic rate of normal brain tissue. ^{18}F-FDG uptake of low-grade tumours is generally similar to that of normal white matter, whereas high-grade tumour uptake can be similar to that of normal grey matter, resulting in limited sensitivity of lesion detection. In addition, in recurrent tumours the ^{18}F-FDG uptake could be lower than the normal white matter, whereas in necrotic cells the ^{18}F-FDG uptake could be higher than the normal white matter. It can be assumed that ^{18}F-FLT has a theoretical advantage in detecting tumour recurrence as there is little uptake in normal brain. It has been agreed that ^{18}F-FLT may help to define tumour activity by imaging tumours with greater sensitivity than ^{18}F-FDG (Nitzsche *et al*., 2003). Another significant finding arose from a study by Nitzsche and his colleagues in 2003, who determined that ^{18}F-FLT was greater to ^{18}F-FDG for the detection of recurrent brain tumours after brachytherapy.

A study by Dohmen and colleagues in 2000 compared the use of ^{18}F-FLT with L-methyl-11C-methionine (11C-MET) for the detection of brain tumours. They discovered that ^{18}F-FLT showed higher tumour contrast compared to 11C-MET. However, low-grade brain tumours limit the application of ^{18}F-FLT in brain tumour imaging as it showed poor visual distinction in that case (Been *et al*., 2004). Garlip (2003) discovered that the ^{18}F-FLT standardised uptake value was higher than that of 11C-MET. Even though ^{18}F-FLT has shown some advantages compared with ^{18}F-FDG and 11C-MET, relatively small and therefore inconclusive studies have been published. There is a need to provide anatomical information and to further determine whether ^{18}F-FLT is able to differentiate between benign and malignant tissues and between residual tumour and radionecrosis. If ^{18}F-FLT proves to be a sensitive and specific marker for the brain, it will be very useful for the next stages in management; namely establishing the best site for tumour biopsy and for planning of radiotherapy in heterogeneous tumour (Been *et al*., 2004).

Colorectal Cancer (CRC)

Francis and his colleagues in 2003 successfully imaged colorectal cancer using both ^{18}F-FDG and ^{18}F-FLT. Both markers displayed 100% sensitivity when imaging primary colorectal cancer. For visualisation of extra hepatic lesions, ^{18}F-FDG and ^{18}F-FLT demonstrated sensitivities of 100% and 92% respectively (Francis *et al*., 2003).

However, his study also demonstrated an increased uptake of ^{18}F-FDG from non-malignant inflammatory peritoneal lesions, which were thus presumed to be malignant. This would lead to false-positive scans when using ^{18}F-FDG. In contrast, such lesions showed no avidity for ^{18}F-FLT, demonstrating a specificity that may be useful for further characterisation of equivocal lesions (Francis *et al*., 2003). His study concluded that in colorectal cancer, ^{18}F-FLT demonstrated lower cellular trapping compared to ^{18}F-FDG. The poor sensitivity displayed by ^{18}F-FLT makes it a poor candidate as a diagnostic tool for colorectal cancer. Although it lacks in sensitivity (inclusion of free positives), ^{18}F-FLT has the potential to improve the specificity (rejection of false positives) for the detection of colorectal cancer.

Another study led by Wang *et al*. (2009) investigated whether the use of dual-tracers, ^{18}F-FDG and ^{18}F-FLT, could predict the biologic character of metastases in colorectal cancer. Wang *et al*. (2009) used animal modelling to prove that higher uptake of ^{18}F-FLT could be correlated to a higher incidence of metastasis. The human colorectal cancer cell lines SW480 and SW620 were generated in 20 mice, whereby the former was generated in the left front leg and latter was generated in the right front leg. Wang observed high uptake of ^{18}F-FLT in mice from small animal PET/CT which correlated well with the overexpression of HSP27 and integrin ß3 in the left front leg of the mice (SW480) (Wang *et al*., 2009). On the other hand, high uptake of ^{18}F-FDG was observed in the right front leg, which had been generated with SW620 cell lines but not by ^{18}F-FLT. The overexpression of HSP27 and integrin ß3 in SW480, which observed higher uptake of ^{18}F-FLT, was believed to reflect a higher rate of metastasis to lung and liver (Wang *et al*., 2009). Meanwhile, high uptake of ^{18}F-FDG in SW620 cell lines can possibly correlate with lymphatic metastases (Wang *et al*., 2009). From the study, Wang and his colleagues (2009) suggested that a combination of the dual-tracers ^{18}F-FLT and ^{18}F-FDG could be used to predict the biologic behaviour of colorectal cancer.

Lymphoma

Lymphoma is a type of malignancy that originates in lymphocytes of the immune system; particularly in lymph nodes and presenting as an enlargement of these nodes. For high-grade lymphoma visualisation, there is no dispute that ^{18}F-FDG has been proven to be a sensitive method. However, for the low-grade (indolent) lymphoma, the value of ^{18}F-FDG is still unclear (Been *et al*., 2004). Hence, ^{18}F-FLT could in theory have an additional value as a tracer of proliferative tissues. Been (2004) also compared ^{18}F-FLT and ^{18}F-FDG in lymphoma patients. It was found that the mean standardised uptake value (SUV) for ^{18}F-FLT was 4.5 whereas the mean SUV for ^{18}F-FDG was 5. This showed that ^{18}F-FDG had higher uptake in lymphoma. In terms of sensitivity, both markers were found to be comparable. As ^{18}F-FLT uptake in lymphoma is closely correlated with the rate of proliferation, problems may arise during the prognosis in lymphoma. In the case of prognosis in lymphoma, the rate of proliferation is not always

correlated with lymphoma's prediction (Been *et al*., 2004). In haematopoietic dysfunction cases, the ^{18}F-FLT marker is able to determine the activity, extent and distribution of bone marrow reserve and hence, assist in decision making for a variety of clinical indications. ^{18}F-FLT findings complement results of bone marrow aspiration and trephine biopsy (BMAT) and could be a useful tool for assessing response to novel treatments in patients with myeloproliferative diseases (Hofman *et al*., 2012).

Melanoma

Melanoma is a malignant tumour of pigment cells (melanocytes), which are found predominantly in skin but also in the bowel and eye. Cobben and colleagues in 2003 used ^{18}F-FLT in imaging of melanoma to compare with ^{18}F-FDG. They discovered that the specificity and sensitivity of ^{18}F-FLT in imaging of melanoma was 60% and 88%, respectively. In contrast, the specificity and sensitivity using ^{18}F-FDG was 83% and 92%, respectively. This indicates that the specificity and sensitivity of ^{18}F-FLT for melanoma are lower than those of ^{18}F-FDG. It appears that ^{18}F-FLT is not a preferential marker when it comes to detection of melanoma.

LIMIT OF ^{18}F-FLT AS A CELLULAR PROLIFERATION MARKER

The extent of the agreement on whether ^{18}F-FLT shows a net benefit in cellular proliferation has been continuously debated. The dispute arises due to the nature of DNA synthesis mechanisms: the thymidine salvage pathway and de novo synthesis pathway. In thymidine salvage pathway, thymidine is transported across the cell membrane and phosphorylated by TK1 into thymidine monosphosphate (TMP) before it is further phosphorylated into thymidine diphosphate (TDP) and thymidine triphosphate (TTP) (McKinley *et al*., 2013). TTP then is incorporated into the DNA.

In contrast to thymidine salvage, the de novo synthesis pathway uses deoxyuridine monophosphate as an alternative for conversion into TMP through the action of the thymidylate synthase (TS) enzyme. TPM is then further phosphorylated and incorporated into the DNA. Due to this nature of the DNA synthesis mechanism, it is assumed that previous studies using ^{18}F-FLT may underestimate cell proliferation in de novo pathway-dependent tumours. In 2013, McKinley and his colleagues conducted a study to demonstrate that ^{18}F-FLT is poorly reflected as a proliferative index in some tumours that utilise the de novo pathway. They generated the human colorectal cancer cell lines, HCT-116 (parental line) and HCT-116p21 in the cell lines and also in the xenografts to explore the effect of p21 deletion on ^{18}F-FLT. Interestingly, in HCT-116p21 cells, elevated levels of the TS enzyme was observed. Meanwhile, the level of TK1 diminished. When ^{18}F-FLT PET was performed on the xenografts to demonstrate the sensitivity of ^{18}F-FLT to de novo pathway utilisation, the HCT-116 xenografts manifested greater uptake than the analogous HCT-116p21 xenografts (McKinley *et al*., 2013). The finding were supported by the findings of a previous study led by Moroz *et al*. (2011) who suggested that ^{18}F-FLT uptake was unrepresentative of xenografts growth in tumours utilising the de novo pathway. From the findings, McKinley *et al*. (2013) concluded that ^{18}F-FLT PET cannot discriminate moderately proliferative, thymidine salvage-driven tumours from high-proliferative index tumours that rely primarily upon the de novo pathway.

CONCLUSION

It is well accepted that ^{18}F-FDG is the ubiquitous marker in PET oncological practice. Nevertheless, ^{18}F-FLT is an exciting marker with improved specificity that could be the number one candidate for therapeutic monitoring. Thereby, future research should continue to probe the potential of ^{18}F-FLT as a powerful marker for cellular proliferation.

REFERENCES

Barthel, H., Cleij, M. C., Collingridge, D. R., Hutchinson, O. C., Osman, S., & He, Q. (2003). 3'-Deoxy-3'[^{18}F]Fluorothymidine as a new marker for monitoring tumour response to antiproliferative therapy in vivo with positron emission tomography. *Cancer Research, 63*, 3791-3798.

Been, L. B., Suurmeijer, A. J. H., Cobben, D. C. P., Jager, P. L., Hoekstra, H. J., & Elsinga, P. H. (2004). [^{18}F]FLT-PET in oncology: current status and opportunities. *European Journal of Nuclear Medicine and Molecular Imaging, 31*(12), 1559-1672.

Buck, A. K., Halter, G., Schirrmeister, H., Kotzerke, J., Wurziger, I., & Glatting, G. (2003). Imaging proliferation in lung tumours with PET: ^{18}F-FLT versus ^{18}F-FDG. *Journal of Nuclear Medicine, 44*(9), 1426-1431.

Cancer Imaging Program. (2006). An investigational positron emission tomography (PET) radiopharmaceutical for injection and intended for use as an in vivo diagnostic for imaging active cellular proliferation of malignant tumours. *Division of Cancer Treatment and Diagnosis* (4th ed.). National Institute of Health.

Chen, W., Cloughesy, T., Kamdar, N., Satyamurthy, N., Bergsneider, M., & Liau, L. (2005). Imaging proliferation in brain tumours with ^{18}F-FLT PET: Comparison with ^{18}F-FDG. *Journal of Nuclear Medicine, 46*(6), 945-952.

Cobben, D. C. P., Jager, P. L., Elsinga, P. H., Maas, B., Suurmeijer, A. J. H., & Hoekstra, H. J. (2003). 3'-^{18}Fluoro-3'-deoxy-L-thymidine: A new tracer for staging metastatic melanoma? *Journal of Nuclear Medicine, 44*, 1927-1932.

Dohmen, B. M., Shield, A. F., Grierson, J. R., Kuntzsch, M., Reimold, M., & Sloan, A. (2000). [^{18}F] FLT-PET in brain tumours. *Journal of Nuclear Medicine, 41*(supplementary), 216P.

Fathinul, F., Nordin, A. J., & Lau, W. F. E. (2013). 18(F) FDG-PET/CT is a useful molecular marker in evaluating tumor aggressiveness; A revised understanding of an in-vivo FDG PET imaging that alludes the alteration of cancer biology. *Cell Biochemistry and Biophysics, 66*(1), 37-43.

Francis, D. L., Visvikis, D., Costa, D. C., Arulampalam, T. H. A., Townsend, C., & Luthra, S. K. (2003). Potential impact of [^{18}F]3'-deoxy-3'-fluorothymidine versus [^{18}F]fluoro-2-deoxy-D-glucose in positron emission tomography for colorectal cancer. *European Journal of Nuclear Medicine and Molecular Imaging, 30*(7), 988-994.

Gambhir, S. S., Czermin, J., Shcwimmer, J., Silverman, D. H., Coleman, R. E., & Phelps, M. E. (2001). A tabulated summary of the FDG PET literature. *Journal of nuclear medicine, 42*(5 suppl), 1S-93S.

Garlip, G., Dittmar, C., Kracht, L., Thomas, A. V., Herholz, K., & Heiss, W. D. (2003). Identification of DNA and amino acid metabolism in human gliomas by PET. *Journal of Nuclear Medicine, 44(*5), 167P-167P.

Grierson, J. R., Shields, A. F., & Eary, J. F. (1997). Development of a radiosynthesis for 3'-[F-18] fluoro-3'-deoxynucleosides. *Journal of Labelled Compounds and Radiopharmaceuticals, 40,* 60-62.

Herrmann, K., Eckel, F., Schmidt, S., Schneidhauer, K., Krause, B. J., & Kleeff, J. (2008). In vivo characterization of proliferation for discriminating cancer from pancreatic pseudotumors. *Journal of Nuclear Medicine, 49*(9), 1437-1444.

Hofman, M., Segard, T., Khan, Z., Seymour, J., & Hicks, R. (2012). Clinical utility of ^{18}F-fluoro-L-thymidine (FLT) PET to evaluate bone marrow distribution and proliferation in patients with haematopoietic dysfunction. *Journal of Nuclear Medicine, 53*(S1), 538.

Kenny, L., Coombes, R. C., Vigushin, D. M., Al-Nahhas, A., Shousha, S., & Aboagye, E. O. (2007). Imaging early changes in proliferation at 1 week post chemotherapy: a pilot study in breast cancer patients with 3'-deoxy-3'-[^{18}F]fluorothymidine positron emission tomography. *European Journal of Nuclear Medicine and Molecular Imaging, 34*(9), 1339-1347.

Kumar, R. (2007). Assessment of therapy response in malignant tumours with ^{18}F-fluorothymidine. *European Journal of Nuclear Medicine and Molecular Imaging, 34*(9), 1334-1338.

Langen, P., Etzol, G., Hintsche, R., & Kowollik, G. (1969). 3'-deoxy-3'-fluorothymidine, a new selective inhibitor of DNA-synthesis. *Acta biologica et medica Germanica, 23*(6), 759-766.

McKinley, E. T., Ayers, G. D., Smith, R. A., Saleh, S. M., Zhao, P., Washington, M. K., Coffey, R. J., & Manning, H. C. (2013). Limits of [^{18}F]-FLT PET as a biomarker of proliferation in oncology. Plos One, 8(3), 1-9.

Moroz, M. A., Kochetkov, T., Cai, S., Wu, J., & Shamis, M. (2011). Imaging colon cancer response following treatment with AZD1152: A preclinical analysis of [^{18}F]fluoro-2-deoxyglucose and 3'-deoxy-3'[^{18}F]fluorothymidine imaging. *Clinical Cancer Research, 17(*5), 1099-1110.

Nitzsche, E. U., Walter, M., Schirp, U., Machulla, H. J., & Mueller, J. (2003). Combined PET imaging of proliferation and glycolysis for follow up of brachytherapy in brain tumours. *Society of Nuclear Medicine 50th Annual Meeting.*

Pio, B. S., Park, C. K., Pietra, R., Hsueh, W. A., Satyamurthy, N., & Pegram, M. D. (2006). Usefulness of 3'-[F-18]Fluoro-3'-deoxythymidine with positron emission tomography in predicting breast cancer response to therapy. *Molecular Imaging and Biology, 8*(1), 36-42.

Quon, A., Chang, S. T., Chin, F., Kamaya, A., Dick, D. W., Loo, J. B. W., Gambhir, S. S., & Koong, A. C. (2008). Initial evaluation of ^{18}F-fluorothymidine (FLT) PET/CT scanning for primary pancreatic cancer. *European Journal of Nuclear Medicine and Molecular Imaging, 35*(3), 527-531.

Seitz, U., Wagner, M., Neumaier, B., Wawra, E., Glatting, G., & Leder, G. (2002). Evaluation of pyrimidine metabolising enzymes and in vitro uptake 3'-[^{18}F]fluoro-3'-deoxythymidine [^{18}F]FLT in pancreatic cancer lines. *European Journal of Nuclear Medicine and Molecular Imaging, 29*(9), 1174-1181.

Shields, A. F., Grierson, J. R., Dohmen, B. M., Machulla, H. J., Stayanoff, J. C., & Lawhorn-Crews, J. M. (1998). Imaging proliferation in vivo with [^{18}F]FLT and positron emission tomography. *Nature Medicine, 4*(11), 1334-1336.

Silverman, D. H., Pio, B. S., Satyamurthy, N., Park, C. K., Chap, L., & Pegram, M. (2002). Monitoring effects of breast cancer chemotherapy with fluorodeoxyglucose and fluoro-L-thymidine. *Journal of Nuclear Medicine, 43*(5), 311.

Smyczek- Gargya, B., Fersis, N., Dittmann, H., Vogel, U., Reischl, G., & Machulla, H. J. (2004). PET with [^{18}F]fluorothymidine for imaging of primary breast cancer: A pilot study. *European Journal of Nuclear Medicine and Molecular Imaging, 31*(5), 720-724.

Wang, H., Jinming, Z., Jiahe, T., Baolin, Q., Tianran, L., Yingmao, C., Jian, L., & Shan, W. (2009). Using dual-tracer PET to predict the biologic behaviour of human colorectal cancer. *Journal of Nuclear Medicine, 50*(11), 1857-1864.

Wilson, I. K., Chatterjee, S., & Wolf, W. (1991). The use of 3'-fluoro-3'-deoxythymidine and studies of its ^{18}F-labelling, as a tracer for the non-invasive monitoring of the biodistribution of drugs against AIDS. *Journal of Fluorine Chemistry, 55*, 283-289.

Yun, M., Oh, S. J., Ha, H. J., Ryu, J. S., & Moon, D. H. (2003). High radiochemical yield synthesis of 3'-deoxy-3'-[^{18}F]fluorothymidine using (5'-O-dimethoxytrityl-2'-deoxy-3'-O-nosyl-β-D-threo pentofuranosyl)thymine and its 3-N-BOC-protected analogue as a labelling precursor. *Nuclear Medicine and Biology, 30*(2), 151-157.

Pertanika J. Sci. & Technol. 24 (1): 53 - 70 (2016)

SCIENCE & TECHNOLOGY

Journal homepage: http://www.pertanika.upm.edu.my/

Scaling Group Transformation for MHD Double-Diffusive Flow Past a Stretching Sheet with Variable Transport Properties Taking into Account Velocity Slip and Thermal Slip Boundary Conditions

Uddin, M. J.[1, 3], Khan, W. A.[2*] and Ismail, A. I. M.[3]

[1]*Department of Mathematics, American International University-Bangladesh, Banani, Dhaka 1213, Bangladesh*

[2]*Department of Engineering Sciences, PN Engineering College, National University of Science and Technology, Karachi 75350, Pakistan*

[3]*School of Mathematical Sciences, Universiti Sains Malaysia, Penang 11800, Malaysia*

ABSTRACT

The steady two-dimensional laminar mixed convective boundary layer flow of a viscous incompressible electrically conducting Newtonian fluid along a moving stretching sheet embedded in a porous medium was studied numerically. We used temperature dependent viscosity and thermal conductivity and concentration dependent mass diffusvity. Further, the velocity and thermal slip boundary conditions were applied at the surface of the sheet. The governing transport equations were reduced to similarity equations using scaling group of transformation, before being sloved numerically by using the fourth-fifth order Runge-Kutta-Fehlberg method from Maple 13. Our analysis revealed that the mass diffusivity parameter causes both temperature and concentration to increase whilst thermal conductivity parameter increases the temperature. It was also revealed that the rate of heat and mass transfer increased with the increasing of velocity slip, viscosity and power law parameters. Comparisons with previous published works are reported and good agreements were found.

Keywords: Variable transport properties, double-diffusion, Lie group, velocity and thermal slip, MHD

INTRODUCTION

Momentum, heat and mass transfer in porous media have applications in the petroleum industry, geothermal processes, control of pollutant spread in ground water, heat exchange between soil and atmosphere, flat plate solar collectors, solar power collectors, food industries, insulation of nuclear reactors, nuclear waste management and many other areas (Nield & Bejan, 2013). Transport

Article history:
Received: 6 June 2013
Accepted: 22 September 2015

E-mail addresses:
Uddin, M. J. (jashim_74@yahoo.com), wkhan_2000@yahoo.com (Khan, W. A.), izani@cs.usm.my (Ismail, A. I. M.)
*Corresponding author

ISSN: 0128-7680

phenomenon due to motion of a stretching sheet has attracted the interest of researchers because of its diverse engineering applications such as the aerodynamic extrusion of plastic sheets, the boundary layer along a liquid film in condensation process and the cooling of the metal plate in a cooling bath as well as its use in the glass and fibre industries (Vajravelu *et al*., 2011). Fluid flow over a linearly stretching surface was first analysed by Crane (1970). This problem was widely studied for natural/combined convective steady/unsteady flow over various geometries for both Newtonian and non-Newtonian fluid in clear/porous media. A few investigations are presented in the paper by Ishak *et al*. (2009) and Abdel-Rahman (2010). Thermal radiation effect plays an important role in controlling heat transfer in the industry where the quality of the final products depends on heat controlling factors to some extent. High temperature plasmas, cooling of nuclear reactors, liquid metal fluids and power generation systems are some important applications of radiative heat transfer from a surface plate to conductive fluids.

Heat flux caused by a concentration gradient is known as diffusion-thermo effect (Dufour effect) whilst species differentiation owing to the gradient of temperature is known as thermal-diffusion effect (Soret effect) (Eckert & Drake, 1972). It is known that these effecst are smaller than the effects described by Fourier and Fick's laws, but there are many practical applications in which their effects are significant. For example, the Soret effect has been used for isotope separation and in the mixing between gasses with very light molecular weight and of medium molecular weight (Hayat *et al*., 2010). The effect of Soret number and Dufour number on MHD free convective heat and mass transfer over a vertical stretching surface in a porous medium was studied by Mansour *et al*. (2008). The steady stagnation point flow over a vertical stretching surface in the presence of species concentration and mass diffusion under the Soret and Dufour effects was studied by Tsai and Huang (2009). Postelnicu (2010) describes Dufour and Soret effects on two-dimensional stagnation point flow in a saturated porous medium.

The above literature review revealed that the previous analyses are concerned with the boundary layer flow and heat and mass transfer in a Newtonian fluid using a conventional no-slip boundary conditions. However, fluid flow in micro/nanoscale such as micropumps, microtubines, micro heat exchangers, sensors and actuators are important for micro- and nanoscience and the conventional no slip boundary condition at the solid–fluid interface must be replaced with the slip condition (Jiji, 2010). Slip flows occur in a variety of technological applications, for example, extrusion dies (Gifford 2004), foam production (Ireland & Jameson, 2009), fabrication, the design of microelectromechanical systems (Lahjomri & Oubarra, 2013) and fluidic cells in medicine (Khaled & Vafai, 2004), in which increasing wall slip has been shown to generate enhanced cooling and flow fluctuations. Slip effect on flow field has been studied by various authors: Aziz (2010), Uddin *et al*. (2012) and Noghrehabadi *et al*. (2012). All of these researchers restricted their investigation to constant transport properties. However, they are not constants. No study, as far as these authors are aware, has been reported in the literature for the investigations of MHD mixed convective flow past a stretching sheet with slip boundary conditions and variable transport properties.

The aim of this study was to extend the work of Abdel Rahman (2010) to include the effect of velocity and thermal slip as well as temperature dependent thermal conductivity and concentration dependent mass diffusivity. The transport equations were reduced to similarity equations using similarity variables obtained by a scaling group analysis and then

solved numerically. The effect of the key physical parameters on the dimensionless velocity, temperature, concentration, skin friction, rate of heat transfer and the rate of mass transfer were examined and discussed. The problem reported in this paper has not been investigated in the literature despite its applications in many engineering processes, such as nuclear waste, polymer production, dispersion of chemical pollutants through water-saturated soil, geothermal energy extractions, plasma studies, liquid metal fluids, power generation systems, molecular dynamics and micro/nanofluidics.

FORMULATION OF THE BASIC TRANSPORT EQUATIONS

A steady two-dimensional magnetohydrodynamic (MHD) double-diffusive combined convective laminar incompressible Newtonian fluid flow in a Darcian porous medium along a moving vertical stretching surface was considered. The flow model and coordinate system is shown in Fig.1.

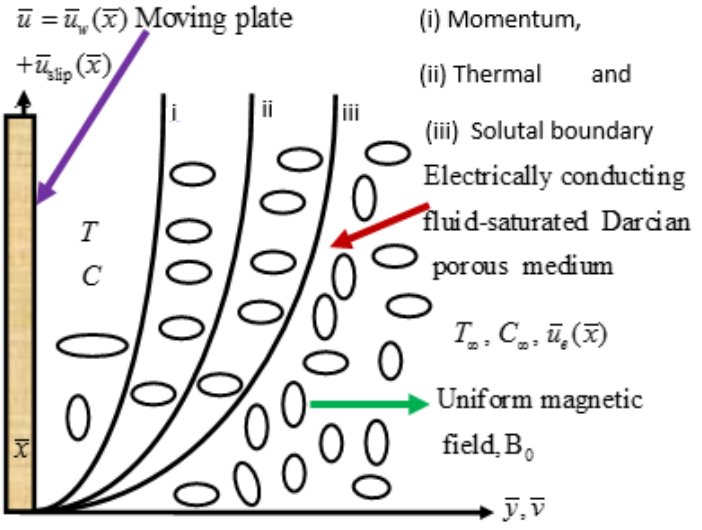

Fig.1: Uptake mechanism of thymidine and ^{18}F-FLT.

A magnetic field of uniform strength B_0 was applied perpendicular to the plate. We ignored induced magnetic fields and hence ingored the magnetic Reynolds number. It was assumed that a first-order homogenous isothermal irreversible chemical reaction would take place between the chemical constitute of the plate and the ambient fluid. The Boussinesq approximation was taken into account. Following Seddeek and Salem (2005), we assumed the temperature dependent viscosity would vary according to $\mu(T) = \mu_\infty e^{-\alpha_0 \theta}$, where μ_∞ is the constant viscosity far away from the plate and α_0 is the viscosity parameter depending on the nature of the fluid, Θ is the dimensionless temperature defined in Eqn. (6). It was further assumed that the temperature dependent thermal conductivity varied linearly as $k(T) = k_\infty [1 + c_1 (T - T_\infty)] = k_\infty [1 + A\theta]$, where k_∞ is the constant undisturbed thermal conductivity far away from the plate, c_1 is a

constant which depends on the fluid and $A = c_1 \Delta T$ is the thermal conductivity parameter. We further assumed that mass diffusivity varied linearly as where D_∞ is the constant concentration diffusivity far away from the plate and $Dc = c_2 \Delta C$ is a concentration diffusivity parameter (White & Subramanian, 2010), ϕ is the dimensionless concentration defined in Eqn. (6). Here c_2 is a constant. The boundary layer equations in dimensional form are (Abdel-Rahman, 2010):

$$\frac{\partial \bar{u}}{\partial \bar{x}} + \frac{\partial \bar{v}}{\partial \bar{y}} = 0, \tag{1}$$

$$\bar{u}\frac{\partial \bar{u}}{\partial \bar{x}} + \bar{v}\frac{\partial \bar{u}}{\partial \bar{y}} = \nu_\infty \frac{\partial}{\partial \bar{y}}\left(e^{-\alpha_0 \theta}\frac{\partial \bar{u}}{\partial \bar{y}}\right) + \bar{u}_e \frac{d\bar{u}_e}{d\bar{x}} - \frac{\nu_\infty}{k}(\bar{u} - \bar{u}_e) - \frac{\sigma B_0^2}{\rho}(\bar{u} - \bar{u}_e) \tag{2}$$
$$+ g\beta_T (T - T_\infty) + g\beta_C (C - C_\infty),$$

$$\bar{u}\frac{\partial T}{\partial \bar{x}} + \bar{v}\frac{\partial T}{\partial \bar{y}} = k_\infty \frac{\partial}{\partial \bar{y}}\left[(1 + A\theta)\frac{\partial T}{\partial \bar{y}}\right] + \frac{16\sigma_1 T_\infty^3}{3\rho_\infty c_p k_1}\frac{\partial^2 T}{\partial \bar{y}^2} + \frac{Q_0}{\rho_\infty c_p}(T - T_\infty) \tag{3}$$
$$+ \frac{k_T D_m}{c_s c_p}\frac{\partial}{\partial \bar{y}}\left[(1 + Dc\phi)\frac{\partial C}{\partial \bar{y}}\right],$$

$$\bar{u}\frac{\partial C}{\partial \bar{x}} + \bar{v}\frac{\partial C}{\partial \bar{y}} = D_\infty \frac{\partial}{\partial \bar{y}}\left[(1 + Dc\phi)\frac{\partial C}{\partial \bar{y}}\right] - k_0 (C - C_\infty) \tag{4}$$
$$+ \frac{K_T D_\infty}{T_m}(1 + Dc\phi)\frac{\partial^2 T}{\partial \bar{y}^2}.$$

The relevant boundary conditions are (Jiji, 2010):

$$\bar{u} = c\bar{x} + N_1 \nu_\infty \frac{\partial \bar{u}}{\partial \bar{y}},\ \bar{v} = 0,\ T = T_w(\bar{x}) + D_1 \frac{\partial T}{\partial \bar{y}}, C = C_w(\bar{x}) \text{ at } \quad \bar{y} = 0, \tag{5}$$
$$\bar{u} \to \bar{u}_e(\bar{x}) = a_1 \bar{x},\ \ T \to T_\infty,\ \ C \to C_\infty \quad \text{as} \quad \bar{y} \to \infty.$$

Here $(\bar{u}, \bar{v})$: Darcian velocity components along the $\bar{x}$ and $\bar{y}$ -axes, $\mu(T)$: temperature dependent viscosity, ρ_∞: density of the ambient fluid, ν_∞ constant kinematic viscosity, $\bar{u}$ free stream velocity, K_0: permeability of the porous media, σ: electric conductivity, g: acceleration due to gravity, β_T: volumetric coefficient of thermal expansion, β_c: volumetric coefficient of mass expansion, C_p: specific heat at constant pressure, $k(T)$: temperature dependent thermal conductivity, Q_0: heat generation/absorption constant, k_T: thermal diffusion ratio, C_s: concentration susceptibility, $D(C)$: concentration dependent mass diffusivity, T_m: mean fluid temperature, k_0: reaction rate constant, N_1: velocity slip factor and D_1: thermal slip factor. Also, c and a_1 are the positive constant σ_1 : Stefan-Boltzmann constant, while k_1: Rosseland means absorption coefficient.

Using the following are dimensionless variables:

$$x=\frac{\overline{x}}{\sqrt{\nu_\infty / c}},\ y=\frac{\overline{y}}{\sqrt{\nu_\infty / c}},\ u=\frac{\overline{u}}{\sqrt{c\nu_\infty}},\ v=\frac{\overline{v}}{\sqrt{c\nu_\infty}},\ u_e=\frac{\overline{u}_e}{\sqrt{c\nu_\infty}},$$
$$\theta=\frac{T-T_\infty}{\Delta T},\phi=\frac{C-C_\infty}{\Delta C},\Delta T=T_w-T_\infty,\Delta C=C_w-C_\infty. \tag{6}$$

and hence, using the stream function Ψ defined by $u=\frac{\partial\psi}{\partial y},\ v=-\frac{\partial\psi}{\partial x},$ we have from Eqns. (2)-(4):

$$\Delta_1\equiv\frac{\partial\psi}{\partial y}\frac{\partial^2\psi}{\partial x\partial y}-\frac{\partial\psi}{\partial x}\frac{\partial^2\psi}{\partial y^2}+\alpha_0\,e^{-\alpha_0\theta}\frac{\partial\theta}{\partial y}\frac{\partial^2\psi}{\partial y^2}-e^{-\alpha_0\theta}\frac{\partial^3\psi}{\partial y^3}$$
$$-u_e\frac{du_e}{dx}+(\Omega+M)\left(\frac{\partial\psi}{\partial y}-u_e\right)-\frac{g\,\beta_T\,\Delta T}{c\sqrt{c\nu_\infty}}\theta-\frac{g\,\beta_C\,\Delta C}{c\sqrt{c\nu_\infty}}\phi=0, \tag{7}$$

$$\Delta_2\equiv\frac{\partial\psi}{\partial y}\frac{\partial\theta}{\partial x}-\frac{\partial\psi}{\partial x}\frac{\partial\theta}{\partial y}+\frac{\partial\psi}{\partial y}\theta\frac{\partial}{\partial x}[\ln(\Delta T)]-\frac{1}{\mathrm{Pr}}\left[\frac{R+1+A\theta}{R}\right]\frac{\partial^2\theta}{\partial y^2}$$
$$-\frac{1}{\mathrm{Pr}}A\left(\frac{\partial\theta}{\partial y}\right)^2-Q\theta-Df\frac{\partial}{\partial y}\left[(1+Dc\phi)\frac{\partial\phi}{\partial y}\right]=0, \tag{8}$$

$$\Delta_3\equiv\frac{\partial\psi}{\partial y}\frac{\partial\phi}{\partial x}-\frac{\partial\psi}{\partial x}\frac{\partial\phi}{\partial y}+\frac{\partial}{\partial x}[\ln(\Delta C)]-\frac{1}{Le}\frac{\partial}{\partial y}\left[(1+Dc\phi)\frac{\partial\phi}{\partial y}\right]+K\phi$$
$$-Sr(1+Dc\phi)\frac{\partial^2\theta}{\partial y^2}=0. \tag{9}$$

The boundary conditions in Eqn. (5) become:

$$\frac{\partial\psi}{\partial y}=x+a\frac{\partial^2\psi}{\partial y^2},\ \frac{\partial\psi}{\partial x}=0,\ \phi=1,\ \theta=1+b\frac{\partial\theta}{\partial y}\ \text{ at }\ y=0,$$
$$\frac{\partial\psi}{\partial y}\to S\,x,\ \theta\to 0,\ \phi\to 0\quad\text{as}\quad y\to\infty. \tag{10}$$

The controlling parameters are: Dufour ($D_f = D_\infty K_T\Delta C/C_sC_p\alpha_m\Delta T$), Soret ($S_r = D_\infty K_T\Delta T/T_m\alpha_m\Delta C$), magnetic field ($M = \sigma B^2{}_0/\rho_\infty c$), radiation ($R=3k_1k_\infty/16\sigma_1T^3{}_\infty$), generation/absorption ($Q=Q_0/c\,\rho_\infty c_\mathrm{p}$), porosity ($\Omega=\nu/c\,K_0$), velocity slip ($a=\sqrt{c\nu_\infty}\ N_1$), thermal slip ($b=\sqrt{c/\nu_\infty}\ D_1$), stretching ($S=a_1/c$), chemical reaction ($K=k_0/c$), Prandtl number ($\mathrm{Pr}=\mu_\infty c_\mathrm{p}/k_\infty$), Lewis number ($Le=\nu_\infty/D_\infty$). The wall temperature and concentration varied nonlinearly as $Tw=T_\infty + c_3x^n$ and $C_w = C_\infty + c_4x^n$, where C_3, C_4 are constants and n is the power law index.

SYMMETRY ANALYSIS

In this section, we shall show how scaling group transformation (special form of Lie group) transforms the governing equations into similarity equations. We begin our analysis by selecting the following scaling group of transformation (Seshadri & Na, 1985; Uddin *et al*., 2012),

$$\Gamma: x^* = xe^{\varepsilon\alpha_1}, y^* = ye^{\varepsilon\alpha_2}, \psi^* = \psi e^{\varepsilon\alpha_3}, \theta^* = \theta e^{\varepsilon\alpha_4}, \quad \phi^* = \phi e^{\varepsilon\alpha_5}, \beta_T^* = \beta_T e^{\varepsilon\alpha_6}, \beta_C^* = \beta_C e^{\varepsilon\alpha_7}. \tag{11}$$

Here ε ($\neq 0$) is a parameter and α_i (i = 1,2,3,...,7) are all arbitrary, real constants not all-zero simultaneously. Transformations in Eqn. (11) may be treated as a point transformation transforming the coordinates:

$$(x, y, \psi, u_e, \theta, \phi, \beta_T, \beta_C) \text{ to } (x^*, y^*, \psi^*, u_e^*, \theta^*, \phi^*, \beta_T^*, \beta_C^*).$$

We now investigate the relationship among the exponents $\alpha's$ such that:

$$\Delta_j\left(x^*, y^*, , u^*, v^* \cdots, \frac{\partial^3 \psi^*}{\partial y^{*3}}\right) = H_j\left(x, y, u, v, \cdots, \frac{\partial^3 \psi}{\partial y^3}; a\right)\Delta_j\left(x, y, \cdots, \frac{\partial^3 \psi}{\partial y^3}\right), (j = 1,2,3)$$

since this is the requirement for the differential forms Δ_1, Δ_2 and Δ_3 to be conformally invariant under the transformation group (11). Substituting the transformations (11) in Eqns. (14)-(16), we have:

$$\begin{aligned}
&\Delta_1 \equiv \frac{\partial \psi^*}{\partial y^*}\frac{\partial^2 \psi^*}{\partial x^* \partial y^*} - \frac{\partial \psi^*}{\partial x^*}\frac{\partial^2 \psi^*}{\partial y^{*2}} + \alpha_0 e^{-\alpha_0 \theta^*}\frac{\partial \theta^*}{\partial y^*}\frac{\partial^2 \psi^*}{\partial y^{*2}} - e^{-\alpha_0 \theta^*}\frac{\partial^3 \psi^*}{\partial y^{*3}} \\
&-u_e^*\frac{du_e^*}{dx^*} - (\Omega + M)\frac{\partial \psi^*}{\partial y^*} + (\Omega + M)u_e^* - \frac{g\,\Delta T}{c\sqrt{c\nu_\infty}}\beta_T^*\theta^* - \frac{g\,\beta_C\,\Delta C}{c\sqrt{c\nu_\infty}}\beta_C^*\phi \\
&= e^{\varepsilon(2\alpha_3 - \alpha_1 - 2\alpha_2)}\left[\frac{\partial \psi}{\partial y}\frac{\partial^2 \psi}{\partial x \partial y} - \frac{\partial \psi}{\partial x}\frac{\partial^2 \psi}{\partial y^2}\right] \\
&+ e^{\varepsilon(\alpha_4 + \alpha_3 - 3\alpha_1)}\alpha_0 e^{-\alpha_0 e^{\alpha_4}\theta}\frac{\partial \theta}{\partial y}\frac{\partial^2 \psi}{\partial y^2} - e^{\varepsilon(\alpha_3 - 3\alpha_1)}e^{-\alpha_0 e^{\alpha_4}\theta}\frac{\partial^3 \psi}{\partial y^3} \\
&-e^{\varepsilon\alpha_1}u_e\frac{du_e}{dx} - (\Omega + M)e^{\varepsilon(\alpha_3 - \alpha_2)}\frac{\partial \psi^*}{\partial y^*} + (\Omega + M)e^{\varepsilon\alpha_1}u_e \\
&-\frac{g\,\Delta T}{c\sqrt{c\nu_\infty}}e^{\varepsilon(\alpha_4 + \alpha_6)}\beta_T\theta - e^{\varepsilon(\alpha_5 + \alpha_7)}\frac{g\,\beta_C\,\Delta C}{c\sqrt{c\nu_\infty}}\beta_C\phi,
\end{aligned} \tag{12}$$

$$\Delta_2 \equiv \frac{\partial \psi^*}{\partial y^*}\frac{\partial \theta^*}{\partial x^*} - \frac{\partial \psi^*}{\partial x^*}\frac{\partial \theta^*}{\partial y^*} + \frac{\partial \psi^*}{\partial y^*}\theta^* \frac{\partial}{\partial x^*}\left[\ln(\Delta T)\right]$$
$$-\frac{1}{\mathrm{Pr}}\left[\frac{R+1+A\theta^*}{R}\right]\frac{\partial^2 \theta^*}{\partial y^{*2}} - \frac{1}{\mathrm{Pr}}A\left(\frac{\partial \theta^*}{\partial y^*}\right)^2 - Q\theta^* - Df\frac{\partial}{\partial y^*}\left[(1+Dc\,\phi^*)\frac{\partial \phi^*}{\partial y^*}\right] =$$
$$e^{\varepsilon(\alpha_3+\alpha_4-\alpha_1-\alpha_2)}\left[\frac{\partial \psi}{\partial y}\frac{\partial \theta}{\partial x} - \frac{\partial \psi}{\partial x}\frac{\partial \theta}{\partial y} + \frac{\partial \psi}{\partial y}\theta\frac{\partial}{\partial x}\left[\ln(\Delta T)\right]\right]$$
$$-\frac{1}{\mathrm{Pr}}e^{\varepsilon(\alpha_4-2\alpha_2)}\left[\frac{R+1+e^{\varepsilon\alpha_4}A\theta}{R}\right]\frac{\partial^2 \theta}{\partial y^2} - \frac{1}{\mathrm{Pr}}A\,e^{\varepsilon(2\alpha_4-2\alpha_2)}\left(\frac{\partial \theta}{\partial y}\right)^2$$
$$-Qe^{\varepsilon\alpha_4}\theta - Dfe^{\varepsilon(\alpha_5-2\alpha_2)}(1+Dc\,e^{\varepsilon\alpha_5}\phi)\frac{\partial^2 \phi}{\partial y^2} - Df\,Dce^{\varepsilon(2\alpha_5-2\alpha_2)}\left(\frac{\partial \phi}{\partial y}\right)^2 \quad (13)$$

$$\Delta_3 \equiv \frac{\partial \psi^*}{\partial y^*}\frac{\partial \phi^*}{\partial x^*} - \frac{\partial \psi^*}{\partial x^*}\frac{\partial \phi^*}{\partial y^*} + \frac{\partial}{\partial x^*}\left[\ln(\Delta C)\right] - \frac{1}{Le}\frac{\partial}{\partial y^*}\left[(1+Dc\,\phi^*)\frac{\partial \phi^*}{\partial y^*}\right]$$
$$+K\,\phi^* - Sr(1+Dc\,\phi)\frac{\partial^2 \theta}{\partial y^2} = e^{\varepsilon(\alpha_3+\alpha_5-\alpha_1-\alpha_2)}\left[\frac{\partial \psi}{\partial y}\frac{\partial \phi}{\partial x} - \frac{\partial \psi}{\partial x}\frac{\partial \phi}{\partial y} + \frac{\partial}{\partial x}\left[\ln(\Delta C)\right]\right]$$
$$-\frac{1}{Le}\left[1+Dc\,e^{\varepsilon\alpha_5}\phi\right]e^{\varepsilon(\alpha_5-2\alpha_2)}\frac{\partial^2 \phi}{\partial y^2} - \frac{Dc}{Le}e^{\varepsilon(\alpha_5-2\alpha_2)}\left(\frac{\partial \phi}{\partial y}\right)^2 \quad (14)$$
$$-Sr\left[1+Dc\,e^{\varepsilon\alpha_5}\phi\right]e^{\varepsilon(\alpha_4-2\alpha_2)}\frac{\partial^2 \theta}{\partial y^2}.$$

The system remains invariant under the group transformation Γ if the exponent satisfies the following relationship:

$$\alpha_2 = \alpha_4 = \alpha_5 = 0,\ \alpha_1 = \alpha_3 = \alpha_6 = \alpha_7. \quad (15)$$

The set of transformations (11) reduces to:

$$x^* = xe^{\varepsilon\alpha_1}, y^* = y, \psi^* = \psi e^{\varepsilon\alpha_1}, \theta^* = \theta, \phi^* = \phi, \beta_T^* = \beta_T e^{\varepsilon\alpha_1}, \beta_C^* = \beta_C e^{\varepsilon\alpha_1}. \quad (16)$$

Using Taylor series expansion in powers of $\mathcal{E}$, keeping the terms up to the first degree and neglecting higher powers of $\mathcal{E}$, we have:

$$x^* - x = \varepsilon\alpha_1 x, y^* - y = 0, \psi^* - \psi = \varepsilon\alpha_1\psi, \theta^* - \theta = \phi^* - \phi = 0,$$
$$\beta_T^* - \beta_T = \varepsilon\alpha_1\beta_T, \beta_C^* - \beta_C = \varepsilon\alpha_1\beta_C. \quad (17)$$

SIMILARITY TRANSFORMATIONS

It is clear that $y^* = y, \theta^* = \theta, \phi^* = \phi$ are invariant. Let us define them by

$$\eta = y,\ \theta = \theta(\eta),\ \phi = \phi(\eta). \tag{18}$$

The other invariants can be found by solving the following characteristic equations:

$$\frac{dx}{\alpha_1 x} = \frac{d\psi}{\alpha_1 \psi} = \frac{d\beta_T}{\alpha_1 \beta_T} = \frac{d\beta_C}{\alpha_1 \beta_C}. \tag{19}$$

Solving (18), we get the following absolute invariants (similarity transformations):

$$\psi = x f(\eta),\ \beta_T = \beta_{T_0} x,\ \beta_C = \beta_{C_0} x. \tag{20}$$

Here β_{T_0} and β_{C_0} are constant thermal and mass expansion coefficients, η is the similarity independent variable and $f(\eta)$ is the dimensionless stream function.ηf

SIMILARITY EQUATIONS

With the use of the definitions in Eqns. (18) and (20), Eqns. (7)-(10) reduce to the following similarity equations:

$$f''' - \alpha_0 f''\theta' + e^{\alpha_0 \theta}\left[ff'' - f'^2 + S^2 - (\Omega + M)(f' - S) + Gr\theta + Gc\phi \right] = 0,$$

$$\left[\frac{R + 1 + A\theta}{\Pr R}\right]\theta'' + A\theta'^2 + f\theta' - n f'\theta + Q\theta + Df\left(1 + Dc\phi\right)\phi'' + Df\, Dc\,\phi'^2 = 0, \tag{21}$$

$$(1 + Dc\phi)\phi'' + Dc\,\phi'^2 + Le\left[f\phi' - n f'\phi - K\phi + Sr(1 + Dc\phi)\theta'' \right] = 0. \tag{22}$$

The boundary conditions (10) yield:

$$\begin{aligned} &f(0) = 0,\ f'(0) = 1 + af''(0),\ \theta(0) = 1 + b\theta'(0),\ \phi(0) = 1, \\ &f'(\infty) - S = \theta(\infty) = \phi(\infty) = 0. \end{aligned} \tag{23}$$

Here $Gr = g\beta_{T_0} L\Delta T / c\sqrt{c\nu_\infty}$, $Gc = g\,\beta_{C_0} L\Delta C / c\sqrt{c\nu_\infty}$ are thermal and mass Grashof numbers respectively.

It is interesting to note that in the case of no-slip boundary conditions ($a = b = 0$) and in the case of the constant thermal conductivity and mass diffusivity ($A = Dc = 0$) we can recover the similarity solution reported by Abdel-Rahman (2010).

QUANTITIES OF ENGINEERING INTEREST

The quantities of interest are the friction factor $C_{f\bar{x}}$, local Nusselt number $Nu_{\bar{x}}$ and the local Sherwood number $Sh_{\bar{x}}$ respectively. These quantities can be conveniently calculated from the following relations:

$$C_{f\bar{x}} = \frac{\mu}{\rho \bar{u}_w^2}\left(\frac{\partial \bar{u}}{\partial \bar{y}}\right)_{\bar{y}=0}, Nu_{\bar{x}} = \frac{-\bar{x}}{T_w - T_\infty}\left(\frac{\partial T}{\partial \bar{y}}\right)_{\bar{y}=0}, Sh_{\bar{x}} = \frac{-\bar{x}}{C_w - C_\infty}\left(\frac{\partial C}{\partial \bar{y}}\right)_{\bar{y}=0}. \quad (24)$$

Substituting Eqns. (6), (18) and (20) into Eqn. (24), the physical quantities can be written as:

$$\sqrt{\mathrm{Re}_{\bar{x}}}\, C_{f\bar{x}} = \left[1 + A(1-\theta(0)\right] f''(0), \frac{Nu_{\bar{x}}}{\sqrt{\mathrm{Re}_{\bar{x}}}} = -\theta'(0), \frac{Sh_{\bar{x}}}{\sqrt{\mathrm{Re}_{\bar{x}}}} = -\phi'(0), \quad (25)$$

where $\mathrm{Re}_{\bar{x}} = \frac{u_w \bar{x}}{\nu}$ is the local Reynolds number.

RESULTS AND DISCUSSION

The similarity Eqns. (20)-(22) with boundary conditions in Eqn. (23) were solved numerically using the Runge-Kutta-Fehlberg fourth-fifth order numerical method in Maple 13 (White & Subramanian, 2010). The details of the method were described in a recent paper by Uddin *et al*. (2013). The effect of the controlling parameters on the dimensionless velocity, temperature, concentration, friction factor, heat transfer and mass transfer rates were investigated and presented in graphs. In the case of constant viscosity $\alpha_0 = 0$, constant thermal conductivity A = 0 and constant mass diffusivity (Dc = 0), the results of the skin friction factor, the rate of heat and mass transfer were compared with the published results for some special cases. The comparisons are given in Tables 1-3 and were found to have a good agreement.

Fig.2 illustrates the effect of the porosity and viscosity parameters on the diemsionless velocity. It was noticed that both the parameters reduced the dimensionless velocity. The numerical computations for these graphs were performed for and , which corresponded to assisting mixed convective flow. This (assisting flow) happens in many engineering applications such as cooling of electronic components and nuclear reactors. Fig.3 shows the influence of the radiation and thermal conductivity parameters on the dimensionless temperature. The dimensionless temperature decreased with the radiation parameter. It was further found that temperature increased with the increase in the thermal conductivity parameter. Physically increasing thermal diffusivity parameter means the increasing of the thermal conductivity of the fluid. Increasing thermal conductivity implies an increase in temperature. The effect of the thermal slip and heat generation parameters on the dimensionless temperature is shown in Fig.4. It was noticed that the temperature reduced with the increase of the thermal slip parameter. We also noticed that due to the increasing value of the generation parameter, the temperature increased. This was because physically, heat generation ( ) in the fluid will enhance thermal energy to the flow and hence, for a positive , temperature will rise. The effect of the mass diffusivity and Dufour number on the dimensionless temperature is shown in Fig.5. We observed from Fig.5 that the temperature enhances with improvements in the mass diffusivity parameter.

TABLE 1: Comparison of the Heat and Mass Transfer Rates Under Soret and Dufour Effects for Different Q when $R = 0.4$, K=0.6, α_0 - $Gr = Gc = M = a = 6 = A = Dc = 0$, $S = Le = \Pr = n = \Omega = 1$

Q	Sr	Df	$\sqrt{\mathrm{Re}_{\bar{x}}}\,Nu_{\bar{x}}$			$\sqrt{\mathrm{Re}_{\bar{x}}}\,Sh_{\bar{x}}$		
			Tsai et al. (2009)	Abdel Rahman (2010)	Present results	Tsai et al. (2009)	Abdel Rahman (2010)	Present results
0.0	2.0	0.03	0.6641	0.6636	0.66405	1.0726	1.0724	1.07262
	1.0	0.12	0.6403	0.6401	0.64030	1.2858	1.2856	1.28579
	0.5	0.30	0.5881	0.5876	0.58806	1.3941	1.3939	1.39409
	0.1	0.60	0.4972	0.4966	0.49716	1.4589	1.4588	1.45897
0.5	2.0	0.03	0.5518	0.551	0.55178	1.2070	1.2070	1.20707
	1.0	0.12	0.5254	0.5238	0.52544	1.3545	1.3546	1.35453
	0.5	0.30	0.4695	0.4687	0.46947	1.4293	1.4292	1.42938
	0.1	0.60	0.3749	0.3740	0.37486	1.4661	1.4660	1.46613
-0.5	1.0	0.03	0.7619	0.7616	0.76188	0.9499	0.9497	0.94992
	1.0	0.12	0.7403	0.740	0.74029	1.2231	1.2230	1.22313
	0.5	0.30	0.6911	0.6907	0.69107	1.3620	1.3618	1.36198
	0.1	0.60	0.603	0.6027	0.60303	1.4524	1.4523	1.45247

TABLE 2: Comparison of the Skin Friction, the Heat and Mass Transfer Rates for Different Values of M when $R = 0.4$, $K = 0.6$, $S = 0.5$, $Df = 0.12$, $\Pr = n = Le = 1$, α_0 = Gr=Gc=Ω=a=b=A=Dc=0

M	$\sqrt{\mathrm{Re}_{\bar{x}}}\,C_{f\bar{x}}$		$\sqrt{\mathrm{Re}_{\bar{x}}}\,Nu_{\bar{x}}$		$\sqrt{\mathrm{Re}_{\bar{x}}}\,Sh_{\bar{x}}$	
	Abdel Rahman (2010)	Present results	Abdel Rahman (2010)	Present results	Abdel Rahman (2010)	Present Results
1	0.8321	0.832126	0.5267	0.526593	1.2001	1.200041
3	1.0910	1.091021	0.5144	0.514332	1.1856	1.185622
5	1.2998	1.299798	0.5069	0.506775	1.1759	1.175899

TABLE 3 : Comparison of the Skin Friction, the Heat and Mass Transfer Rates for different Values of S when K= 0.6, R = 0.4, Df = 0.12, $\Pr = n = Le = Sr = 1$, α_0 = Gr =Gc = A = Dc =Ω = a = b = 0

S	$\sqrt{\mathrm{Re}_{\bar{x}}}\,C_{f\bar{x}}$			$\sqrt{\mathrm{Re}_{\bar{x}}}\,Nu_{\bar{x}}$			$\sqrt{\mathrm{Re}_{\bar{x}}}\,Sh_{\bar{x}}$		
	Tsai et al. (2009)	Abdel Rahman (2010)	Present	Tsai et al. (2009)	Abdel Rahman (2010)	Present	Tsai et al. (2009)	Abdel Rahman (2010)	Present
0.5	-0.6673	-0.6673	-0.6673	0.5368	0.5368	0.5367	1.2109	1.2109	1.2109
1.0	0	0.0132	0.0000	0.6403	0.6359	0.6403	1.2858	1.2835	1.2857
1.5	0.9095	0.8989	0.9095	0.7282	0.7258	0.7282	1.3653	1.3638	1.3653

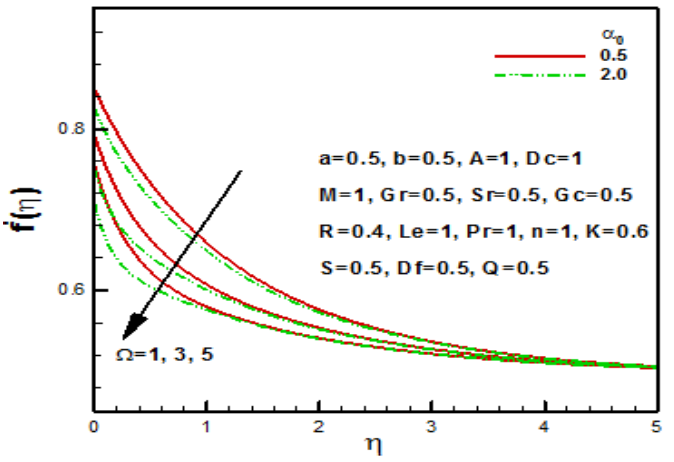

Fig.2: Effect of the porosity and viscosity parameters on dimensionless velocity.

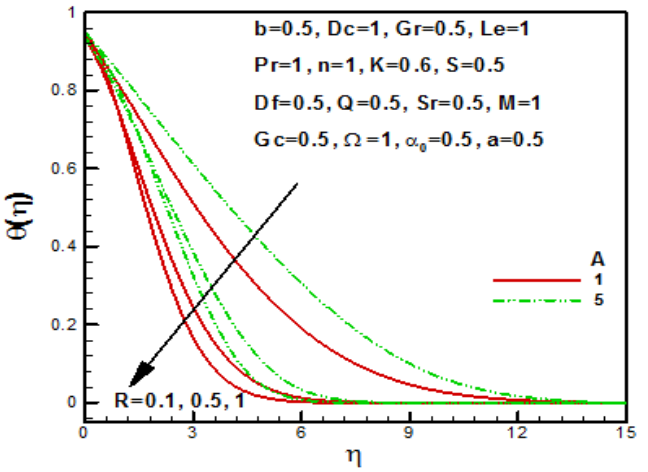

Fig.3: Effect of the radiation and thermal conductivity parameters on dimensionless temperature.

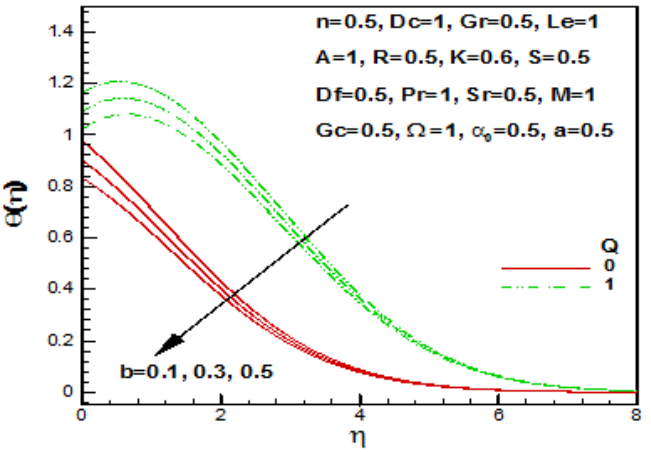

Fig.4: Effect of thermal slip and heat generation parameters on dimensionless temperature.

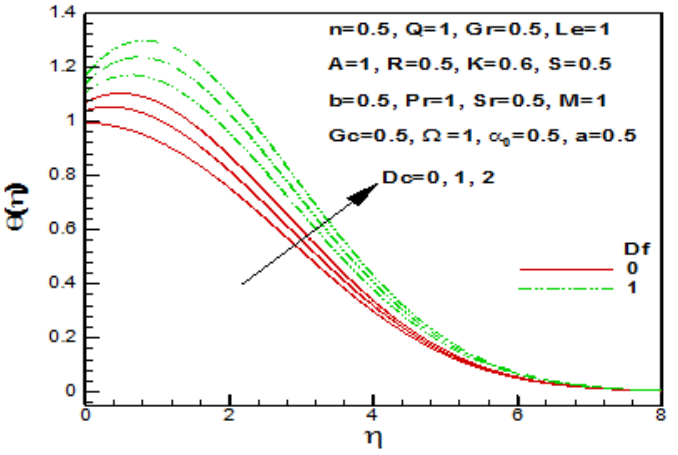

Fig.5: Effect of the Dufour and concentration diffusivity parameters on dimensionless temperature.

Fig.6 shows that the dimensionless concentration increased as the mass diffusivity parameter increased. This was due to the fact that an increase in the mass diffusivity parameter caused an increase in the mass diffusivity, which is a linear function of concentration. As a result, increasing mass diffusivity increased the concentration. This important finding was overlooked by all of the previous authors. Concentration variations due to Lewis number and Soret number are shown in Fig.7. It was observed that concentration as well as the concentration boundary layer thickness was increased as the Lewis number increases.

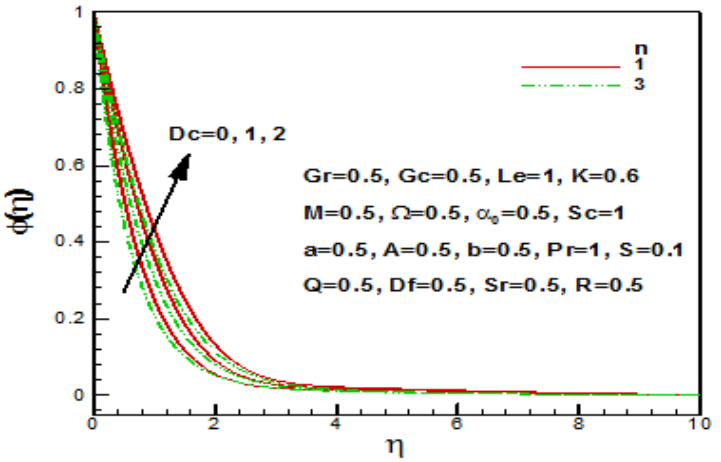

Fig.6: Effect of concentration diffusivity and power-law index parameters on dimensionless concentration.

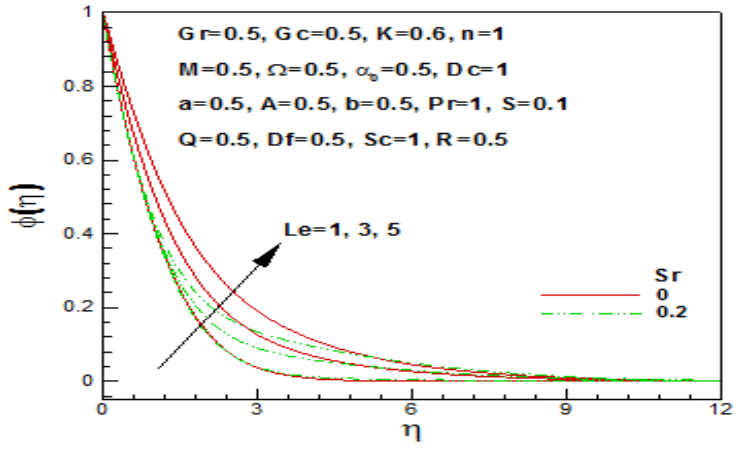

Fig.7: Effect of the Schmidt number and Soret number on dimensionless concentration.

The effect of different parameters on skin friction is illustrated in Fig.8 and Fig.9. It was observed from Fig.8 that skin friction was a decreasing function of the velocity slip parameter and the thermal and concentration Grashof number. This was due to the fact that in the presence of a magnetic field, the slip parameter increased the velocity at the surface, which reduced the friction. In this case, it was assumed that the viscosity was constant. Also, the decrease in the wall temperature and concentration decreased the thermal and concentration Grashof numbers, which helped in reducing the skin friction. The variation of the skin friction with magnetic field for different values of stretching and porosity parameters is illustrated in Fig.9. It was clear that the skin friction increased with an increase in the magnetic and porosity parameters. This was due to the fact that the magnetic field decreased the velocity at the surface, which increased the skin friction. Similarly, the increase in the porosity parameter reduced the velocity at the surface and as a result, the skin friction increased. It is important to note that the stretching of the plate increased the velocity and hence, decreased the skin friction.

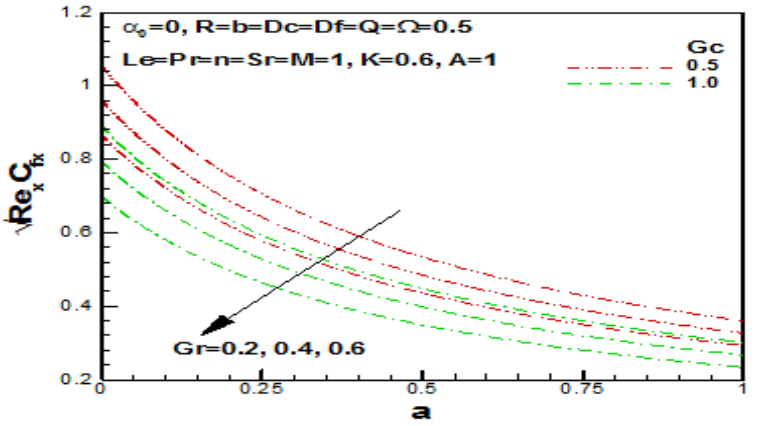

Fig.8: Effect of slip parameter and thermal and concentration Grashof numbers on skin friction.

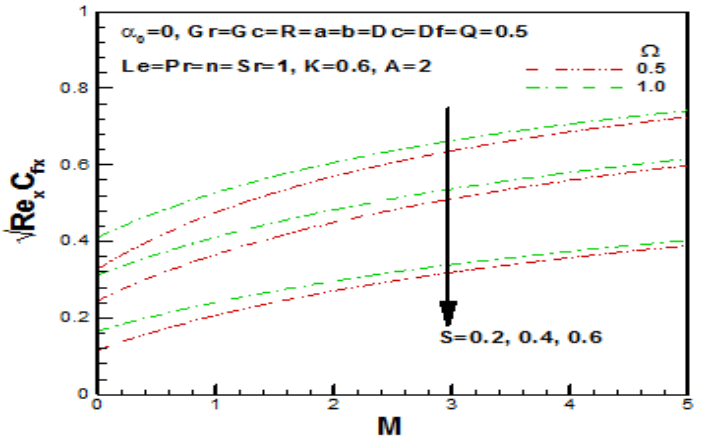

Fig.9: Effect of the magnetic, stretching and porosity parameters on skin friction.

The variation of the dimensionless heat transfer rates versus different parameters is depicted in Fig.10-12. Fig.10 reveals that the dimensionless heat transfer rate was a weak function of Soret and Dufour numbers. It was found that the dimensionless heat transfer rates decreased with an increase in the heat generation parameter. The variation of the dimensionless heat transfer rates versus the stretching parameter for different values of the power-law index and chemical reaction parameter is shown in Fig.11. Observe that the rate of heat transfer increased due to increases in the stretching, power-law index and chemical reaction parameters. The variation of the dimensionless heat transfer rates versus magnetic parameters for different values of the velocity slip and viscosity parameters is illustrated in Fig.12. We may see in Fugure 12 that the heat transfer rate increased for increasing values of slip and viscosity parameter whilst it decreased with increasing values of the magnetic field parameter.

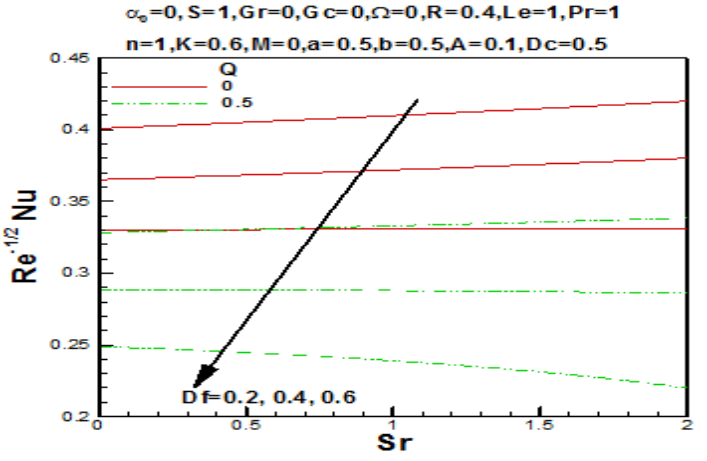

Fig.10: Variation of the dimensionless heat transfer rates versus Soret numbers for different Dufour numbers and heat generation parameters.

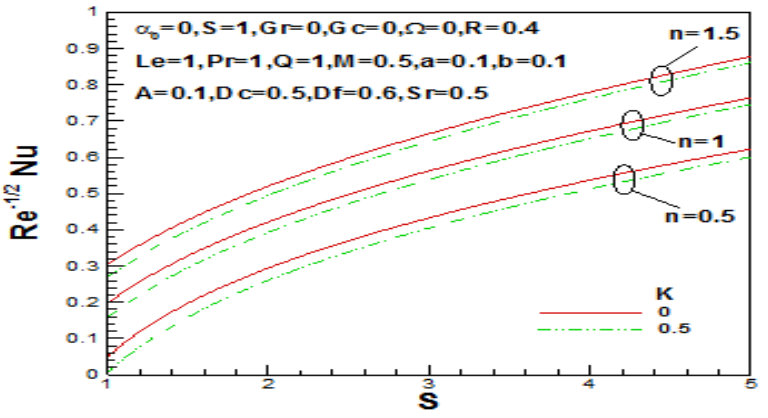

Fig.11: Variation of the dimensionless heat transfer rates versus stretching parameter for different power-law index and chemical reaction parameters.

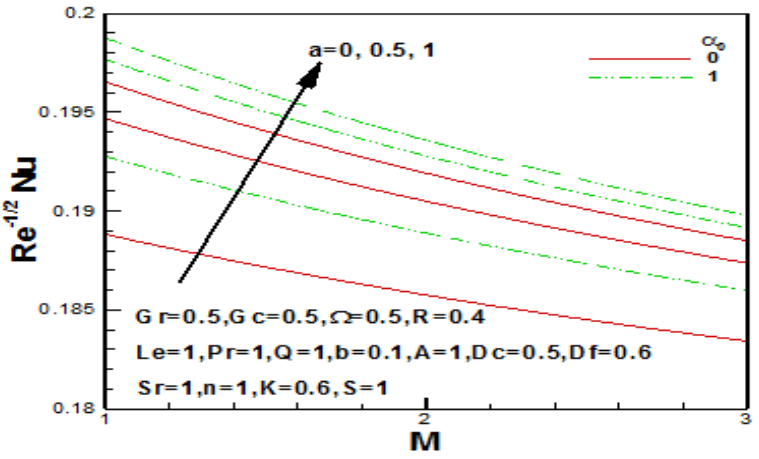

Fig.12: Variation of the dimensionless heat transfer rates versus magnetic parameter for different velocity slip and viscosity parameters.

The variation of the dimensionless mass transfer rates versus different parameters is depicted in Fig.13-15. Fig.13 exhibits that the rate of mass transfer rose with the rise in heat generation and the Dufour numbers but decreased as the value of the Soret number declined. It is important to note that in the absence of heat generation, dimensionless mass transfer rates decreased for small Dufour numbers and become almost constant for large Dufour numbers. But as heat generation increased, the dimensionless mass transfer rates started increasing with the increase in both Soret and Dufour numbers. We noticed from Fig.14 that the dimensionless mass transfer rates increased with the stretching parameter, power-law index and chemical reaction parameters. The variation of dimensionless mass transfer rates versus magnetic parameter for different values of velocity slip and viscosity parameters is shown in Fig.15. It was found that the mass transfer rate increased with the velocity slip and viscosity parameters.

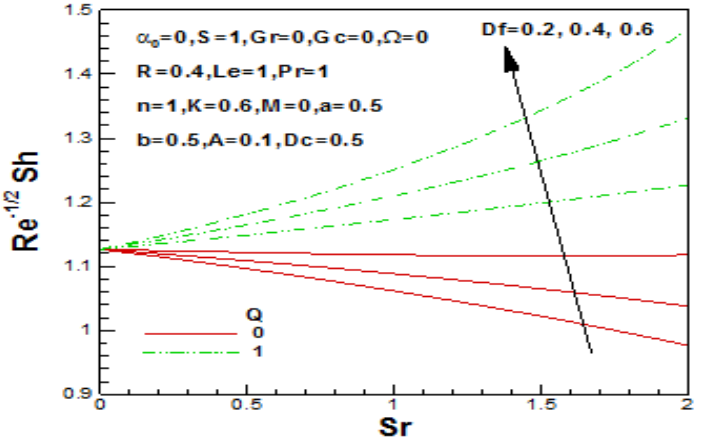

Fig.13: Variation of the dimensionless mass transfer rates versus Soret numbers for different Dufour numbers and heat generation parameters.

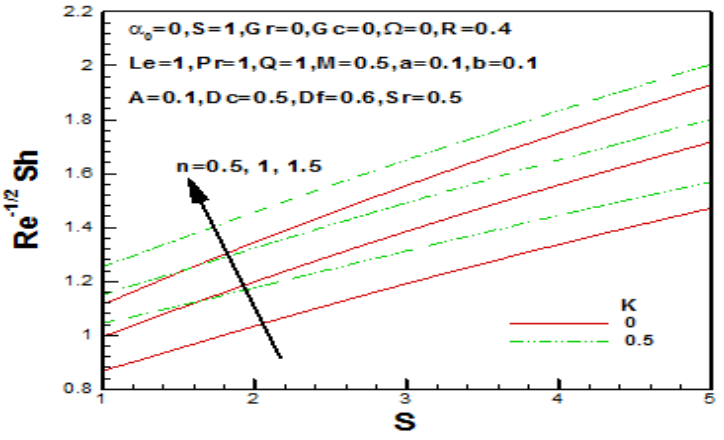

Fig.14: Variation of the dimensionless mass transfer rates versus stretching parameter for different power-law index and chemical reaction parameters.

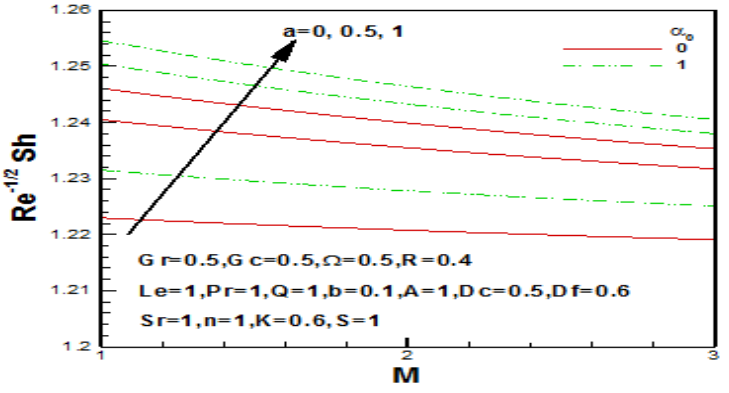

Fig.15: Variation of the dimensionless mass transfer rates versus magnetic parameter for different velocity slip and viscosity parameters.

CONCLUSION

The steady laminar boundary layer slip flow of a viscous incompressible Newtonian fluid along a moving stretching sheet immersed in a porous medium was studied numerically. The temperature- dependent viscosity and thermal conductivity and concentration-dependent mass diffusivity were taken into account. By using a scaling group transformation, the transport equations along with the boundary conditions were converted to similarity equations. From our analysis, we concluded that for some types of mixture (for example, H2-air) with the light and medium molecular weight, the magnetic field and the Soret and Dufour's effects with the variable mass diffusivity play an important role and should be taken into consideration as well.

REFERENCES

Abdel-Rahman, G. M. (2010). Thermal-diffusion and MHD for Soret and Dufour's effects on Hiemenz flow and mass transfer of fluid flow through porous medium onto a stretching surface. *Physica B, 405*, 2560-2569.

Aziz, A. (2010). Hydrodynamic and thermal slip flow boundary layers over a flat plate with constant heat flux boundary condition. *Communication in Nonlinear Science and Numerical Simulation, 15*, 573-580.

Crane, L. J. (1970). Flow past a stretching plate. *Zeitschrift für angewandte Mathematik und Physik ZAMP, 21*, 645-647.

Eckert, E. R., & Drake, R. M. (1972). *Analysis of heat and mass transfer.* New York: McGraw Hill.

Gifford, W. A. (2004). The effect of wall slip on the performance of flat extrusion dies. *Polymer Engineering. & Science, 41*, 1886-1892.

Hayat, T., Mustafa, M., & Pop, I. (2010). Heat and mass transfer for Soret and Dufour's effect on mixed convection boundary layer flow over a stretching vertical surface in a porous medium filled with a viscoelastic fluid. *Communication in Nonlinear Science and Numerical Simulation, 15,* 183-1196.

Ireland, P. M., & Jameson, G. J. (2009). Foam slip on surfaces of intermediate or low wettability. *Chemical Engineering Science, 64*, 3859-3867.

Ishak, A., Nazar, R., & Pop, I. (2009). Boundary layer flow and heat transfer over an unsteady stretching vertical surface. *Mecanica, 44,* 369-375.

Jiji, L. M. (2009). *Heat convection.* (2nd ed., Chapter 11). Springer, New York.

Khaled, A. R. A., & Vafai, K. (2004). Analysis of oscillatory flow disturbances and thermal characteristics inside fluidic cells due to fluid leakage and wall slip conditions. *Journal of Biomechanics, 37,* 721-729.

Lahjomri, J., & Oubarra A. (2013). Hydrodynamic and thermal characteristics of laminar slip flow over a horizontal isothermal flat plate. *ASME Journal of Heat Transfer, 135*(2), 021704.

Mansour, M. A., & El-Anssary, N. F., & Aly, A. M. (2008). Effects of chemical reaction and thermal stratification on MHD free convective heat and mass transfer over a vertical stretching surface embedded in porous media considering Soret and Dufour numbers. *Chemical Engineering Journal,145*, 340-345.

Nield, D. A., & Bejan, A. (2013). *Convection in porous media.* (4th ed.). New York: Springer.

Noghrehabadi, A., Pourrajab, R., & Ghalambaz, M. (2012). Effect of partial slip boundary condition on the flow and heat transfer of nanofluids past stretching sheet prescribed constant wall temperature. *International Journal of Thermal Sciences, 54,* 253-261.

Postelnicu, A. (2010). Heat and mass transfer by natural convection at a stagnation point in a porous medium considering Soret and Dufour effects. *Heat Mass Transfer, 46,* 831-840.

Seddeek, M. A. & Salem, A. M. (2005). Laminar mixed convection adjacent to vertical continuously stretching sheets with variable viscosity and variable thermal diffusivity. *Heat Mass Transfer, 41*, 1048-1055.

Seshadri R., & Na T. Y. (1985). *Group invariance in engineering boundary value problems*. Springer, New York, USA.

Tsai, R., & Huang, J. S. (2009). Heat and mass transfer for Soret and Dufour's effects on Hiemenz flow through porous medium onto a stretching surface. *International Journal of Heat Mass Transfer, 52*(9), 2399-2406.

Uddin, M. J., Ferdows, M., Be´g, O. A. (2013). Group analysis and numerical computation of magneto-convective non-Newtonian nanofluid slip flow from a permeable stretching sheet, *Applied Nanoscience, 4*(7), 897-910.

Uddin, M. J., Khan, W. A., & Ismail, A. I. M. (2012). Scaling group transformation for MHD boundary layer slip flow of a nanofluid over a convectively heated stretching sheet with heat generation. *Mathematical Problems in Engineering, 2012*, Article ID 934964, 20 pp.

Vajravelu, K., Prasad, K. V., Lee, J., Lee, C., Pop, I., Robert, A., & Van Gorder. (2011). Convective heat transfer in the flow of viscous Ag–water and Cu–water nanofluids over a stretching surface. *International Journal of Thermal Sciences, 50*(5), 843-851.

White, R. E., & Subramanian, V. R. (2010). *Computational methods in chemical engineering with maple*. New York: Springer

Pertanika J. Sci. & Technol. 24 (1): 71 - 87 (2016)

PERTANIKA JOURNALS

SCIENCE & TECHNOLOGY

Journal homepage: http://www.pertanika.upm.edu.my/

Morphological and Physico-Chemical Characteristics of Soils in the Tasik Chini Catchment in Pahang, Malaysia

Sujaul, I. M., Ismail, B. S.*, Tayeb M. A., Muhammad Barzani, G. and Sahibin, A. R.

School of Environmental and Natural Resource Sciences, Faculty of Science and Technology, Universiti Kebangsaan Malaysia, 43600 UKM, Bangi, Selangor, Malaysia

ABSTRACT

The morphological and physico-chemical properties of 11 soil series representing the major soil types in the Tasik Chini catchment in Pahang, Malaysia were studied. Soil types of the study area showed wide variations in their morphological and physico-chemical properties as a result of mean annual precipitation, soil parent material, vegetation and topography. Analyses showed that low values of silt were recorded in the horizon and the content of clay increased with soil depth. All the soil series contained low amounts of organic matter. Physical properties showed higher values for bulk density in the disturbed soils compared to the undisturbed forest soils. Regarding the chemical properties, these soils were strongly acidic. Electrical conductivity was also very low. Due to low pH, the contents of exchangeable base in all the soil types were very low. The cation exchange capacity of all the soil series were low with values less than 13.34 meq/100g soil.

Keywords: Soil series, morphology, physico-chemical properties, soil profile, Tasik Chini

INTRODUCTION

Soils are the essential components of the environment and foundation resources for nearly all types of land use, besides being the most important component of sustainable agriculture (Bech *et al*., 2008). Therefore, an assessment of soil quality and its direction of change with time is an ideal and primary indicator of sustainable agricultural land management (Doran, 2002). Soil quality indicators refer to the measurable soil attributes that influence the capacity of a soil to function within the limits imposed by the ecosystem, to preserve biological productivity and environmental quality and to promote plant, animal and human health (Arshad & Martin, 2002). These attributes could be physical, chemical and/or biological properties of the soil (Arshad & Martin, 2002; Doran, 2002; Zornoza *et al*., 2007).

Article history:
Received: 22 September 2014
Accepted: 30 July 2015

E-mail addresses:
sujaulbd@gmail.com (Sujaul, I. M.),
ismail@ukm.edu.my (Ismail, B. S.),
atayeb91@yahoo.com (Tayeb M. A.),
barzanigasim@unisza.edu.my (Muhammad Barzani, G.),
haiyan@ukm.edu.my (Sahibin, A. R.)
*Corresponding author

ISSN: 0128-7680

Any disturbing practice will lead to disruptions in the natural equilibrium of the soil, and the expression should be capable of reflecting this alteration. In addition, the climate (mainly temperature and precipitation) can have an important influence on soil properties and dynamics. Soil organic matter content is the result of the balance between inputs (litter and root exudates) and outputs (decomposition and leaching as soluble organic compounds) (Zornoza *et al*., 2007).

Soils are dramatically altered by human activity in agriculture and urban environments, and these alterations distinguish these soils from those in other systems and within urban environments (Scharenbroch *et al*., 2005). Research has enabled assessment of the unique physical, biological and chemical properties of urban soils. Specifically, urban soil bulk density, soil microbial biomass and activity and soil organic matter quantity and quality have been studied and found to be affected by urban conditions (Pouyat *et al*., 2002). Deforestation caused by logging, land conversion, road construction and other disturbances by human activities will invariably result in increased erosion rate with larger amounts of sediment being transported into the rivers, lakes, reservoirs and seas. Although erosion is an external process on the land surface, it is greatly accelerated by human activities, and it inundates and contaminates lakes with sediment. Heavy sedimentation rates shorten the lifespan of lakes and reservoirs, destroys aquatic habitats, reduces reservoir' storage capacity and reduces the flood control capacity of reservoirs (Alin & Cohen, 1999).

The recurring process of sedimentation has an impact on Tasik Chini i.e. shallower bottom, while the chemical influx from pesticides and fertilizer that come from agricultural activities increase the chemical concentration in water and sediment. Three characteristics of soil such as erodibility, heavy metal content and adsorption capability of chemical waste influence the degradation process.

The Tasik Chini catchment consists of various land forms comprising 31 soil series (Fig.1). Eleven soil series were selected for the study and they covered nearly 2741.52 ha or 41.10% of the study area. They were the Malacca, Prang, Gong Chenak, Serdang, Tebok, Kedah, Bungor, Kekura, Kuala Brang, Lating and Rasau series. The Malacca soil series is lateritic in nature, highly weathered, brown to reddish brown in colour and is distributed around the Chini Resort. Laterisation usually occurs when silicates are washed out, but the remaining sesquioxides of aluminium and iron accumulate and impart a deep red colour to the soil (Brady, 1990). The Rasau soil series is a weakly weathered soil, whitish in colour and has weakly developed profiles. The Kekura soil series is also a weakly weathered soil, grey in colour. Weathering is not intense and constitutes structural development. The Bungor soil series is a moderately weathered soil, yellowish brown in colour. The Kuala Bang series is a moderately weathered soil, bright reddish brown in colour. The Prang series is also a highly weathered soil, yellowish in colour. The Serdang, Gong Chenak, Tebok, Lating and Kedah series constitutes moderately weathered soils. These 11 soil series are scattered within the lake or around it (Fig.1). According to the USDA soil classification, the Malacca and Prang series belongs to Oxisols; the Bungor, Serdang, Tebok, Gong Chenak, Kedah, Lating and Kuala Brang to Ultisols and the Rasau and Kekura to Entisols. Elaborate studies and clear knowledge of the soil types around Tasik Chini including their characteristics are important in order to predict their potential physical and chemical impact on the quality of the lake water. The aim of this study was to identify the morphological and physico-chemical characteristics of the soil types in the Tasik Chini catchment area.

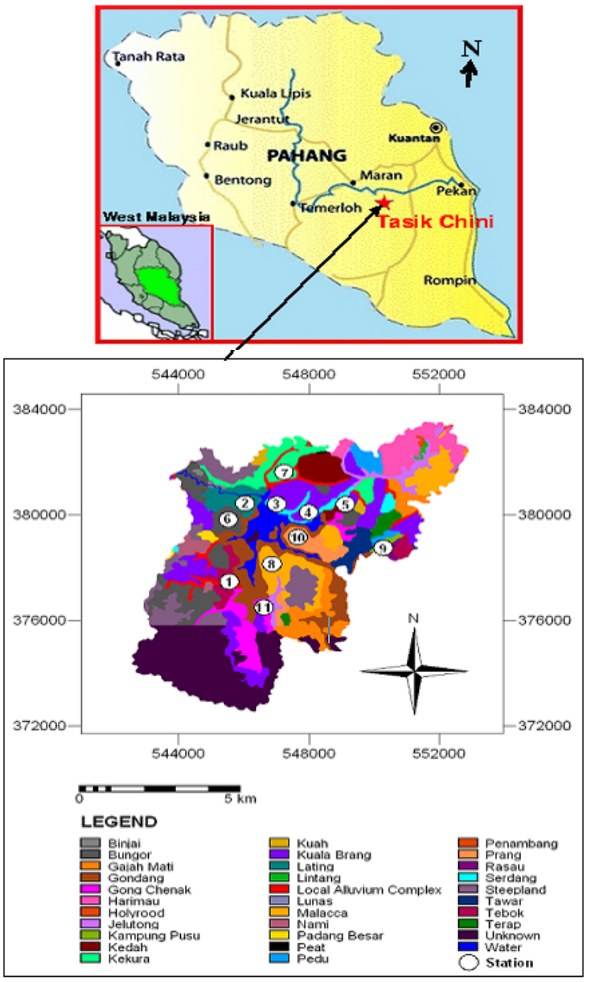

Fig.1: Location map of the study area and sampling stations.

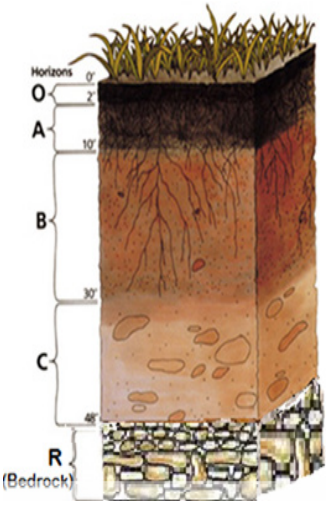

Fig.2: Soil profile

STUDY AREA

Tasik Chini is located in the southeastern region of the state of Pahang in Malaysia. It is approximately 100 km from Kuantan, the capital of Pahang. The lake system, which lies between 3°22′30″ to 3°28′00″N and 102°52′40″ to 102°58′10″E, is made up of 12 open water bodies called "laut" by the local people and it is linked to the Pahang River by the Chini River (Fig.1). A few communities of the indigenous Jakun tribe live around the lake. Tasik Chini is the second largest natural fresh-water lake in Malaysia encompassing 202 ha of open water and 700 ha of Riparian, Peat, Mountain and Lowland Dipterocarp forests (Wetlands International Asia Pacific, 1998). Tasik Chini is surrounded by diversely vegetated low hills and undulating land, which constitute the catchment of the region. There are three hilly areas surrounding the lake, namely, the Ketaya hills (209 m) located southeast, the Tebakang hills (210 m) to the north and the Chini hills (641 m) located southwest. The Tasik Chini catchment is representative of the upstream site of the Pahang River in the town of Pekan, Pahang. The area has a humid

tropical climate with two monsoon periods, characterised by the following bimodal pattern: southwest and northeast monsoons that bring an annual rainfall that varies from 1488 to 3071 mm. The mean annual rainfall is 2,500 mm and the temperature ranges from 21 to 32°C. The potential evapotranspiration (PE) is between 500 and 1000 mm.

MATERIALS AND METHODS

Soil Sampling and Morphological Description

Soil sampling was carried out at selected sampling sites located around the lake (Fig.1). Topsoil (0-20 cm) was collected randomly with a Dutch auger (five replicates). Approximately 500 g samples were collected from each sampling site. The soil at every sampling location was dug deep to expose the profile and complete profile descriptions were recorded. Soil samples were also taken from every identifiable horizon within the profile for laboratory analysis. Soil morphological description and soil sampling were done in accordance with the procedures of the Soil Survey Manual (Soil Survey Division Staff, 1993). Soil samples were sealed in plastic bags and transported to the laboratory. In the laboratory the samples were air dried, broken into smaller-sized particles with a wooden mortar and pestle and sieved through a 2-mm sieve.

Soil Analysis

The air-dried and sieved soil samples were used for determination of the physico-chemical characteristics, which included soil particle size distribution, density, organic matter (OM) content, exchangeable acid cations (Al and H), exchangeable basic cations (Ca, Mg, K and Na), cation exchange capacity (CEC), soil pH and electrical conductivity (EC). Particle size distribution was determined by the pipette method together with dry sieving (Abdulla, 1966). Texture of the soils was using the soil texture triangle. Soil bulk density was obtained using the open-ended metal cylinder (Ring) method (Rowell, 1996) and true density was calculated using the equation derived by Adams (1973). Porosity was calculated using the true and bulk densities. Organic matter content was obtained by weight loss on ignition (Ball, 1964). The pH of the soil was determined by the soil: water ratio of 1:2.5 (Metson, 1956). The exchangeable acid cations (Al and H) were obtained by titration with 1.0 M KCl extract (McLean, 1965). The exchangeable basic cations were obtained using 1.0 M ammonium acetate extract and the Flame Atomic Absorption Spectrophotometer (FAAS, model Perkin Elmer 3300) (Peech *et al*., 1947; Drohan & Sharpe, 1997). The cation exchange capacity was determined by summation of the acid and basic cations. The electrical conductivity was determined using a saturated gypsum extract (Massey & Windsor, 1967).

Statistical Analysis

Statistical analysis was performed using SAS software. Analysis of variance was performed on soil physical and chemical properties.

RESULTS AND DISCUSSION

Morphological Description

The profile description of the selected soil series was carried out based on hand specimens. The descriptions of the soil series are shown in Table 1.

TABLE 1 : Soil Series Profile Description

Soil Series	Horizon	Depth (cm)	Description
Tebok	A	0-10	Light grey (7.5Y7/1); clay; fine sub-angular blocky; non-sticky, non-plastic, very friable; many fine to coarse roots; clear smooth boundary.
	B	>10	Light grey (10Y8/2); clay; moderate to weak medium and fine sub-angular blocky; non-sticky, non-plastic, friable; common medium roots; clear smooth boundary.
Lating	A	0-8	Dull yellow orange (10YR6/3); heavy clay; strong coarse sub-angular blocky; slightly sticky, slightly plastic; friable; abundant medium and fine roots; clear smooth boundary.
	AB	8-20	Dull yellow orange (10YR6/4); heavy clay; moderate to weak, coarse sub-angular blocky; slightly sticky, slightly plastic; friable to firm; many medium roots; clear smooth boundary.
	BA	20-30	Bright yellowish brown (10YR6/6); heavy clay; moderate, coarse sub-angular blocky; slightly sticky, slightly plastic; firm; common medium roots; clear smooth boundary.
	B	>30	Bright yellowish brown (10YR7/6); heavy clay; moderate, coarse sub-angular blocky; slightly sticky; slightly plastic; firm; few medium roots; clear smooth boundary.
Serdang	A	0-20	Light yellow (2.5Y7/3); clay loam; weak, coarse and medium sub-angular blocky; friable; many fine and medium roots; gradual smooth boundary.
	B	>20	Light yellow (2.5Y7/4); clay loam; weak to moderate, coarse sub-angular blocky; friable; few fine and medium roots; diffuse smooth boundary.
Kuala Brang	A	0-12	Bright reddish brown (5YR5/6); clay; strong medium granular; friable; abundant fine roots, some medium and coarse roots; clear smooth boundary.
	B	>12	Bright reddish brown (5YR5/8); clay; weak coarse and very coarse sub-angular blocky; friable; few fine and medium roots; clear smooth boundary.
Kedah	A	0-8	Bright yellowish brown (10YR 6/6); clay loam; fine granular and weak to medium, very fine sub-angular blocky; loose to very friable; many small roots, many channels, few casts; many pores; distinct boundary.

TABLE 1 : (Continued)

	E	8-18	Bright yellowish brown (10YR6/8); clay loam; weak to moderate fine and medium sub-angular blocky; very friable; many small roots, many channels, common pores; diffuse boundary.
	B	18-30	Bright reddish brown (5YR5/6); clay loam; moderate to weak, fine and medium sub-angular blocky; friable to firm; few roots, common channels, common pores; distinct and irregular boundary.
	C	>30	Bright reddish brown (5YR5/8); clay loam; weak fine and medium sub-angular blocky; friable to firm; roots rare, few channels, common pores; unconsolidated material, little evidence of profile development- stones increasing with depth.
Bungor	A	0-21	Yellowish brown (2.5Y5/4); clay loam; very weak to moderately developed fine and medium sub-angular blocky; friable to firm; many fine and medium roots; few channels, high biological activities, worm casts common; diffuse boundary.
	B	>21	Yellowish brown (2.5Y5/6); silty clay loam; weak, medium and fine sub-angular blocky; friable; moderate biological activities, few fine roots, few channels; diffuse smooth boundary.
Kekura	A	0-10	Grey (7.5Y 6/1); sandy loam; moderate to strong, fine and medium sub-angular blocky; friable to slightly firm; many fine and medium roots; numerous pores due to ant activities; gradual boundary
	AB	10-18	Light grey (10Y8/1); sandy loam; moderate, medium and fine sub-angular blocky; friable to slightly firm; many fine and medium roots, few ant activities; diffuse boundary.
	BA	18-29	Light grey (10Y8/2); sandy loam; weak to moderate, coarse and medium sub-angular blocky; friable; many medium and some fine roots; diffuse boundary.
	B	>29	Pale Yellow (7.5Y8/3); sandy clay loam; weak to moderate, coarse and medium sub-angular blocky; friable; few medium and fine roots; abrupt boundary.
Malacca	A	0-10	Yellowish brown (10YR5/4); clay; weak, fine sub-angular blocky; friable; many fine and medium roots; few ant nests; abundant pores; clear smooth boundary.
	B	>10	Yellowish red (5YR5/6); clay; weak medium and fine sub-angular blocky; friable; many fine and medium roots, few ant nests; many pores, abrupt smooth boundary.
Rasau	A	0-8	Whitish (10YR8/1); sandy loam; medium and fine sub-angular blocky; very friable; many coarse and medium roots; clear and smooth boundary.

TABLE 1 : (Continued)

	AB	8-20	Light brownish grey (2.5Y6/2); sandy loam; medium and fine sub-angular blocky; friable; many coarse and medium roots; clear smooth boundary.
	BA	20-30	Pale yellow (2.5Y8/3); sandy loam; moderate, medium and fine sub-angular blocky; friable; many coarse and medium roots; smooth boundary.
	B	>30	Pale yellow (2.5Y8/3); sandy loam; moderate to weak, medium and fine sub-angular blocky; friable; few medium and fine roots; smooth boundary.
Prang	A	0-15	Dark reddish brown (5YR3/4); clay; weak, fine sub-angular blocky; very friable; many fine and few coarse roots; many fine pores; diffuse boundary.
	B	>15	Yellowish red (5YR4/6); clay; weak, fine sub-angular blocky; very friable; few medium roots; many fine pores; diffuse smooth boundary.
Gong Chenak	A	0-10	Dark brown (10YR 4/3); clay; moderate, medium sub-angular blocky; non-sticky, non-plastic; friable; few fine roots; clear smooth boundary.
	AB	10-18	Brownish yellow (10YR6/8); clay; moderate, coarse sub-angular blocky; non-sticky, non-plastic; friable to firm, no roots; clear smooth boundary.
	BA	18-30	Brownish yellow (10YR6/8) with common medium clear red (10YR4/8); clay; moderate, coarse sub-angular blocky; non-sticky, non-plastic; friable; no roots; clear smooth boundary.
	B	>30	Light grey (10YR7/1) with many medium clear red (10YR4/8); clay; non-sticky, non-plastic; friable; no roots; clear smooth Boundary.

Soil texture. Sand was dominant in the Serdang, Kuala Brang, Rasau and Kekura soil series, ranging from 46.10 to 48.95%, 34.84 to 43.81%, 53.90 to 56.28% and 58.87 to 62.79%, respectively. The Malacca and Gong Chenak series had low levels of sand that ranged from 14.17 to 19.40% and 15.07 to 26.14%, respectively. On the other hand, the Lating series had the lowest level of sand that ranged from 2.02 to 3.48% both in the top soil and at the different horizons. Coarse sand was present in most of the soil types except at the lower horizons of the Lating series and the laterite nodules of the Malacca series. Size distribution and texture of the different soil series are shown in Table 2.

The percentage of silt in the Tebok, Lating, Serdang, Kuala Brang, Kedah, Bungor, Kekura, Malacca, Rasau, Prang and Gong Chenak soil series are shown in Table 2. The highest percentage (46.49%) of silt was recorded in the Kedah series and the lowest (17.71%) in the Kuala Brang soil series. Low levels of silt were recorded in the horizon and maximum levels were found in the topsoil. Khresat *et al*. (1998) emphasised that the proportion of silt decreased with the depth of the horizon in soils in north-western Jordan.

TABLE 2 : Properties, Size Distribution and Texture of Topsoils and Subsoils

Station	Soil Series	Horizon	Depth (cm)	Sand %	Silt %	Clay %	Texture
1	Tebok	A	0 – 10	25.53	29.04	45.43	Clay
		B	> 10	23.08	30.18	46.74	Clay
Top soil (Mean of 5 replications)			0 – 20	28.03	31.52	40.45	Clay
2	Lating	A	0 – 8	3.48	37.14	59.38	Clay
		AB	8 – 20	3.02	34.96	62.02	Clay
		BA	20 – 30	2.65	30.51	66.84	Clay
		B	> 30	2.02	19.39	78.59	Clay
Top soil (Mean of 5 replications)			0 – 20	3.28	31.58	65.14	Clay
3	Serdang	A	0 – 20	48.95	31.10	19.95	Clay loam
		B	> 20	46.10	32.26	21.64	Clay loam
Top soil (Mean of 5 replications)			0 – 20	47.91	31.51	20.58	Clay loam
4	Kuala Brang	A	0 – 12	43.81	17.71	38.48	Clay
		B	> 12	34.84	23.43	41.73	Clay
Top soil (Mean of 5 replications)			0 – 20	41.22	22.22	36.56	Clay
5	Kedah	A	0 – 8	32.71	46.21	21.08	Clay loam
		E	8 – 18	25.84	46.47	27.69	Clay loam
		B	18 – 30	24.88	44.91	30.21	Clay loam
		C	> 30	20.23	39.76	40.01	Clay loam
Top soil (Mean of 5 replications)			0 – 20	27.12	46.49	26.39	Clay loam
6	Bungor	A	0 – 21	37.23	36.80	25.97	Clay loam
		B	> 21	33.89	37.05	29.06	Clay loam
Top soil (Mean of 5 replications)			0 – 20	36.08	36.87	27.05	Clay loam
7	Kekura	A	0 – 8	61.29	23.35	15.36	Sandy loan
		AB	8 – 18	61.21	22.59	16.20	Sandy loam
		BA	18 – 29	60.32	22.21	17.47	Sandy loam
		B	> 29	58.87	22.95	18.18	Sandy loam
Top soil (Mean of 5 replications)			0 – 20	62.79	23.28	13.93	Sandy loan
8	Malacca	A	0 – 10	18.16	35.97	45.87	Clay
		B	> 10	14.17	36.80	49.03	Clay
Top soil (Mean of 5 replications			0 – 20	19.40	30.82	49.78	Clay
9	Rasau	A	0 – 8	55.13	31.39	13.48	Sandy loam
		AB	8 – 20	56.28	29.91	13.81	Sandy loam
		BA	20 – 30	53.90	30.70	15.40	Sandy loam
		B	> 30	54.14	30.32	15.54	Sandy loam
Top soil (Mean of 5 replications)			0 – 20	58.44	28.00	13.56	Sandy loam

TABLE 2 : (Continued)

10	Prang	A	0 – 15	42.13	20.21	37.66	Clay
		B	> 15	33.15	24.46	42.39	Clay
Top soil (Mean of 5 replications)			0 – 20	34.56	25.09	40.35	Clay
11	Gong Chenak	A	0 – 10	26.14	24.05	49.81	Clay
		AB	10 – 18	23.45	24.36	52.19	Clay
		BA	18 – 30	18.02	27.08	54.90	Clay
		B	> 30	15.07	28.05	56.88	Clay
Top soil (Mean of 5 replications)			0 – 20	21.84	24.88	53.28	Clay

Clay content was variable in the studied soils. The highest percentage (78.59%) of clay was recorded in the Lating and the lowest (13.48%) in the Rasau soil series. The Rasau and Kekura series contained low levels of clay while the Tebok, Lating, Kuala Brang, Malacca, Prang and Gong Chenak had higher percentages. The distribution of clay increased with depth in the soil. There was higher clay content in the subsoil compared to the surface soil for all the soils studied. Khresat *et al*. (1998) also concluded that clay content in Pedon increased from 35.40% at the surface to 44.80% below 170 cm depth in the soil in north-western Jordan.

Physical properties of the soils studied. The physical properties of the soils are given in Table 3. All the soil series studied contained low amounts of organic matter (OM). The highest values of OM were recorded in the Lating, Kuala Brang, Malacca, Prang and Gong Chenak soil series, which ranged from 1.12 to 9.34%. These soils were clayey in texture. The distribution of OM was found to decrease with depth of horizon in the soil. High OM in the topsoil was due to decomposition of massive leaf litter, which was observed on the surface. The OM content was the lowest in the sandy soils, such as the Rasau and Kekura soils. Similar results have also been reported by Othman *et al*. (1979) where OM in sandy soils ranged from 0.49 to 1.56%. Due to intensive weathering and erosion in Malaysia, all the soil series studied contained less than 10% organic matter in the soil. According to the classification of Acres *et al*. (1975), OM in the studied soils was categorised in the low to medium class (OM< 10%).

The bulk density values of the 11 soil series ranged from 1.03 to 1.33 g/cm^3 with a mean value of 1.13 g/cm^3. The highest (1.33 g/cm^3) and lowest values (1.03 g/cm^3) were recorded in the Rasau and Prang series, respectively. The bulk densities of topsoil were always lower than those of the subsoil, due to the presence of organic matter. Lemenih *et al*. (2005) indicated that the significant increase in soil bulk density and decrease in percent pore space in the soil was most probably caused by the decline in the soils' organic matter content. Due to the sandy loam texture and low organic matter content in the Rasau and Kekura series, the bulk density values were high. On the other hand, the Lating, Kuala Brang, Prang, Bungor and Gong Chenak soil series were under primary forest and lowland dipterocarp forest vegetation, which apparently resulted in higher content of organic matter and high root penetration. Moreover, the bulk density was lower than that of the Rasau and Kekura soil series. The reported value was close to the one reported by Peh (1978) for soils in a dipterocarp forest at Pasoh Forest Reserve in which the OM recorded was 1.12 g/cm^3. Kamaruzaman (1987) also reported a lower bulk density (0.97 g/cm^3) for undisturbed soils at the Tekan Forest Reserve in Pahang, Malaysia.

TABLE 3 : Physical Properties of Topsoil's and Profiles of 11 Soil Series

Station	Soil Series	Horizon	Depth (cm)	Bulk Density (g/cm^3)	True Density (g/cm^3)	Porosity %
1	Tebok	A	0 – 10	1.07	2.60	58.85
		B	> 10	1.15	2.66	56.77
Top Soil (Mean of 5 replications)			0 – 20	1.08±0.01	2.62±0.01	59.00±0.160
2	Lating	A	0 – 8	1.06	2.54	58.27
		AB	8 – 20	1.09	2.62	58.40
		BA	20 – 30	1.11	2.64	57.96
		B	> 30	1.14	2.65	56.98
Top Soil (Mean of 5 replications)			0 – 20	1.04±0.05	2.56±0.04	59.23±1.15
3	Serdang	A	0 – 20	1.26	2.72	53.68
		B	> 20	1.32	2.73	51.65
Top Soil (Mean of 5 replications			0 – 20	1.13±0.02	2.67±0.01	57.80±0.80
4	Kuala Brang	A	0 – 12	1.07	2.59	58.69
		B	> 12	1.09	2.60	58.08
Top Soil (Mean of 5 replications)			0 – 20	1.03±0.03	2.56±0.02	59.55±0.75
5	Kedah	A	0 – 8	1.09	2.67	59.20
		E	8 – 18	1.10	2.70	59.24
		B	18 – 30	1.11	2.71	58.96
		C	> 30	1.12	2.72	58.75
Top Soil (Mean of 5 replications)			0 – 20	1.09±0.01	2.64±0.02	58.58±0.28
6	Bungor	A	0 – 21	1.09	2.62	58.40
		B	> 21	1.12	2.64	57.58
Top Soil (Mean of 5 replications)			0 – 20	1.09±0.01	2.65±0.01	58.75±0.30
7	Kekura	A	0 – 8	1.14	2.70	57.83
		AB	8 – 18	1.17	2.73	57.06
		BA	18 – 29	1.19	2.73	56.39
		B	> 29	1.21	2.74	55.76
Top Soil (Mean of 5 replications)			0 – 20	1.21±0.03	2.68±0.01	55.03±1.24
8	Malacca	A	0 – 10	1.09	2.56	57.37
		B	> 10	1.13	2.60	56.54
Top Soil (Mean of 5 replications)			0 – 20	1.12±0.10	2.56±0.02	56.13±3.52
9	Rasau	A	0 – 8	1.19	2.70	56.04
		AB	8 – 20	1.27	2.72	53.25
		BA	20 – 30	1.33	2.73	51.40
		B	> 30	1.27	2.73	53.60
Top Soil (Mean of 5 replications)			0 – 20	1.06±0.03	2.69±0.01	57.5±1.40

TABLE 3 : (Continued)

10	Prang	A	0 – 15	1.06	2.57	58.75
		B	> 15	1.08	2.61	58.62
Top Soil (Mean of 5 replications)			0 – 20	1.03±0.05	2.52±0.02	59.18±2.37
11	Gong Chenak	A	0 – 10	1.06	2.57	58.81
		AB	10 – 18	1.07	2.61	59.15
		BA	18 – 30	1.09	2.70	58.15
		B	> 30	1.12	2.71	58.64
Top Soil (Mean of 5 replications)			0 – 20	1.06±0.05	2.51±0.16	59.49±2.30

Hati *et al*. (2007) and Tiarks *et al*. (1974) noted that the reduction in bulk density could be attributed to higher organic matter content of the soil.

The true density values of the 11 soil series ranged from 2.51 to 2.74 g/cm^3 with an average value of 2.65 g/cm^3. Due to higher content of being sand and lower organic matter content, the highest value of true density recorded (2.74 g/cm^3) was for the Kekura soil series. The Gong Chenak series had the lowest true density value (2.51 g/cm^3). Clearly, the amount of organic matter in a soil markedly affected the particle density (Brady, 1990). Porosity values ranged from 51.40 to 59.55% with an average value of 57.42%. The highest value (59.55%) was recorded in the Kuala Brang series and the lowest (51.40%) in the Malacca soil series. The highest total porosity occurred on undisturbed forest soils of the Kuala Brang, Kedah, Lating, Tebok, Prang, Bungor and Gong chenak soils series. The Malacca soil series was disturbed soil and had the lowest porosity value. The Malacca soil series was distributed throughout the oil palm plantation area. Porosity of the surface soil was slightly higher than that of the subsoil. Pagliai *et al*. (1983) noted that porosity was directly affected by root penetration, storage and movement of water and gases. Lower porosity values in disturbed soils have also been reported by Pagliai *et al*. (1983) and Pagliai (1987).

Chemical properties of the studied soil series. The data on specific chemical properties of the studied soils are given in Table 4. The uniformity of pH values and the low range recorded were the unique features of Malaysian soils. The pH values ranged from 3.14 to 4.82 with an average value of 4.04. Most of the pH values were below 4.50 and were considered very low (pH < 4.50) in the classification by Landon (1991). The value was normal for forest soils where the weathering and leaching processes occur continuously in addition to the decomposition of organic matter effect. Most profiles showed a slight increase in the pH values down the profile, with the exception of the Prang and Gong Chenak soil series. Zhenghu *et al*. (2007) found that soil pH values increased slightly with depth in the profile, indicating that they experienced moderate leaching and weathering. Low range of electrical conductivity (EC) was recorded in the different soil series. The Malacca series had the lowest value (2.00 dS/m) while the highest value (3.32 dS/m) was recorded for the Kekura series. The mean value of EC was 2.67 dS/m. The values of EC were below 4.00 dS/m, indicating that these soils were not saline. The EC ranged from 2.00 to 3.32 dS/m, and these values were classified as low (Landon, 1991).

TABLE 4 : Chemical Properties of the 11 Soil Series Studied

Station	Soil Series	Horizon	Depth (cm)	OM %	pH	EC dS/m	CEC (cmol c/ kg)
1	Tebok	A	0 – 10	5.93	3.89	3.25	6.28
		B	> 10	3.72	4.27	3.11	8.28
Top Soil (Mean of 5 replications)			0 – 20	6.93±0.20	4.25±0.05	2.70±0.03	6.97±0.52
2	Lating	A	0 – 8	8.09	4.29	2.96	6.50
		AB	8 – 20	5.17	4.36	2.93	6.63
		BA	20 – 30	4.31	4.45	2.78	7.79
		B	> 30	3.88	4.48	2.66	8.62
Top Soil (Mean of 5 replications)			0 – 20	7.26±3.43	4.35±0.05	2.45±0.05	7.97±1.05
3	Serdang	A	0 – 20	1.68	4.38	3.18	4.09
		B	> 20	1.17	4.49	3.15	5.12
Top Soil (Mean of 5 replications)			0 – 20	3.36±0.13	4.27±0.08	2.70±0.02	4.10±0.47
4	Kuala Brang	A	0 – 12	6.23	4.48	2.88	5.54
		B	> 12	5.88	4.53	2.85	5.69
Top Soil (Mean of 5 replications)			0 – 20	7.35±0.78	4.41±0.09	2.44±0.02	5.02±0.87
5	Kedah	A	0 – 8	3.27	4.32	3.17	6.05
		E	8 – 18	2.34	4.41	3.11	7.12
		B	18 – 30	2.13	4.43	3.08	7.91
		C	> 30	1.78	4.49	3.05	9.70
Top Soil (Mean of 5 replications)			0 – 20	4.48±0.66	4.32±0.03	2.56±0.03	7.60±1.33
6	Bungor	A	0 – 21	5.09	4.72	3.12	4.37
		B	> 21	4.36	4.78	3.01	3.90
Top Soil (Mean of 5 replications)			0 – 20	3.95±0.47	4.80±0.09	2.54±0.04	4.34±0.63
7	Kekura	A	0 – 8	2.19	4.56	3.32	2.58
		AB	8 – 18	1.46	4.57	3.29	2.46
		BA	18 – 29	1.34	4.58	3.26	2.47
		B	> 29	1.14	4.59	3.18	2.56
Top Soil (Mean of 5 replications)			0 – 20	2.90±0.19	4.82±0.04	2.55±0.04	2.47±0.37
8	Malacca	A	0 – 10	7.36	3.47	2.18	1.96
		B	> 10	5.63	3.81	2.00	2.06
Top Soil (Mean of 5 replications)			0 – 20	7.16±0.96	3.68±0.09	2.24±0.16	3.47±0.60
9	Rasau	A	0 – 8	2.35	3.14	2.55	3.12
		AB	8 – 20	1.77	3.15	2.44	3.37
		BA	20 – 30	1.10	3.21	2.42	2.75
		B	> 30	1.37	3.25	2.45	2.54
Top Soil (Mean of 5 replications)			0 – 20	2.76±0.38	3.20±0.15	2.21±0.12	3.74±0.34

TABLE 4 : (Continued)

10	Prang	A	0 – 15	6.69	3.32	2.03	2.23
		B	> 15	5.10	3.22	2.02	1.08
Top Soil (Mean of 5 replications)			0 – 20	8.73±0.85	3.31±0.07	2.11±0.14	2.72±0.19
11	Gong Chenak	A	0 – 10	6.75	3.34	2.13	12.81
		AB	10 – 18	5.10	3.35	2.05	13.34
		BA	18 – 30	1.12	3.37	2.22	5.79
		B	> 30	2.03	3.30	2.30	6.09
Top Soil (Mean of 5 replications)			0 – 20	9.34±6.29	3.32±0.16	2.22±0.16	11.27±2.78

The values for the cation exchange capacity (CEC) of the studied soils ranged from 1.08 to 13.34 cmol c/kg soil, with an average value of 5.36 cmol c /kg soil. The values of the CEC of all the top soils were comparatively higher than those down the soil profiles (Table 4). Zhenghu *et al*. (2007) found that the cation exchange capacity (CEC) was higher on the surface than in the subsurface horizons and decreased with depth in all the studied soils. This was due to the effect of the higher organic matter content in the surface and the correlation between organic matter and CEC. The CEC of the Gong Chenak soil series was the highest (13.34 cmol c /kg soil) and that of the Prang series the lowest (1.08 cmol c /kg soil). Due to low pH, the contents of basic cations of all the soils were very low, indicating that the exchange cations in surface soil were dominated by acidic cations like Al and H. The soil of the Rasau series was sandy loam in texture but the CEC was higher compared to those obtained from the Prang and Malacca (clay in texture) soil series. Apparently the Rasau soil had low pH and was dominated by acidic cations of Al and H (3.00 cmol c /kg soil) as opposed to the Malacca (1.65 cmol c /kg soil) and Prang (1.90 cmol c /kg soil) soil series. Razi *et al*. (2005) also reported similar characteristics of acidic soils in their studied area. The range of the CEC values of all the soil series studied were considered low in the classification by Acres *et al*. (1975). In Peninsular Malaysia, more than two thirds of the total land area are covered by acidic soils, of which Ultisols and Oxisols are the most abundant (IBSRAM 1985). Ultisols and Oxisols are soils with low pH, cation exchange capacity and basic cation content (Tessens & Shamshuddin, 1983; Ismail *et al*., 1993; Syed Omar *et al*., 2001). The highly weathered soil materials, having kaolinitic clay mineralogy, showed very low CEC of up to 4 cmol c /kg soil and sum of exchangeable basic cations of <2 cmol c /kg soil (Baert *et al*., 1999).

Correlation Study

The soil erodibility factor (K) represents the effect of soil properties and soil profile characteristics on soil loss in the Tasik Chini catchment area. The physical, chemical and mineralogical soil properties and their interactions that affect the K values are varied, the reason being mainly geogenic.

Anthropogenic activities also affect the principal component of soil in this area. In recent years, Tasik Chini has experienced major development in agricultural activities. Large areas of forest have been converted into oil palm plantations. Illegal logging activities also contributed

to the loss of forest area. Agricultural activities resulted in the release of pollutants such as nitrate and phosphate into the soil. Mining activity was the most important man-made reason for soil degradation. Different types of minerals were exposed to the soil surface due to mining, which directly affected the principal soil component. The activities of a few of the indigenous people who live in Tasik Chini also played some role in soil degradation.

CONCLUSION

A detailed study of the morphology and physico-chemical characteristics of a soil is essential in order to understand the behaviour of the soil. The soils in the study area were well weathered and leached. The Malacca and Prang series was highly weathered soils and clayey in texture. The Kuala Brang, Tebok, Lating and Gong Chenak series was moderately weathered soil and clayey in texture. The Kedah, Bungor and Serdang series was also moderately weathered soil but had a clay loam texture. The Rasau series constituted weakly weathered soil with a sandy loam texture. The clay content of all the soil series increased with depth. The highest total porosity occurred in the undisturbed forest soils of the Bungor, Tebok, Lating, Kuala Brang, Prang, Gong Chenak and Kedah series. The lowest total porosity was recorded on the logged soils such as the Malacca, Serdang, Kekura and Rasau series. The present study revealed that all the soil series contained low organic matter content and were highly porous. The distribution of OM decreased with depth. Low values of OM (1.10%) were recorded in the Rasau series and the highest percentage OM (9.34%) was recorded in the Gong Chenak series. The studied soils had acidic pH, low cation exchange capacity and low exchangeable bases. Due to the dominance of acidic cations (Al and H), the CEC of the Rasau series was higher than that of the Malacca and Prang soil series. The Gong Chenak soil was less leached and had higher values for most of the properties considered in the study. The study also indicated that supply of organic matter to the soils and plantations is important in order to increase both the soil OM content and the cation exchange capacity. Productivity of soils depends not only on the plant nutrient stored but also on the physical characteristics of the soils such as bulk density and porosity. Soil properties, such as particle-size distribution, structural stability, organic matter content, soil chemistry and clay mineralogy, affect soil degradation. Mining and deforestation are the main causes of soil degradation and environmental problems in the Tasik Chini catchment area.

ACKNOWLEDGEMENTS

This study was conducted and supported by the Ministry of Science and Technology, Malaysia through the IRPA grant, code: 09-02-02-0117-EA294, Zamalah Scheme and OUP fund (Code: UKM-OUP-FST-2008) UKM.

REFERENCES

Abdulla, H. H. (1966). *A study on the development of podzol profile in Dovey Forest*. (PhD thesis). University of Wales, United Kingdom.

Acres, B. D., Bower, R. P., Borrough, P. A., Folland, C. J., Kalsi, M. S., Thomas, P., & Wright, P. S. (1975). *The soils of Sabah. Volume 1. Classification and description*. Land Resource Study No. 20. Land Resource Division, Ministry of Overseas Development, England.

Adams, W. A. (1973). The effect of organic matter on the bulk and true densities of some uncultivated podzolic soils. *Journal of Soil Science, 24*(1), 10-17.

Alin, S., & Cohen, A. (1999). Effect of landscape disturbance on animal communities in Lake Tanganyika, East Africa. *Conservation Biology, 13*(5), 1017-1028.

Arshad, M. A., & Martin, S. (2002). Identifying critical limits for soil quality indicators in agro-ecosystem. *Agriculture, Ecosystems and Environment, 88(*2), 153-160.

Baert, G., Ranst, V., Vandenberghe, R. E., & Weirdt, D. J. (1999). Estimation of Al-for-Fe substitution in goethite by selective dissolution and mossbauer spectroscopy in a weathering sequence on mafic rocks in the Lower Congo. *Malaysian Journal of Soil Science, 3*, 11-27.

Ball, D. F. (1964). Loss on ignition as an estimate of organic matter and organic carbon in non-calcareous soil. *Journal of Soil Science, 15*(1), 84-92.

Bech, J., Tume, P., Sokolovska, M., Reverter, F., Sanchez, P. Longan, L., Bech, J., Puente, A., & Oliver, T. (2008). Pedogeochemical mapping of Cr, Ni, and Cu in soils of the Barcelona Province (Catalonia, Spain): Relationships with soil physico-chemical characteristics. J*ournal of Geochemical Exploration, 96*(2), 106-116.

Brady, N. C. (1990). *The nature and properties of soil.* (10th ed.). New York: Macmillan.

Doran, J. W. (2002). Soil health and global sustainability: Translating science into practice. *Agriculture Ecosystems and Environment, 88*(2), 119-127.

Drohan, J. R., & Sharpe, W. E. (1997). Long-term changes in forest soil acidity in Pennsylvania, U.S.A. *Water, Air and Soil Pollution, 95*(1-4), 299-311.

Hati, K. M., Swarup, A., Dwivedi, A. K., Misra, A. K., & Bandyopadhyay, K. K. (2007). Changes in soil physical properties and organic carbon status at the topsoil horizon of a vertisol of central India after 28 years of continuous cropping, fertilization and manuring. *Agriculture Ecosystems and Environment, 119*(1), 127-134.

IBSRAM. (1985). *Report of the inaugural workshop and proposal for implementation of the tropical soil management network*. International Board of Soil Research and Management, Bangkok, Thailand.

Ismail, H., Shamshuddin, J., & Syed Omar, S. R. (1993). Alleviation of soil acidity in Ultisol and Oxisol for corn growth. *Plant and Soil, 151*(1), 55-65.

Kamaruzaman, J. (1987). *Impact of ground-based logging machine on soil physical properties and tree growth.* (MSc. Thesis dissertation). Universiti Pertanian Malaysia, Serdang, Selangor, Malaysia.

Khresat, S. A., Rawajfih, Z., & Mohammad, M. (1998). Morphological, physical and chemical properties of selected soils in the arid and semi-arid region in north-western Jordan. *Journal of Arid Environments, 40*(1), 15-25.

Landon, J. R. (1991). Booker tropical soil manual. *In A handbook for soil survey and agricultural land evaluation in the tropics.* New York: Longman.

Lemenih, M., Karltun, E., & Olsson, M. (2005). Assessing soil chemical and physical property responses to deforestation and subsequent cultivation in smallholders farming system in Ethiopia. Agriculture, *Ecosystems and Environment, 105*(1), 373-386.

Massey, D. M., & Windsor, G. W. (1967). *Rep. glasshouse crops research institute*, pp. 72.

McLean, E. O. (1965). Exchangeable aluminum. In C. A. Black (Ed.), *Methods of soil analysis-Part 2,* Agronomy Monograph No. 9, American Society of Agronomy and Soil Science Society of America. (p. 985). Madison: WI.

Metson, A. J. (1956). *Methods of chemical analysis for soil survey samples.* New Zealand, NZ DSIR. (NZ Soil Bureau Scientific Report 12. p 21.

Othman, Y., Tan, K. H., & Tham, K. C. (1979). Organic matter and nitrogen studies in Malaysian soils. In *Proceeding Seminar on Chemistry and Fertility of Malaysian Soils*, December 10, 1979 (pp. 3-11). Serdang, Malaysia.

Pagliai, M. (1987). Effects of different management practices on soil structure and surface crusting. In N. Fedoroff, L. M. Bresson, & M. A. Coutry (Eds.), *Soil Micromorphology* (pp. 415-421). France: Française pour 1'Etude du Sol, Plaisir.

Pagliai, M., Guidi, G., La Marca, M., & Lucamante, G. (1983). Micromorphometric and micromorphological investigation of a clay loam soil in viticulture under zero and conventional tillage. *Journal of Soil Science, 34*(2), 391-403.

Peech, M., Alexander, L. T., Dean, L. A., & Reed, J. E. (1947). *Methods of soil analysis for soil-fertility investigations* (p. 25). Washington, D.C.: USDA Circular 757.

Peh, C. H. (1978). *Rates of sediment transport by surface wash in three forested areas of Peninsular Malaysia*. Kuala Lumpur: Occasional Paper No. 3 University of Malaya.

Pouyat, R., Groffman, P., Yesilonis, I., & Hernandez, L. (2002). Soil carbon pools and fluxes in urban ecosystems. *Environmental Pollution, 116,* S107-S118.

Razi, W. M. I., Tukimat, L., Azman, H., Shahril Nizam, & Sahibin, A. R. (2005). *Impact of mining activities on physico-chemical properties of soil in Kota Tinggi, Johor, Malaysia.* Proceedings of Second Regional Symposium on Environment and Natural Resources, March 22-23, 2005 (pp. 187-189). Pan Pacific Hotel, Kuala Lumpur, Malaysia.

Rowell, D. R. (1996). *Soil science: Methods and application.* England: Addison Wesley Longman.

Scharenbroch, B. C., Lloyd, J. E., & Johnson-Maynard, J. L. (2005). Distinguishing urban soils with physical, chemical, and biological properties. *Pedobiologia, 49*(4), 283-296.

Soil Survey Division Staff. (1993). *Soil survey manual.* U.S. Dept. of Agriculture Handbook No. 18. Washington, D.C.: U.S. Govt. Printing Office.

Syed Omar, S. R., Zubaidah, I., Shamshuddin, J., & Husni, M. H. A. (2001). Ammonium and potassium exchange in acid tropical soil treated with zeolites. *Malaysian Journal of Soil Science, 5,* 59-70.

Tessens, E., & Shamshuddin, J. (1983). *Quantitative relationship between mineralogy and properties of tropical soils*. Serdang: UPM Press.

Tiarks, A.E., Mazurak, A.P. & Chesnin, L. (1974). Physical and chemical properties of soil associated with heavy applications of manure from cattle feedlots. *Soil Science Society of America Proceedings, 38*, 826-830.

Wetlands International Asia Pacific. (1998). *The ecological assessment of Chini Lake, Pahang, Peninsular Malaysia*: *An evaluation of its conservation value and environmental improvement requirements*. Kuala Lumpur: Wetlands International Asia Pacific.

Zhenghu, D., Honglang, X., Zhibao, D., Gang, W., & Drake, S. (2007). Morphological, physical and chemical properties of aeolian sandy soils in northern China. *Journal of Arid Environments, 68*(1), 66-76.

Zornoza, R., Mataix-Solera, J., Guerrero, C., Arcenegui, V., Mayoral, A. M., Morales, J., & Mataix-Benyto, J. (2007). Soil properties under natural forest in the Alicante Province of Spain. *Geoderma, 142*(3), 334-341.

Pertanika J. Sci. & Technol. 24 (1): 89 - 99 (2016)

SCIENCE & TECHNOLOGY

Journal homepage: http://www.pertanika.upm.edu.my/

Development of Integrated Catalytic Membrane-Based Unit for Biofuel Production

El-Zanati, E.[1], Ritchie, S. M. C.[2] and Abdallah, H.[1*]

[1]*Chemical Engineering Pilot Plant, Engineering Research Division, National Research Centre, Dokki, Egypt*

[2]*Chemical and Biological Engineering Department, University of Alabama, Tuscaloosa, Alabama, USA*

ABSTRACT

Flow-through catalytic membrane system for ester production is one of the competitive alternatives to the conventional esterification system. This article presents the development of an integrated reaction/regeneration unit that was established to study the reaction followed by the regeneration step using two consecutive membrane reactor units working alternately. The hypothesis led to continuous ester production with a relatively high average conversion. The esterification reaction conversion of ethylhexanoic acid with ethanol and acetic acid with ethanol using catalytic membrane reactor reached up to 97.7% and 96%, respectively at room temperature after a reaction time of 10 sec, then slowly decreased; this is attributed to the decrease of catalytic membrane efficiency due to water adsorption on active functional groups, making a regeneration step mandatory. The developed unit was used to produce biofuel/biodiesel by esterification of acetic acid and fatty acid with ethanol.

Keywords: Catalytic membrane, esterification, regeneration, integrated pilot unit

INTRODUCTION

Functionalised membranes with catalytic active groups have recently attracted significant attention in chemical production, where the membranes are capable of achieving dual purposes: reaction and separation, where each single process intensifies performance and operation, which will lead to cost effectiveness of the production system. The removal of one or more products in reversible reaction promotes the forward direction by breaking the thermodynamic equilibrium barrier. Among the merits of membrane catalytic reactors are supra conversion, high productivity and product quality (Mbaraka *et al*., 2003; Shah *et al*., 2005; Maria *et al*., 2006; Sawant *et al*., 2007; El-Zanati *et al*., 2011).

Furthermore, the functionalised catalytic membranes containing sulfonated polystyrene grafts have successfully been used as an

Article history:
Received: 29 May 2014
Accepted: 29 June 2015

E-mail addresses:
ieelzanati@gmail.com (El-Zanati, E.),
sritchie@coe.eng.ua.ed (Ritchie, S. M. C.),
heba_nasr94@yahoo.com (Abdallah, H.)
*Corresponding author

ISSN: 0128-7680

alternative to conventional catalysts that are applied in esterification processes (El–Zanati *et al*., 2012; Abdallah *et al*., 2013). A flow-through catalytic membrane reactor describes the concept for continuous heterogeneous reactions, where the catalyst is immobilised in the pores of the membrane. The porous membrane does not perform any separation tasks; it is exclusively used as a microstructure catalyst carrier (Shah *et al*., 2005; Shi *et al*., 2013). This type of reactor allows high catalytic activity due to intensive contact between the reactants and catalyst and it provides potentially a narrow residence time (Ozdemir *et al*., 2006; Westermann & Melin., 2009; Westermann *et al*., 2009; Buonomenna *et al*., 2010). Accordingly, functionalised membranes are considered a type of multi microreactors since the reaction actually takes place inside the membrane pores. However, functionalised catalytic membranes have exhibited high catalytic efficiency and great potential for some important reactions, such as esterification, isomerisation, oxidation, hydrogenation, dehydrogenation etc. (Shah & Ritchie., 2005; Shah *et al*., 2005).

Shah and Ritchie (2005) implanted sulfonic acid groups onto the pore surface of polyethersulfone (PES) microfiltration membrane to catalyse the esterification of ethanol and acetic acid. In a previous study Abdallah *et al*. (2013) made up suitable microfiltration membranes for reaction catalysis, where grafting of sulfonic groups on polyethersulphone membranes was developed to catalyse esterification reactions; the reaction conversion reached more than 90% after 10 sec. Also, El Zanati and Abdallah (2012) investigated the same reaction using a modified grafted membrane by increasing the catalytic efficiency of the membrane up to 33.7% and using a large membrane area, the reaction conversion reached 97% after 10 sec process time. Likewise, in a former study a set of parameters influencing the esterification reaction was conducted (El-Zanati *et al*., 2011), where the results indicated that increasing the molar ratio increases catalytic efficiency (by increasing styrene percentage in the membrane-grafting step) and the internal surface area of the pores in terms of reaction conversion and productivity.

In a catalytic membrane reactor, the reaction conversion is suddenly increased to maximum value, which is attributed to water adsorption on the sulfonic groups. It then starts to decline slowly, owing to deactivation of the catalytic active sites by the adsorbed water within the membrane pores. Therefore, the membrane becomes progressively saturated; this behaviour creates an optimisation problem; therefore, at optimum time the membrane could be shifted to the regeneration step for further uses (El-Zanati *et al*., 2012; Abdallah *et al*., 2013).

Shi *et al*. (2013) studied a novel composite catalytic membrane that was prepared from a sulfonated polyethersulfone and polyethersulfone blend and supported by non-woven fabrics as a heterogeneous catalyst to produce biodiesel from continuous esterification of oleic acid with methanol in a flow-through mode, where an oleic acid conversion was kept at over 98% for 500 hours, running continuously.

The difference between this work and our previous work is the intention to design and develop an integrated catalytic membrane pilot unit for continuous esterification/regeneration steps; in Abdallah *et al*. (2013), the authors studied the polyethersulfone membrane preparation parameters to produce a microfiltration polyethersulfone that could be grafted by catalytic groups and then applied in esterification reaction of ethanol with acetic acid, with the reaction carried out in a small membrane holder with diameter 47mm. In their article, El Zanati and Abdallah (2012) showed how the membrane grafting parameters were studied and the

mathematical model of the grafting polymerisation steps were studied to reach optimum grafting parameters. El-Zanati *et al*. (2011) investigated the parametric study of the esterification reaction of ethanol and acetic acid using a small-sized 47mm catalytic membrane holder, where the membrane was purchased and not prepared in the lab.

The aim of the present work was the development of an integrated catalytic membrane pilot unit for continuous esterification/regeneration. The design was established on using two parallel membrane reactors for esterification/regeneration steps.

EXPERIMENTAL WORK

Design of an Integrated Continuous Esterification System

A conceptual design of an integrated continuous catalytic membrane system used to produce ester was developed. The design approach was based on experimental results and a pre-developed mathematical model that was obtained from previous work (El-Zanati *et al*., 2011; El–Zanati *et al*., 2012; Abdallah *et al*., 2013; El-Zanati *et al*., 2014). These results revealed that the reaction conversion was increased suddenly and reached maximum value after 10 sec and this lasted for a certain time depending on reaction design parameters. Since the reaction conversion started to slowly decrease with time, this phenomenon was attributed to membrane deactivation due to adsorbed water on functionalised sulfonic active groups. The adsorbed water is accompanied by deactivation of the catalytic membrane efficiency; therefore, membrane regeneration became mandatory to dehydrate the membrane.

The dehydration was conducted by sulfuric acid and it enabled membrane reuse and, consequently, enhanced system cost-effectiveness. The conceptual design principal was based on conducting reaction and regeneration simulinuously.The membrane regeneration was achieved by treating the used membrane with 1N sulfuric acid (acting as water adsorbing agent) at 25°C under 2 bar nitrogen pressure. The regeneration step was stopped when the sulfuric acid concentration left the membrane without changes; this process takes approximately 20 min (El- Zanati *et al*., 2011). Results of the esterification process obtained from an earlier study (El-Zanati *et al*., 2011) are illustrated in Fig.1, where is shown the change of reaction conversion with time at the internal pore surface area of 125510 cm2. This study also investigated the optimum regeneration time, as shown in Fig.2. Fig.3 exhibits the conceptual design flow sheet; it indicates that the first reactor shifted to functioning as a regenerator when the conversion reached a set point; this point was later determined by feedback on experimental results. The second reactor was then in service and started the reaction until the conversion reached the set point; then it shifted to regeneration, while the reaction was transferred to the first reactor and so on.

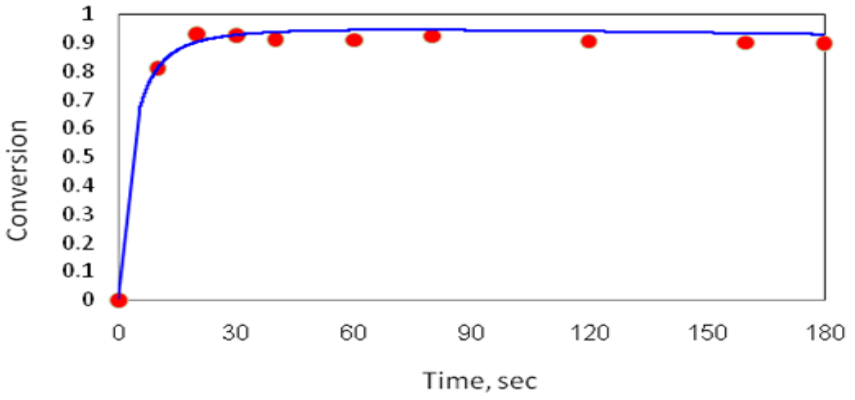

Fig.1: Change of reaction conversion with time (El-Zanati *et al.*, 2011).

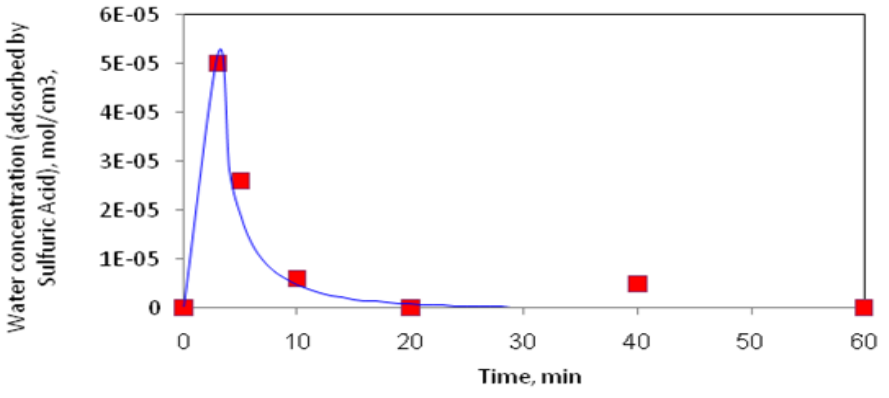

Fig.2: Regeneration time (El-Zanati et al., 2014).

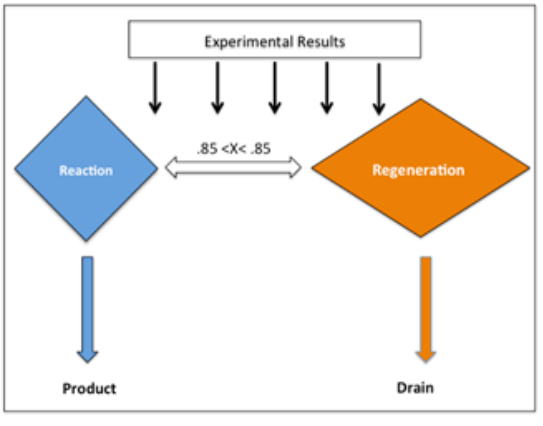

Fig.3: The conceptual design flow sheet.

Process Design

The esterification flow-through process using a catalytic membrane was designed according to previous experimental conditions (El-Zanati *et al*., 2011; El-Zanati *et al*., 2012; Abdallah *et al*., 2013; El-Zanati *et al*., 2014). The design that was proposed was based on using two reactors working alternately to conduct the esterification reactions (ethanol with acetic acid and ethanol with ethyhexanoic acid) and membrane regeneration. The design depended on some basis on the previous experiment, which rested on the following principles:

1. Asymmetric flat sheet poyethersufone (PES) membranes of 14.2 cm diameter were prepared by phase-inversion method. The polymer solution was prepared using 16% PES in DMF, 2.5% PEG 400 as polymeric additive (Abdallah *et al*., 2013).
2. The grafting process of the membranes was conducted by permeating a 1N H2SO4 solution through a PES membrane at 60ºC under pressure drop of about 2 bars for 1 hour and 12% volume of styrene in toluene was used for 10 minutes at a constant pressure drop of 2 bar and at 25ºC. The final step was to terminate the graft through permeation of 1N H2SO4 through the membrane for 1 hour at a constant pressure drop of 2 bar and at 25ºC (Zanati *et al*., 2012).
3. Two stainless steel 316L reactors of same size (14.2 cm diameter) were used to carry out the reaction and regeneration.
4. The first reactor worked continuously for 1 hour in reaction step (starting from t=0 to t=1 hr), then worked 20 min in regeneration step (starting from t=1 hr to t=20 min, where the total time was 1 hr and 20 min for reaction/regeneration steps).
5. Meanwhile, the second reactor started the reaction step at t=1 hr to t=2 hr, then started for regeneration to t=20 min. This process was performed continuously for 6 hr.
6. The product was collected continuously from each reactor and collected in a holding tank.

The process design depended on parameters that were selected according to the optimum parameters from previous experiments (El-Zanati *et al*., 2011; El-Zanati *et al*., 2012; Abdallah *et al*., 2013) where, the molar ratio of the feed in the esterification reactions were (2:1) ethanol to acetic acid and (5:1) ethanol to fatty acid. The reactions were carried out in membrane reactors with a diameter of 14.2 cm. The reaction temperature was 25°C. The working time in each reactor was 1 hr and the regeneration duration for each reactor was 1 hr, where the two reactors were working in alternately.

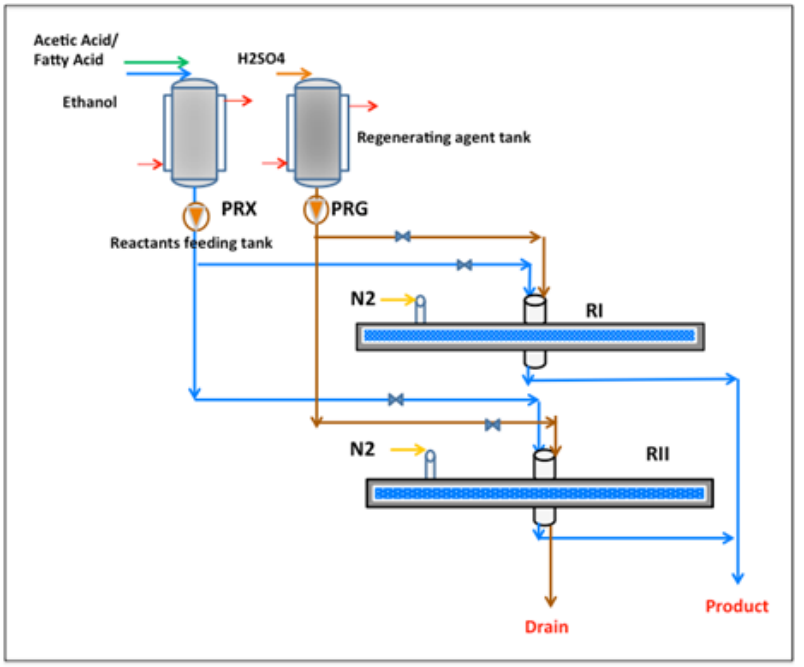

Fig.4: Flow sheet of pilot integrated unit for reaction and regeneration.

Implementation of Integrated Esterification/Regeneration Unit

The basic process design of the pilot unit comprised two reactors and their auxiliaries were manufactured in the workshop of the National Research Centre, Egypt except for the membrane holders that were purchased from Sartorius Company, Germany (Fig.4). The reaction/ regeneration unit comprised a feeding tank of stainless steel 316 L, 1 L capacity, which was connected to the first and second reactors by a network of stainless steel pipes (316 L, 1/4"diameter) and valves to facilitate the manoeuver from reaction step to regeneration step and from one unit to another easily. The feeding vessel had two openings, one for applying nitrogen, used as a blanket and as a support for the feeding step for both steps (reaction and regeneration), and the other for charging either the reactants or regenerating solution.

The reactor (membrane holder) of stainless steel (316 L) and a diameter of 14.2 cm had an upper and lower ticked cover, and the grafted membrane was sandwiched between them and supported on a Teflon support screen. The membrane holder had three openings: the first was a feed entrance and the second was for N2 feeding, both on the top cover, while the third was located at the bottom, and was used for product collection. A stainless steel (316 L) vessel was used as a surge tank for regenerating solution (1N H2SO4).

Testing and Evaluation of the Integrated Unit to Produce Biofuel/Biodiesel

Two experiments were performed using the developed pilot unit. The first esterification reaction was carried out to produce ethyl acetate at operating conditions of molar ratio 2:1 ethanol to acetic acid at 25°C under 2 bar nitrogen pressure for 60 min then shifted to the other reactor, while the first one was subjected to the regeneration step using 1N H2SO4 at 25°C under

the same nitrogen pressure for 20 min; subsequently the esterification reaction returned to the regenerated membrane in the first reactor, while the other membrane in the second reactor was exposed to the regeneration step. This trend was repeated alternately for 6 hours. The second esterification reaction was carried out to produce fatty ester using fatty acid (ethyl hexanoic acid) with ethanol. It was conducted using the same procedures and conditions except that the reaction was performed at molar ratio 5:1 ethanol to fatty acid. The samples were collected and analysed by gas chromatography.

The reaction conversion was calculated based on the change in the concentration of acetic acid or fatty acid in the product compared by the feed using the following equation:

$$Conversion\ \% = 100 * \frac{C_f - C_p}{C_f}$$

where C_f is the concentration of acid in the feed and C_p is the concentration of acid in the product.

RESULTS AND DISCUSSION

Membrane Preparation, Grafting and Characterisation

Asymmetric flat sheet poyethersufone (PES) membranes were prepared by the phase-inversion method; the prepared membrane before and after grafting is illustrated in Fig.5. The grafting process of the prepared membrane was carried out using one reactor of the developed unit, passing a solution of 1N H2SO4 at temperature 60°C for 1 hr at the initiation step and 12% styrene at 25°C for 10 min in the polymerisation step and finally 1N H2SO4at 25°C for 1 hr in the termination step of the grafting process. A scanning electron micrograph was used to assess the grafted membrane surface; Fig.6 indicates that the grafted membrane pores were wider than the original one and seemed lesser in number (El-Zanati *et al*., 2011, Abdallah *et al*., 2013).

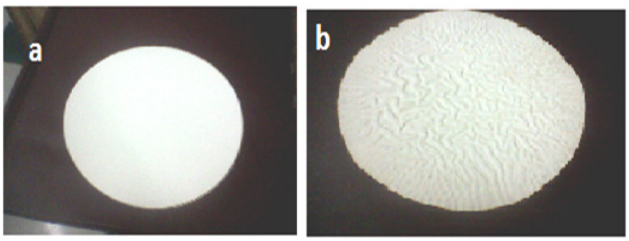

Fig.5: Prepared membrane (a) before grafting and (b) after grafting.

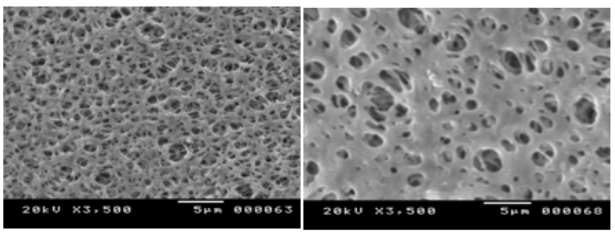

(a) **(b)**

Fig.6: SEM picture of grafted membrane surface, the magnification power was 10 kv.

Integrated of Esterification/Regeneration Processes Set-Up

The integrated reaction/regeneration unit is captured in Fig.7. The unit was used in an NRC workshop. It operates as described earlier; each reactor is fed with reactants from a surge vessel of capacity sufficient for a running time of 1 hr and provided with an adjustable valve to control the flow rate. Also, each reactor was connected with a tank of diluted sulphuric acid of a capacity sufficient for running 20 min for regeneration. The product is collected continuously from each reactor and collected in a holding tank. An example of the scheme using two consecutive cycles, comprising all equipment and operating time, follows this process: the filling of tanks, reaction and regeneration steps etc. Table 1 illustrates the GANTT chart and schedule of working time i.e. 210 min.

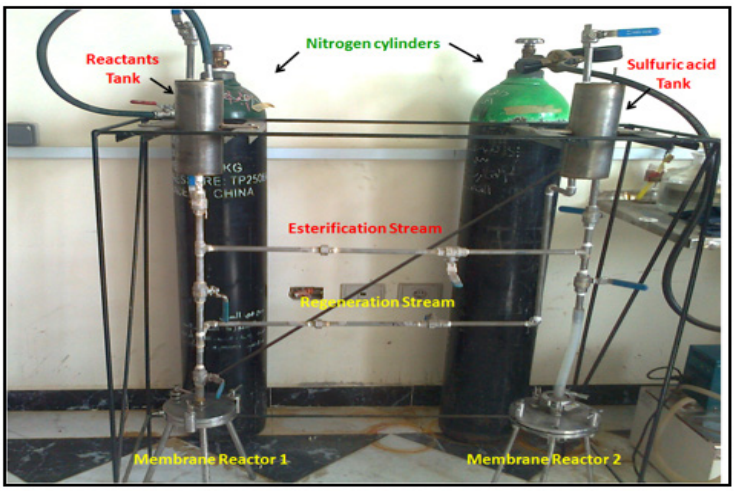

Fig.7: Pilot integrated unit for reaction and regeneration.

TABLE 1 : GANTT Chart and Schedule Working Time for Two Cycles (210 min)

Process/task	Time*10 (min)
Filling of reactant feeding vessel	
Filling of regeneration solution feeding vessel	
Feeding R1 with reactants	
Esterification reaction in R1	
Feeding regeneration solution to R1	
Regeneration of membrane of R1	
Feeding R2 with reactants	
Esterification reaction in R2	
Feeding regeneration solution to R2	
Regeneration of membrane of R2	
Feeding R1 with reactants	
Esterification reaction in R1	
Feeding regeneration solution to R1	
Regeneration of membrane of R1	
Feeding R2 with reactants	
Esterification reaction in R2	

Testing and Evaluation by Flow-Through Esterification Reaction

The esterification reaction using a catalytic membrane at 2:1 ethanol to acetic acid, at room temperature and under 2 bar nitrogen pressure was conducted. The change of reaction conversion with time is illustrated in Fig.8. The results indicated a maximum peak at the beginning of the reaction, where the conversion reached about 96% after 10 sec of reaction time. During the process the conversion decreased until it reached 93% after 60 min; at this point the regeneration step was started and the other membrane holder was used to continue the reaction. This was repeated for six hours.

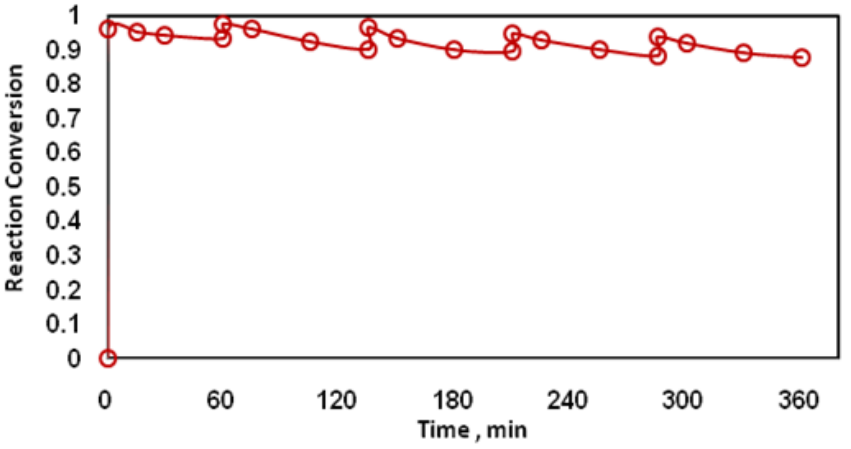

Fig.8: Flow-through esterification process with catalytic membrane using 2:1 ethanol to acetic acid.

The experiments were repeated to produce fatty ester. Fig.9 illustrates the flow-through esterification reaction by catalytic membrane using 5:1 ethanol to fatty acid (ethylhexanoic acid). The maximum peak conversion reached 97.7 % at the beginning of the reaction and decreased during the reaction time to minimum peak conversion at 92% after 60 min. This was repeated for six hours.

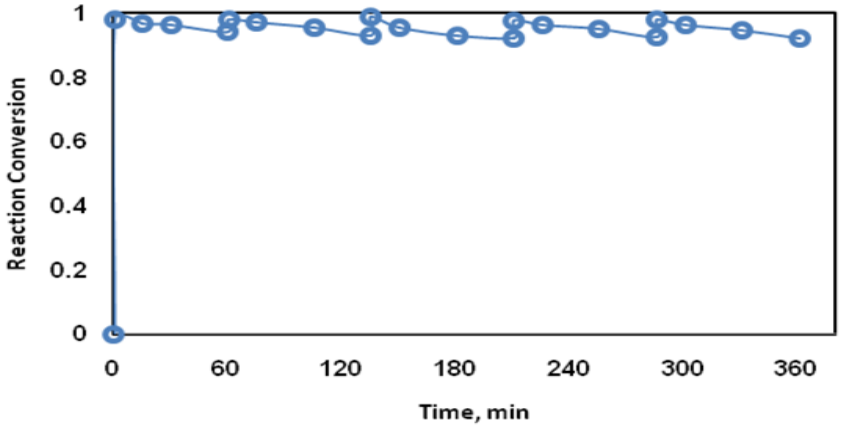

Fig.9: Flow-through esterification process with catalytic membrane using 5:1 ethanol to fatty acid.

The experiment succeeded in obtaining almost constant reaction conversion for both investigated reactions to assess and evaluate the designed unit where the average reaction conversion was 96-98%. However, this process increased productivity in a short time and decreased the separation cost (Abdallah *et al*., 2013).

CONCLUSION

The functionalised catalytic membrane of sulfonated polystyrene grafts acts as an alternative to the conventional esterification process. An integrated pilot unit was developed to produce esters continuously; it comprised two units working simultaneously at two steps i.e. the reaction and regeneration steps. The first reactor operated for a period of 60 minutes before the reactant flow was shifted to the second reactor. The first reactor was then subjected to dewatering and membrane regeneration for 20 minutes. The integrated pilot unit afforded a high esterification comprehensive reaction conversion of 96-98% for esterification of acetic acid and fatty acid with ethanol, respectively.

REFERENCES

Abdallah, H., Said, F., Ahmed, E., El-Ardy, O., & El-Zanati, E. (2013). Development and preparation of microfiltration polyethersulfone membrane for catalytic membrane application. *Journal of Applied Sciences Research, 9,* 1623-1634.

Abdallah, H., El-Gendi, A., El-Zanati, E., & Matsuura, T. (2013). Pervaporation of methanol from methylacetate mixture using polyamide-6 membrane. *Desalination and Water Treatment, 51*(40-42), 7807-7814.

Buonomenna, M., G., Choi, S., H., & Drioli, E. (2010). Catalysis in polymeric membrane reactors: The membrane role. *Asia-Pacific Journal of Chemical Engineering, 5*(1), 26-34.

El-Zanati, E., Ritchie, S., Abdallah, H., Ettouny, R., & El-Rifai, M. (2011). Esterification catalysis through functionalized membranes. *International Journal of Chemical Reactor Engineering, 9(*1), 1542-6580.

El–Zanati, E., & Abdallah, H. (2012). Development of functionalized catalytic membrane for ethyl ester production. *International Journal of Emerging Trends in Engineering and Development, 5,* 505-521.

El-Zanati, E., Ritchie, S.M.C., Abdallah, H., & Elnashaie, S. (2014). Mathematical modeling, verification and optimization for catalytic membrane esterification micro-reactor. *International Journal of Chemical Reactor Engineering, 13(*1), 71-82.

Maria, T., Sanza, J., & Urgen, G. (2006). Esterification of acetic acid with isopropanol coupled with pervaporation Part II. Study of a pervaporation reactor. *Chemical Engineering Journal, 123*(1), 9-14.

Mbaraka, I. K., Radu, D. R., Lin, V. S. Y., & Shanks, B. H. (2003). Organosulfonic acid functionalized mesoporous silicates for the esterification of fatty acid. *Journal of Catalysis, 219*(2), 329-336.

Ozdemir, S. S., Buonomenna, M. G., & Drioli, E. (2006). Catalytic polymeric membranes: Preparation and application. *Applied Catalysis A: General, 307(*2), 167-183.

Sawant, D. P., Vinub, A., Justus, J., Srinivasu, P., & Halligudi, S. B. (2007). Catalytic performances of silicotungstic acid/zirconia supported SBA-15 in an esterification of benzyl alcohol with acetic acid. *Journal of Molecular Catalysis A: Chemical, 276*(1), 150-157.

Shah, T. N., & Ritchie, S. M. C. (2005). Esterification catalysis using functionalized membranes. *Applied Catalysis A: General, 296*(1), 12-20.

Shah, T. N., Goodwin, J. C., & Ritchie, S. M. C. (2005). Development and characterization of a microfiltration membrane catalyst containing sulfonated polystyrene grafts. *Journal of Membrane Science, 251*(1), 81-89.

Shi, W., He, B., Cao, X., Li, J., Yan, F., Cui, Z., Zou, Z., Guo, S., & Qian, X. (2013). Continuous esterification to produce biodiesel by SPES/PES/NWF composite catalytic membrane in flow-through membrane reactor: Experimental and kinetic studies. *Bioresource Technology, 129*, 100-107.

Westermann, T., & Melin T. (2009). Flow-through catalytic membrane reactors: Principles and applications. *Chemical Engineering Processing, 48*(1), 17-28.

Westermann, T., Kretzschmar, E., Pitsch, F., & Melin, T. (2009). Heat transfer and temperature profiles in flow-through catalytic membrane reactors, *Chemical Engineering Journal, 155*(1), 371-379.

Pertanika J. Sci. & Technol. 24 (1): 101 - 121 (2016)

PERTANIKA JOURNALS

SCIENCE & TECHNOLOGY

Journal homepage: http://www.pertanika.upm.edu.my/

Beyond Barebones Cloud Infrastructure Services: Stumbling Competitiveness During Economic Turbulence

JosephNg, P. S.[1,2] and Kang, C. M.[1]

[1]*School of Computing and Creative Media, KDU University College, Jalan Kontraktor U1/14, Seksyen U1, 40150 Shah Alam, Selangor, Malaysia*

[2]*Faculty of Computer and Information Science, University Technology Petronas, Bandar Seri Iskandar, 31750, Tronoh, Perak, Malaysia*

ABSTRACT

The hyper competitiveness of medium-size enterprise is not only heavily dependent on its cloud computing infrastructure evolution but also on its adaptation for sustainability to global web interconnection ecosystems. While the bigger multinationals have experienced positive business values due to their economies of scale, the medium-size manufacturing plant still faces greater challenges. We update the view on two similar but evolved theoretical perspectives from Harvard University: Commodity of IT infrastructure and Disruptive Technology into a catalyst model for optimum technology maximisation. This paper proposes the establishment of a new dynamic barebones yet optimised internet infrastructure that will integrate the existing client server into the extranet to form an extended cloud environment. The study's three-stage primary data collection procedure consistently validated our findings. Our results suggest that enterprise should continue to invest in optimised IT infrastructure despite the economic turbulence for competitive gearing in the future.

Keywords: Cloud computing, economic turbulence, exostructure, framework, IaaS, ICT infrastructure, Small and Medium Size Enterprise

INTRODUCTION

The Small and Medium Enterprise (SME) is a major force that constitutes 99.2% of Malaysia's total business establishments. Organic local growth is insufficient to fend off the rise of global SMEs. East Asian countries have in the past embraced technologies and are now enjoying the fruits of early adaptation (Tsai, 2012). More significant is the contribution of the Medium Size Manufacturing Plant (MSMPs), although comprising only 3% of Malaysia's total business establishments; the MSMPs have, however, contributed around RM1 billion (equivalent to USD$330 million) to Malaysia's total Gross Domestic Product

Article history:
Received: 22 September 2014
Accepted: 23 September 2015

E-mail addresses:
josephnps@hotmail.my (JosephNg P.S.)
cmkang@kdu.edu.my (Kang, C.M.)
*Corresponding author

ISSN: 0128-7680

(GDP) in 2012. For MSMPs to continue their dominance and move up to become larger power houses, there is a need to energise them even further to create new global competitive market efficiency.

As MSMPs expand globally, so does the availability of computing services. The Internet has created a technology innovation, a new digital market place. The advent of cloud service is unavoidable and optimising the next generation cloud service seems to be the next best solution (Abareshi, 2012; Li, 2012; Luftman, 2012; Otim, 2012; Venters, 2012; Vinekar & Teng, 2012; Wang, 2012; Antonov, 2013; Chandio, 2013; Daim, 2013; Dihal, 2013; Drnevich, 2013; Gannon, 2013; Kun, 2013; Schryen, 2013;). As enterprises begin to embrace the Internet of Things (IOT) via the ability to communicate more digitally, the promise of business improvement at a reduced shared cost grows as well. MSMPs are still using outdated technology.

MSMPs face serious resource poverty with fragmented IT operation that focuses on day-to-day tactical strategies. MSMPs lack in relevant research on the utilisation of cloud computing optimisation due to perceived low commercial value when compared to larger multinationals. Past research has shown that many MSMPs have over invested in IT infrastructure, and this has increased the operation cost and inevitably hampered sustainability (Ng, 2011, 2012; Marston, 2011). But with the advancement in IT resources outsourcing, MSMPs should be able to embrace much more complex solutions. Kun (2012) has suggested that as MSMP start to grow, they should "invest in information systems, which allow the organization to process more information without overloading the communications channels". This paper highlights the evolved technology innovation that has lagged to enhance the competitiveness of MSMPs.

Uncertainty has been enterprise's greatest worry and has translated into opportunities lost. While most would assume that a volatile economy is a period of reconciliation and hibernation, the period is actually used as strategic reconsolidation of new business strategies (Linden, 2013; Ng, 2013). Economic turbulence can be actually transformed from a mere sustainability shield to a strategic weapon for competitive advantages. This period can be used to implement and stabilise the new IT infrastructure.

IT infrastructure has been at the forefront to enable various solutions in today's digital businesses. Its new innovation is available in almost every enterprise but this however turns "IT" into a commodity technology, which Carr (2003, 2005) has termed "IT Doesn't Matter" anymore. Cloud services can no longer provide the technological edge that is required for competitive advantage. As technology matures and becomes more affordable for the mass market, it will lose its competitive edge, as stated by Clayton (2006): "Disruptive Technology [provides] insignificant competitive advantage" to enterprise. Both these theories have forced enterprise to reconsider their actual IT infrastructure specification needs before jumping into unnecessary over investment.

These challenges indicate that there are insufficient frameworks or models designed specifically for MSMPs to move beyond cloud infrastructure services, and this becomes a stumbling block for their competitiveness during economic turbulence. Cloud service is undeniably still the best option for shared solutions; however, there is still room for improvement. This paper proposes a new paradigm for consensus shifting of the legacy theory evolved from the practice of multinational corporations (MNC) that can be used for MSMPs during a volatile period.

TABLE 1 : Null Hypothesis

H_N1: Disruptive technology has low influence to competitive advantage contribution.
H_N2: IT infrastructures have positive relation to commodity product classification.
H_N3: Scarce resources are associated with MSMPs' IT infrastructure performance.
H_N4: Economic turbulence has positive correlation to infrastructure investment decisions.

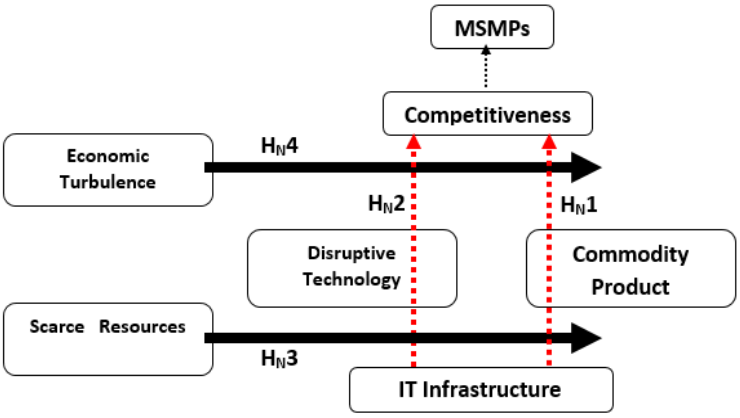

Fig.1: Initial null hypothesis relationship.

We draw a new paradigm shift that may be important in overcoming economic turbulence, uncertainty and dynamism in an evolving competitive landscape. This qualitative research initially started with the traditional Null Hypothesis shown in Table 1 with the relationship shown in Fig.1 and was then concluded with a revised Directional Correlation Hypothesis based on new findings from three data collection instruments (mass survey, personalised interview and expert group discussion). For this paper, the term "barebones" is defined as the minimum infrastructure specification needed to maintain and operate the ICT requirement for an enterprise. The new framework proposed for MSMPs cloud optimisation can also be extended to MNCs as a benchmark barebones model.

The conceptual explanatory results were deployed in sequential mixed mode process of quantitative generalisation to justify further qualitative reasoning. The quantitative results derived from previous research were used in this paper to reaffirm the current qualitative findings to conclude the analysis. This paper, however, will provide contradictive views to the above and propose the following research objectives:-

1. To explore the relationship between technology uniqueness at the point of time of disruptive technology.
2. To identify the period of product commoditisation during the product's life cycle.
3. To explore the criteria that attract enterprise to adopt the utility model.
4. To access the impact of economic turbulence towards IT infrastructure investment.

Medium-Size Manufacturing Plant Infrastructure Investment Outlook Literature

Economic turbulence has significantly impacted many enterprises. Kappelman (2014) in his survey across 484 enterprises found that IT spending represented an average of 5% of the total spending, equivalent to USD215 million annually. Marston (2011) also reported that "2/3 of the average corporate IT staffing budget goes towards standard support and maintenance" and this has increased their operation cost significantly. This has forced many enterprises to wait for the next positive outlook cycle. However, when bullish opportunities appear, the crowded market space and slow technology could not stand out to ice the cream.

Malaysia's poor economic performance continues to raise doubts globally as the country's economic outlook has been downgraded from "Stable" to "Negative" and its competitive ranking has dropped to 25th spot. MSMPs today need to re-energise for a positive bounce back or risk future survival impact (Reuters, 2013; Bloomberg, 2013; Starbiz, 2013; Sunbiz, 2013). Outside the country, the rise of global MSMPs has also put pressure on local MSMPs.

Malaysia's Medium Size Manufacturing Plant is experiencing booming growth as information technology becomes part of the day-to-day operation cycle. New advancement in industrial robotics, namely computer-aided manufacturing and enterprise resources planning, have helped not only to automate traditional manual processes but also improved production efficiency. These highly sensitive technologies require sophisticated local control to interact with embedded tools while integrating multi-source information systems that are geographically diverse in location. Understandably, as production sales are demand driven with challenging cycles, the need for on-demand shared services is unavoidable.

We substantiated Nicholas Carr's (2003, 2005) theory of commodity of technology and Christensen Clayton's (2006) theory on disruptive technology to understand how technology adoption was being applied. Many enterprises have over time come to believe that having the best and latest technology delivers superior results. These enterprises failed to understand that their competitors also had the same idea and, therefore, also invested in similar technology to neutralise competition (Bannister & Remenyi, 2005). Furthermore, technology catch-up is a never-ending race with exponential improvement over time that will disrupt the supply chain environment of the manufacturing plant. The whole exercise of business process reengineering will require more resources, which MSMPs lack. The integration of both theories here brings in the synergistic value of fencing off technology glories that could impact enterprise relearning.

Nicholas Carr's (2003, 2005) theory of commodity of technology argued that the normalisation of available IT infrastructure superiority reduces the competitiveness of the enterprise. This is the reverse of what happened during the golden era when technology opened up new opportunities for servicing client needs and the market place. However his research was only confined to larger Multinational Corporations (his example focused on the railway, telegraph and electrical supply system enterprise), which is not entirely applicable to the MSMP environment. Bannister and Remenyi (2005) in their paper, however, contemplated Carr's statement that "IT is not of strategic importance anymore" while Bhatt and Grover (2005) disagreed on the "delineating of infrastructure capabilities". These larger enterprises focused on larger capital expenditure using their huge almost bottomless operating expenses while patiently waiting for longer strategic returns. This luxury, however, could not be enjoyed by the MSMPs that required technological advantages to open up greater digital market place

or to streamline traditional manual processes as they grew bigger. Carr also stated that IT infrastructure is now considered a commodity product and, therefore, enterprise should no longer lead in technology advancement to gain competitiveness. This is clearly shown by the exponential increase in George's (2004) paper on 'Outsourcing and Globalization: The View from the United States'. We recommend that MSMPs adopt existing available technology from MNCs and not venture into reinventing technology.

Another Harvard University scholar, Christensen Clayton (2006) shared his theory on disruptive technology, which put greater emphasis on the dynamic nature of the IT infrastructure product life cycle that causes distortion to a product's contribution to the current ecosystem. He warned about the insignificant competitive advantages that are originally perceived by using the best of new technology. Stratechery (2013), Tellis (2006) and Danneels (2004) have, however, questioned Clayton's definition of "disruptive" and "technology", asking at what point these should be considered. While Clayton's theory focused on mainstream market saturation, so-called disruptive technologies still provide a golden opportunity for tapping into the MSMP, as discussed by Lucan and Goh (2009) in 'Disruptive technology: How Kodak missed the digital photography revolution'.

Both these two fundamental theories have put a hold on MSMPs' traditional infrastructure investment outlook. As cloud services can no longer provide the expected uniqueness, economic turbulence adds a further complication to the low-cost replacement of outsource services by service providers. However, after considering the time IT infrastructure requires for making significant contributions to the results and given the current disruptive economic happenings, cloud computing investment needs a fresh outlook assessment, as explained in the latter part of this paper. Past research shows that MSMPs have over invested in IT infrastructure after being pressured by their peers' competitive advantage, resulting in significant impact on their financial returns (Marston, 2011; Joseph, 2013, 2014). When a competitor makes an IT infrastructure investment based on a new technological innovation and finds it incompatible, they seldom make public their failure. Other enterprises unaware of the real issues hear of the adoption news, join the bandwagon and, thus, create an industry-wide tsunami. His finding further affirms that the reason IT infrastructure was classified as a commodity was not due to the saturation of technological advantages but because of discrepancies in investment decisions. At a time when almost all enterprises have been digitised, the option of not digitising is unthinkable but just when to digitise is a critical question. MSMPs, however, have glorified their technology chasing, yet are unable to maximise their utilisation efficiency. There are others who have ignored the infrastructure investment due to its non-direct revenue contribution and its high initial capital expenditure.

In this research, the focus is on Table 2 where cell M3, 3 indicates slightly high turbulence with reasonable competitive pressure to sustain operations. This is a group that can still invest in IT infrastructure to make an edge for competitive change without having much difficulty in sustainability. The current turbulence experienced in Malaysia is at T3 as defined by Fong YS and Tan CK as the country is experiencing spillover effects of the European crisis and the USA's fiscal cliff while undergoing moderate competitive business competition locally. This was also reaffirmed during the Top Management Interview conducted by Ng (2013). The current business competition is positioned at midpoint at C3 as there is sufficient business opportunity for aggressive enterprises, although this requires hard work.

TABLE 2 : ICT Infrastructure Turbulence Sustainability and Competitive 3-Dimensional Matrix

			Competitive Level				
			High Competitive Requirement				Low Competitve Requirement
			5	4	3	2	1
Turbulence Level	High Turbulence	5	M5,5				M5,1
		4					
		3			M3,3		
	Low Turbulence	2					
		1	M1,5				M1,1

Sustainability Level

Cloud Computing Utility Model Characteristic Literature

Lee (2013) highlighted that "the success of a firm depends on its ability to take advantage of the technology shifts to innovate in their business models and eventually to compete differently". The globalisation of MSMPs requires an IT infrastructure solution that is available geographically 24/7. Given their constraints on resources and the complexity of technology management, cloud computing is undeniably a must-have infrastructure for MSMPs (Venters, 2012; Chandio, 2013; Gupta, 2013; Lee, 2013; Sultan, 2013; Kleis, 2013). The inclusion of cloud computing as the 5th utility variable component besides electricity, water, gas and the telephone, the expectation of the pay-per-use economic factor seems to have motivated many MSMPs to jump on the bandwagon. This allows MSMPs to pay for only the additional service utilised while having greater flexibility with market environment dynamics. When compared to the traditional investments, some IT infrastructure may not be fully utilised due to low requirement and may become obsolete by the time they are actually used. However, considering that 73% of the 484 respondents in Kappelman's (2014) survey still used their internal cloud shows there is still room for improvement.

The utility cloud is the best fit model that allows MSMPs to focus on their core business activity in relation to smaller capacity requirements. This has provided a cost reduction of between 20 and 30% in IT operations (Venters, 2012). However, Clayton advocated that the pitfalls of innovative value contributor in new market contributor. Furthermore, Carr highlighted that most enterprises that require digital communication have already embraced the cloud model and, therefore, provided insignificant technology uniqueness and some may even experience decreasing values. Although consensus is for the adoption of this model in general, an argument can also be produced for the MSMPs that consider cloud utility to be new innovations as it expands from the traditional local market to the international market, citing an example of the use of a payment gateway for electronic commerce.

Although Infrastructure as a Service (IaaS) may seem to have reached its saturation period for most enterprises, there is, however, still room for optimisation of its use by medium-size enterprises. In this research, the emphasis was on the extension of IaaS as enterprises today operate a variety of solutions that require specific infrastructure specifications to host localised web application systems. Nevertheless, these specific infrastructures are now readily available

on shared services provided by cloud services solution providers. MSMPs are more receptive to a cheaper but good enough solution in what is called a Low End Disruptive Technology to make reasonable competitive advantages in the New Market Disruption innovative value contributor.

RESEARCH METHODOLOGY

This research extracted views and opinions to explain the phenomena sequence that leads to technology adoption (Czamecki & Spiliopoulou, 2012; Paliokaite, 2012; Venkatesh, 2013). The hypothesis proposed earlier aimed to test the conceptual framework in an economically turbulent environment to extract its correlation. The research methodology is summarised in Table 3.

This research identified and compared various empirical literature to review the historic dynamics that lead to the need to start the research. The analysis highlighted the imbalance of IaaS technology adoption in the MSMPs that led to an environment of unjustified differentiation in investment returns. Previous research from Ng (2011; 2012a, 2012b) highlighted the availability of sufficient resources to drive computing infrastructure investment as compared to the earlier mindset of ill resources held by MSMPs. This improved condition is supported by the advancement of shared service through the utilisation of cloud computing and service outsourcing.

The novelty of these phenomena in this research is unique as there is limited discussion on economic turbulence in the case of a small enterprise. The use of Mix Mode methods can help to provide greater insight into many phenomena of interest that are difficult to explain using either the qualitative or quantitative method alone (Venkatesh, 2013). In this method, the initial mass survey was first carried out to test the quantitative volume needed to plan the research project's resources. Numerical justification was used to generalise the issues faced by MSMPs and also to relate the magnitude of impact from the issues. It was then backed by qualitative reasoning to define the hypothesis. As IaaS is a long-term strategic investment decision, it also requires the input of top management. This requires qualitative interpretation from the research instrument. This narrative statement was then customised to narrow down the area of improvement for competitiveness.

The (1) Focus Group interactive Delphi method used in current research to gather primary data was an extension of the previous (2) mass survey with operational team and (3) personalised interview with top management. Table 3 shows the profile of the respondents selected for this research. In this current Focus Group data gathering, 10 experts, who were experienced IT personnel, were gathered in an email group to discuss various questions pertaining to this study. Three different instruments were used, as shown in Table 4. The Concurrent Validity method aimed to affirm the consistent views and opinions of all executive ranks within the enterprise.

As for Construct Validation as shown in Table 4, the instruments were tested in both the university and at industry level. The views and opinions of the lecturers helped to test the research theoretical framework to ensure all possible theories were revisited. The industry respondents were required to test the practical implication of the framework in a non-controlled environment with multi-factored constraints. Validation was gathered from the executive interview with top management on the MSMP's strategic direction of computing infrastructure

TABLE 3 : Research Methodology Summary

Activity / Phase	Phase 1 Quantitative Generalisation	Phase 2 Qualitative Reasoning	Phase 3 Testing	Phase 4 Validation
Research Dimension	Phenomena Explanatory Sequential Dimension			
Research Design	Random Survey	Personal Interview	Focus Group Discussion – Technical Level	Focus Group Discussion – Strategic Level
Data Collection	• End users – Managerial level • Across Peninsular Malaysia • January to February, 2012 • 228 respondents	• End users – Top management level • Central Malaysia • January to March 2013 • 10 respondents	• Consultants, vendors & end-users • Central Malaysia • October 2013 • 10 respondents	• Malaysian Manufacturing Federation • Central Malaysia • Targeted October 2014 • 10 respondents
Research Methods	• Convenient sampling using available organisation hosting final-year industrial-training students • Distributed by undergraduate students to the site supervisor during their industrial internship	• Convenient sampling of who was willing to participate and share information • Interviewed by first author	• Convenient sampling of who was willing to participate and share information • Facilitated by first author	• Convenient sampling who are willing to participate and share information • Facilitated by first author
Data Analysis	Spearman Correlation Quantitative Exploration	Qualitative Reasoning Explanation	Delphi Inductive Conclusion	Qualitative Reasoning Explanation
Contribution	Conceptual framework	Draft framework	Preliminary framework	Pilot framework

TABLE 4 : Research Validation

1.	Content validity -Domain distribution -Language, Depth
2.	Concurrent Validity -Mass Survey -Personalised interview -Focus group
3.	Construct Validity -Lecturer -Industry experts

(Joseph, 2013). As the infrastructure investment was higher, the deliverable was mapped to the long-term strategic direction of the enterprise, which was set by top management. Further validation was obtained from the focus group discussion via email with the technology subject matter experts. This was conducted between March and May 2013 (Joseph, 2014). The Delphi method was used to share views and comments from the experts, and their feedback was analysed.

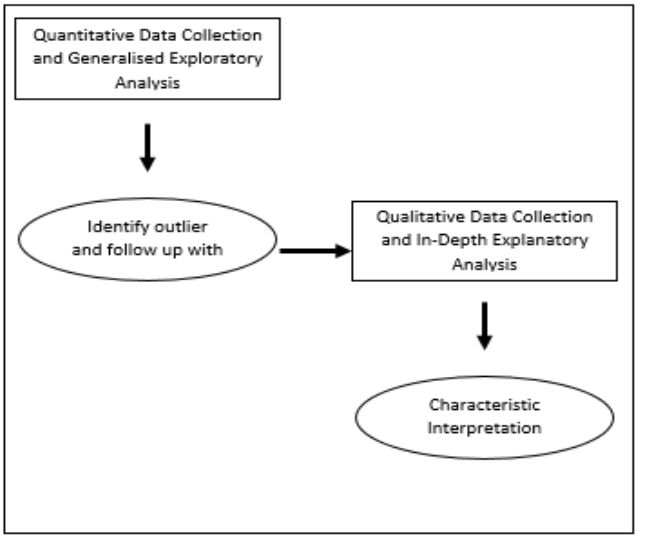

Fig.2: Sequential design.

The sequential design shown in Fig.2 explained the factors that led to a series of actions taken by MSMPs when deciding to adopt cloud computing IaaS for the environment. The preliminary descriptive explained the metamorphosis transition that MSMPs endured in adopting the new IaaS while the inductive reasoning explained the cause of the results in each transition. All this led to the explanatory findings that were used to understand the phenomenon progression. The mass survey aimed to gather quantitative operational reasoning;

the personalised interview aimed to extract deeper strategic direction while the focus group interview provided opportunity for expert debates. The expert groups were given the feedback gathered from the top management interview to evaluate. The use of multiple methods of data collection in the study enhanced the reliability of the data collected, yielding consistent results when the characteristic being measured was not significantly changed. This helped to "address why a particular sample was chosen" (Zhang, 2012). The instruments used in the study (questions) were distributed to different experts in the field for pre-testing of language, depth, technical and knowledge jargon. This also ensured that an appropriate question proportion was distributed to reflect various parts of the research domain.

FINDINGS AND DISCUSSION

The medium-size enterprise is a mature group that can project economical maturity to up-class itself by staying in line with IaaS to fend off economic turbulence. ICT is now a common tool that not only helps to automate business process but will also distinguish each competitor in the future (Brown, 2012; Santos, 2012; Bharadwaj, 2013; Gu, 2013; Rong, 2013; Sen, 2013; Tambe, 2013). Based on the original theory of commodity by Carr (2003, 2005), it can be argued that although each technological edge is swiftly available to almost all the enterprises within the same horizontal industry or across the industry, there has not been much discussion on MSMPs that are sitting just below the fence. They do not have the privilege of exploring IaaS technology superiority just because these commodity IT infrastructure is considered too fanciful for them to enjoy. Indeed, a new technology may not necessarily help an enterprise to leap-frog ahead of competition as mentioned by Clayton's (2006) theory of disruptive technology. Lee (2013) has pointed out that "the sustainability of any specific business model has become unclear as technology changes from outside an organization can be highly disruptive". However, when economic turbulence becomes the real disruptive force, new technologies become the equaliser to form equilibrium to balance between sustainability and competitiveness. There have also been insufficient research studies to develop a shield technology that can defend the medium enterprise from any sustainability issues during the volatile period of economic turbulence. This is where this new novel theory of barebones IaaS for competitiveness during economic turbulence comes from. Table 5 summarises the findings.

TABLE 5 : Research Findings Summary

Managerial Survey Findings Summary	Top Management Interview Findings Summary	Expert Focus Group Findings Summary
A1. Continuous IT infrastructure investment currently	B1.Currently economic turbulence has limited impact on IT investment decision due to it medium- and long-term deliverables.	C1. Current economic turbulence is a seasonal factor that may be beyond the work scope of the budgeting process.

TABLE 5 : (Continued)

A2. IT infrastructure investment is based on pressure from having what competitors have.	B2. Sufficient technology to fulfil operation requirements	C2. IT infrastructure is a medium- and long-term planning requirement where contribution may be experienced during or after the economic turbulence
A3. Technology focuses on day-to-day electronic business.	B3. IT infrastructure investments to provide the platform to differentiate the market player	C3. Technological-edge service is a major differentiation in technological product competition.
A4. Felt that their organisation has over invested in ICT	B4. Slow migration to IaaS due to security and capacity concerns on shared services	C4. IaaS high baseline charges forcing impractical utility model for lower range users
A5. A technological edge is highly dynamic and evolving.	B5. IT infrastructures are nowadays considered a utility tool for day-to-day operation support.	C5. Current market saturation is forcing a competitive pricing war to attract customers.
A6. Lacking in internal IT expertise to implement technology solution	B6. Focus mainly on core operations like client service and manufacturing flow	C6. Technology resources are now available from outsourcing

Based on the findings, the following revised Directional Correlation hypothesis was developed and is discussed together with the earlier NULL hypothesis.

H_N1: Disruptive technology has low influence to competitive advantage contribution.

H_R1: Technology differentiation has high influence on disruptive technology at the point of time.

Competitive advantage can be derived from having a technological edge that is superior to what a current competitor has. Granted the fact that a mature technology can no longer provide an advantage in the mainstream market, this technology, however, can still provide golden opportunities to the emerging market where this technology is still under development. This can be concluded from the findings obtained from the top management interview shown in Table 4 under Section A5, B4 and B5. One man's shield is another man's weapon.

In the case of IaaS, it is already a stable and readily adopted product by larger enterprises in day-to-day operation. These premium products are considered luxury 'wants' by most MSMPs; however, as MSMPs cross over the fence to compete with more advanced enterprises, a want becomes a critical 'need'. According to Bannister and Remenyi (2005), "IT has revolutionized the way business is conducted as well as how businesses communicate with different entities". Furthermore, at this point of time, MSMPs need to focus on delivering their core competencies and not be distracted by complex IT infrastructure management.

H_N2: IT infrastructures have positive relation to commodity product classification.

H_R2: Commodity product classification has positive relation to IT infrastructure life cycle.

Each enterprise requires a product or services that give it a form of competitive advantage to differentiate itself from the market. When the product or service can no longer provide that edge during its product life cycle, then it becomes a disruptive technology. This is where the product becomes so saturated that almost all enterprises use it as part of their standard operating product and, therefore, it is categorised as a commodity product. Section A2 and A4 in Table 5 show this while C5 shows the product normalisation stage where the product has lost it technology superiority edge.

While the product goes through its life cycle, the same product has a different life cycle in a different environment. IaaS may have reached its peak contribution in the large enterprise, but it is growing for the MSMPs. In the example of Kodak, they "experienced a nearly 80% decline in its workforces, loss of market share, a tumbling stock price and significant internal turmoil as a result of its failure to take advantage of new technology" (Lucas & Goh, 2009). Using the utility model, MSMPs can be seen as enjoying the cream of the technological edge provided by the cloud service provider without worrying about when the product will become obsolete and be classified as a commodity product as seen in feedback by top management in Table 4 B5.

H_N3: Scare resources are associated with Medium-Size Enterprise performance.

H_R3: Utility model has high association to scarce resource.

Medium-size enterprises are constrained by resources and seek solutions with minimum capital outlay and are not usually amazed by technology skimming. Additionally, with the high uncertainty during an economic turbulence, enterprises are not confident of the direction technology might take. They seek technologies that are mature and easily available without much commitment in capital expenditure. Complex solutions require highly skilled expertise and tools to configure and maintain where MSMPs are currently lacking as shown in Table 4 Section A6 and B6. Even managing an expert is a complex process of recruitment, reskilling and retention. Therefore medium-size enterprises are enticed by all-in-one solutions that can be implemented by general users. This is where cloud service has helped to minimise the problem as suggested in Table 4 Section C6. While smaller enterprises are facing difficulties in fulfilling the minimum baseline requirement of typical cloud service as highlighted in Section C4, medium-size enterprises, on the other hand, have found the fit.

IaaS provides "IT efficiency, whereby the power of modern computers is utilized more efficiently through highly scalable hardware and software resources" (Marston, 2011) and is a product that is charged based on actual utilisation without much initial investment required. Furthermore, it also requires minimum expertise to configure and it is an advantage to enterprises that lack in-house skilled and knowledge manpower.

H_N4: Economic turbulence has positive correlation to infrastructure investment decisions.

H_R4: IT Infrastructure investment decision has low correlation with economic turbulence.

While economic turbulence can be experienced in a short period of less than a year, most IT infrastructure requires a longer period of two to three years to demonstrate positive results. This can be seen from all three respondent groups in Table 4 Section A1, B1, C1 and C2. Therefore, enterprise todays should continue to invest in IT infrastructure during this current uncertainty to prepare for future opportunities. However, prudent decisions on barebones specification for hibernation is also a strategic survival consideration.

The impact of economic turbulence is "perceived to be a secondary temporary IT importance in strategic alignment from the perspective of top management" (Leelien, 2012). Despite the economic uncertainty, businesses today are globally connected in a digital environment that still requires the same solutions irrespective of whether services are hosted internally or externally.

The interrelated findings in Table 4 showed consistent concurrent validity as seen from the feedback obtained through all three data collection instruments (survey, interview and focus group) to validate the research results. In summarising the four revised hypotheses above, it can be noted that technology life cycle is an important component in mapping technology adoption where crafting product specification is a management art for future decision makers. IT infrastructure is a medium- and long- term investment and returns can only be experienced later. While economic turbulence has created a storm for many enterprises, the cloud utility model has provided much sunshine for emerging enterprises.

Exostructure as a Service (EaaS)

In this paper, we introduce a new cycle of cloud computing service that provides the technology difference that is required by the MSMPs for sustainability during a period of economic turbulence yet competitive enough to penetrate into the larger and more lucrative multinational market places. The solution is the provision of a new service that must be resilient to the potential disruptive technology dumped by the MNC to the MSMPs. While understanding that each technology will somehow move into the commoditisation stage during their life cycle, it must have the capability to revitalise itself from the best of LAN and WAN technology. As the cloud services are embedded within the concept of a utility model, this new service should have the components of flexible costing. Assuming that the economic turbulence is a seasonal occurrence, new technology introduction should incorporate a dynamic upgrade as shown in Fig.3.

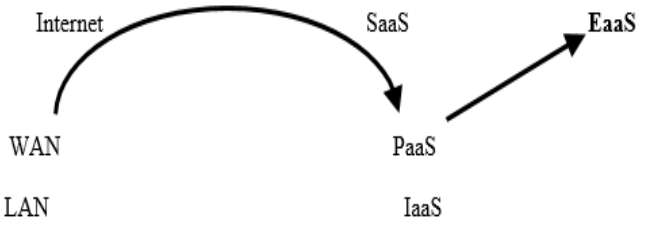

Fig.3: Infrastructure quantum leap.

Recalling Ng (2014) and Marston's (2011) findings that most MSMPs have over invested in their current IT infrastructure, EaaS will optimise the existing Local Area Network (LAN) infrastructure before expanding it into the shared services Wide Area Network (WAN). Exostructure is an extension of local IT infrastructure to a cloud computing environment. The cloud service is an integrated IaaS deployed in a Client Server environment compared to traditional SaaS and PaaS. This allows the benefits of the LAN to be integrated with the benefits of the WAN. This ensures local infrastructure is optimised while maximising the utility model for the excess resources.

EaaS will provide the technological edge for the enterprise to differentiate itself from other medium-size enterprises to penetrate the new market place when they move into the global market share of larger enterprises. In the example of an enterprise moving towards electronic businesses, many new servers or solutions are required, namely electronic payment servers or store front web servers. While servers that are costly require complex configurations, they are easily available to MSMPs via shared cloud services. Therefore MSMPs can now compete more equally in the international market instead of depending only on the local market.

Local servers will communicate with local devices like industrial robotics, input-output controllers and local applications that are sensitive to acute response time with high data transmission load. Speed and localised infrastructures are required due to specific local application that is indispensable and non-substitutable factors in the core processes. This could be a typical Network Access Solution (NAS), Manufacturing Resource Planning (MRP) or Enterprise Resource Planning (ERP). However, Ng's (2013) research highlighted the alarming over-investment by most MSMPs. With EaaS, local infrastructure investment is kept to the minimum barebones level, thus saving cost especially during economic turbulence when cost does matter for sustainability reasons. However, other additional processing and storage requirements can be offloaded into a remote infrastructure for batch processing. As the infrastructure requirement grows beyond local capabilities, this excess requirement is then extended to shared cloud services like Infrastructure as a Service (IaaS). This is done via configuration of network (router and switches) parameters to make the IaaS transparent to local client servers. Depending on the economic sales cycle, these requirements can have a volatile high and low. Deploying the utility model of paying for what you use, this method balances with the enterprise's real business requirement as shown in Fig.4.

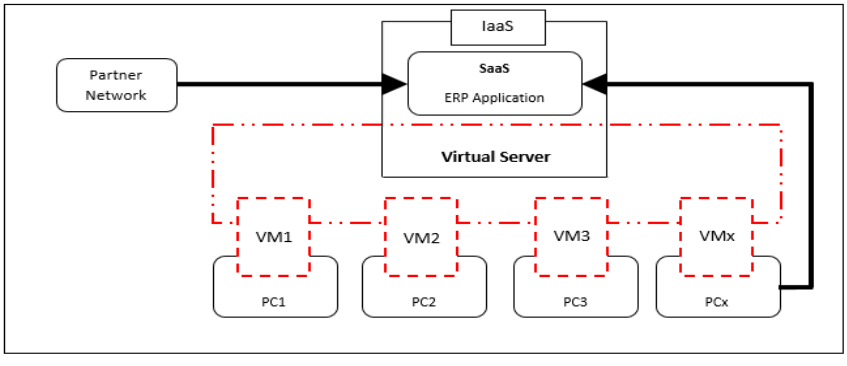

Fig. 4: EaaS logical architecture.

The local server, however, is a virtual server that emerges from the virtualisation of many local desktops that are traditionally underutilised. Here, each desktop will be installed with a tool to enable virtual machine partition to form a grid computing network that connects to a virtual server that will host the application software (like SAP financial application) in a Software as a Service (SaaS) platform. The desktop will then be reconnected to the virtual server to access the application software as if it were a normal server. As the number of desktop clients increase, the demand for processing capabilities of the virtual servers would also increase, and this is provided by the same increase in desktop. Thus, this parallel increment provides a balanced demand versus supply of resources without idle or redundant infrastructures.

Management Implications

Gartner's (2013) IT Market Clock is a powerful analysis tool to classify and describe the characteristic of a particular product or service in a simple quadratic life cycle for easier visual presentation. Fig.5 shows a revised version of the clock incorporating EaaS as the main actor in moving the arm of technology life cycle.

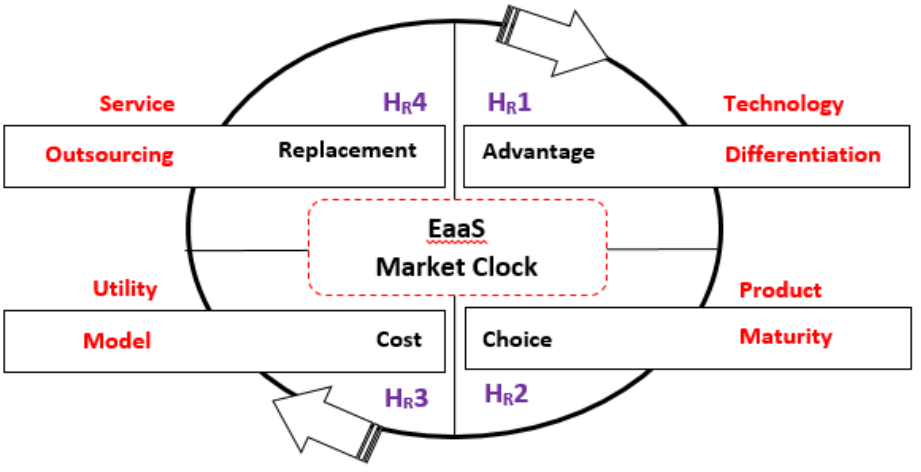

Fig.5: EaaS market clock.

As the market place becomes more saturated and turbulent, aggressive MSMPs need to acquire a new technological edge to gain the competitive advantages and differentiate themselves among the players. MSMPs today are global multi-site enterprises with networks of factory, sales office and distribution centres integrating with customers and suppliers who also have multi-site locations where speed of deployment for new products and services does matter. All these require electronic commercial solutions like payment gateways and a centralised solution for a multi-branch network that requires high capital expenses (CAPEX) that are traditional unaffordable for the MSMPs, but are now easily deployed via cloud services. This readily available solution allows for a rapid response to changing technological needs via fast deployment with minimum startup delay. Furthermore, these cloud services are more tolerant of innovation with extensive third-party connectivity to merchant banks and major

regulatory services. Enterprise sales are a seasonable contribution where holding excessive infrastructure can be wastage yet on the other hand, they are unable to support growth opportunity when it arises, which is indeed a loss. With the dynamics of economic turbulence, EaaS can allow MSMPs to mitigate negative business turnover with options to terminate or scale down services. This operating expenses (OPEX) model will avoid any potential pitfall of underutilised investment as highlighted earlier.

Cloud services have now matured as a standard operating platform of choice for enterprise as the product is already a mature technology. This allows for the creation of a standard operating procedure in the enterprise and also with partner enterprises as they share the same cloud platform. This allows the MSMPs to securely add capacity on demand. A variety of multiple vendors allows for wider comparison and competitive solution costs, making it more affordable. The standardisation of the cloud services comes with more open architectural interoperability of products and providers, thus eliminating proprietary legacy technology dependencies and customer locking. This flexibility allows MSMPs greater choice when deciding the value differentiations, thus avoiding commoditisation of product or services.

Economic turbulence is a major factor that causes enterprises to hold or take a wait-and-see attitude on their next investment decision. This is where the utility model is highly elastic as the enterprise only pays for the service acquired and thus avoids unproductive asset idling especially for enterprises that have flat or declining IT budgets. The utility model also allows greater values from superior technology returns at lower investment with internal savings for internal support services to operate IT operations and these may include electricity to power up their data centre. Non-IT services can also include human-resource services to hire IT personnel and stationery. This helps MSMPs to concentrate on their core operation and avoid distractions from IT operations. The utility model also allows the MSMPs to obtain the required level of support assurance in line with the service level agreement, thus providing measurable management implications. Threats to one enterprise may be an opportunity for another enterprise, and this is the period where MSMPs can seize the opportunity to negotiate further discounts on charges from their cloud service providers. EaaS also enhances MSMPs' corporate social responsibility activities by being more environmental-friendly as it replaces their internal data centre with a centralised cloud provider and, thus, reduces carbon footprint and physical space usage.

MSMPs currently face challenges in up-scaling experts, skills and knowledge especially in high-end systems such as complex human capital management to accommodate flexible growth. With the outsourcing of backend infrastructure to cloud service providers, already scarce MSMPs may focus on their core competencies to maintain sustainability during economic turbulence. Outsourcing also helps to reduce training cost associated with continuous development of in-house expertise or even retiring redundant IT personnel. The implementation of EaaS also allows enterprises be up-to-date on competitive emerging technologies and to seek strategic advantages. With the outsourcing of IT infrastructure, huge office floor space can be reused to house MSMPs' core support services including more space for sales and marketing personnel to bring in more revenue.

IT infrastructure requires higher capital expenditure upfront while results can only be experienced years later with a market clock constraint. These products have a dynamic shelf

life and, therefore, requires future upgrade or replacements to avoid becoming just an expensive tool. By implementing EaaS as a pay-per-service utility model, this burden is transferred to the cloud service provider while relieving the MSMPs of complex IT strategic and divestment decision.

CONCLUSION

As the current economic environment is still very vulnerable, MSMPs need to have a strategic IT infrastructure strategy not only for sustainability but also to gain competitive advantage. Economic turbulence is no longer a period for lazy hibernation but a golden opportunity for reenergising. Enterprises need to spend less, follow the emerging trend, adopt less risky investment while understanding their own vulnerabilities. EaaS makes eminent sense to a new framework for MSMPs, which for the time being, have been suppressed by unavailable new ideas for a competitive advantage leap. MSMPs should not fear economic turbulence but rather embrace it in order to differentiate between sustainability and competitiveness.

Despite the poor resources of MSMPs, IT infrastructure has revolutionised the way MSMPs must compete to contribute to national productivity. While volatile economies can be largely attributed to many uncontrollable factors, strategic IT infrastructure investment decisions can still be optimised internally. EaaS enables MSMPs to shift from traditional slow organic growth hierarchies to a more aggressive one capable of penetrating into a larger enterprise marketplace while other less aggressive ones remain indecisive during a volatile economy.

In this paper, we have highlighted the evolved meaning of commodity IT infrastructure and revised it by redefining the 'disruptive environment' to mean moire than purely 'disruptive technology'. The findings appear to contradict Carr and Clayton's theory that IT infrastructure still has potential growth opportunity before it reaches the commodity level for emerging medium-size enterprises. This paper highlights new consequences of basing long-term IT infrastructure solely on their evolved theories. Furthermore, the argument that technology has saturated and no longer provides a competitive edge is no longer valid as it can explore new, untapped new enterprises. While IaaS is focused on pooling of Internet shared resources and client servers are focused on local interaction with backend processing, EaaS is an integrated barebones of a LAN and WAN infrastructure environment. EaaS is a solution that will provide the flexibility to grow while MSMPs transition themselves during critical periods of economic turbulence.

Localised cloud services are far from complete, and this allows deeper research into the EaaS specification development. This paper has focused on the qualitative framework development and opportunities for future quantitative research are still wide. This paper further serves as a reference for future implementation during a volatile economy that may recur and, therefore, MSMPs must be prepared, as reminded by Pong (2013), "US recession: it's closer than we think". MSMPs must strategise themselves beyond barebones cloud infrastructure services that may be the stumbling block to competitiveness during economic turbulence or risk becoming irrelevant.

REFERENCES

Abareshi, A., Martin, W., & Molla, A. (2012). The role of information and communication technologies in moving toward new forms of organizing. *International Journal of Business Information Systems, 9*(2), 169-188.

Antonov, A. (2013). New business-oriented global/regional information network. *International Journal of Business Information Systems, 12*(3), 321-334.

April manufacturing sales down 5.2%. (2013, Jun 12). *SunBiz, The Sun*. p. 18.

Bannister, F., & Remenyi, D. (2005). Why IT continues to matter: Reflection on the strategic value of IT. *Electronic Journal Information Systems Evaluation, 8*(3), 159-168.

Bharadwaj, A., Sawy, O. A. E., Pavlou, P. A., & Venkatraman, N. (2013). Visions and voice on emerging challenges in digital business strategy. *MIS Quarterly, 37*(2), 633-661.

Bhatt, G. D., & Grover, V. (2005, Fall). Types of information technology capabilites and their tole in competive advantage: An emperical study. *Journal of Management Information Systems Evaluation, 22*(2), 253-277.

Bloomberg. (2013). *Najib sees Malaysia escaping Fitch rating cut Southeast Asia. Bloomberg.* Retrieved from http://www.bloomberg.com/news/2013-10-13/najib-sees-malaysia-escaping-fitch-rating-cut-southeast-asia.html. Accessed on 2013, Jul 11, 2013.

Brigg, R. O., & Numamaker, J. (2013). Special issue: Multiple dimension of value in information system. *Journal of Management Information Systems, 29*(4), Spring 2013, 97-102.

Brown, S. A., Venkatesh, V., & Goyal, S. (2012). Expectation confirmation in technology use. *Information Systems Research, 23(*2), 474-487.

Carr, N. G. (2003, May). IT doesn't matter. *Harvard Business Review,* pp.41-49.

Carr, N. G. (2005, May). The end of corporate IT. Computerworld, *MIT Sloan Management Review, 46*(3), 66-73.

Chandio, F. H., Abbasi, M. S., Nizamani, H. A., & Nizamani, Q. U. A. (2013). Online banking information systems acceptance: A structural equation modelling analysis. *International Journal of Business Information Systems, 12*(2), 177-193.

Christensen, C. M. (2006). The ongoing process of building a theory of disruption. *Journal of Product Innovation Management, 23*(1), 39-55.

Czamecki, C., & Spiliopoulou, M. (2012). A holistic framework for the implementation of a next generattion network. *International Journal of Business Information Systems, 9*(4), 385-401.

Daim, T. U., Basoglu, A. N., Gunay, D., Yildiz, C., & Gomez, F. (2013). Exploring technology acceptance for online food services. *International Journal of Business Information Systems, 12*(4), 383-403.

Danneels, E. (2004). Disruptive technology reconsidered: A critique and research agenda. *Journal of Product Innovation Management, 21*(4), 246-258.

Dihal, S., Bouwman, H., Reuver, M. D., Warnier, M., & Carlsson, C. (2013). Mobile cloud computing: State of the are and outlook. *Info, 15*(1), 4-16.

Drnevich, P. L., & Croson, D. C. (2013). Information technology and business level strategy: Toward an integrated theoretical perspective. *MIS Quarterly, 37*(2), 483-509.

Fitch revises Malaysia outlook to negative. (2013). *Reuters*. Retrieved from http://www.reuters.com/article/2013/07/30/fitch-revises-malaysias-outlook-to-negat-idUSFit66566620130730. Accessed on 2013 Jul, 11, 2013.

Gannon, B. (2013). Outsiders: An exploratory history of IS in Corporation. *Journal of Information Technology, 28*(1), 50-62.

George, J. F., Valacich, J. S., & Valor, J. (2004). Does IT still matter? *Twenty-Fifth International Conference on Information Systems,* pp.1039-1048.

Gu, J. W., & Jung, H. W. (2013). The effects of IS resources, capabilities and qualities on organizational performance: *An integrated approach. Information & Management, 50*(2-3), 87-97.

Gupta, P., Seetharaman, A., & Raj J. R. (2013). The usage and adoption of cloud computing by small and medium businesses. *International Journal of Information Management, 33*(5), 861-874.

Joseph Ng, P. S., Choo, P. Y., Wong, S. W., Phan, K. Y., & Lim, E. H. (2012). Hibernating ICT infrastructure during rainy days. *Journal of Emerging Trends in Computing and Information Sciences, 3*(1), 112-116.

Joseph, N. P. S. (2011). Energizing ICT infrastructure for SMES competitiveness during economic turbulence. *SCOReD 2011,* Putrajaya, Malaysia, 328-332.

Joseph, N. P. S., Mahmood, A. K., Choo, P. Y., Wong, S. W., Phan, K. Y., & Lim, E. H. (2013). Battles in volatile information and communication technology landscape: the Malaysia small and medium enterprise case. *International Journal of Business Information Systems, 13*(2), 217-234.

Joseph, N. P. S., Mahmood, A. K., Choo, P. Y., Wong, S. W., Phan, K. Y., & Lim, E. H. (2014). IaaS cloud optimisation during economic turbulence for Malaysia small and medium enterprise. *International Journal of Business Information Systems, 16*(2), 196-208.

Joseph, N. P. S., Mahmood, A. K., Yin, C. P., Wan, W. S., Yuen, P. K., & Heng, L. E. (2014). Barebone cloud IaaS: revitalisation disruptive technology. *International Journal of Business Information Systems, 18*(1), 107-126.

Kappelman, L., Luftman, J., & McLean, E. (2014). SIM IT trend study 2013, SIMposium, 2013, November, Boston, http://bit.ly/1asjfDN, Accessed on 2014, Jan 18, 2014.

Kaurffman, R. J., Weber, T. J., & Wu, D. J. (2012, Fall). Special section: Information and competitive strategy in a networked economy. *Journal of Management Information Systems, 29*(2), 7-10.

Kleis, L., Chwelos, P., Ramirez, R. V., & Cockburn, I. (2013). Information technology & intangible output: The impact of IT investment on innovation productivity. *Information Systems Research, 53*(1), 42-59.

Kun, S. I., Grover, V., & Teng, James T. C. (2013). Research note, do large firms becomes smaller by using information technology? *Information Systems Research, 24*(2), 470-491.

Lee, C. Y., Park, H. J., & Park, Y. T. (2013). Keeping abreast of technology driven business model evolution: A dynamic patent analysis approach. *Technology Analysis and Strategic Management, 25*(5), 487-505.

Leelien, K. H. (2012, Winter). The impact of IT management sophistication on perceived IT importance in strategic alignment. *Journal of Computer Information Systems, 53*(2), 50-64.

Li, X. X., & Chen, Y. X. (2012). Corporate IT standardization: Product compatibility, exclusive purchase commitment and competition effects. *Information Systems Research, 23*(4), 1158-1174.

Linden, A., Tampereen, T. Y., & Porin, Y. (2013). The importance of technology in the ICT requirement definition process, *PICMET 2013*, 2283-2295.

Lucas, H. C., & Goh, J. M. (2009). Disruptive technology: How Kodak missed the digital photography revolution. *Journal of Strategic Information Systems, 18*(1), 46-55.

Luftman, J., Zadeh, H. S., Derksen, B., Santana, M., Rigoni, E. H., & Huang, Z. D. (2012). Key information technology and management issues 2011-2012: An international study. *Journal of Information Technology, 27*(3), 198-212.

Marston, S., Li, Z., Bandyopadhyay, S., Zhang, J., & Ghalsasi, A. (2011). Cloud computing – The business perspective. *Decision Support Systems, 51*(1), 176-189.

Otim, S., Dow, K. E., Grover, V., & Wong, J. A. (2012). The impact of information technology investments on downside risk of the firm: alternative measurement of the business value of IT. *Journal of Management Information Systems, 29*(1), 159-194.

Paliokaite, A. (2012). The relationship between organisational foresight and product innovation in small and medium size enterprise. *8th International PhD Conference, School on National Systems of Innovation and Economic Development.* Globelic Academy.

Rong, K., Lin, Y., Shi, Y., & Yu, J. (2013). Linking business ecosystem lifecycle with platform strategy: A triple view of technology, application or orgnisaton. *International Journal of Technology Management, 62*(1), 75-105.

Santos, B. L. D., Zheng, Z., Mookerjee, V. S., & Chen, H. Y. (2012). Are new IT enable investment opportunies dimishing for firms? *Information Systems Research, 23*(2), 287-305.

Schryen, G. (2013). Revisting IS business value research: What we already know, what we still need to know and how we can get there. *European Journal of Information Systems, 22*(2), 139-169.

Sen, S., & Raghu, T. S. (2013). Interdepencies in IT infrastructure services: Analyzing service processes for optimal incentive design. *Information Systems Research, 24*(3), 822-841.

Starbiz. (2013). *World Bank cuts growth outlook as world enters new normal*. Retrieved from http://biz.thestar.com.my/news/ story.asp?file=/2013/6/13/business/20130613085623&sec=business. Accessed on 2103, Jun 13.

Stratechery.com (2013). *What Clayton Christensen got wrong*. http://stratecgery.com/2013/clayton-christensen-got-wrong. Accessed on 2013, Dec 2.

Sultan, N. (2013). Making use of cloud computing for healthcare provision: Opportunities and challenges. *International Journal of Information Management, 34(*2), 861-874.

Tambe, P., & Hitt, L. M. (2013). Measuring information technology spillover. *Information System Research, 25*(1), 53-71.

Tellis, G. J. (2006). Disruptive technology or visionary leadership? *Journal of Product Innovation Management, 23*(1), 34-38.

Tsai, K. H., & Hsu, T. J. (2012). Linking cross functional collaboration, innovation performance and competitive intensity: Towards a medicated moderation perspective. *Asian Journal of Technology Innovation, 20*(1), 113-126.

Venkatesh, V., Brown, S. A., & Bala, H. (2013). Bridging the qualitative-quantitative divide: Guideline for conducting mixed methods research in information systems. *MIS quarterly, 37*(1), 21-54.

Venters, W., & Whitley, E. A. (2012). A critical review of cloud computing: researching desires and realities. Journal of Information Technology, 27(3), 179-197.

Vinekar, V., & Teng, J. T. C. (2012). IT impacts in information and physical product industries. Journal of Computer Information Systems, 53(1), 65-71.

Wang, N. X., Liang, H. G., Zhong, W. J. Xue, Y. J., & Xiao, J. H. (2012, Fall). Resource structuring or capability building? An empirical study of the business value of Information Technology. Journal of Management Information Systems, 29(2), 325-367.

Zhang, Y., & Shaw, J. D. (2012). From the editors, Publishing in AMJ – Part 5, Crafting the methods and results. Academy of Management Journal, 55(1), 8-12.

Pertanika J. Sci. & Technol. 24 (1): 123 - 136 (2016)

SCIENCE & TECHNOLOGY

Journal homepage: http://www.pertanika.upm.edu.my/

Optimisation of Combined Acid and Enzymatic Hydrolysis of Cocoyam Starch to Produce Fermentable Hydrolysate

Amenaghawon, N. A.*, Osagie, E. I. and Ogbeide, S. E.

Department of Chemical Engineering, Faculty of Engineering. University of Benin, PMB 1154, Ugbowo, Benin City, Edo State, Nigeria

ABSTRACT

Dilute acid hydrolysis and enzymatic hydrolysis were sequentially combined for the purpose of producing fermentable hydrolysate from cocoyam starch. A three variable Box Behnken design was used to study the effect of temperature, time and acid concentration for the acid hydrolysis step while for the enzymatic hydrolysis step, the variables optimised were temperature, time and pH. A total of 17 individual experiments were generated for each step of the hydrolysis and were used to develop regression models for each step. The regression models developed to represent the acid and enzymatic hydrolysis steps were statistically significant ($p<0.05$) and did not show lack of fit ($R^2>0.9$). For the acid hydrolysis step, the regression model predicted the maximum sugar concentration to be 79.81 g/L at optimum temperature 100°C, time 11.66 min and acid concentration 1.5% w/w. For the enzymatic hydrolysis step, the regression model predicted the maximum sugar concentration to be 93.44 g/L at optimum temperature 58ºC, time 55 min and pH of 5.5.

Keywords: Acid hydrolysis, box Behnken design, cocoyam, enzymatic hydrolysis, reducing sugar

INTRODUCTION

Root and tuber crops are among the most important group of food crops in many tropical African countries. In Nigeria for instance, cassava (Manihot esculenta) is the most important of these crops in terms of total production, importance and economic value (Okoye *et al*., 2008). Cocoyam (*Colocasia esculenta*), which belongs to the Araceae family, ranks third after cassava and yam (Onyenweaku & Okoye, 2007). According to a report by Ogunniyi (2008), Nigeria is the world's largest producer of cocoyam, accounting for about 40% of total world output as recorded by the Food and Agriculture Organisation in 2007 (FAO, 2007). Despite this, Nigeria and other developing nations are beset by the problem of lack of proper storage facilities for these tubers and as such, a large number of these tubers in the order of millions of tons are destroyed through pest infestation,

Article history:
Received: 22 September 2014
Accepted: 9 June 2015

E-mail addresses:
andrew.amenaghawon@uniben.edu (Amenaghawon, N. A.),
osagie.ebuwa@uniben.edu (Osagie, E. I.),
samuel.ogbeide@uniben.edu (Ogbeide, S. E.)
*Corresponding author

ISSN: 0128-7680

deterioration, physical damage to the tubers, pilfering etc. (Omemu *et al*., 2005). In order to recover the losses resulting from this wastage, it is important to expand the usage range of these tubers with particular focus on converting them into value-added products.

The cocoyam tuber is rich in carbohydrate, containing about 77.9% starch (Akpata & Babalola, 2012). This starch can be hydrolysed to sugar syrups, which are employed by the food industry to make sweet drinks and juices (Betiku & Adesina, 2013). It can also be fermented by a suitable microorganism to produce organic acids such as citric acid, gluconic acid, oxalic acid and bioalcohols such as bioethanol and biobutanol (Kunamneni & Singh, 2005; Amenaghawon & Aisien, 2012). Conventionally, starch is converted to reducing sugars via dilute acid catalysed hydrolysis (Anozie & Aderibigbe, 2011; Amenaghawon *et al*., 2013a). It typically involves the use of dilute acids such as sulphuric acid, hydrochloric acid, phosphoric acid and nitric acid to hydrolyse the starch by cleaving the α and β linkages in the starch molecule (Najafpour *et al*., 2007). Nevertheless, the conversion of starch to glucose is never complete; hence, acid hydrolysis is typically combined with enzymatic hydrolysis in a sequential manner to obtain improved yield of reducing sugars (Woiciechowski *et al*., 2002; Amenaghawon *et al*., 2013b).

The conditions of hydrolysis such as temperature, time, pH etc. influence the yield of reducing sugars. Very little work has been done on the hydrolysis of cocoyam starch to produce hydrolysates (Omemu *et al*., 2005; Ajao *et al*., 2009; Braide & Nwaoguikpe, 2011). To the author's knowledge, no attempt has been made to sequentially combine acid hydrolysis with enzymatic hydrolysis to produce fermentable hydrolysate from cocoyam starch. In addition, none of these studies attempted to optimise the conditions of hydrolysis using statistically designed experiments for response surface methodology (RSM). It is important to optimise the variables that could influence the hydrolysis process in order to obtain the maximum yield of sugars during hydrolysis. RSM is a comprehensive experimental design and statistical modelling tool that is utilised for the optimisation of multivariable processes (Box & Wilson, 1951). Its main advantage is the ability to minimise the number of experimental runs needed to be conducted in order to obtain statistically acceptable results (Betiku *et al*., 2013).

In this work, cocoyam starch was converted into reducing sugars in a sequentially combined two-step acid and enzymatic hydrolysis. To optimise the process, RSM was applied to determine the effects of three factors (temperature, time and acid concentration) over three levels and their interactions on the amount of reducing sugar released during the acid hydrolysis step. For the enzymatic hydrolysis step, the factors considered were temperature, time and pH.

MATERIALS AND METHODS

Cocoyam Starch Preparation

Cocoyam tubers were obtained from the Faculty of Agriculture model farm in the University of Benin, Benin City, Edo State, Nigeria. The tubers were washed in clean water to remove the adhering dirt, after which they were peeled manually and crushed using a roller mill. The crushed pulp was sieved with a sieve of Teflon cloth. The starch obtained was allowed to settle for about 12 hours. It was decanted and the starch cake obtained was oven dried. The dried starch was then packed in a container for storage (Betiku & Adesina, 2013).

Enzymes

Amyloglucosidase obtained from the biotechnology division of the Federal Institute of Industrial Research Oshodi (FIIRO), Lagos, Nigeria was used for the enzymatic hydrolysis step.

Dilute Acid Hydrolysis

Dilute acid hydrolysis of the prepared cocoyam starch was carried out in a 500 mL Duran round-bottom flask using dilute hydrochloric acid concentration in the range 0.5-1.5% w/w and 10 g of cocoyam starch. The operating conditions of the hydrolysis reaction were as follows: temperature (80-100°C) and time (5-15 min). The mixture of starch in acid was heated rapidly to the set point temperature and upon completion of the hydrolysis reaction, the reaction vessel was removed from the thermostat heating mantle and cooled under running tap water. Once cooled, the liquid content of the round-bottom flask was filtered using a Whatman No. 4 filter paper to obtain a clear hydrolysate that was subsequently analysed for fermentable sugars.

Enzymatic Hydrolysis

The hydrolysate resulting from the acid hydrolysis step at the optimised conditions was subjected to enzyme treatment. The pH was adjusted to the appropriate level using a citrate-phosphate buffer as required. Amyloglucosidase of concentration 1% (v/v) was added for the enzymatic hydrolysis to take place. After the hydrolysis reaction, the enzyme was deactivated by heating the mixture to 100°C for 10 min. The final mixture was centrifuged at 10,000 rpm for 10 min and the supernatant was analysed for reducing sugar.

Analytical Methods

The reducing sugars recovered from the cocoyam starch during hydrolysis were quantified using the method of Miller (1959). To 1 mL of the supernatant, 3 mL of dinitrosalicylic acid (DNS) reagent was added in the test tube and the mixture was boiled for 5 min. It was subsequently cooled and diluted appropriately, after which the absorbance was measured at a wavelength of 540 nm using the UV-Visible Spectrophotometer (PG Instruments model T70).

Experimental Design

TABLE 1 : Box Behnken Design for Acid Hydrolysis Step

Independent Variable	Symbols	Coded and Actual Levels		
		-1	0	+1
Temperature (°C)	X_1	80	90	100
Time (min)	X_2	5	10	15
Acid Concentration (w/w %)	X_3	0.5	1.0	1.5

TABLE 2 : Box Behnken Design for Enzymatic Hydrolysis Step

Independent Variable	Symbols	Coded and Actual Levels		
		-1	0	+1
Temperature (°C)	X_1	55	60	65
Time (min)	X_2	55	60	65
pH (-)	X_3	5.5	6.0	6.5

A three variable Box Behnken design (BBD) for response surface methodology was used to develop a statistical model for both hydrolysis steps. The range of the variables that were optimised for both steps are shown in Tables 1 and 2. The experimental design made up of 17 runs for each step was developed using Design Expert® 7.0.0 (Stat-ease, Inc. Minneapolis, USA).

The coded and actual values of the independent variables were calculated as follows

$$x_i = \frac{X_i - X_o}{\Delta X_i} \qquad [1]$$

where x_i and X_i are the coded and actual values of the independent variable, respectively. X_o is the actual value of the independent variable at the centre point and ΔX_i is the step change in the actual value of the independent variable. The following generalised second-order polynomial equation was used to estimate the response of the dependent variable:

$$Y_i = b_o + \sum b_i X_j + \sum b_{ij} X_i X_j + \sum b_{ii} X_i^2 + e_i \qquad [2]$$

where Y_i is the dependent variable or predicted response, X_i and X_j are the independent variables, b_o is the offset term, b_i and b_{ij} are the single and interaction effect coefficients and ei is the error term.

RESULTS AND DISCUSSION

Statistical Modelling of the Acid Hydrolysis Step

Table 3 shows the Box-Behnken design matrix for the acid hydrolysis step. The response variable was chosen as the reducing sugar concentration. Equation (3) is the quadratic regression model in terms of actual variables that was obtained after applying a multiple regression analysis to the experimental data presented in Table 3.

$$Y = 87.81 + 0.53X_1 - 2.42X_2 - 55.98X_3 + 0.076X_1X_2 + 0.84X_1X_3 + 0.67X_2X_3 - 0.012X_1^2 - 0.26X_2^2 - 10.32X_3^2 \qquad [3]$$

The values of total sugar concentration as predicted by Equation (3) are also presented in Table 3. The results of the analysis of variance (ANOVA) carried out to determine the fit of the regression model are presented in Tables 4 and 5.

TABLE 3 : Box Behnken Design Matrix for the Optimisation of the Acid Hydrolysis Step

Run No	Factors						Response	
	Coded Values			Actual Values			Sugar Concentration (g/L)	
	X_1	X_2	X_3	X_1	X_2	X_3	Observed	Predicted
1	-1	0	-1	80	10	0.5	72.06	72.32
2	-1	1	0	80	15	1.0	61.47	62.21
3	1	1	0	100	15	1.0	69.25	70.51
4	0	0	0	90	10	1.0	75.22	75.22
5	0	1	1	90	15	1.5	70.64	69.64
6	1	0	-1	100	10	0.5	64.85	64.59
7	1	0	1	100	10	1.5	79.33	79.07
8	0	-1	-1	90	5	0.5	64.74	65.74
9	0	0	0	90	10	1.0	75.22	75.22
10	-1	-1	0	80	5	1.0	73.20	71.94
11	0	0	0	90	10	1.0	75.22	75.22
12	-1	0	1	80	10	1.5	69.66	69.92
13	0	0	0	90	10	1.0	75.22	75.22
14	0	-1	1	90	5	1.5	67.44	68.44
15	0	0	0	90	10	1.0	75.22	75.22
16	0	1	-1	90	15	0.5	61.25	60.25
17	1	-1	0	100	5	1.0	65.80	65.06

TABLE 4 : Analysis of Variance (ANOVA) of Regression Model for the Acid Hydrolysis Step

Sources	Sum of Squares	df	Mean Squares	F value	p value
Model	456.08	9	50.68	41.63	< 0.0001
X_1	1.01	1	1.01	0.83	0.3930
X_2	9.18	1	9.18	7.54	0.0287
X_3	73.02	1	73.02	59.99	0.0001
X_1X_2	57.61	1	57.61	47.33	0.0002
X_1X_3	71.23	1	71.23	58.52	0.0001
X_2X_3	11.19	1	11.19	9.19	0.0191
X_1^2	5.73	1	5.73	4.70	0.0667
X_2^2	184.73	1	184.73	151.76	< 0.0001
X_3^2	28.00	1	28.00	23.00	0.0020
Residual	8.52	7	1.22		
Lack of Fit	5.52	3	1.84	2.45	0.2034
Pure Error	3.00	4	0.75		
Cor Total	464.60	16			

TABLE 5 : Statistical Information for ANOVA for the Acid Hydrolysis Step

Source	Response Value
R_2	0.98
CV %	1.57
Adeq. Precision	22.24

The model F value of 41.63 and very low p value (<0.0001) showed that the model was significant. The lack-of-fit F value of 2.45 implies that there was insignificant lack of fit. The coefficient of variation (CV) obtained was 1.57% (Table 5). The coefficient of variation gives a measure of the degree of precision with which the treatments were carried out; a low value of CV typically implies that the treatments were carried out with high precision and reliability (XuJie & Wei, 2008). The adequate precision value of 22.24 indicates an adequate signal, and shows that the model can be used to navigate the design space (Cao *et al*., 2009). An R^2 value of 0.98 indicates that 98% of the variability in the response could be explained by the regression model (Amenaghawon *et al*., 2014). The R^2 value indicates the degree to which the model was able to predict the response. Qi *et al*. (2009) reported that the closer the R^2 value is to unity, the better the model can predict the response.

Optimisation of Dilute Acid Hydrolysis Step

The graphical representations of the regression equation for the optimisation of the acid hydrolysis step are displayed as three dimensional (3D) response surface curves in Figures 1 to 3. Fig.1 shows the effect of acid concentration and time on the total sugar concentration. For the range of time investigated, the total sugar concentration increased progressively with increase in acid concentration. This trend may be attributed to the catalytic activity of the acid. Since the hydrogen ions in a solution are responsible for the catalytic activity of the acid, increasing the acid concentration results in an increase in the number of hydrogen ions in the solution, which in turn results in a corresponding increase in the catalytic activity of the acid. Hence, the rate at which the glycosidic bonds are cleaved will increase, resulting in the formation of more fermentable sugars (Kumar *et al*., 2009). Similar observations have been reported by other researchers (Hu *et al*., 2010; Lenihan *et al*., 2010). The hydrolysis time showed a quadratic effect on the total sugar concentration as shown in Fig.1. For the range of acid concentrations investigated, intermediate levels of time were needed to obtain high fermentable sugar concentrations, and any further increase in time resulted in a decrease in sugar concentration. The decline might have resulted from the degradation of fermentable sugars to by-products such as furfural and hydroxyl methyl furfural (Najafpour *et al*., 2007).

The effect of temperature and time on the total sugar concentration is shown in Fig.2. At low values of hydrolysis time, the total sugar concentration increased with an increase in temperature. Although a similar trend was observed at high values of hydrolysis time, the rate of the hydrolysis reaction was, however, faster. This observation might be attributed to the increase in the rate of collision of the molecules of the reacting species during the reaction. Hence, the higher the temperature, the more frequently the molecules collided with each other, resulting in a reaction. With respect to time, a trend similar to that shown in Fig.1 was observed. Anozie

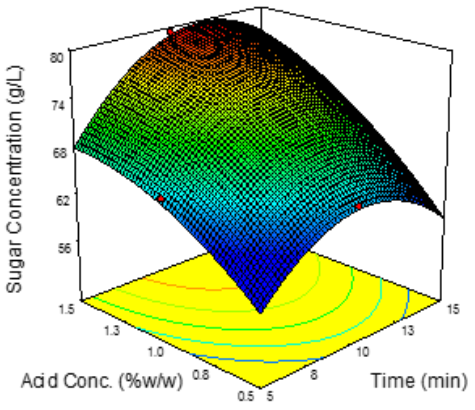

Fig.1: Effect of acid concentration and time on total sugar concentration for acid hydrolysis.

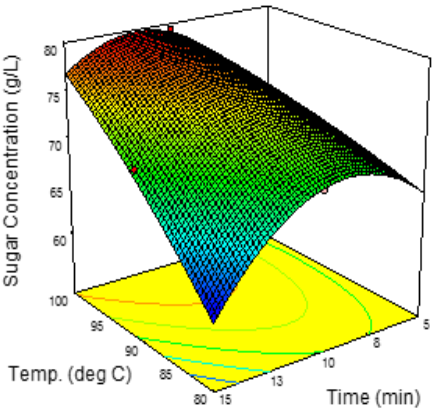

Fig.2: Effect of temperature and time on total sugar concentration for acid hydrolysis.

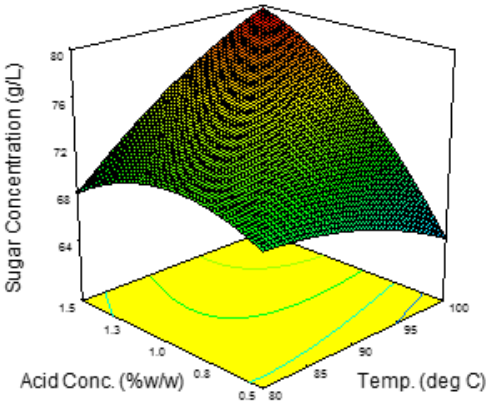

Fig.3: Effect of acid concentration and temperature on total sugar concentration for acid hydrolysis.

and Aderibigbe (2011) reported a similar trend for the optimisation of fermentable hydrolysate production from cassava starch using the response surface methodology. They observed that temperature had a positive influence on the hydrolysis reaction.

The effect of acid concentration and temperature on the hydrolysis process is shown in Fig.3. At low values of temperature, the total sugar concentration increased albeit not very significantly with an increase in acid concentration. At high values of temperature, a similar trend was observed but the hydrolysis reaction was observed to be faster as seen in the rapid increase in the total sugar concentration. This observation might not be unconnected with the enhancement of the rate of the hydrolysis reaction at high temperatures. With respect to acid concentration, the rate of the reaction was observed to be higher at higher concentrations of acid and this could also be attributed to the enhancement of the catalytic activity of the acid as a result of the increase in the amount of hydrogen ions in solution.

The regression model (Equation 3) was optimised to determine the optimum values of acid concentration, hydrolysis temperature and time that resulted in the maximum sugar concentration. The result of optimisation by RSM indicated a maximum reducing sugar concentration of 79.81 g/L. The optimum conditions of hydrolysis that resulted in this value were as follows: acid concentration, 1.5% w/w; hydrolysis temperature, 100 °C and hydrolysis time, 11.66 min. To confirm the validity of the results predicted by the model, experiments were performed in triplicate at the established optimal hydrolysis conditions. The results obtained showed that the total sugar concentration (79.14 g/L) obtained was close to the predicted value (79.81 g/L). The excellent correlation between the predicted and measured values shows the validity of the response model. Similar results have been reported by previous researchers. Anozie and Aderibigbe (2011) investigated the application of dilute acid hydrolysis for the recovery of fermentable sugars from cassava starch. Their results showed the optimum value of temperature, time and agitation speed to be 80 °C, 60 min and 200 rpm respectively. Under these conditions, the maximum reducing sugar production was recorded as 46.12 g/L. In another study, Gaewchingduang and Pengthemkeerati (2010) reported optimal hydrolysis conditions (acid concentration, time and temperature) of 0.98 %, 60 min and 120°C respectively for the conversion of starch present in cassava bagasse to fermentable sugars. This work reports a higher sugar concentration at milder conditions. Mild conditions of hydrolysis are important in the sense that there is the possibility of degradation of sugars to inhibitory products such as furfural and hydroxymethylfurfural when the hydrolysis is carried out under harsh conditions (Najafpour *et al*., 2007).

Statistical Modelling of the Enzymatic Hydrolysis Step

Results of the enzymatic hydrolysis step are shown in Table 6, which contains the coded and actual values of the variables that were optimised. The Table contains experimental sugar concentrations as well as those predicted by the regression model (Equation 4).

$$Y = 1337.42 + 29.39X_1 - 32.60X_2 - 362.54X_3 - 0.060X_1X_2 + 3.95X_1X_3 + 6.69X_2X_3 - 0.41X_1^2 - 0.045X_2^2 - 24.00X_3^2 \quad [4]$$

Table 7 shows the analysis of variance of the regression model (Equation 4). The model F-value of 9.03 and a low p value of 0.0042 implied that the model was significant. The data obtained fit the quadratic model best with an R^2 value of 0.92, showing that the model proved suitable for the adequate representation of the actual relationship between the selected variables. The lack-of-fit p value of 0.1734 showed that the lack-of-fit of the model was not significant. According to Vázquez *et al*. (2009), a non-significant lack of fit is actually desirable. This shows that the model could be used in theoretical prediction of the enzymatic hydrolysis of cocoyam starch.

The low value of CV obtained (Table 8) shows that the treatments were carried out with high reliablility (XuJie & Wei, 2008). The model can be used to navigate the design space as evident from the Adeq. Precision value obtained (Cao *et al*., 2009).

TABLE 6: Box Behnken Design Matrix for the Optimisation of the Enzymatic Hydrolysis Step

Run No	Factors						Response	
	Coded Values			Actual Values			Sugar Concentration (g/L)	
	X_1	X_2	X_3	X_1	X_2	X_3	Observed	Predicted
1	-1	0	-1	80	10	0.5	72.06	72.32
2	-1	1	0	80	15	1.0	61.47	62.21
3	1	1	0	100	15	1.0	69.25	70.51
4	0	0	0	90	10	1.0	75.22	75.22
5	0	1	1	90	15	1.5	70.64	69.64
6	1	0	-1	100	10	0.5	64.85	64.59
7	1	0	1	100	10	1.5	79.33	79.07
8	0	-1	-1	90	5	0.5	64.74	65.74
9	0	0	0	90	10	1.0	75.22	75.22
10	-1	-1	0	80	5	1.0	73.20	71.94
11	0	0	0	90	10	1.0	75.22	75.22
12	-1	0	1	80	10	1.5	69.66	69.92
13	0	0	0	90	10	1.0	75.22	75.22
14	0	-1	1	90	5	1.5	67.44	68.44
15	0	0	0	90	10	1.0	75.22	75.22
16	0	1	-1	90	15	0.5	61.25	60.25
17	1	-1	0	100	5	1.0	65.80	65.06

TABLE 7: Analysis of Variance (ANOVA) of Regression Model for the Enzymatic Hydrolysis Step

Sources	Sum of Squares	df	Mean Squares	F value	p value
Model	2879.08	9	319.90	9.03	0.0042
X_1	6.44	1	6.44	0.18	0.6827
X_2	397.95	1	397.95	11.23	0.0122
X_3	308.68	1	308.68	8.71	0.0214
X_1X_2	8.88	1	8.88	0.25	0.6320
X_1X_3	389.47	1	389.47	10.99	0.0129
X_2X3	1118.44	1	1118.44	31.56	0.0008
X_1^2	450.94	1	450.94	12.72	0.0091
X_2^2	5.26	1	5.26	0.15	0.7114
X_3^2	151.60	1	151.60	4.28	0.0774
Residual	248.11	7	35.44		
Lack of Fit	248.00	3	82.67	2.79	0.1734
Pure Error	0.10	4	0.03		
Cor Total	3127.19	16			

TABLE 8: Statistical Information for ANOVA for the Enzymatic Hydrolysis Step

Source	Response Value
R^2	0.92
CV %	9.88
Adeq. Precision	11.91

Optimisation of the Enzymatic Hydrolysis Step

The graphical representations of the regression model for the optimisation of the enzymatic hydrolysis step are displayed as three-dimensional (3D) response surface curves in Fig.4 to Fig.6. Fig.4 shows the effect of time and temperature on the concentration of sugars produced during enzymatic hydrolysis. Within the range of temperature investigated, the total sugar concentration increased with increase in time. This suggests that the residual starch in the acid hydrolysate was being converted to more sugars. Increasing the hydrolysis temperature did not favour the formation of reducing sugars. As noted earlier, this might be attributed to the degradation of sugars to unwanted products (Najafpour *et al*., 2007).

The response surface plot representing the effect of pH and temperature on sugar concentration while keeping time constant is presented in Fig.5. The results showed that more sugars were produced at low pH values, indicating that acidic conditions favoured the production of fermentable sugars during enzymatic hydrolysis. This observation was recorded both at high and low temperatures. The pH of the solution is important to the biochemical functioning of the enzyme. Changes in pH could affect the configuration of an enzyme as well as the charge properties of the substrate. Extremely high or low pH values generally result in complete loss of activity for enzymes. The loss of activity results from the inability of the substrate to bind to the active site on the enzyme as a result of the change in its configuration. In general, enzymes typically have a pH optimum with the optimum differing from one enzyme to another. The results obtained are in agreement with the fact that amyloglucosidase has the most acidic optimum pH of all amylases. It is reportedly most active at a pH value of around 5.

Fig.6 shows the effect of pH and time on the hydrolysis process. In terms of pH, a trend similar to that presented in Fig.5 was observed. However, the effect of pH was not very significant at high values of hydrolysis time.

The regression model for the enzymatic hydrolysis step (Equation 4) was optimised to determine the optimum values of hydrolysis temperature, time and pH that resulted in the maximum sugar concentration. The result of optimisation by RSM indicated a maximum reducing sugar concentration of 93.44 g/L. The optimum conditions of hydrolysis that resulted in this value were as follows: hydrolysis temperature, 58 °C; hydrolysis time, 55 min and pH, 5.5. To confirm the validity of the results predicted by the statistical model, experiments were performed in triplicate under the established optimal hydrolysis conditions. The results obtained showed that the total sugar concentration (93.14 g/L) obtained was close to the predicted value (93.44 g/L). The excellent correlation between the predicted and measured values shows the validity of the response model. Similar results have been obtained by other researchers. Sunaryanto *et al*. (2013) subjected sago starch to a combined process of acid and enzymatic

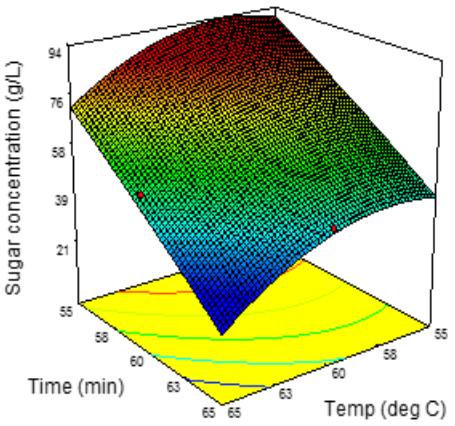

Fig.4: Effect of time and temperature on total sugar concentration for enzymatic hydrolysis.

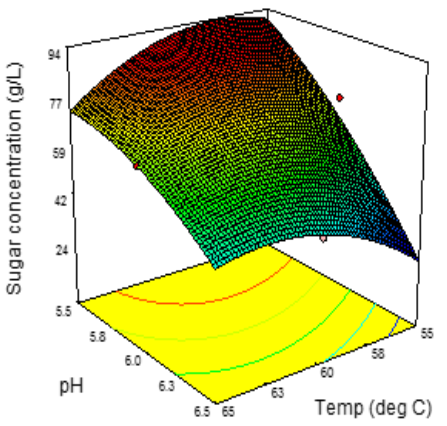

Fig.5: Effect of pH and temperature on total sugar concentration for enzymatic hydrolysis.

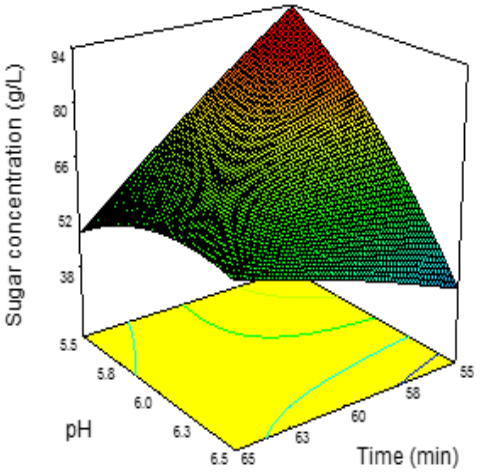

Fig.6: Effect of pH and time on total sugar concentration for enzymatic hydrolysis.

hydrolysis for the purpose of producing bioethanol. Their results showed that the maximum sugar concentration obtained for the acid hydrolysis step was 66 g/L while a value of 70 g/L was obtained for the enzymatic hydrolysis step. In another study, Betiku and Adesina (2013) reported optimum hydrolysis conditions (temperature, time and pH) of 61.05 °C, 55.02 min and 6.5 respectively for the enzymatic hydrolysis of potato starch. At these optimised conditions, the maximum sugar concentration was obtained as 172.23 g/L. The significantly higher amount of sugar recovered by Betiku and Adesina (2013) compared to the result obtained in this work could be attributed to the fact that they used twice the amount of starch used in this work.

CONCLUSION

The response surface methodology was successfully applied to the optimisation of sequentially combined acid and enzymatic hydrolysis of cocoyam starch. The regression models developed to represent the acid and enzymatic hydrolysis steps were statistically significant ($p<0.05$) and did not show lack-of-fit ($R^2>0.9$). The maximum reducing sugar concentration obtained for the acid hydrolysis step was 79.81 g/L at temperature 60 ºC, time 60 min and pH 6.5. For the enzymatic hydrolysis step, the maximum reducing sugar concentration obtained was 93.44 g/L at temperature 58 ºC, time 55 min and pH 5.5. The hydrolysate obtained in this work may be utilised as a carbon source for the biotechnological production of useful products like citric acid, gluconic acid, oxalic acid and ethanol.

REFERENCES

Ajao, A. T., Abdullahi, H. J., Atere, T. G., & Kolawole, O. M. (2009). Studies on the biodegradation and utilization of selected tuber wastes by Penicillium expansum. *Bioscience Research Communications, 21(*5), 221-227.

Akpata, D. F., & Babalola, T. O. (2012). The use of cassava, sweet potato and cocoyam, and their by-products by non-ruminants. *International Journal of Food Science and Nutrition Engineering, 2*(4), 54-62.

Amenaghawon, N. A, Nwaru, K. I., Aisien, F. A., Ogbeide, S. E., & Okieimen, C. O. (2013a). Application of Box-Behnken design for the optimization of citric acid production from corn starch using Aspergillus niger. *British Biotechnology Journal, 3*(3), 236-245.

Amenaghawon, N. A., & Aisien, F. A. (2012). Modelling and simulation of citric acid production from corn starch hydrolysate using Aspergillus niger. *Environment and Natural Resources Research, 2*(1), 73-85.

Amenaghawon, N. A., Aisien, F. A., & Ogbeide, S. E. (2013b). Bioethanol production from pretreated cassava bagasse using combined acid and enzymatic hydrolysis. University of Benin *Journal of Science and Technology, 1*(2), 48-53.

Amenaghawon, N. A., Okieimen, C. O., & Ogbeide, S. E. (2014). Modelling and statistical optimization of dilute acid hydrolysis of eucalyptus wood chips using response surface methodology. *Pacific Journal of Science and Technology, 15*(1), 245-256.

Anozie, A. N., & Aderibigbe, A. F. (2011). Optimization studies of cassava starch hydrolysis using response surface method. *New Clues in Science, 1*, 37-43.

Betiku, E., & Adesina, O. A. (2013). Optimization of sweet potato starch hydrolyzate production and its potential utilization as substrate for citric acid production. *British Biotechnology Journal, 3*(2), 169-182.

Betiku, E., Akindolani, O. O., & Ismaila, A. R. (2013). Enzymatic hydrolysis optimization of sweet potato (ipomoea batatas) peel using a statistical approach. *Brazilian Journal of Chemical Engineering, 30(*3), 467-476.

Box, G. E. P., & Wilson, K. B. (1951). On the experimental attainment of optimum conditions (with discussion). *Journal of the Royal Statistical Society Series B, 13*(1), 1-45.

Braide, W., & Nwaoguikpe, R. N. (2011). Production of ethanol from cocoyam (*Colocasia esculenta*). *International Journal of Plant Physiology and Biochemistry, 3*(3), 64-66.

Cao, G., Ren, N., Wang, A., Lee, D. J., Guo, W., Liu, B., Feng, Y., & Zhao, Q. (2009). Acid hydrolysis of corn stover for biohydrogen production using Thermoanaerobacterium thermosaccharolyticum W16. *International Journal of Hydrogen Energy, 34(*17), 7182-7188.

FAO (2007). *FAOSTAT Statistics Division of the Food and Agriculture Organization.* Retrieved from http://faostat.fao.org.

Gaewchingduang, S., & Pengthemkeerati, P. (2010). Enhancing efficiency for reducing sugar from cassava bagasse by pretreatment. *World Academy of Science, Engineering and Technology, 46,* 727-730.

Hu, R., Lin, L., Liu, T., & Liu, S. (2010). Dilute sulfuric acid hydrolysis of sugar maple wood extract at atmospheric pressure. *Bioresource Technology, 101*(10), 3586-3594.

Kumar, P., Barrett, D. M., Delwiche, M. J., & Stroeve, P. (2009). Methods for pretreatment of lignocellulosic biomass for efficient hydrolysis and biofuel production. *Industrial and Engineering Chemistry Research, 48*(8), 371-3729.

Kunamneni, A., & Singh, S. (2005). Response surface optimization of enzymatic hydrolysis of maize starch for higher glucose production. *Biochemical Engineering Journal, 27*(2), 179-190.

Lenihan, P., Orozco, A., O'Neill, E., Ahmad, M. N. M., Rooney, D. W., & Walker, G. M. (2010). Dilute acid hydrolysis of lignocellulosic biomass. *Chemical Engineering Journal, 156*(2), 395-403.

Miller, G. L. (1959). Use of dinitrosalicylic acid reagent for determination of reducing sugar. *Analytical Chemistry, 31*(3), 426-428.

Najafpour, G., Ideris, A., Salmanpour, S., & Norouzi, M. (2007). Acid hydrolysis of pretreated palm oil lignocellulosic wastes. *IJE Transactions, 20*(2), 147-156.

Ogunniyi, L. T. (2008). Profit efficiency among cocoyam producers in Osun State, Nigeria. International *Journal of Agricultural Economics & Rural Development, 1*(1), 38-46.

Okoye, B. C., Onyenweaku, C. E., & Agwu, A. E. (2008). Technical efficiency of small-holder cocoyam farmers in Anambra State Nigeria: Implications for agricultural extension policy. *Journal of Agricultural Extension, 12*(1), 107-116.

Omemu, A. M., Akpan, I., Bankole, M. O., & Teniola, O. D. (2005). Hydrolysis of raw tuber starches by amylase of Aspergillus niger AM07 isolated from the soil. *African Journal of Biotechnology, 4*(1), 19-25.

Onyenweaku, C. E., & Okoye, B. C. (2007). Technical efficiency of small-holder cocoyam farmers in Anambra State, Nigeria: A translog stochastic frontier production function approach. *International Journal of Agriculture and Rural Development, 9*(1), 1-6.

Qi, B., Chen, X., Shen, F., & Wan, Y. (2009). Optimization of enzymatic hydrolysis of wheat straw pretreated by alkaline peroxide using response surface methodology. *Industrial and Engineering Chemistry Research, 48*(15), 7346-7353.

Sunaryanto, R., Handayani, B. H., & Safitri, R. (2013). Enzymatic and acid hydrolysis of sago starch for preparation of ethanol production. *Microbiology Indonesia, 7*(2), 68-74.

Vázquez, M., Delgado, R., & Castro, A. J. (2009). Modelling of the enzymatic hydrolysis of potato (*Solanum tuberosum*) using response surface methodology. *Starch, 61*(10), 601-609.

Woiciechowski, A. L., Nitsche, S., Pandey, A., & Soccol, C. R. (2002). Acid and enzymatic hydrolysis to recover reducing sugars from cassava bagasse: An economic study. *Brazilian Archives of Biology and Technology, 45*(3), 393-400.

XuJie, H., & Wei, C. (2008). Optimization of extraction process of crude polysaccharides from wild edible BaChu mushroom by response surface methodology. *Carbohydrate Polymers, 72*(1), 67-74.

Pertanika J. Sci. & Technol. 24 (1): 137 - 163 (2016)

PERTANIKA JOURNALS

SCIENCE & TECHNOLOGY

Journal homepage: http://www.pertanika.upm.edu.my/

Simulation of a Bioreactor with an Improved Fermentation Kinetics – Fluid Flow Model

Emily Liew Wan Teng[1] and Law Ming Chiat[2*]

[1]*Department of Chemical Engineering, Faculty of Engineering and Sciences, Curtin University, Sarawak Campus, CDT 250, 98009 Miri, Sarawak, Malaysia*

[2]*Department of Mechanical Engineering, Faculty of Engineering and Sciences, Curtin University, Sarawak Campus, CDT 250, 98009 Miri, Sarawak, Malaysia*

ABSTRACT

Ethanolic fermentation experiments were carried out using a stirred tank equipped with a Rushton turbine. The data were used to estimate kinetic parameters based on a newly developed kinetics model originated from Herbert's microbial kinetics model. This newly developed model took into account the effects of aeration rate (*AR*) and stirrer speed (*SS*). Experiment data i.e. glucose, ethanol and biomass concentrations obtained from different experiment sets were used for kinetics prediction. Assuming a perfectly-stirred condition, the kinetic parameters were initially estimated through solving Herbert's model equations. These estimated kinetic parameters were then incorporated in a Computational Fluid Dynamics (CFD) model but the simulation results did not agree well with the experiment findings. Based on the proposed CFD model, the kinetic parameters were corrected. The correction factors were expressed as functions of *AR* and *SS*. This analysis highlighted the need to estimate kinetic parameters based on CFD simulation because it is able to account for the spatial variation in a reactor. A sensitivity analysis of the kinetic parameters using the coupled CFD-fermentation kinetic model was carried out to further understand the influence of each set of kinetic parameters on the model prediction. It was found that the sensitivities of the kinetic parameters varied with the concentrations of glucose, ethanol and biomass.

Keywords: Bioreactor, CFD, ethanol, fermentation, kinetics, Rushton turbine

INTRODUCTION

Bioreactors are most widely used in chemical and bioprocess industries such as fermentation, for mixing and combining liquids for biochemical reactions (Harvey & Rogers, 1996). It is vital to ensure that the requirements of the microbial environment were met for maximum microbial growth, such as temperature, pH and oxygen content

Article history:
Received: 14 October 2014
Accepted: 14 April 2015

E-mail addresses:
emily2703@gmail.com (Emily Liew Wan Teng),
m.c.law@curtin.edu.my (Law Ming Chiat)
*Corresponding author

ISSN: 0128-7680

(Hutmacher & Singh, 2008). As a result, the bioreactor performance is complex due to the complicated interrelations between the microbial cells and the governing environment. The exact description of flow movement by a simple model is not possible as the flow caused by the impeller embedded in the bioreactor is overlapped by turbulence fluctuations.

Another main issue to be addressed is the kinetics of ethanolic fermentation. It is evident that an ideally mixed assumption is inadequate to describe the wide range of length scales present in stirred tanks (Fox, 1998). Thus, it is vital to employ micro-mixing behaviour for a stirred tank. So far, most kinetics is limited to macro-kinetics i.e. the interactions of the microenvironment around the microbial cells with its dependency on the biological reaction are not taken into account. The metabolism of microorganisms is very complex, whereby the metabolism varies during the cycle of cell growth and replication. These phenomena cause inhomogeneity of the microorganism population. There might be morphological differentiation of microbial cells accompanied by changes in the cell metabolisms. Thus, what is observed is only an averaged behaviour over the great number of cells in different states. It is tough to establish a very detailed model to describe all the microbial metabolic activities. One of the ways suggested is the consideration of aeration rate (*AR*) and stirrer speed (*SS*) as manipulated variables in the bioreactor system. According to García-Ochoa and Gomez (2009), the most important operating conditions in a stirred tank bioreactor are *AR* and *SS*. This is due to the fact that in a stirred tank bioreactor, high values of mass and heat transfer rates are attained. Oxygen mass transfer is influenced by both *AR* and *SS* (García-Ochoa *et al*., 1995). Both *AR* and *SS* offer more effects via the mixing mechanism of a stirred tank bioreactor compared to other operating conditions as both affect the mass, heat and oxygen transfer throughout the bioreactor operation and provide turbulence in the bioreactor.

Starzak *et al*. (1994) summarised a list of kinetic models that were used to simulate the kinetic ethanolic fermentation process. These kinetic models consist of a set of ordinary differential equations (ODE), which describe the material balance of biomass, product (ethanol) and substrate (glucose). Optimisation techniques were used to obtain the model constants by minimising the error between the kinetic models and experiment data. All these approaches assumed perfectly mixed behavior, which neglects the spatial variation of the fermentation process. Spatial variation of the fermentation process is defined as the variation throughout the bioreactor tank that is associated with microorganism population.

In order to analyse the highly complex fluid flow in mechanically stirred reactors, computational fluid dynamics (CFD) offers a potentially useful tool for this purpose. In recent years, CFD has been used intensively in the simulation of single-phase and multiphase flow within relatively simple geometries, whereby simulation results are to be compared with experiment data (Kuipers & van Swaaij, 1998). Nevertheless, there are only a few CFD simulations that coupled fluid flow and fermentation in the models. This is due to large-time scale difference between fluid flow and its reactions. Consequently, CFD simulation of fermentation process is too time-consuming. Van Zyl (2012) developed a three-dimensional (3-D) CFD model with the incorporation of fermentation reactions. However, the reaction terms were not strongly coupled with the fluid flow physics and the CFD results were not compared with the experiment data. In addition, there were also a number of CFD-reaction models but these were on different reactions such as gluconic acid (Elqotbi *et al*., 2013) and

polymerisation processes (Patel *et al*., 2010; Roudsari *et al*., 2013). To avoid an excessive computing effort, Bezzo and Macchietto (2004) proposed a hybrid multizonal/CFD approach to the model bioreactor. The computational domain was divided into 20 zones and a perfectly-stirred reactor model was assumed in each zone. Liew *et al*. (2013) simulated a CFD with fermentation reaction; however, since it was a steady-state model, it is impossible to assess the accuracy of the simulation with experiment data as a function of time.

The objectives of this study were: (a) to carry out an experimental study on *AR* and *SS* on biomass, substrate (glucose) and product (ethanol) concentrations in a mechanically-stirred tank bioreactor; (b) to determine the kinetic parameters of the fermentation process using a perfectly-stirred reactor model and experiment data from (a); (c) to incorporate the kinetic parameters obtained in (b) with a simplified time-dependent CFD model that does not require much computational time, and (d) to conduct CFD simulations for the prediction of the bioreactor performance, in terms of ethanol production in the gas-liquid mechanically-stirred bioreactor and validation with experiment results obtained in (a).

MATERIALS AND METHODS

The schematic diagram of the experiment setup is shown in Fig.1. Experiments were carried out in a 2L elliptical-bottom shaped cylindrical tank of internal diameter of 0.128m that was transparent to light. A six-bladed Rushton turbine impeller of diameter 0.044m was utilised for this experimental study. Glucose was utilised as the main substrate for the fermentation medium. Air was admitted to the bioreactor using a cylindrical sparger located at the bottom of the tank, beneath the impeller. Agitation was carried out using a variable speed DC motor. The speed ranged from 30 to 1,100 rpm for the 2L bioreactor tank specification. The DC motor drive was a maintenance free, 150W quiet, direct motor-driven operation.

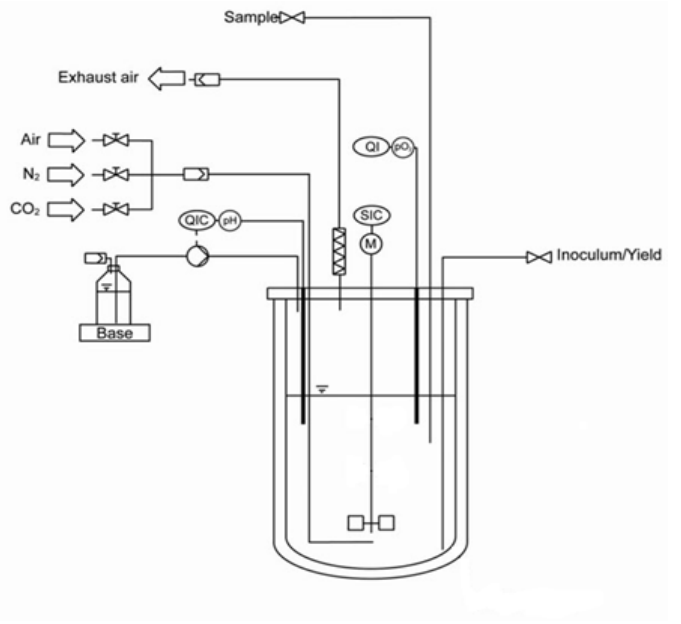

Fig.1: Schematic diagram of experiment setup used for this study.

Microorganism and Inoculum

Experiments were conducted using a BIOSTAT A-plus 2L, MO-Assembly bioreactor operated in batch mode. This bioreactor was a solid, autoclavable laboratory bioreactor system that was suitable for a wide range of research and industrial applications. It was applicable for microbial culture for the growth of bacteria, yeast and fungi as well as cell culture for the growth of animal, insect and plant cells.

A Rushton turbine was utilised to study the effect of agitation, whereas an air sparger was utilised to study the effect of aeration. Commonly used for efficient mixing and maximum oxygen transfer within the bioreactor, the Rushton turbine is a disc turbine that was used in many fermentation processes for fast air stream break-up without itself becoming flooded in air bubbles (Stanbury & Whitaker, 1995).

On the other hand, 40 mL of inoculum was prepared in a conical flask and was incubated at 28 °C for 8 hours. The microorganism used in this study was *Saccharomyces cerevisiae*, which is the most commonly used microorganism in fermentation processes (Schugerl & Bellgardt, 2000). *Saccharomyces cerevisiae* was purchased in ready-made powder form from Sigma Aldrich. Thus, there was no isolation and screening of the microorganisms. *Saccharomyces cerevisiae* was directly added into the inoculum for growth to occur, and the pH was adjusted to pH 5 for optimum growth. It was vital that the inoculum was prepared in a contamination-free environment due to its physiological condition, which had a major effect on fermentation. Therefore, the conical flask was sterilised before usage to avoid any contamination. Steam was utilised for sterilisation and was applied at 15 psi. The inoculum was prepared based on the formulation by Thatipamala *et al*. (1992), which is outlined in Table 1, along with an addition of 1 g of Baker's yeast. Baker's yeast was added after the inoculum was autoclaved. The inoculum was then incubated for 8 hours.

TABLE 1 : Inoculum Preparation Formulation

Constituents	Amount (g/L)
Glucose	50
Yeast extract	5.0
NH_4Cl	2.5
Na_2HPO_4	2.91
KH_2PO_4	3.0
$MgSO_4$	0.25
$CaCl_2$	0.08
Citric acid	4.3
Sodium citrate	3.0

Fermentation Medium

The composition of the fermentation medium was also prepared by Thatipamala *et al*. (1992). 1.5 L of the fermentation medium was prepared in the bioreactor tank by adding the constituents listed in Table 1 that were similar to the inoculum preparation formulation, without the addition

of Baker's yeast. The fermentation medium was then sterilised under 121 °C for 20 mins and allowed to cool down under room temperature at 30 °C. After 4 hours, the freshly prepared 40 mL of inoculum was added to the cooled fermentation medium and mixed thoroughly.

Operating Conditions

Once the fermentation medium had been mixed, the pH of the medium was measured and subsequently adjusted to pH 5 with the addition of acid (sulphuric acid) or alkali (sodium hydroxide). The temperature was adjusted to 30 °C and maintained with the utilisation of a temperature controller, which was embedded in the bioreactor. *AR* and *SS* were set according to the preferred conditions, respectively.

The fermentation process was started after all these operating conditions were maintained at the desired settings. Samples taken at sampling intervals of 2 to 4 hours were analysed for glucose and ethanol concentrations immediately after the samples were extracted from the bioreactor. The experiments were repeated at various conditions of *AR* and *SS* within the range of 1.0-1.5LPM of *AR* and 100-150rpm of *SS*. The operating ranges of *AR* (1.0LPM-1.5LPM) and *SS* (100-150rpm) were selected for this study as a preliminary study for the improved kinetics model. The operating ranges for both *AR* and *SS* were not within a large range as it would be easier to analyse the possibility of both parameters in future studies. Should the effects of both parameters in the improved kinetics model be low, the range would be increased in future studies.

Bioreactor Operating Cycle

The bioreactor was ready for operation once the inoculum and fermentation mediums were ready. The bioreactor was connected to a computer that was fully automated with control systems, with operating parameters such as pH, temperature, oxygen content, *AR* and *SS* that could be controlled automatically. Once all operating parameters were set based on the desired conditions, the fermentation process began, and the operating parameters were recorded in the computer throughout the fermentation process. Samples were extracted during the fermentation process every 2 hours; sampling was stopped once the fermentation process was completed after 45 hours.

Analytical Procedures

After the samples were extracted from the bioreactor, the samples were first filtered and then analysed for the concentrations of glucose and ethanol concentrations, as well as optical density. Glucose and ethanol concentrations were analysed using R-Biopharm test kits and UV spectrophotometer under a wavelength of 340 nm, as outlined in the procedures manual provided by the test kits. The UV spectrophotometer utilised was Perkin Elmer Lambda 25 UV/Vis Systems with a range between 190 and 1,100 nm (with a fixed bandwidth of 1 nm). However, for the analysis of optical density, no test kits were required as the UV spectrophotometer could directly analyse the optical density measurements. All samples were tested under room temperature for consistency. Optical density was measured to observe the microorganisms'

growth throughout the fermentation process. The optical density decreased subsequently with fermentation time. Once the optical density decreased steadily, the results indicated that the fermentation process was completed as the microorganisms' growth had halted.

Modelling

Assumptions. It is expensive to simulate a complete three-dimensional (3-D) model of the bioreactor. To reduce the computational time, a two-dimensional (2-D) model was developed. In addition, air was not accounted for in the 2-D model due to its small volume fraction in the bioreactor. To verify this assumption, a 3-D CFD model of the bioreactor (without reaction) was simulated using commercial software STAR-CCM+ (version 8.04, CD-adapco, UK) and it was found that average volume fraction of air was about 0.8%, as shown in Fig.2. In addition, the oxygen consumption rate was not calculated in the model. Consequently, the gas phase was not considered. Nevertheless, the effect of the oxygen was accounted implicitly throughout the kinetic scheme discussed in the later section.

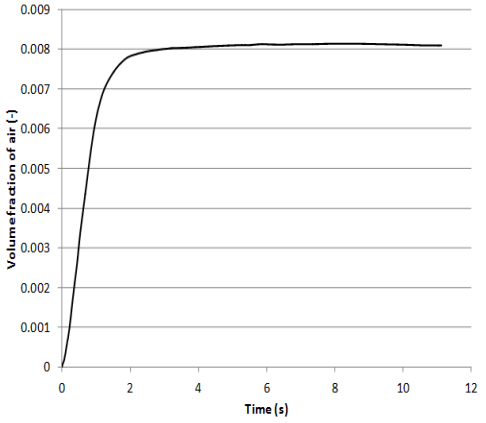

Fig.2: The average volume fraction of air simulated by a 3-D CFD model.

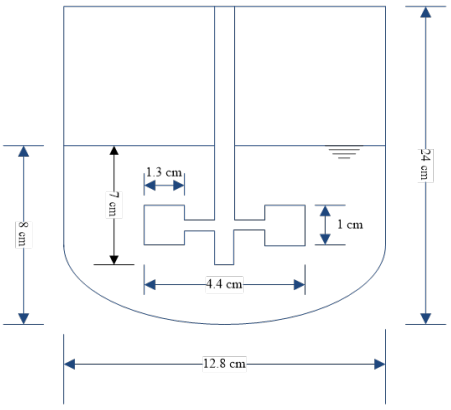

Fig.3: Geometry of the bioreactor.

Model description. Generally, a CFD analysis often involves a number of procedures. Firstly, a computational domain of the problem under investigation has to be identified. After that, a set of governing equations that describe the physics of the phenomenon has to be determined. These governing equations are often presented in the form of partial differential and algebraic equations. The initial input and boundary conditions for the governing equations are required in order to obtain a unique solution for the CFD analysis. The following section describes the methodology used in the CFD analysis of this current work.

Computational domain. The dimensions of the stirred stank are shown in Fig.3. However, due to the symmetry of the tank, only half of the bioreactor tank was simulated in this current study.

Governing transport equations. To calculate the liquid velocity in the bioreactor, Navier-Stokes equations were required to be solved. These equations consist of mass and momentum conservation equations. The equations were required to be solved simultaneously as they are

coupled. As the experiment was carried out at isothermal condition, the density change was negligible. The specific temperature used in this study was room temperature at 30 ºC. Thus, incompressible flow was assumed. The mass conservation equation for the incompressible bioreactor solution can be expressed as:

$$\rho\nabla\cdot\mathbf{u}=0 \qquad [1]$$

where ρ is the density of the bioreactor solution, $\mathbf{u}$ is the velocity vector and ∇ is the divergence operator (Versteeg & Malalasekera, 2007).

On the other hand, since the liquid density was significant ($\rho \approx 1023$ kg/m^3), the volume force due to the liquid mixture, $\rho\mathbf{g}$, was accounted for in the momentum conservation equation, which is expressed as:

$$\rho\frac{\partial\mathbf{u}}{\partial t}+\rho(\mathbf{u}\cdot\nabla)\mathbf{u}=\nabla\cdot\left[-p\mathbf{I}+(\mu+\mu_T)\left(\nabla\mathbf{u}+(\nabla\mathbf{u})^T\right)-\frac{2}{3}\rho k\mathbf{I}\right]-\rho\mathbf{g} \qquad [2]$$

where ρ is the liquid pressure; μ is the liquid dynamic viscosity; μ_T is the turbulent viscosity and k is the turbulent kinetic energy.

The bioreactor normally operates in turbulent regime ($\mathrm{Re}\approx 40{,}000$) so the turbulent phenomenon has to be accounted for by solving the $k-\varepsilon$ equations. The turbulent kinetic energy, k can be calculated as:

$$\rho\frac{\partial k}{\partial t}+\rho(\mathbf{u}\cdot\nabla)k=\nabla\cdot\left[\left(\mu+\frac{\mu_T}{\sigma_k}\right)\nabla k\right]+P_k-\rho\varepsilon \qquad [3]$$

On the other hand, the turbulent dissipation rate, ε was obtained as follows:

$$\rho\frac{\partial\varepsilon}{\partial t}+\rho(\mathbf{u}\cdot\nabla)\varepsilon=\nabla\cdot\left[\left(\mu+\frac{\mu_T}{\sigma_\varepsilon}\right)\nabla\varepsilon\right]+C_{\varepsilon1}\frac{\varepsilon}{k}P_k-C_{\varepsilon2}\rho\frac{\varepsilon^2}{k} \qquad [4]$$

where $\mu_T=\rho C_\mu\frac{k^2}{\varepsilon}$, P_k is the turbulent kinetic energy production rate, $P_k=\mu_T+[\nabla\mathbf{u}:(\nabla\mathbf{u}+(\nabla\mathbf{u})^T)-\frac{2}{3}\rho k.\mathbf{u}]$. The values for various coefficients are $C\mu = 0.09$, $C_{\varepsilon1} = 1.44$, $C_{\varepsilon2}= 1.92$, $\sigma_k = 1.0$ and $\sigma_\varepsilon = 1.3$. These numerical values are based on curve-fitting of comprehensive turbulent flow data (Versteeg & Malalasekera, 2007).

The medium contained four main components i.e. water as well as glucose, ethanol and biomass concentrations. Since water was present in excessive amount, the remaining components were modelled as diluted species. Thus, the concentration of a component in the solution can be calculated by the following transport equation:

$$\frac{\partial c_i}{\partial t}+\mathbf{u}\cdot\nabla c_i=\nabla\cdot(D_i\nabla c_i)+R_i \qquad [5]$$

where D_i is the diffusion coefficient of the component i (i = substrate, product, biomass) and is the corresponding reaction rate. The reaction rate of each of these components is discussed in Section 3.3.

Boundary conditions and solution procedure. Wall function based on the logarithmic wall law (Kuzmin *et al*., 2007) was used at the bioreactor tank wall while the slip boundary condition was used for the liquid surface for k - ε model. The rotational speed, μ_Θ, is defined at the impeller wall by:

$$u_\theta = r\omega \qquad [6]$$

where r is the radial distance from the centre of the tank and ω is the angular velocity.

As for the species equation, zero normal gradient is implemented at the liquid surface:

$$-\mathbf{n} \cdot D_i \nabla c_i = 0 \qquad [7]$$

where $\mathbf{n}$ is the outward normal vector at the boundary.

At the bioreactor walls, no flux condition was prescribed:

$$-\mathbf{n} \cdot \left(-D_i \nabla c_i + \mathbf{u} c_i\right) = 0 \qquad [8]$$

The governing equations [1] - [8] were solved using COMSOL Multiphysics v4.1 (COMSOL, Sweden). The computational domain was meshed using 4886, 11222, 26416 elements. No appreciable difference was observed for the cases with 11222 and 26416 elements. The simulations were carried out using 26416 elements. It takes approximately 2 hours for a simulation to be completed over a 45-hour fermentation process. The model also avoids the need to simulate a three-dimensional two-phase flow model, which requires a simulation time of approximately 1 week.

Reaction kinetics of the fermentation process. In this study, the hydrodynamics of liquid-gas flows in a mechanically-stirred bioreactor tank was simulated using Herbert's concept of endogenous metabolism. This kinetics concept has been used in numerous studies to describe the kinetics of ethanolic fermentation with sufficient accuracy (Starzak *et al*., 1994). Studies on the impacts of *AR* and *SS* were focused on the concentration profiles of biomass (X), substrate (glucose) (S) and product (ethanol) (P) in terms of product yield and productivity.

In the kinetics hybrid model development, experiment data of X, S and P concentrations for different conditions of *AR* and *SS* were used to predict the kinetics parameters, k_1, k_2, k_3,..., k_6 using Herbert's concept. The range of *AR* was set to be in the range from 1.0-1.5LPM and *SS* from 100-150rpm, which is similar to the experiment range. For this purpose, Herbert's concept was applied as follows: It is assumed that the observed rate of biomass formation comprised the growth rate and the rate of endogenous metabolism, which are known as Herbert's microbial kinetics model (Starzak *et al*., 1994):

$$\begin{aligned} R_x &= (R_x)_{growth} + (R_x)_{end} \\ &= \left(\frac{k_1 S X}{k_2 + S} \exp(-k_5 P) - k_6 X \right) / 3600 \end{aligned} \qquad [9]$$

where $-k_6 X$ is the rate of growth due to endogenous metabolism by a linear dependence. The division of a constant of 3600 is to convert the reaction rate from kg/(m^{3}hr) to kg/(m^{3}s).

It was also assumed that the rates of substrate consumption and product formation were proportional to the biomass growth rate:

$$R_s = \left(-k_3 \frac{k_1 SX}{k_2 + S} \exp(-k_5 P) \right) / 3600 \quad [10]$$

$$R_p = \left(k_4 \frac{k_1 SX}{k_2 + S} \exp(-k_5 P) \right) / 3600 \quad [11]$$

Kinetic parameters based on perfectly-stirred bioreactor assumption. The kinetic parameters' estimation was obtained by minimising the errors between the experiment data and the model equations. The model formulation consisted of equations [9]-[11], which implied a perfectly-stirred tank condition (Liew *et al*., 2013). MATLAB v2006 (The MathWorks, Inc, US) was utilised to predict the values of to . Any set of experiment data within the experiment range was utilised for prediction. The experiment data was first arranged in a spreadsheet and imported into MATLAB. All initial values of substrate concentration, product concentration and biomass concentration (based on experiment data), along with the *AR* and *SS* conditions, were clearly stated in MATLAB before the prediction began. Next, initial values of k_1 to k_6 were provided as well. Any initial values of k_1 to k_6 could be assumed since the values of to would change based on different sets of experiment data provided. The initial k_1 to k_6 values could be changed after the first prediction if the values were not satisfied. ODE45 was selected as the solver for the prediction as it was the most common solver used for prediction purposes.

Next, iterations were performed to predict the values of k_1 to k_6 by utilising the solver selected. During iterations, the solver would fit the experiment data with the kinetic model embedded with the kinetics from k_1 to k_6. Iterations would stop once the values of k_1 to k_6 were predicted. The values of k_1 to k_6 were considered acceptable if the exit flag value were positive, where an exit flag was an integer that showed that iterations had been halted and completed. Positive exit flags correspond to successful outcomes whereas negative exit flags correspond to failure outcomes. Based on the assumptions proposed in this study, the total number of iterations used in ODE45 to obtain the positive and negative exit flags were approximately 1,500 and 500, respectively.

In order to check and compare the fitness of the kinetics with respect to the experiment data, plots of model fitting with respect to the experiment data were generated. In the case of unsatisfied fitness, initial values of k_1 to k_6 can be reassumed for new predictions of k_1 to k_6 values. Iterations can be done again for new predictions.

Improved kinetic parameters for CFD analysis. It was discovered that when the equation [9]-[11] were coupled with the CFD model (equations [1]-[8]), the kinetic parameters obtained from Section 3.3.1 were found to over-estimate the fermentation reaction. Hence, correction factors were introduced to the rate expressions i.e. [9]-[11]. These corrected expressions, denoted by a subscript, c , are shown as follows:

$$R_{x,c} = \left(\alpha_1 \frac{k_1 SX}{k_2 + S} \exp(-\alpha_5 k_5 P) - \alpha_6 k_6 X \right) / 3600 \quad [12]$$

$$R_{s,c} = \left(-\alpha_3 k_3 \frac{k_1 SX}{k_2 + S} \exp(-\alpha_5 k_5 P) \right) / 3600 \quad [13]$$

$$R_{p,c} = \left(\alpha_4 k_4 \frac{k_1 SX}{k_2 + S} \exp(-\alpha_5 k_5 P) \right) / 3600 \quad [14]$$

Each correction factor, i, α_i was modelled using a second-order spline, which is defined as:

$$\beta_0 + \beta_1 X_1 + \beta_2 X_2 + \beta_3 X_1 X_2 + \beta_4 X_1^2 + \beta_5 X_2^2 \quad [15]$$

where $X_1 = AR - 2$ and $X_2 = \dfrac{(SS - 225)}{75}$

The expressions of the kinetic parameters, $k_1, ..., k_6$ and the correction factors $\alpha_1, ..., \alpha_6$ are listed in Table 2.

TABLE 2 : Expressions of the Kinetic Parameters and Correction Factors

$k_1 = (1.3998 - 0.2852X_1 + 0.3692X_2) \left[\frac{\text{g}}{\text{L.hr}} \right]$	$\alpha_1 = 3.3324 + 1.4669X_1 - 0.2010X_2 + 5.8336X_1X_2 - 4.7719X_1^2 - 2.1244X_2^2$
$k_2 = 0.01 \left[\frac{\text{g}}{\text{L}} \right]$	$\alpha_2 = 1$
$k_3 = (0.5377 - 0.0148X_1 + 0.022X_2)[-]$	$\alpha_3 = 13.6026 + 13.2693X_1 + 8.3081X_2 + 7.0327X_1X_2 + 1.9638X_1^2 + 0.4782X_2^2$
$k_4 = (0.0738 + 0.0142X_1 + 0.0128X_2)[-]$	$\alpha_4 = 6.9135 + 1.0897X_1 - 0.6332X_2 + 13.5979X_1X_2 - 11.719X_1^2 - 5.336X_2^2$
$k_5 = (0.8072 - 0.1019X_1 - 0.0211X_2) \left[\frac{\text{L}}{\text{g}} \right]$	$\alpha_5 = 0.8171 + 0.3420X_1 + 0.0978X_2 - 0.4513X_1X_2 + 0.7962X_1^2 + 0.1778X_2^2$
$k_6 = (0.0228 - 0.0001X_1 - 0.0019X_2) \left[\text{hr}^{-1} \right]$	$\alpha_1 = 1.1003 + 1.60X_1 - 0.5964X_2 + 0.1664X_1X_2 + 0.2152X_1^2 - 0.1765X_2^2$

RESULTS

Experiments were conducted to study the impact of *AR* and *SS* on the production of biomass, glucose and ethanol concentrations respectively. Generally, similar trends can be identified where there is increment in ethanol concentration and biomass concentration with the increase in *AR* and *SS*. On the other hand, glucose concentration decreased with the increase in *AR* and SS. These trends are generally identified with the increase in time. In each section below, the effect of *AR* and *SS* on each concentration is discussed.

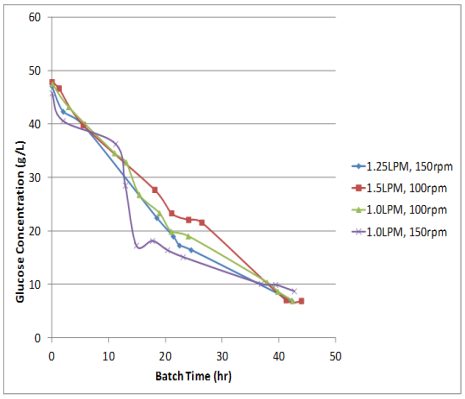

Fig.4: Graph of glucose concentration (g/L) vs. batch age (hr)

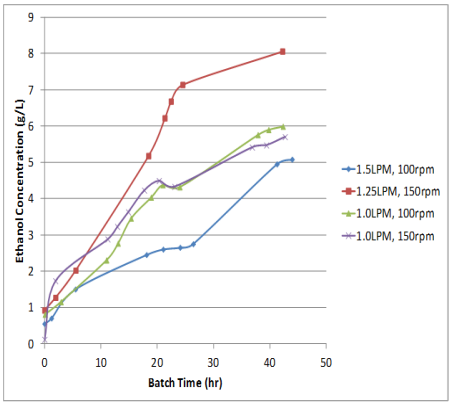

Fig.5: Graph of ethanol concentration (g/L) vs. batch age (hr).

Effect of Aeration Rate (AR) and Stirred Speed (SS) on Glucose Concentration

Fig.4 shows the trend of glucose concentration under different sets of *AR* and *SS*. As predicted, the glucose concentrations decreased with time under the influence of different sets of *AR* and *SS*. Glucose was consumed with time to produce ethanol. The rates of glucose consumption were quite comparable for all sets of *AR* and *SS*. This showed that although different conditions of *AR* and *SS* were implemented, the final glucose concentration attained was comparable. However, it is vital to investigate the amount of ethanol and biomass concentrations which can be produced under different *AR* and *SS* conditions since different amounts of glucose will be utilised to produce different amounts of ethanol and biomass concentrations.

Effect of Aeration Rate (AR) and Stirrer Speed (SS) on Ethanol Concentration

Fig.5 displays the ethanol concentration profiles under the influence of different *AR* and *SS* conditions. As predicted, as glucose concentration decreased, ethanol concentration increased with respect to time.

Generally, as observed from Fig.5, the ethanol concentration trend was not comparable under different conditions of *AR* and *SS* as compared to the glucose concentration trend from Fig.4. Notice that, when *AR* and *SS* was at 1.25 LPM and 150 rpm respectively (red line), ethanol concentration showed the highest value i.e. at 8.0 g/L. As observed from other *AR*

and *SS* conditions, the ethanol concentrations varied from 5.0 to 6.0 g/L, which were not significantly higher than 1.25 LPM *AR* and 150 rpm *SS*. These results show that although the glucose concentration trend was comparable, the ethanol concentration, however, varied under different conditions of *AR* and *SS*. Therefore, with the same amount of glucose concentration utilised, different amounts of ethanol concentration will be produced under different *AR* and *SS* conditions. Based on the ranges of *AR* and *SS* set for this study, the highest attainable ethanol concentration was at the mid-level range of *AR* i.e. 1.25 LPM, and the highest level range of *SS* i.e. at 150 rpm. The demands of the culture medium varied throughout the fermentation process, whereby the oxygen demand was low at the beginning of the process (Stanbury & Whitaker, 1995). However, due to high biomass content towards the end of the process, the oxygen demand was high. Therefore, it is evitable that at *AR* of 1.25 LPM and SS of 150rpm, highest ethanol concentration was achieved. Although 1.25 LPM was not the highest level of *AR*, with the aid of *SS*, the highest ethanol concentration was produced at this level. These results show the importance of engaging both *AR* and *SS* in the production of ethanol.

Effect of Aeration Rate (AR) and Stirrer Speed (SS) on Biomass Concentration

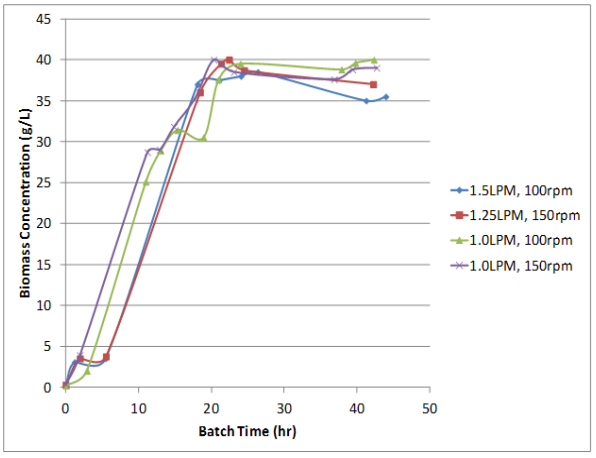

Fig.6: Graph of biomass concentration (g/L) vs. batch age (hr).

Fig.6 displays the variation of biomass concentration profile with different sets of *AR* and SS. As predicted, the biomass concentration increased with fermentation time. The rates of growth were comparable under different conditions of *AR* and *SS*. Compared to the trends of glucose and ethanol concentrations, glucose and biomass concentrations were comparable with fermentation time under different conditions of *AR* and *SS*. These observations showed that both glucose and biomass concentrations did not experience much variation within the *AR* and SS range. However, the ethanol concentration trend showed different variations with fermentation time.

Based on studies done by Cot *et al*. (2007), the different amount of ethanol concentration was not likely due to the glucose and biomass concentrations produced. It was due to the cell viability with respect to the ethanol and biomass concentrations produced. During the fermentation process, the rate of ethanol concentration formation increased. Thus, the cell viability decreased. This phenomenon is due to the inhibition of ATP synthesis or leakage of metabolites from the cells while the yeast cells were metabolically inactive (Ghareib *et al*., 1988). The plasma membrane was damaged and thus, the ethanol tolerance decreased. This caused the phospholipid content to decrease, which eventually caused cell death (Emily *et al*., 2009). Due to this condition, different amounts of glucose were utilised to produce ethanol. Biomass concentration increased throughout the fermentation process and a vast proportion of biomass was produced towards the end of the fermentation process (Stanbury & Whitaker, 1995).

CFD Results

Validation of CFD simulation result. Table 3 gives the numerical values of the corrected kinetic parameters $(\alpha_i k_i)$ and uncorrected kinetic parameters (k_i) for three different operating conditions. Simulations were carried out using these kinetic parameters and the accuracy of the models was compared with the experiment data.

TABLE 3 : Numerical Values of Corrected and Uncorrected Kinetic Parameters

Parameters	Uncorrected values	Corrected values
AR = 1 LPM, SS = 100 rpm	$k_1 = 1.0697$	$k_{1,c} = 1.3373$
	$k_2 = 0.01$	$k_{2,c} = 0.01$
	$k_3 = 0.5158$	$k_{3,c} = 0.7736$
	$k_4 = 0.03827$	$k_{4,c} = 0.1148$
	$k_5 = 0.9443$	$k_{5,c} = 0.7743$
	$k_6 = 0.02607$	$k_{6,c} = 0.01294$
AR = 1.5 LPM, SS = 100 rpm	$k_1 = 0.9271$	$k_{1,c} = 0.65$
	$k_2 = 0.01$	$k_{2,c} = 0.01$
	$k_3 = 0.5084$	$k_{3,c} = 0.4072$
	$k_4 = 0.04537$	$k_{4,c} = 0.04553$
	$k_5 = 0.8933$	$k_{5,c} = 0.7079$
	$k_6 = 0.02602$	$k_{6,c} = 0.02593$
AR = 1.25 LPM, SS = 150 rpm	$k_1 = 1.25$	$k_{1,c} = 2.50$
	$k_2 = 0.01$	$k_{2,c} = 0.01$
	$k_3 = 0.5268$	$k_{3,c} = 1.16$
	$k_4 = 0.05035$	$k_{4,c} = 0.2517$
	$k_5 = 0.90473$	$k_{5,c} =0.6633$
	$k_6 = 0.02478$	$k_{6,c} = 0.01402$

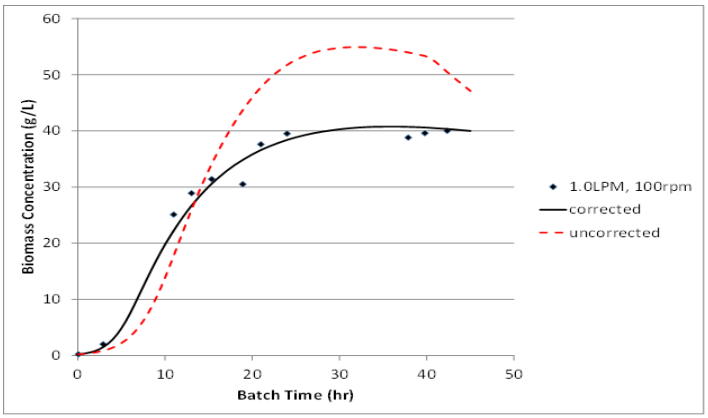

(a)

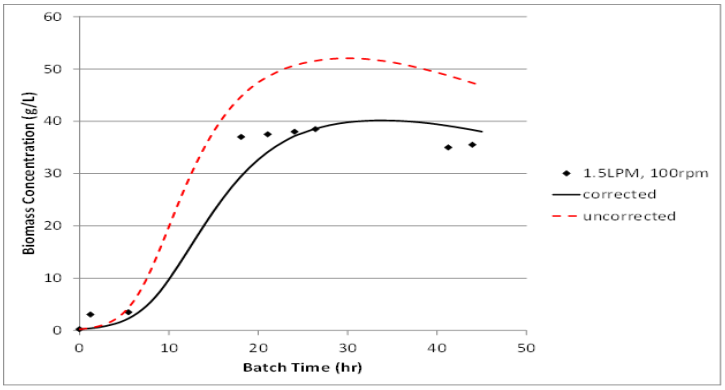

(b)

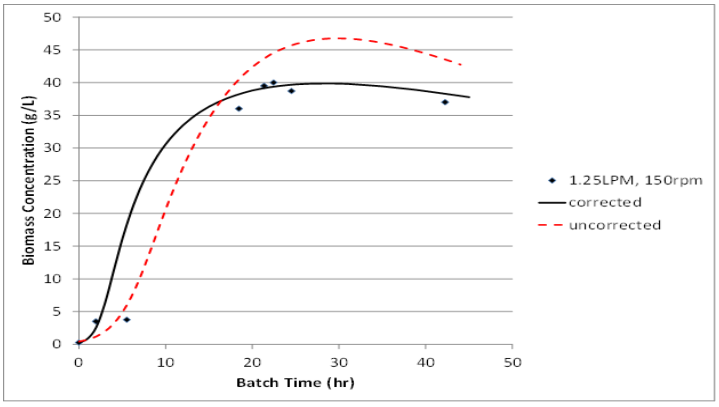

(c)

Fig.7: Prediction of biomass concentrations for (a) AR = 1.0 LPM and SS = 100 rpm; (b) AR = 1.5 LPM and SS = 100 rpm; (c) AR = 1.25 LPM and SS = 150 rpm using corrected and uncorrected kinetic parameters.

Figures 7 (a)-(c) show that the corrected kinetic model was able to predict the growth of biomass reasonably well compared to the uncorrected model for three different operating conditions. Generally, the biomass production was slow in the first few hours, e.g. batch time ≈ 4 hours for *AR* = 1.0 LPM and *SS* = 100 rpm. This is known as the lag phase, where the cells were adjusting to the medium (Rao, 2010). Then the biomass started to increase rapidly, up to batch time ≈ 20 hours. After that, the biomass content remained constant. The biomass was converted to ethanol during this process (Rao, 2010). Due to the shortage of the substrate (glucose), the biomass started to decrease. The biomass production was modelled using Monod-Herbert model, as shown in equation [9]. The growth rate was inhibited by the exponential term which was a function of ethanol concentration. The decay phase of the biomass was modelled as a linear function of biomass itself, which was significant at a high biomass concentration.

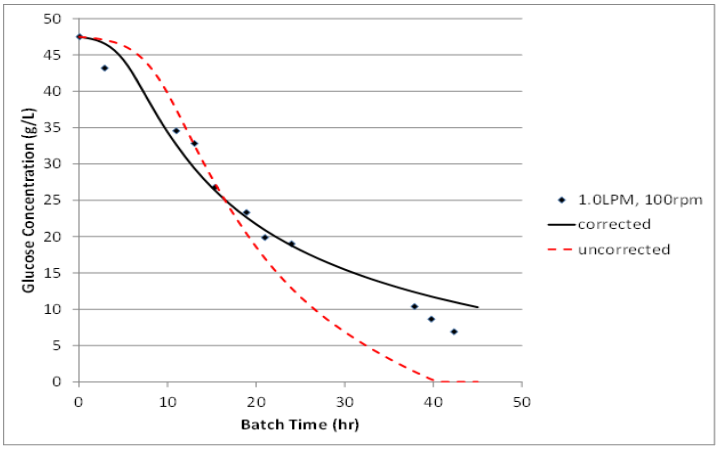

(a)

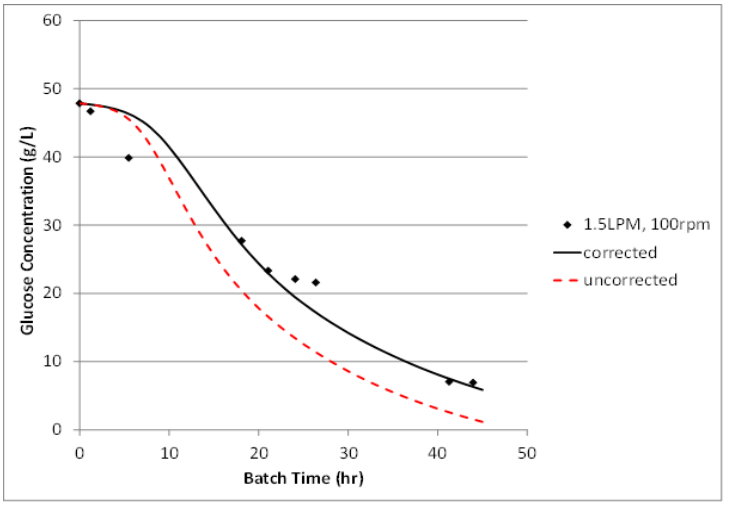

(b)

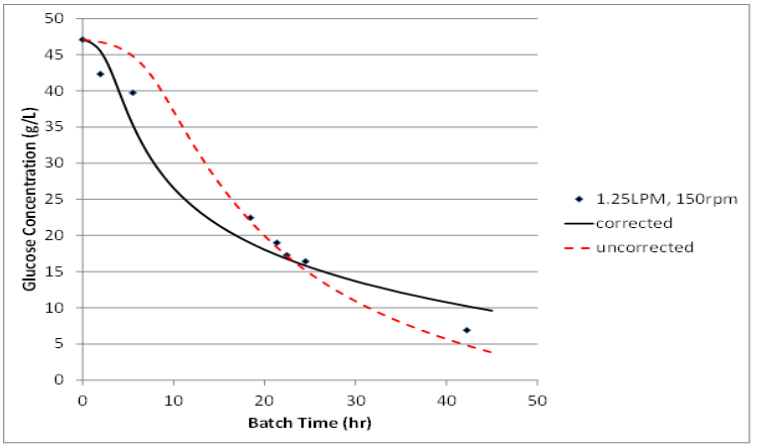

(c)

Fig.8: Prediction of glucose concentrations for (a) AR = 1.0 LPM, SS = 100 rpm; (b) AR = 1.5 LPM, SS = 100 rpm; (c) AR = 1.25 LPM, SS = 150 rpm using corrected and uncorrected kinetic parameters.

Fig.8 (a)-(c) show the simulated results of glucose consumption using the corrected and uncorrected kinetic parameters under different operating conditions. The experiment data was also shown. The results show that the uncorrected kinetics model predicted higher glucose consumption compared with the experiment findings. Similarly, the production of ethanol is assumed to be proportional to the growth of biomass; the uncorrected kinetic model underestimated the ethanol production as shown in Fig.9 (a)-(c). In both the glucose consumption and ethanol production models, the reaction rates were both inhibited at the higher ethanol concentration.

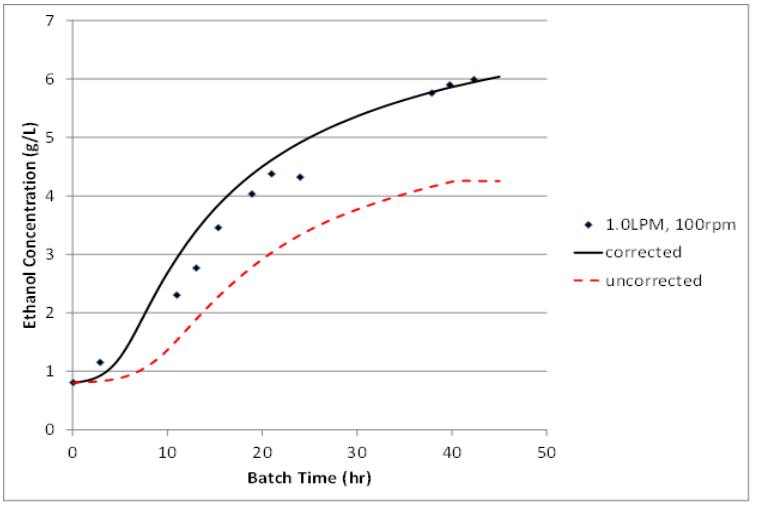

(a)

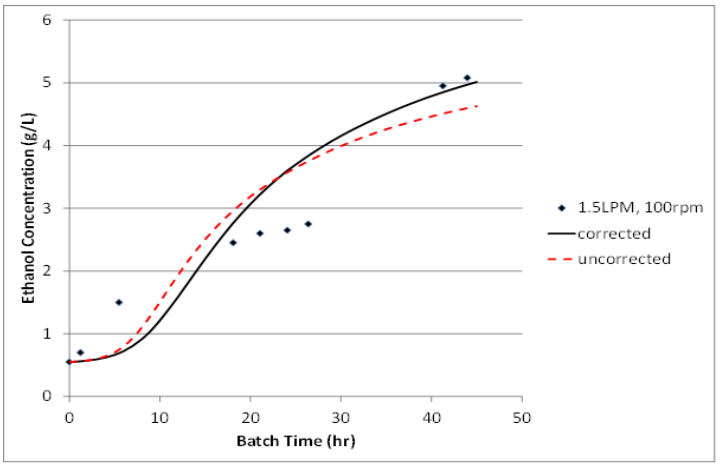

(b)

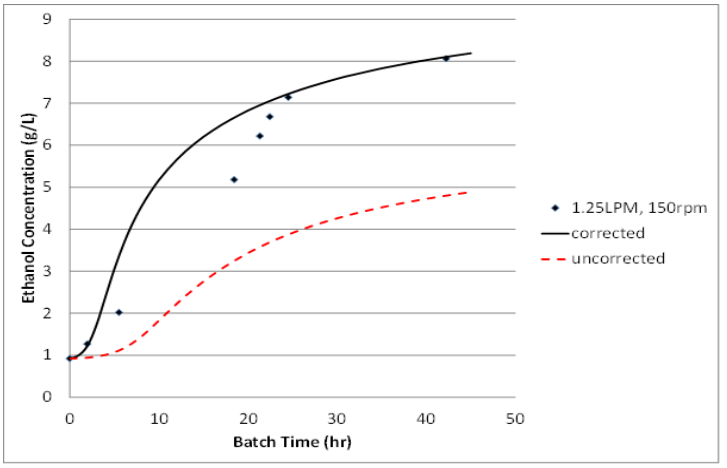

(c)

Fig.9: Prediction of ethanol concentrations for (a) AR = 1.0 LPM and SS = 100 rpm; (b) AR = 1.5 LPM and SS = 100 rpm; (c) AR = 1.25 LPM and SS = 150 rpm using corrected and uncorrected kinetic parameters.

Sensitivity Analysis of the Kinetic Parameters

The fermentation kinetics model often requires a number of parameter estimations. There are six parameters in the current study i.e. k_1 to k_6 To obtain the optimum values, it was important to carry out the sensitivity analysis of the parameter required. The analysis will reveal which parameters had a strong effect on the model results. Thus, the information was helpful in developing an optimisation algorithm for parameter estimation (Alcázar & Ancheyta, 2007). The sensitivity of the kinetic parameters, k_1 to k_6 on the biomass, ethanol and glucose was investigated for the case of AR = 1.25 LPM and SS = 150 rpm. This was treated as the baseline of the study. Each of the kinetic parameters was varied by $\pm 10\%$; the percentage differences of the material concentrations are presented in Fig.10 to Fig.15.

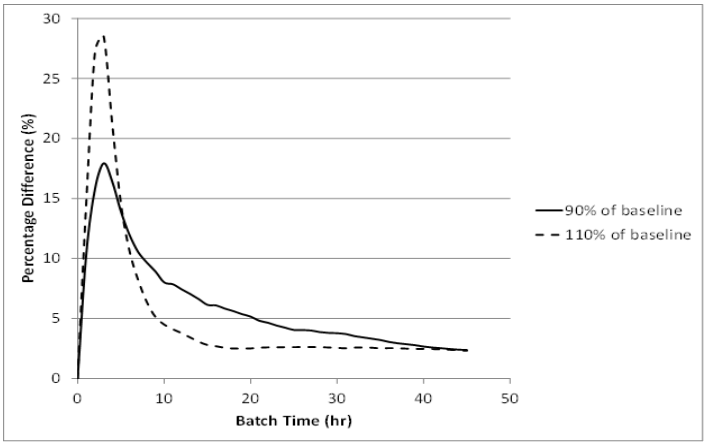

(a)

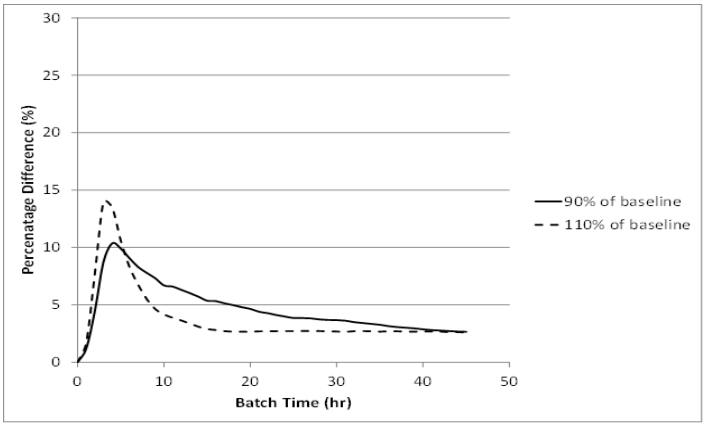

(b)

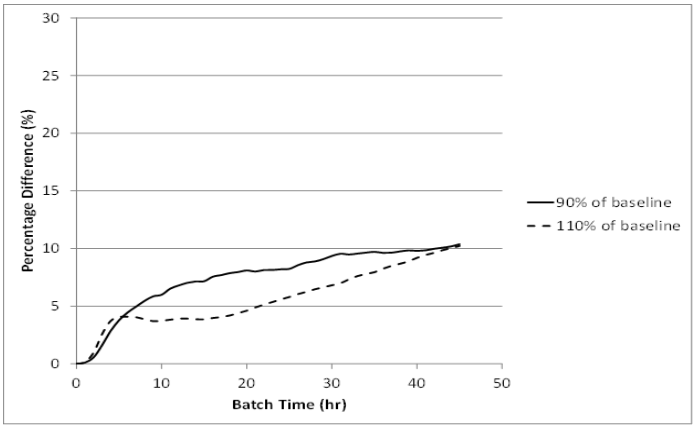

(c)

Fig.10: Percentage difference in the (a) production of biomass; (b) production of ethanol; (c) consumption of glucose, when the parameter, k_1 is changed by $\pm 10\%$.

Fig.10 (a) shows that 10% variation in k_1 caused the biomass concentration difference to increase from zero to a maximum of 28%, after which, it decreased. The initial rapid increase was due to the biomass production and the availability of the high substrate (glucose) concentration. The rapid decrease of the percentage difference was caused by lower $(R_x)_{growth}$, which was due to the inhibition effect of the product (i.e. exp $(-k_5P)$ $\frac{k_1SX}{k_2+S}$). Since biomass content was high as the batch time was longer, additional biomass produced did not cause a larger percentage difference. A similar trend was observed for the ethanol production as seen in Fig.10 (b). On the other hand, the percentage difference of the glucose increased with the batch time [Fig.10 (c)]. This was because although the glucose consumption rate was high at the initial stage, the availability of the glucose was high enough that the percentage difference was not significant. As the fermentation process proceeded, the glucose concentration was scarce and the percentage difference started to increase noticeably.

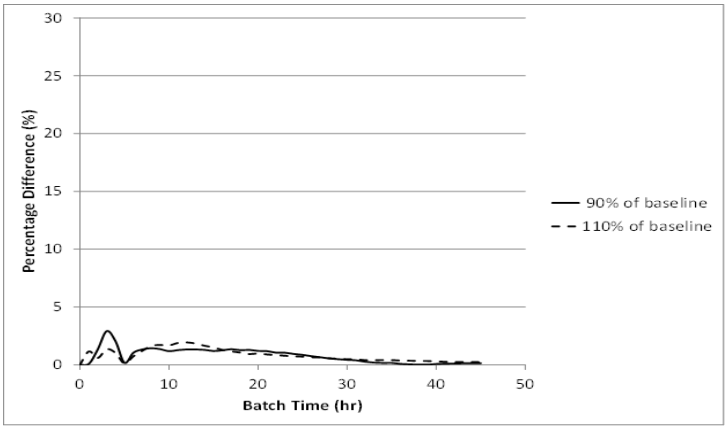

(a)

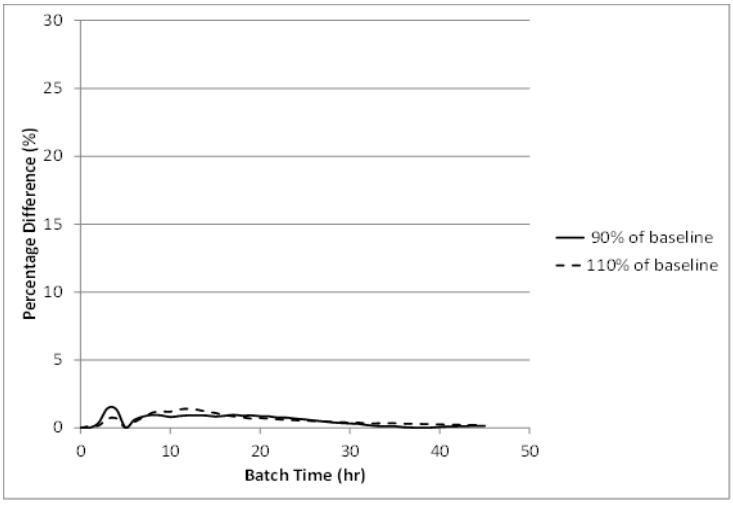

(b)

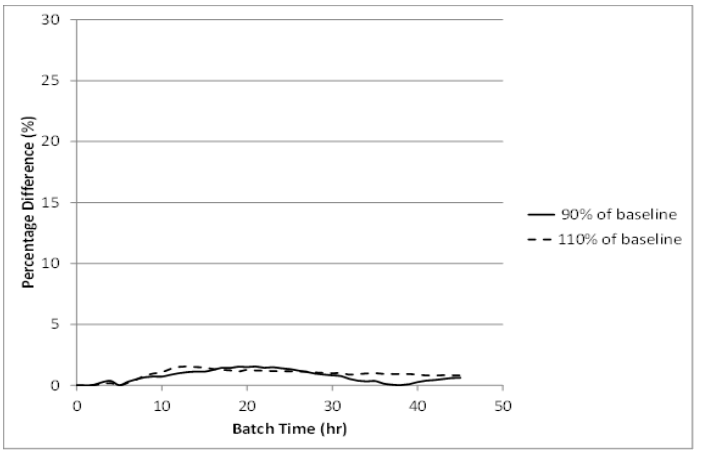

(c)

Fig.11: Percentage difference in the (a) production of biomass; (b) production of ethanol; (c) consumption of glucose, when the parameter, k_2 is changed by $\pm 10\%$.

The parameter k_2 did not have a significant effect on these three substances. Fig.11 (a)-(c) showed that the percentage differences were around 2-3% when k_2 was varied by 10%. This suggests that k_2 does not play an important role in optimum parameters estimation.

The parameter k_3 did not greatly affect the concentration of biomass and ethanol but it had a strong effect on the glucose utilisation as shown in Fig.12. Fig.12(c) indicates that the percentage difference of the glucose could be as high as 35% in the simulation, which is 3 times that of the k_3 variation.

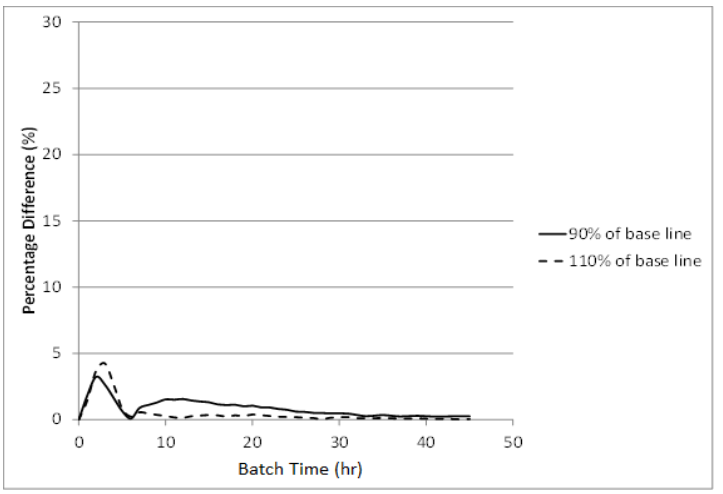

(a)

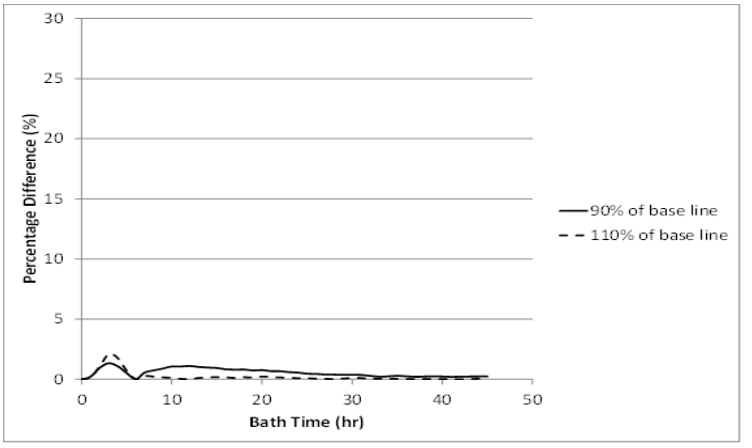

(b)

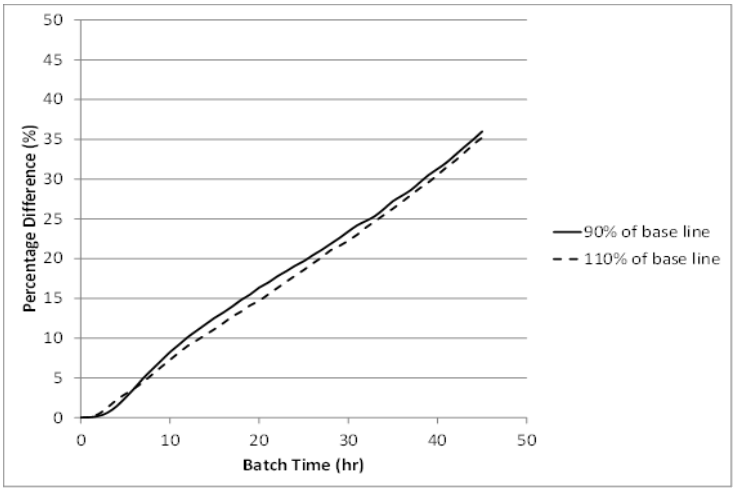

(c)

Fig.12: Percentage difference in the (a) production of biomass; (b) production of ethanol; (c) consumption of glucose, when the parameter, k_3 is changed by $\pm 10\%$.

Fig.13 (a)-(c) reveal that parameter k_4 affected the biomass and glucose concentrations to a greater extent compared to ethanol concentration. The percentage difference for ethanol concentration was at most 3% compared to 10% and 36% for biomass and glucose concentrations, respectively. This is counter-intuition on hindsight because parameter k_4 was expected to affect ethanol more significantly compared to the others. Nevertheless, the observations are explained as follows: When parameter k_4 was varied, the variation in ethanol concentration was achieved, which in turn affected $(R_x)_{growth}$ in equation (6), as shown in Fig.13(d). $(R_x)_{growth}$ affected the biomass, ethanol and glucose concentrations as shown in equations (9)-(11). However, the reaction rate of the ethanol was much smaller (of the order of 10^{-5} kg/cm^{3}s) compared to that of the biomass (of the order of 10^{-3} kg/m^{3}s) and glucose (of the order of 10^{-4} kg/m^{3}s). Thus, the ethanol concentration did not vary much when parameter was varied.

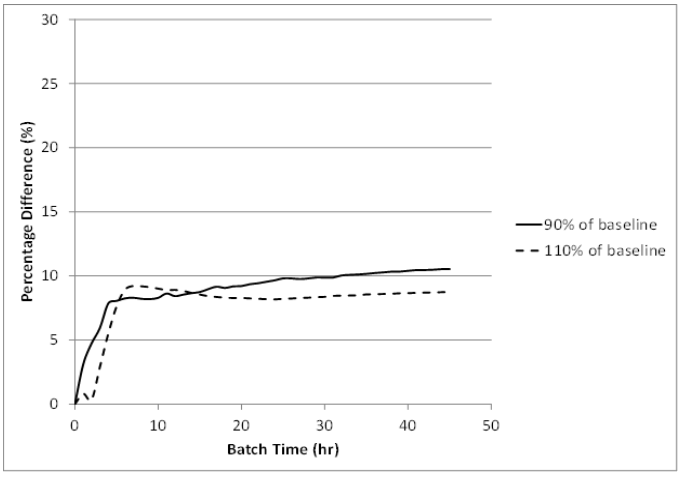
Percentage Difference (%)
Batch Time (hr)
90% of baseline
110% of baseline

(a)

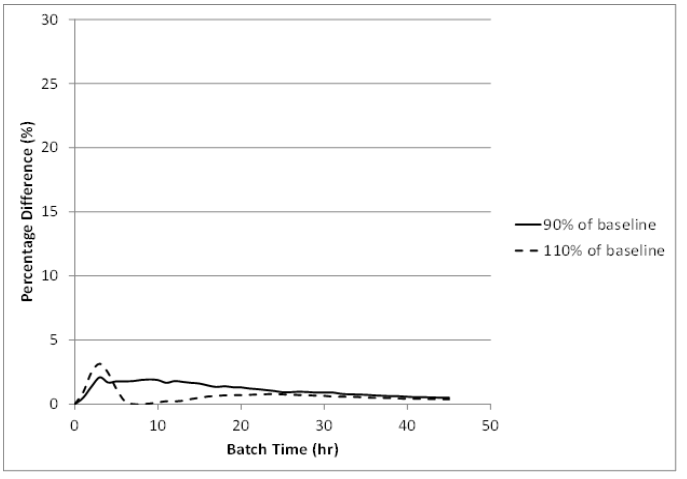
Percentage Difference (%)
Batch Time (hr)
90% of baseline
110% of baseline

(b)

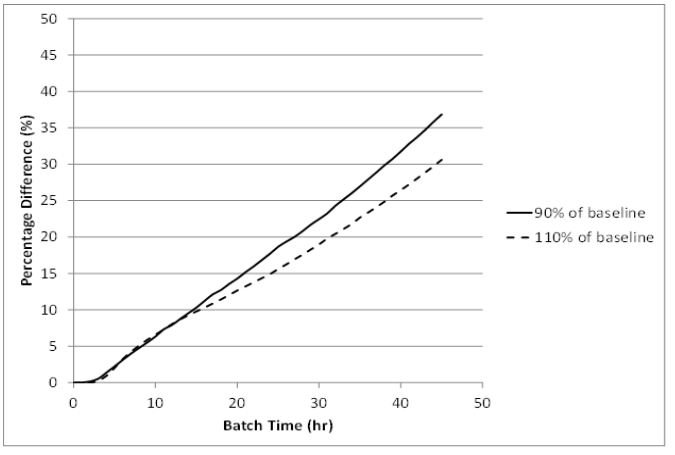
Percentage Difference (%)
Batch Time (hr)
90% of baseline
110% of baseline

(c)

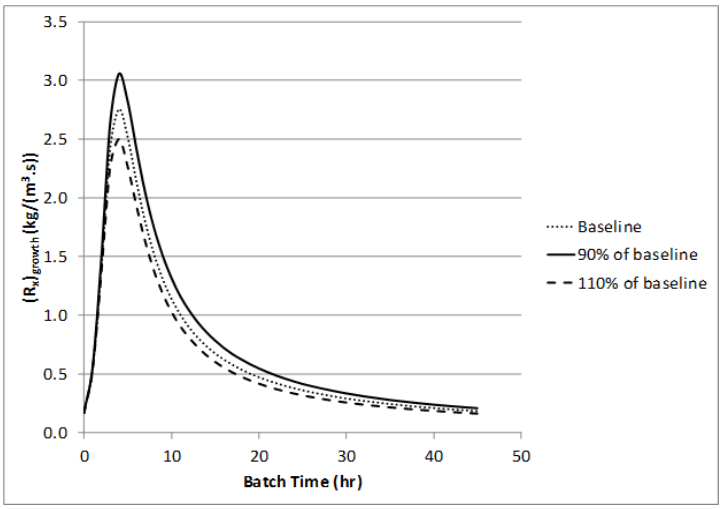

(d)

Fig.13: Percentage difference in the (a) production of biomass; (b) production of ethanol; (c) consumption of glucose; (d) $(R_x)_{growth}$ when the parameter, k_4 is changed by $\pm 10\%$.

When the parameter, k_4 was varied, the maximum percentage difference for the biomass and ethanol concentrations was observed around batch time ≈ 4 hours, which corresponded to the maximum production rate [Fig.14 (a) - (b)]. On the other hand, the percentage difference of the glucose concentrations increased as shown in Fig.14(c).

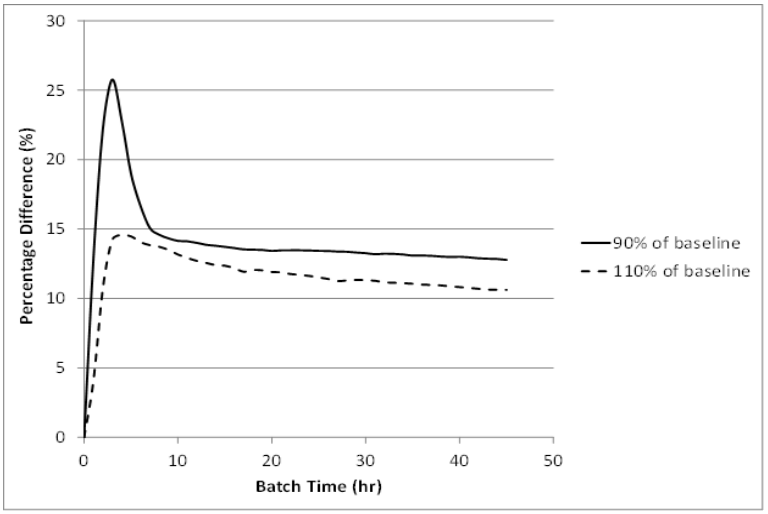

(a)

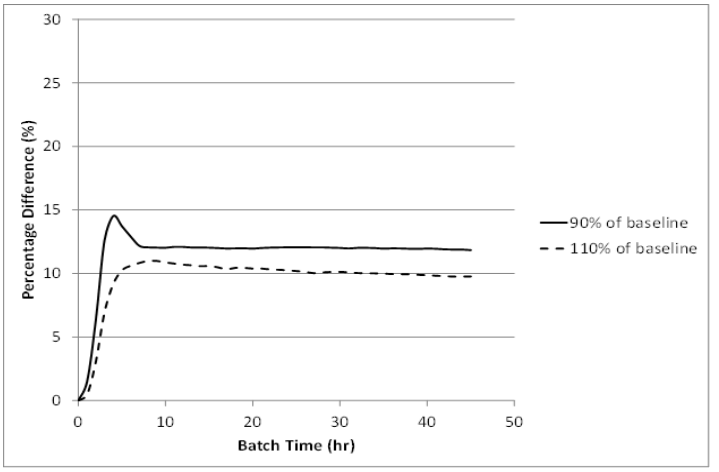

(b)

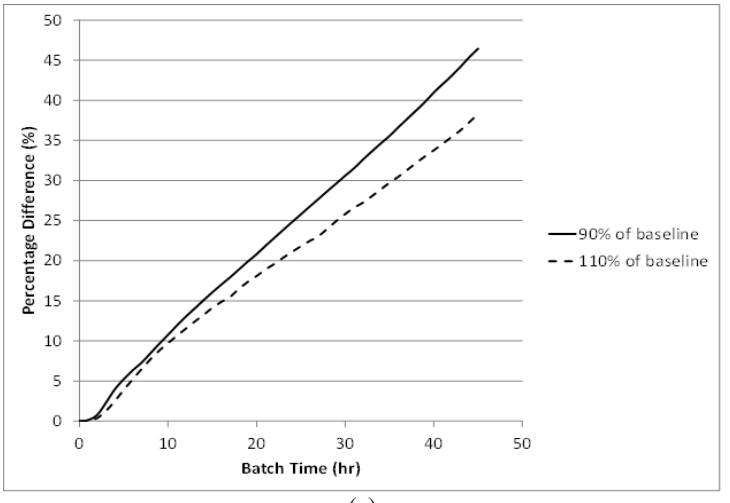

(c)

Fig.14: Percentage difference in the (a) production of biomass; (b) production of ethanol; (c) consumption of glucose, when the parameter, $k_5$is changed by $\pm 10\%$.

Fig.15(a) shows the effects of parameter k_6 on biomass. It was observed that the effect was significant for biomass product. The percentage difference of the biomass increased since was related to biomass utilisation, as seen in equation (9). The ethanol and glucose concentrations were less affected by k_6 as shown in Figures 15 (b)-(c).

The sensitivity analysis showed that the fermentation process was most affected by (in the order of decreasing importance) k_5, k_4, k_3, k_1, k_6 and k_2. This analysis is important as it aids CFD-based optimisation in future work.

The analysis above showed that the influence of each of the kinetic parameters varies with the concentration of biomass, glucose and ethanol, which are a function of the batch time.

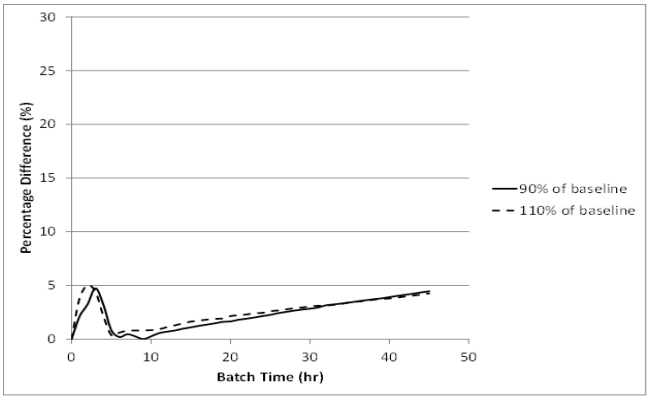

(a)

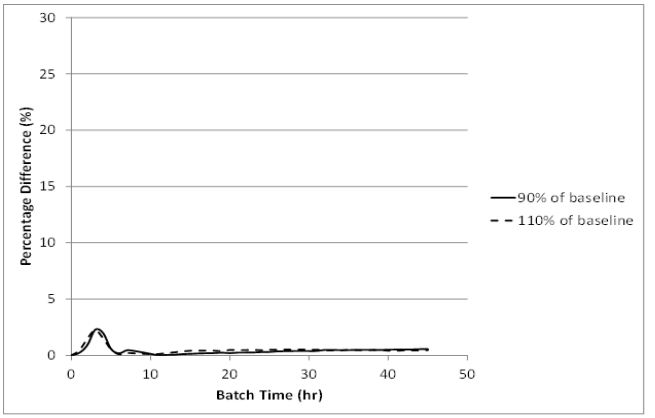

(b)

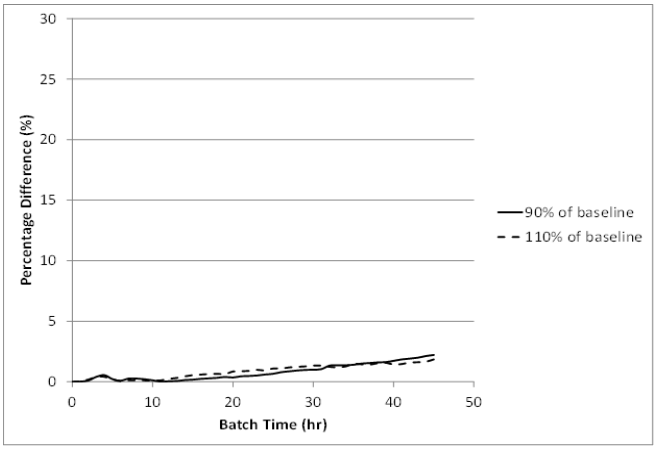

(c)

Fig.15: Percentage difference in the (a) production of biomass; (b) production of ethanol; (c) consumption of glucose, when the parameter,k_6 is changed by $\pm 10\%$.

CONCLUSION AND FUTURE WORK

In this paper, a new kinetics model with the implementation of CFD simulation was proposed. The kinetic parameters of the ethanol fermentation based on Herbert's microbial kinetics, assuming perfectly-stirred condition, were not able to produce good predictions during CFD simulations. Correction factors based on a second-order spline were proposed to improve the CFD-based results. The coupled fermentation kinetics – CFD model is useful for practical purposes since the simulation time required is 2 hours to simulate a 45-hour fermentation process. A typical three dimensional two-phase flow fermentation kinetic-CFD model requires an approximate simulation time of 1 week. The work also highlights the need to incorporate a CFD model to obtain better kinetics parameter estimation. In this study, the maximum ethanol that can be produced was around 8.0 g/L, at the operating conditions of AR = 1.2 LPM and *SS* = 150 rpm. The corresponding kinetic parameters are: $k_{1,c} = 2.50$, $k_{2,c} = 0.01$, $k_{3,c} = 1.16$, $k_{4,c} = 0.2517$, $k_{5,c} = 0.6633$ and $k_{6,c} = 0.01402$. Future work is suggested to incorporate parameters such as temperature and pH into the improved kinetics model for further enhancement and improvement of the kinetics model.

REFERENCES

Alcázar, L. A., & Ancheyta, J. (2007). Sensitivity analysis based methodology to estimate the best set of parameters for heterogeneous kinetic models. *Chemical Engineering Journal, 128*(2), 85-93.

Bezzo, F., & Macchietto, S. (2004). A general methodology for hybrid multizonal/CFD models: Part II. Automatic zoning. *Computers & Chemical Engineering, 28*(4), 513-525.

Cot, M., Loret, M., Francois, J., & Benbadis, L. (2007). Physiological behaviour of *Saccharomyces cerevisiae* in aerated fed-batch fermentation for high level production of bioethanol. *FEMS Yeast Research, 7*(1), 22-32.

Elqotbi, M., Valev, S. D., Montastruc, L., & Nikov, I. (2013). CFD modelling of two-phase stirred bioreaction systems by segregated solution of the Euler-Euler model. *Computers and Chemical Engineering, 48*, 113-120.

Emily, L. W. T., Nandong, J., & Samyudia, Y. (2009). Experimental investigation on the impact of aeration rate and stirrer speed on micro-aerobic batch fermentation. *Journal of Applied Sciences, 9*(17), 3126-3130.

Fox, R. O., (1998). On the relationship between Lagrangian micromixing models and computational fluid dynamics. *Chemical Engineering and Processing: Process Intensification, 37*(6), 521-535.

Garcia-Ochoa, F., & Gomez, E. (2009). Bioreactor scale-up and oxygen transfer rate in microbial processes: An overview. *Biotechnology Advances, 27*(2), 153-176.

García-Ochoa, F., Santos, V. E., & Alcón, A. (1995). Xanthan gum production: An unstructured kinetic model. *Enzyme and Microbial Technology, 17*(3), 206-217.

Ghareib, M., Youssef, K. A., & Khalil, A. A. (1988). Ethanol tolerance of *Saccharomyces cerevisiae* and its relationship to lipid content and composition. *Folia Microbiologica (Praha), 33(*6), 447-452.

Harvey, A. D., & Rogers, S. E. (1996). Steady and unsteady computation of impeller-stirred reactors. *AIChE Journal, 42*(10), 2701-2712.

Hutmacher, D. W., & Singh, H. (2008). Computational fluid dynamics for improved bioreactor design and 3D culture. *Trends in Biotechnology, 26*(4), 166-172.

Kuipers, J. A. M., & van Swaaij, W. P. M. (1998). Computational fluid dynamics applied to chemical reaction engineering. In F. Keil, W. Mackens, H. Voβ, J. Werther (Eds.), *Scientific computing in chemical engineering ii: computational fluid dynamics, reaction engineering and molecular properties* (pP. 383-390). Berlin: Springer-Verlag.

Kuzmin, D., Mierka, O., & Turek, S. (2007). On the Implementation of the k- turbulence model in incompressible flow solvers based in a finite element discretization. *International Journal of Computing Science and Mathematics, 1*, 193-206.

Liew, E. W. T., Nandong, J., & Samyudia, Y. (2013). Multi-scale models for the optimization of batch bioreactors. *Chemical Engineering Sciences, 95*, 257-266.

Patel, H., Ein-Mozaffari, F., & Dhib, R. (2010). CFD analysis of mixing in thermal polymerization of styrene. *Computers and Chemical Engineering, 34*(4), 421-429.

Rao, D. G. (2010). *Introduction to biochemical engineering.* New Delhi: Tata McGraw Hill.

Roudsari, S. F., Ein-Mozaffari, F., & Dhib, R. (2013). Use of CFD in modeling MMA solution polymerization in a CSTR. *Chemical Engineering Journal, 219,* 429-442.

Schugerl, K., & Bellgardt, K. H. (2000). Bioreaction engineering, modeling and control. Springer-Verlag.

Stanbury, P. F., Whitaker, A., & Hall, S. J. (1995). *Principles of fermentation technology.* Butterworth-Heinemann.

Starzak, M., Kryzstek, L., Nowicki, L., & Michalski, H. (1994). Macroapproach kinetics of ethanol fermentation by *Saccharomyces cerevisiae*: Experimental studies and mathematical modelling. *The Chemical Engineering Journal and the Biochemical Engineering Journal, 54*(3), 221-240.

Thatipamala, R., Rohani, S., & Hill, G. A. (1992). Effects of high product and substrate inhibitions on the kinetics and biomass and product yields during ethanol batch fermentation. *Biotechnology and Bioengineering, 40*(2), 289-297.

Versteeg, H., & Malalasekera, W. (2007). *An introduction to computational fluid dynamics: The finite volume method*. Essex: Pearson.

Van Zyl, J. M. (2012). *Three-dimensional modelling of simultaneous saccharification and fermentation of cellulose to ethanol* (Doctoral dissertation). Stellenbosch: Stellenbosch University.

Pertanika J. Sci. & Technol. 24 (1): 165 - 176 (2016)

PERTANIKA JOURNALS

SCIENCE & TECHNOLOGY

Journal homepage: http://www.pertanika.upm.edu.my/

Expression of C5a and its Receptor in Canine Spontaneous Tumours: A Preliminary Finding

Norhaifa, G.[1], Bachek, N. F. [1], Kamarudin, N. H. [1], Nashreq, K. N. [1], Ajat, M. M.[1], Hafandi, A. [1], Selvarajah, G. T.[2] and Hezmee, M. N. M.[1*]

[1]Department of Veterinary Preclinical Sciences, Faculty of Veterinary Medicine, Universiti Putra Malaysia, 43400 Serdang, Selangor, Malaysia

[2]Department of Veterinary Clinical Studies, Faculty of Veterinary Medicine, Universiti Putra Malaysia, 43400 Serdang, Selangor, Malaysia

ABSTRACT

A study of the development of spontaneous tumours in dogs gives many benefits in oncology research due to the similarity between dog and human cancer in terms of epidemiologic, biologic and clinical features. There is evidence that the complement component 5 anaphylatoxin (C5a) and its receptor are involved in the development of many types of tumour due to its inflammatory properties. The purpose of this study was to determine the expression of C5a on several types of canine spontaneous tumour i.e. mammary tumour, lung tumour, testicular tumour and melanoma. The expression of C5a in these tumours was compared with normal tissue from the breasts, lungs, testes and skin. The total of eight post-mortem canine tissues were collected from University Veterinary Hospital (UVH), University Putra Malaysia and stored in a preservative solution (RNAlater) to keep the RNA from degrading. The RNA was extracted using the Qiagen RNA Extraction Kit and a cDNA synthesis was carried out using a one-step PCR kit (Promega, USA). The expression of C5a was determined using reverse transcriptase PCR (RT-PCR) and Quantitative real-time PCR (qPCR) techniques. The results showed that all types of tumour gave higher expression of C5a compared to normal tissue. This means that the CT value for the tumours was below 30 cycles except for melanoma and the expression of C5a of normal tissues was above 30 cycles. This finding suggests that C5a and its receptor may be involved in the development of tumours in dogs and can be used as a tumour biomarker for both animals and humans in the future. Nevertheless, further studies investigating the mechanisms of C5a and its receptor in canine spontaneous tumour are necessary.

Keywords: Canine spontaneous tumour, C5a, C5a receptor

Article history:
Received: 8 January 2015
Accepted: 27 April 2015

E-mail addresses:
farhanabachek@gmail.com (Bachek, N. F.),
nhazwani02@gmail.com (Kamarudin, N. H.),
nashreq90@gmail.com (Nashreq, K. N.),
mokrish@upm.edu.my (Ajat, M. M.),
hafandi@upm.edu.my (Hafandi, A.),
hezmee@upm.edu.my (Hezmee, M. N. M.)
*Corresponding author

ISSN: 0128-7680

INTRODUCTION

The choice of dogs as the animal model to study the role of the complementary protein C5a in the development of spontaneous tumours justifies its role as a good and reliable tool to gain further knowledge about spontaneous tumours and potential remedies. Dogs with spontaneous tumours may be used as good animal models based on several characteristics that have been studied by previous researchers (Rowell *et al*., 2011; Pinho *et al*., 2012). These similarities between canine and human tumours have been known to be related to genetics, treatment targets and physiology (Khanna *et al*., 2006; Breen & Modiano, 2008; Paoloni & Khanna, 2008).

C5a is one of the proteins in the immune system that is involved in the inflammation reaction resulting in recruiting inflammatory cells to targeted regions in the body. Previous studies found that C5a was involved in many types of disease related to inflammation reaction (Dondorp *et al*., 2005) and cancers (Kim *et al*., 2005; Markiewski *et al*., 2008; Hezmee *et al*., 2011). However, the exact role of C5a in the body is still unclear due to lack of research and information about this complement.

Complement proteins, particularly of C5a, have been always thought to be one of the most vital substances in the host defence mechanisms. Nonetheless, many studies recently have implicated the role of complement activation in the development of multiple inflammatory and immunological diseases, including sepsis (Ward, 2004), acute respiratory distress syndrome (Robbins *et al*., 1987), glomerulonephritis (Welch, 2002), ischemia-reperfusion injury (Arumugam *et al*., 2004a), rheumatoid arthritis (Linton & Morgan, 1999) and asthma (Hawlisch *et al*., 2004).

C5a receptors (C5aR) can be located on the myeloid cells such as the phagocytic leukocytes (Chenoweth & Hugli, 1978; Kurimoto *et al*., 1989; Gerard & Gerard, 1991; Werfel *et al*., 1992; Revollo *et al*., 2005), as well as those of a non-myeloid origin such as hepatocytes, lung vascular smooth muscle cells, bronchial and alveolar epithelial cells (Haviland *et al*., 1995; Riedemann *et al*., 2002), articular chondrocytes (Onuma *et al*., 2002) and astrocytes (Gasque *et al*., 1995). Previous studies showed that there was a 70-percent similarity of the C5a receptor between canines, humans, rats and bovines. Therefore, the canine C5a receptor is considered orthologous to the human C5a receptor, and this represents a surprisingly high interspecies variability compared with other G-protein-coupled-receptors (Perret *et al*., 1992).

There are various functions of this receptor in the cells and tissues. One of the most important functions of this receptor is in the development of sepsis. It is achieved by the recruitment of neutrophils by C5a/C5aR signalling. C5a/C5aR signalling in neutrophils leads to activation of phosphatidylinositol 3-kinases (PI3K)/ a serine/threonine kinase (PI3K/Akt) pathways, which provide survival signals for neutrophils. Assembly of NADPH oxidase can be triggered by C5a/C5aR signalling, resulting in H_2O_2 productions in organs and tissues. An increased number of neutrophils together with H_2O_2 generation may be linked to tissue injury and multiple organ failure (Guo & Ward, 2005).

With this discovery, attention is shifted towards the prevention of the excessive complement activation that may lead to the development of multiple diseases. Therapeutic research has been conducted on laboratory animal models using trial antagonistic and agonist drugs to further understand the actions of complement proteins, particularly C5a. Therefore, the objective of

this preliminary study is to determine the availability of C5a receptors in the spontaneous tumour tissue of dogs. With the vast advancement of anti-complementary drugs available commercially, this study will provide a stepping stone for more detailed research into the use of these drugs to treat these tumours in dogs and, subsequently, in humans as well.

MATERIALS AND METHOD

Canine Spontaneous Tumours and Sample Preparation

A total of eight samples of different spontaneous canine tumours and normal tissues were obtained from excised tissues of diagnosed cases of canine spontaneous tumours from the University Veterinary Hospital (UVH), Faculty of Veterinary Medicine, Universiti Putra Malaysia (UPM). Table 1 shows the types of tumour based on their histopathological findings as diagnosed by the veterinary pathologist in Faculty of Veterinary Medicine, Universiti Putra Malaysia. A number of normal tissues were also obtained from pathological archives of the post mortem unit of Faculty of Veterinary Medicine for comparison. All the tissues were submerged in a sterile RNAlater® solution (Ambion, Inc., USA) for PCR analysis and sequencing of C5aR expression.

TABLE 1 : Types of Tumour Obtained

Lung carcinoma
Mammary carcinoma
Melanoma
Testicular tumour

The tissues that were submerged in the RNAlater® solution were treated for conversion to PCR products. The tissues were finely chopped into pieces of size 1-mm in diameter (50-100mg) and then transferred into a tube containing TRIZOL® solution (Invitrogen™, USA) for preparation of PCR products.

RNA Isolation and cDNA Synthesis

The tissues in the TRIZOL® were homogenised using scalpel blade into much smaller pieces and vortexed vigorously. The digested tissues were left at 25 ºC for 5 min. The insoluble materials were removed by centrifuge to obtain solutions containing the digested tissues at 13,000 rpm for 10 min at 4 ºC. The supernatants were transferred into a new tube. Chloroform was then added to the supernatants and the tubes were shaken vigorously and left at 25 ºC for 5 min and centrifuged at 13,000 rpm for 10 min at 4 ºC. The clear supernatant was transferred to a fresh tube containing isopropanol solution. The solutions were left at 25 ºC for 10 min and were centrifuged at 13,000 rpm for 15 min at 4 ºC. The supernatants were discarded. The pelleted RNAs were washed with a 75% ethanol solution and the solutions were centrifuged at 9,000 rpm for 5 min at 4 ºC. The RNA in the tubes was left to dry for 5 min. The process was continued with the RNA extractions. The pellets containing RNA products were re-suspended with nuclease-free water and heated at 55 ºC for 15 min. DNAse1 (Invitrogen™, USA) treatment

was conducted to remove traces of contaminating DNA. For the final preparation of the RNA extraction, cDNA syntheses of the RNA-treated cells were performed using the Universal RiboClone® cDNA synthesis system (Promega Corporation, USA). The RNAs from tumour tissues were used for C5a receptor detection and expression using a PCR machine.

Cloning and Sequence Analysis of Canine C5aR (CD88)

The primers for this study were designed according to the study by Perret *et al*. (1992). The C5aR cloning sequences and Hypoxanthine phosphoribosyltransferase (HPRT) genea used in this study were as follows:

C5aF = 5' GCT CAT CCT GCT CAA CAT GTA C 3'
C5aR = 5' CCG CGG AAG ATG AAC GA 3'
HPRTF = 5' TGC TCG AGA TGT GAT GAA GG 3'
HPRTR = 5' TCC CCT GTT GAC TGG TCA TT 3'

The primer sequences were obtained from BASE Life Sciences Holdings (Singapore). The primers were aliquot into smaller tubes and the leftover aliquot were stored in -80ºC. One vial of each primer was used for this assay. Routine thermal reaction work out was conducted on the cDNA aliquots of 4µg of mammary tumour samples in 40 cycles in these conditions: pre-denaturing step for 10 min at 95 ºC, denaturation step for 1 min at 94 ºC, annealing temperature of 1 min at 50 ºC, extension step for 1 min at 72 ºC and extension procedure for 10 min at 72 ºC. Other annealing temperature tested was 55 ºC while HPRT primers were used to serve as canine housekeeping genes. Each PCR product from the thermal reaction was then subjected to gel electrophoresis through a 1.5% agarose gel and stained with ethidium bromide for screening purposes.

Quantification of Target Gene Expression

The quantification and negative control of C5aR gene transcripts were carried out by real time quantitative PCR using the Applied Biosystems (Victoria, Australia) and Sybr Green qPCR kit (Promega, USA). The PCR reaction mixture (20 µl) contained 10 µl of Sybr Green qPCR mix, 0.5 µl of the above-described primer mix 10 nM each, 1 µl RNAs inhibitor and 2 µl of cDNA template. The PCR protocol was: UNG enzyme incubation at 45 °C for 45 min; initial denaturation at 94 °C for 5 min; 40 cycles for primer annealing, 60 °C for 30 s for primer extension and an elevated temperature of 72 °C for 30 s for fluorescent data acquisition; and a final extension step at 80 °C for 2 s to allow the formation of fully duplexed DNA. To check the specificity of the amplified products, a melting curve analysis was performed immediately following the completion of the PCR. The melting protocol consisted of heating from 65 to 95 °C at a rate of 0.2 °C per step, and each step was held for 1 s for data acquisition. For each sample analysed, the mean Ct value based on the results of all experiments was calculated, together with that of the corresponding standard samples. The canine C5aR cDNA copy numbers were then normalised using the calculated HPRT cDNA copy numbers (the mean) of the same sample and run. This number was obtained by applying the respective Ct values for HPRT in the standard dilution curve of the same dilution.

RESULTS AND DISCUSSION

The study of complement 5a (C5a) is a new field of study in Malaysia. It is important to study C5a due to lack of information regarding the exact role of C5a in the body and the involvement of this protein in various diseases. Many studies have shown that C5a is involved in many pathological states related to inflammatory disease and cancer (Dondorp *et al*., 2005; Fitzpatrick, 2001; Hong *et al*., 2010). The expression of C5a and its receptor can be defined using the reverse transcriptase Polymerase Chain Reaction (rt-PCR) and real time PCR (qPCR). These techniques are suitable for use in detecting the expression of C5a biology due to its properties, which are inexpensive, rapid response and high sensitivity in producing millions of copies of DNA even though the quality of the DNA may be poor (Erlich, 1989).

Expression of C5a Receptor Protein in Canine Tumours

Fig.1 (A) shows the band for the housekeeping gene i.e. the HPRT gene. Meanwhile, Fig.1 (B) shows the single bands that were obtained from the C5a primer in tumour tissues in which Lane 1 is mammary carcinoma, lane 2 is lung carcinoma, lane 3 is melanoma and lane 4 is testicular tumour. The result indicates that C5a was expressed in all types of tumour except melanoma tissues while there was none in normal tissue (data not shown). The DNA ladder marker (Promega, USA) was used as a reference in which each band contributed to 100 bp size.

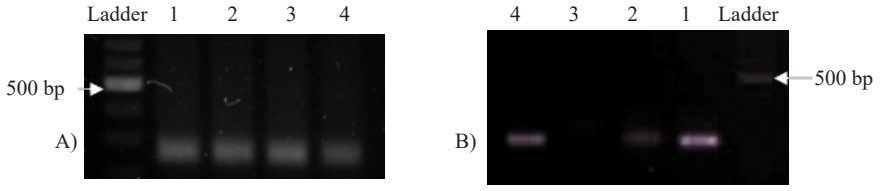

Fig.1: The expression of C5a receptor via Reverse Transcriptase PCR. Result of electrophoresis in 1.5% TBE-agarose gel of RT-PCR product using two sets of primers; A) HPRT primer as a housekeeping gene for each tumour tissues and B) C5a Primer with tumour tissues in which lane 1: Mammary carcinoma; lane 2: Lung carcinoma; lane 3: Melanoma and lane 4: Testicular tumour using 100bp ladder (Promega, USA).

The single band given for the PCR products showed that the polymerisation of C5aR using specific C5aR primers had occurred in the tissues. This result is a positive indicator for determining the role of the C5a and its receptor in the development of spontaneous cancer. It is due to the presence of PCR products in most of the tumour tissues; PCR products are absent in normal tissues. The presence of PCR products indicates that there was an abundance of C5a receptors in the tissues. This finding was consistent with previous studies that showed the involvement of C5a in many pathological states especially cancer (Smedegård *et al*., 1989; Czermak *et al*., 1999; Huber-Lang *et al*., 2001; Huber-Lang *et al*., 2006; Markiewski, 2008; Patel *et al*., 2008). RT-PCR is the most sensitive procedure to detect RNA because it can detect and amplify much smaller samples (Kim & Kim, 2003) and also from a single cell. Housekeeping genes or internal control genes are normally used as a reference for the genes of interest (Suzuki *et al*., 2000). It is constant in certain cell types but varies in other types of cell or tissue (Thellin *et al*., 1999; Warrington *et al*., 2000). Thus, the use of housekeeping genes is important in gene expression analysis.

Determination of cDNA Sequencing of Canine C5aR (CD88)

Nucleotide sequencing of canine C5aR cDNA revealed a coding region of 1357 bp. The deduced amino acid sequences of canine C5aR contained 657 residues. Sequencing of these digests showed that the recombinant was 97% homologous to the canine C5aR gene sequence deposited in GenBank under the accession no. X65860. The homologies of the cDNA and amino acid sequences among some mammalian species were calculated (Table 2).

TABLE 2: Nucleic Acid and Amino Acid Sequence Homologies of Canine C5aR, Compared with Other Mammalian Species

Dog	Human	Mouse	Rats	Sheep	Pig	Cattle
Nucleic acid (%)	91.0	91.0	92.0	85.0	88.0	85.0
Amino acid (%)	82.0	86.0	85.0	85.0	89.0	85.0

At the cDNA sequence level, canine C5aR was found to show high homologies with human C5aR (91%) and rats C5aR (92%). This result indicates that the role of C5a in the canine cells provided a direct indicator of the development of tumours in humans regarding the high sequence homology among them. Although rat models have a higher sequence homology for C5aR sequence, in terms of genome sequence, canine models have a higher similarity with human (79%) compared to rat (69%) models (Davis *et al*., 2014). Besides that, the use of rats in research cannot always be faithfully extrapolated to human patients. Canines are more suitable for use in the study of cancer due to their characteristics of experiencing spontaneous disease with high frequency, developing the same types of cancer observed in humans and being receptive to the same therapeutic strategies (Pontius *et al*., 2007). In addition, both canines and owners are susceptible to getting the same type of cancer due to exposure to the same environmental factors.

The use of dogs as a model of a variety of cancers in human has been suggested due to the fact that the characteristics and gene sequence of C5a in canines mimic those in humans (Rowell *et al*., 2011; Pinho *et al*., 2012). Hence, it is important to study the effects of C5a/c5aR on the development of tumours in canines. Unfortunately, due to the limited number of samples because of difficulty in getting spontaneous tumour samples from veterinary hospital in Malaysia, this study was unable to statistically exhibit these arguments on a much bigger scale. Nevertheless, this preliminary study provided a good platform for exploring the potential of using C5a/C5aR markers in clinical applications for diagnostic tools. It also highlighted prognostic indicators and potential targets for therapeutic and preventive strategies and supports efforts to evaluate clinical trials on the efficacy of C5a/C5aR-blockers in the treatment of canine tumours.

Quantification of C5aR Gene Expression

Four types of canine tumour were used in this study i.e. mammary carcinoma, lung carcinoma, melanoma and testicular tumour. Each tumour was compared to its normal tissue from the particular part of the body. The result showed that the mean CT value for the tumours was below 30 cycles except for melanoma and that the expression of C5a of normal tissues was

above 30 cycles. The differentiation of CT value between tumour tissues and normal tissues for mammary carcinoma, testicular tumour, lung carcinoma and melanoma were 15, 11, 5 and 2 cycles, respectively.

The CT value is a parameter used in detection and quantification of C5a expression in canine spontaneous tumours. The CT value form is in indirect proportion to the amount of PCR product in a reaction (Higuchi *et al*., 1993). The higher expression of gene of interest gives a lower CT value due to the principle of RT-PCR i.e. the detection of samples depends on the fluorescent signal that is captured by computer software where the result is calculated based on cycle threshold (CT) value. The higher the starting copy number of the nucleic acid target, the sooner a significant increase in fluorescence is observed. The result showed that the expression of C5a in canine spontaneous tumours was higher than in normal tissues due to the lower CT value of tumour tissues compared to normal issues.

These findings are supported by the previous study of Hezmee *et al*. (2011) in which the researchers found that the expression of C5a in canine malignant tumours was higher compared to that in benign tumours while there was no expression of C5a in canine normal mammary tissues. This suggests that C5a may have a direct biological effect on cancer cells. This finding is also in agreement with another study done on C5aR expression in bovine mammary tissues, in which C5aR was also expressed by inflammatory cells from bovine mammary tissues, but not from normal or inactive cells (Nemali *et al*., 2008). Hence, this study suggested that activation of C5a receptors may have a consequence in tumour development. However, the use of a small sample size in this study means it is not clearly possible to make a proper correlation between the expression of C5aR and tumour types. Besides that, many precautionary steps starting from preparation protocol to analysing of results need to be emphasised due to the different type of tissues that can lead to a false positive result.

The Real Time Polymerase Chain Reaction (qPCR) is a method that can be used to replace the weakness of PCR (Erlich *et al*., 1989; Whelan *et al*., 2003). This system provides greater sensitivity for amplicon detection compared to conventional PCR that uses gel-based detection. It can be seen in the results, where conventional PCR gave a single band to most of the tumour tissues but there was no band for melanoma and normal tissues. This was due to very low expression of C5a in these tissues. However, when the samples were put through the real-time PCR technique, both tumours and normal tissues gave a CT value result. This was due to the capability of real-time PCR of detecting DNA up to 50 fg and its higher sensitivity, up to tenfold more, than that of conventional PCR. Based on the reverse transcriptase PCR and Real Time PCR, the results showed that the expression of C5a was up-regulated in all the tumour tissues except melanoma and down-regulated in all normal tissues (Fig.2).

Even though the role of C5aR in the development of canine tumours remains unclear, there are studies that suggest a link between chronic inflammatory response and the development of cancer (Coussens & Werb, 2002; Tan & Coussens, 2007). C5a and its receptors play an important role in various other disorders involving chronic inflammatory responses (Robbins *et al*., 1987; Welch, 2002; Arumugam *et al*., 2004a; Hawlisch *et al*., 2004; Ward, 2004) and due to its property of being one of the most potent inflammatory peptides, excessive activation of complement proteins towards their receptors in tissues has been hypothesised to lead to the progression of tumour cells (Tan & Coussens, 2007).

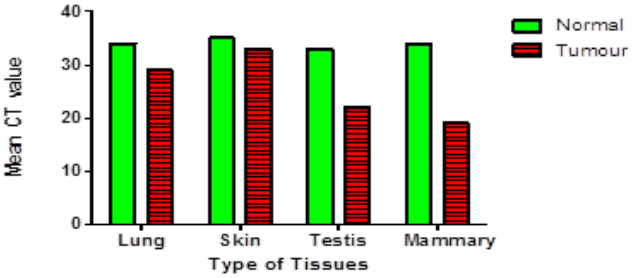

Fig.2: The magnitude of expression of C5a via Real Time PCR. The CT value recorded for C5a is higher in normal tissue compared to the tumour tissue. The CT values recorded is indirectly proportional with concentration of C5a in which the higher the concentration of C5a, the lower the CT values recorded. The HPRT gene was used as a housekeeping gene to validate the results. The red bars show that the tumour tissues started with lane 1: Lung carcinoma; lane 2: Melanoma; lane 3: Testicular tumour; and lane 4: Mammary tumour. The green bars show the normal tissues for each type of tumour starting with the lung tissue followed with skin, testis and mammary tissues.

The complex mechanism of humoral immunity of the host, which includes the activation of C5a and its receptors in tissue and cell surfaces, is still not fully understood; nevertheless, receptors for the Fc portion of IgG (especially FcGRIII) and complement factors (particularly C5a/C5aR) are recognised as co-dominant effectors in the process (Schmidt & Gessner, 2005). Tissues damaged by autoimmune disorders and by cancer have similar characteristics such as in chronic innate immune cell infiltration, tissue re-modelling, angiogenesis, altered survival pathways (Sapir & Shoenfeld, 2005). It would seem there is a possibility that the same immune complex effector pathways are involved in pathogenesis of both disease (Tan & Coussens, 2007). Although this study did not provide any data regarding the treatment of these tumours, there are, however, scientifically tested and proven anti-complement drugs that are used to counter the effects of excessive and chronic C5a/C5aR activation (Short *et al*., 1999; Arumugam *et al*., 2002; Woodruff *et al*., 2003; Arumugam *et al*., 2004b).

CONCLUSION

This preliminary study found that the expression of C5a was up-regulated in most of the spontaneous canine tissues and down-regulated in all normal tissues. This study gave a positive indicator of the role of C5a in the development of spontaneous tumours in canines as well as in humans due to high homology of the C5a sequence in both dogs and humans. However, further study is warranted to fully understand the mechanism of tumour development due to action of C5a/C5aR; data for a higher number of tumour-bearing animals and the effects of C5a/C5aR antagonist and agonist drugs should be included in such study.

REFERENCES

Arumugam, T. V., Shiels, I. A., Woodruff, T. M., Reid, R. C., Fairlie, D. P., & Taylor, S. M. (2002). Protective effect of a new C5a receptor antagonist against ischemia–reperfusion injury in the rat small intestine. *Journal of Surgical Research, 103*(2), 260-267.

Arumugam, T. V., Shiels, I. A., Woodruff, T. M., Granger, D. N., & Taylor, S. M. (2004). The role of the complement system in ischemia-reperfusion injury. *Shock, 21*(5), 401-409.

Arumugam, T. V., Woodruff, T. M., Stocks, S. Z., Proctor, L. M., Pollitt, S., Shiels, I. A., ... & Taylor, S. M. (2004). Protective effect of a human C5a receptor antagonist against hepatic ischaemia-reperfusion injury in rats. *Journal of Hepatology, 40(*6), 934-941.

Breen, M., & Modiano, J. F. (2008). Evolutionarily conserved cytogenetic changes in matological malignancies of dogs and humans--man and his best friend share more than companionship. *Chromosome Research, 16*(1), 145-154.

Chenoweth, D. E., & Hugli, T. E. (1978). Demonstration of specific C5a receptor on intact human polymorphonuclear leukocytes. *Proceedings of the National Academy of Sciences, 75*(8), 3943-3947.

Coussens, L. M., & Werb, Z. (2002). Inflammation and cancer. *Nature, 420(*6917), 860-867.

Czermak, B. J., Sarma, V., Pierson, C. L., Warner, R. L., Huber-Lang, M., Bless, N. M., Schmal, H., Friedl, H. P., & Ward, P. A. (1999). Protective effects of C5a blockade in sepsis. *Nature Medicine, 5*(7), 788-792.

Davis, B. W., & Ostrander, E. A. (2014). Domestic Dogs and cancer research: A Breed-based genomics approach. *ILAR Journal, 55*(1), 59-68.

Dondrop, A., Nosten, F., Stepniewska, K., Day, N., & White, N. (2005). Artesunate versus quinine to treatment of severe falciparum malaria: A randomised trial. *Lancet, 366(*9487), 717-725.

Erlich, H. A. (1989). The polymerase chain reaction. *Journal of Clinical Immunology, 9(*6), 437-447.

Fitzpatrick, F. A. (2001). Inflammation, carcinogenesis and cancer. I*nternational Immunopharmacology, 1*(9-10), 1651-1667.

Gasque, P., Chan, P., Fontaine, M., Ischenko, A., Lamacz, M., Götze, O., & Morgan, B. P. (1995). Identification and characterization of the complement C5a anaphylatoxin receptor on human astrocytes. *The Journal of Immunology, 155*(10), 4882-4889.

Gasque, P., Singhrao, S. K., Neal, J. W., Gotze, O., & Morgan, B. P. (1997). Expression of the receptor for complement C5a (CD88) is up-regulated on reactive astrocytes, microglia, and endothelial cells in the inflamed human central nervous system. *The American Journal of Pathology, 150*(1), 31.

Gerard, N. P., & Gerard, C. (1991). The chemotactic receptor for human C5a anaphylatoxin. *Nature, 349,* 614-617.

Guo, R. F., & Ward, P. A. (2005). Role of C5a in inflammatory responses. *Annual Review of Immunology, 23*, 821-852.

Haviland, D. L., McCoy, R. L., Whitehead, W. T., Akama, H., Molmenti, E. P., Brown, A., & Wetsel, R. A. (1995). Cellular expression of the C5a anaphylatoxin receptor (C5aR): demonstration of C5aR on nonmyeloid cells of the liver and lung. *The Journal of Immunology, 154*(4), 1861-1869.

Hawlisch, H., Wills-Karp, M., Karp, C. L., & Köhl, J. (2004). The anaphylatoxins bridge innate and adaptive immune responses in allergic asthma. *Molecular immunology, 41*(2), 123-131.

Hezmee, M. N. M., Kyaw-Tanner, M., Lee, J. Y. P., Shiels, I. A., Rolfe, B., Woodruff, T., & Mills, P. C. (2011). Increased expression of C5a receptor (CD88) mRNA in canine mammary tumors. *Veterinary immunology and immunopathology, 139*(1), 50-56.

Higuchi, R., Fockler, C., Dollinger, G., & Watson, R. (1993). Kinetic PCR analysis: Real-time monitoring of DNA amplification reactions. *Biotechnology, 11*, 1026-1030.

Hong, S., Lee, H. J., Kim, S. J. & Hahm, K. B. (2010). Connection between inflammation and carcinogenesis in gastrointestinal tract: Focus on TGF-I² signaling. *World Journal of Gastroenterology, 16*(17), 2080-2093.

Huber-Lang, M. S., Sarma, J. V., McGuire, S. R., Lu, K. T., Guo, R. F., Padgaonkar, V. A., ... & Ward, P. A. (2001). Protective effects of anti-C5a peptide antibodies in experimental sepsis. *The FASEB Journal, 15*(3), 568-570.

Huber-Lang, M., Sarma, J. V., Zetoune, F. S., Rittirsch, D., Neff, T. A., McGuire, S. R., ... & Ward, P. A. (2006). Generation of C5a in the absence of C3: a new complement activation pathway. *Nature Medicine, 12*(6), 682-687.

Khanna, C., Lindblad-Toh, K., Vail, D., London, C., Bergman, P., Barber, L., & Withrow, S. (2006). The dog as a cancer model. *Nature Biotechnology, 24*(9), 1065-1066.

Kim, D.-Y., Martin, C. B., Lee, S. N., & Martin, B. K. (2005). Expression of complement protein C5a in a murine mammary cancer model: Tumor regression by interference with the cell cycle. *Cancer Immunology Immunotherapy, 54*(10), 1026-1037.

Kim, S., & Kim, T. (2003). Selection of optimal internal controls for gene expression profiling of liver disease. *Biotechniques, 35*(3), 456-460.

Kurimoto, Y., De Weck, A. L., & Dahinden, C. A. (1989). Interleukin 3-dependent mediator release in basophils triggered by C5a. *The Journal of Experimental Medicine, 170*(2), 467-479.

Linton, S. M., & Morgan, B. P. (1999). Complement activation and inhibition in experimental models of arthritis. *Molecular Immunology, 36*(13), 905-914.

Markiewski, M. M., DeAngelis, R. A., Benencia, F., Ricklin-Lichtsteiner, S. K., Koutoulaki, A., Gerard, C., & Lambris, J. D. (2008). Modulation of the antitumor immune response by complement. *Nature immunology, 9*(11), 1225-1235.

Nemali, S., Siemsen, D. W., Nelson, L. K., Bunger, P. L., Faulkner, C. L., Rainard, P., ... & Quinn, M. T. (2008). Molecular analysis of the bovine anaphylatoxin C5a receptor. *Journal of Leukocyte Biology, 84*(2), 537-549.

Onuma, H., Masuko-Hongo, K., Yuan, G., Sakata, M., Nakamura, H., Kato, T., ... & Nishioka, K. (2002). Expression of the anaphylatoxin receptor C5aR (CD88) by human articular chondrocytes. *Rheumatology International, 22*(2), 52-55.

Paoloni, M., & Khanna, C. (2008). Translation of new cancer treatments from pet dogs to humans. *Nature Reviews Cancer, 8*(2), 147-156.

Patel, S. N., Berghout, J., Lovegrove, F. E., Ayi, K., Conroy, A., Serghides, L., ... & Kain, K. C. (2008). C5 deficiency and C5a or C5aR blockade protects against cerebral malaria. *The Journal of Experimental Medicine, 205*(5), 1133-1143.

Perret, J. J., Raspe, E., Vassart, G., & Parmentier, M. (1992). Cloning and functional expression of the canine anaphylatoxin C5a receptor. Evidence for high interspecies variability. *Biochemical Journal, 288*, 911-917.

Pinho, S. S., Carvalho, S., Cabral, J., Reis, C. A., & Gärtner, F. (2012). Canine tumors: A spontaneous animal model of human carcinogenesis. *Translational Research, 159*(3), 165-172.

Pontius, J. U., Mullikin, J. C., Smith, D. R., Lindblad-Toh, K., Gnerre, S., Clamp, M. B., & O'Brien, S. J. (2007). Initial sequence and comparative analysis of the cat genome. *Genome research, 17*(11), 1675-1689.

Revollo, I., Nishiura, H., Shibuya, Y., Oda, Y., Nishino, N., & Yamamoto, T. (2005). Agonist and antagonist dual effect of the cross-linked S19 ribosomal protein dimer in the C5a receptor-mediated respiratory burst reaction of phagocytic leukocytes. *Inflammation Research, 54*(2), 82-90.

Riedemann, N. C., Guo, R. F., Sarma, V. J., Laudes, I. J., Huber-Lang, M., Warner, R. L., ... & Ward, P. A. (2002). Expression and function of the C5a receptor in rat alveolar epithelial cells. *The Journal of Immunology, 168(*4), 1919-1925.

Robbins, R. A., Russ, W. D., Rasmussen, J. K., & Clayton, M. M. (1987). Activation of the Complement System in the Adult Respiratory Distress Syndrome 1–4. *American Review of Respiratory Disease, 135*(3), 651-658.

Rowell, J. L., McCarthy, D. O., & Alvarez, C. E. (2011). Dog models of naturally occurring cancer. *Trends in Molecular Medicine, 17*(7), 380-388.

Sapir, T., & Shoenfeld, Y. (2005). Uncovering the hidden potential of intravenous immunoglobulin as an anticancer therapy. *Clinical Reviews in Allergy and Immunology, 29*(3), 307-310.

Schmidt, R. E., & Gessner, J. E. (2005). Fc receptors and their interaction with complement in autoimmunity. *Immunology Letters, 100*(1), 56-67.

Short, A., Wong, A. K., Finch, A. M., Haaima, G., Shiels, I. A., Fairlie, D. P., & Taylor, S. M. (1999). Effects of a new C5a receptor antagonist on C5a-and endotoxin-induced neutropenia in the rat. *British journal of pharmacology, 126*(3), 551-554.

Smedegård, G., Cui, L. X., & Hugli, T. E. (1989). Endotoxin-induced shock in the rat. A role for C5a. *The American Journal of Pathology, 135*(3), 489.

Suzuki, T., Higgins, P. J., & Crawford, D. R. (2000). Control selection for RNA quantitation. *Biotechniques, 29*(2), 332-337.

Tan, T. T., & Coussens, L. M. (2007). Humoral immunity, inflammation and cancer. *Curr Opin Immunol, 19*(2), 209-216.

Thellin, O., Zorzi, W., Lakaye, B., De Borman, B., Coumans, B., Hennen, G., ... & Heinen, E. (1999). Housekeeping genes as internal standards: use and limits. *Journal of Biotechnology, 75(*2), 291-295.

Ward, P. A. (2004). The dark side of C5a in sepsis. *Nature Reviews Immunology, 4*(2), 133-142.

Warrington, J. A., Nair, A., Mahadevappa, M., & Syganskayam, T. (2000). Comparison of human adult and fetal expression and identification of 535 housekeeping/ maintenance genes. *Physiology Genomics, 2*(3), 143-147.

Welch, T. R. (2002). Complement in glomerulonephritis. *Nature genetics, 31*(4), 333-334.

Werfel, T., Oppermann, M., Schulze, M., Krieger, G., Weber, M., & Gotze, O. (1992). Binding of fluorescein-labeled anaphylatoxin C5a to human peripheral blood, spleen, and bone marrow leukocytes. *Blood, 79*(1), 152-160.

Whelan, J. A., Russell, N. B., & Whelan, M. A. (2003). A method for the absolute quantification of cDNA using real-time PCR. *Journal of Immunological Methods, 278*(1), 261-269.

Woodruff, T. M., Arumugam, T. V., Shiels, I. A., Reid, R. C., Fairlie, D. P., & Taylor, S. M. (2003). A potent human C5a receptor antagonist protects against disease pathology in a rat model of inflammatory bowel disease. *The Journal of Immunology, 171*(10), 5514-5520.

Pertanika J. Sci. & Technol. 24 (1): 177 - 189 (2016)

SCIENCE & TECHNOLOGY

Journal homepage: http://www.pertanika.upm.edu.my/

A Comparative Study of the Group Runs and Side Sensitive Group Runs Control Charts

Yew, S. Y.[1], Khoo, M. B. C.[1], Teoh, W. L.[2], Teh, S. Y.[3*] and Yeong, W. C.[2]

[1]*School of Mathematical Sciences, Universiti Sains Malaysia, 11800 USM, Penang, Malaysia*

[2]*Department of Physical and Mathematical Science, Faculty of Science, Universiti Tunku Abdul Rahman, Kampar, Perak, Malaysia*

[3]*School of Management, Universiti Sains Malaysia, 11800 USM, Penang, Malaysia*

ABSTRACT

The Group Runs (GR) and Side Sensitive Group Runs (SSGR) control charts are the improvement of the synthetic chart without and with side sensitivity. Both the SSGR and GR charts are effective for detecting small to moderate process mean shifts. The performances of the SSGR and GR charts, in terms of the average time to signal (ATS), are compared in this paper. In this comparative study, the Monte Carlo simulation approach by means of the Statistical Analysis System (SAS) software is used to compute the ATS values for the GR and SSGR charts. The results revealed that the SSGR chart's performance is better than that of the GR chart for all levels of mean shifts.

Keywords: Average time to signal, GR chart, SSGR chart

INTRODUCTION

The Shewhart's $\bar{X}$ chart has wide applications in the service and manufacturing sectors. The Shewhart's $\bar{X}$ chart is effective for detecting large process mean shifts. On the other hand, both the Exponentially Weighted Moving Average (EWMA) and Cumulative Sum (CUSUM) control charts, introduced by Roberts (1959) and Page (1954), respectively, are used to detect small process mean shifts. Recently, many researchers have contributed to a wide variety of control charts to improve process monitoring, such as Costantino *et al*. (2015), Moraes *et al*. (2014), Ali and Riaz (2014), Haq *et al*. (2015), Chong *et al*. (2014), Teoh *et al*. (2014), Costa and Machado (2015) and many more.

The Conforming Run Length (CRL) chart was proposed by Bourke in 1991. Bourke (1991) referred to CRL as the number of inspected units between two consecutive defective units. When CRL < L_{CRL}, the CRL chart will indicate a shift in the process. Here, L_{CRL} is the lower limit of the CRL chart.

Article history:
Received: 6 May 2015
Accepted: 28 July 2015

E-mail addresses:
yyysandra@hotmail.com (Yew, S. Y.),
mkbc@usm.my (Khoo, M. B. C.),
teohwl@utar.edu.my (Teoh, W. L.),
tehsyin@usm.my (Teh, S. Y.),
thomas_yeong@yahoo.com (Yeong, W. C.)
*Corresponding author

ISSN: 0128-7680

The synthetic chart suggested by Wu and Spedding (2000) combines the CRL chart (CRL/S sub-chart) and the Shewhart $\bar{X}$ chart ($\bar{X}/S$ sub-chart). The sample (group) of the CRL/S sub-chart is considered as a unit. This synthetic chart is sensitive to small and moderate process mean shifts. Let μ_0 be the target value of the mean, σ be the standard deviation, k be the multiplier controlling the width of the control limits of the $\bar{X}/S$ sub-chart and n be the sample size. If a group mean is $\bar{X} \notin \left(\mu_0 - k\sigma/\sqrt{n},\ \mu_0 + k\sigma/\sqrt{n}\right)$, the group in the synthetic control chart is declared as non-conforming. The synthetic chart signals an out-of-control status when CRL $\leq L_S$ for the first time. Here, L_S is the lower limit of the CRL/S sub-chart. Davis and Woodall (2002) extended the idea of Wu and Spedding (2000) to propose a side sensitive version of the synthetic control chart. They stated that the synthetic chart with side sensitivity outperforms the synthetic chart. This synthetic chart with side sensitivity has the feature of the run rules chart with a head start. For the synthetic chart with side sensitivity, if two out of $(L_S + 1)$ group means lie outside of the $\bar{X}/S$ sub-chart's limits on the same side of the centre line, the process is declared as being out-of-control.

The Group Runs (GR) control chart proposed by Gadre and Rattihalli (2004) is a combination of an extended version of the CRL chart and the Shewhart $\bar{X}$ chart. Note that this GR chart is an improvement of the synthetic chart. Let L_g be the lower limit of the extended version of the CRL chart, which is a sub-chart of the GR chart.

For the GR chart, a process is declared as being out-of-control when two successive group-based CRLs $\leq L_g$ or the first group-based CRL $\leq L_g$ for the first time. Note that both the non-conforming groups in the two successive CRL values either have shifts on the same or opposite side of μ_0. Besides that, Gadre and Rattihalli (2007) developed a Side Sensitive Group Runs (SSGR) control chart, which is an extension of the group runs chart with side sensitivity. In the SSGR chart, the process is declared as being out-of-control if two successive values CRL $\leq L_{ssg}$ or the first group-based CRL $\leq L_{ssg}$ for the first time. Note that both the non-conforming groups for the two successive CRL values have shifts on the same side of μ_0. Here, L_{ssg} denotes the lower limit of the CRL chart, which is a sub-chart of the SSGR chart. Moreover, Gadre *et al*. (2010) modified the SSGR chart to develop the Side Sensitive Modified Group Runs (SSMGR) chart for detecting shifts in the process mean. Gadre (2014) also extended the univariate GR chart to bivariate and multivariate GR charts for monitoring process variability. The GR and SSGR charts can be used in any process monitoring situations in manufacturing, service industries, healthcare etc. The GR and SSGR charts are found to be better than the EWMA and CUSUM charts in detecting moderate and large shifts.

Gadre and Rattihalli (2007) compared the performance of the SSGR chart with the GR, Shewhart's $\bar{X}$ and synthetic charts. However, in the comparison, the sample size (n) was not fixed, but was chosen to minimise the average time to signal a shift. This resulted in a very large n. For example, in one of the examples, the optimal n was 186, 102, 98 and 89 for the Shewhart's $\bar{X}$, synthetic GR and SSGR charts, respectively. It may not be feasible for practitioners to adopt such a large sample size. Thus, for this paper, we allowed the practitioner to fix the sample size at a particular value, then selected the optimal control limits which would minimise the average time to signal a shift. We focused our attention on small values of n, as small sample sizes are preferred in industrial applications.

The performances, in terms of the average time to signal (ATS), of the SSGR and GR charts for detecting process mean shifts are compared in this paper. The objective of this study was to determine which control chart gives a better performance. The remainder of this paper is organised as follows: Sections 2 and 3 explain the design of the GR and SSGR charts, respectively. Section 4 studies and compares the performance of the GR and SSGR charts. Conclusions are drawn in Section 5.

DESIGN OF THE GR CONTROL CHART

The GR chart operates by declaring a sample of n items as being non-confirming when the sample mean falls outside the lower $\left(L_{\overline{X}|S}\right)$ or upper $\left(U_{\overline{X}|S}\right)$ control limits of the $\overline{X}$ sub-chart. The number of conforming samples between two successive non-conforming samples is defined as the CRL. The process is declared as being out-of-control when the number of two successive CRLs $\leq L_g$ or the first CRL $\leq L_g$ for the first time. Readers may refer to Gadre and Rattihalli (2004) for a detailed explanation of the GR chart.

The average time to signal a shift of size δ, ATS(δ) is given as (Gadre & Rattihalli, 2004):

$$\mathrm{ATS}(\delta) = \frac{n}{P(\delta)} \frac{1}{\left[1-\{1-P(\delta)\}^{L_g}\right]^2}, \tag{1}$$

where $P(\delta)$ is the probability of the occurrence of a non-conforming sample for a shift δ and is given as:

$$\begin{aligned} P(\delta) &= 1 - P\left(L_{\overline{X}|S} < \overline{X} < U_{\overline{X}|S} \,\middle|\, \overline{X} \sim N\left(\mu_0 + \delta\sigma, \frac{\sigma}{\sqrt{n}}\right)\right) \\ &= 1 - \Phi\left(k - \delta\sqrt{n}\right) + \Phi\left(-k - \delta\sqrt{n}\right), \end{aligned} \tag{2}$$

where $\Phi(\cdot)$ is the standard normal cumulative distribution function. The derivation of Equation (1) is shown in Gadre and Rattihalli (2004).

To find the optimal chart parameters (k, L_g) for a given group size, the optimisation algorithm for the GR chart is taken as being similar to that of the synthetic control chart, as proposed by Wu and Spedding (2000). The optimal chart parameters are the parameters that minimise the ATS(δ) subject to the chosen in-control ATS (ATS_0) constraint, where $\mathrm{ATS}_0 = n \times \mathrm{ARL}_0$. The procedure to obtain the optimal chart parameters is outlined as follows:

1. Specify the values of n, μ_0, σ, δ and ARL_0.
2. Let $L_g = 1$.
3. Numerically solve Equation (1) for k when ATS(0) = ATS_0, where $\mathrm{ATS}_0 = n \times \mathrm{ARL}_0$ Parameters (L_g, k) are candidates for an optimal GR chart, since they produce an in-control ATS value of ATS_0.
4. Calculate the out-of-control ATS, ATS(δ) by substituting the current values (L_g, k) into Equation (1).
5. If the out-of-control ATS is reduced to a given precision, let $L_g = L_g + 1$ and go back to Step 3. Otherwise, proceed to Step 6.

6. Take the immediate previous values of (L_g, k) as the optimal control limits of the GR chart.

In this paper, the optimal parameters are computed using Mathematica by implementing Steps 1 to 6.

DESIGN OF THE SSGR CONTROL CHART

The SSGR chart operates by declaring a sample of n items as non-confirming when the sample mean falls outside the lower $\left(L_{\bar{X}|S}\right)$ or upper $\left(U_{\bar{X}|S}\right)$ control limits of the $\bar{X}$ sub-chart. The process is declared as out-of-control when the number of two successive CRLs $\leq L_g$ or the first CRL $\leq L_g$ for the first time. However, unlike the GR chart, the two successive $\bar{X}$ samples corresponding to the two successive CRLs must fall on the same side of the target value μ_0. Readers may refer to Gadre and Rattihalli (2007) for a detailed explanation of the SSGR chart.

The ATS(δ) of the SSGR chart (Gadre and Rattihalli, 2007) is given as:

$$\mathrm{ATS}(\delta) = \frac{n}{P(\delta)} \frac{1-\alpha(1-\alpha)A^2}{A^2[1+\alpha(1-\alpha)(A-2)]} \qquad (3)$$

where $P(\delta) = 1 - \Phi\left(k - \delta\sqrt{n}\right) + \Phi\left(-k - \delta\sqrt{n}\right)$,

$$A = 1 - \left[1 - P(\delta)\right]^{L_{ssg}},$$

and $\alpha = \dfrac{\left[1 - \phi\left(k - \delta\sqrt{n}\right)\right]}{P(\delta)}$,

where $\Phi(\cdot)$ is the standard normal probability density function. The derivation of Equation (3) can be found in Gadre and Rattihalli (2007).

We are interested to search for the optimal chart parameters (k, L_{ssg}) for a given sample size, n. The computation of the optimal chart parameters of the SSGR chart is similar to that of the GR chart described in the previous section but by replacing the notation L_g with L_{ssg} , Equation (1) with Equation (3) and the words 'GR chart' with 'SSGR chart'.

A COMPARISON BETWEEN THE GR AND SSGR CHARTS BASED ON ATS

A comparison between the GR and SSGR charts, in terms of the ATS, is discussed in this section. The Statistical Analysis System (SAS) software was used to calculate the ATS via the simulation methods. The procedure to compute the ATS for the GR chart is outlined as follows:

1. Specify the values of n, μ_0, σ, δ, k and L_g.
2. Compute the lower and upper control limits (LCL and UCL) of the $\bar{X}$ sub-chart.
3. Set CRL = 0 and p = 0.
4. Set i = 1.

5. For $j = 1$ to n, generate X from a normal distribution with mean $\mu 0 + \delta\sigma$ and variance σ^2, then take the sample average as $\bar{X} = \frac{\sum_{j=1}^{n} X_j}{n}$. If LCL < $\bar{X}$ < UCL, go to Step 6; otherwise, go to Step 7.
6. Set $a = 1$, CRL = CRL + 1 and $i = i + 1$, then return to Step 5.
7. Set $p = p + 1$. If $a = 1$, set CRL = CRL + 1 and CRLL (p) = CRL; else if $a \neq 1$, set CRLL (p) = CRL. If $p = 1$, go to Step 8; otherwise, if $p \geq 3$, go to Step 9.
8. If CRLL (p) $\leq L_g$, ATS = $i \times n$; otherwise, i = i + 1 and return to Step 5.
9. If CRLL (p-1) $\leq L_g$ and CRLL (p)$\leq L_g$, ATS = $i \times n$; otherwise, $i = i + 1$ and return to Step 5.

Repeat Steps 3 to 9 for 10,000 times. The ATS is the average value of all the ATS values computed from the 10,000 simulation trials.

The ATS of the SSGR chart was obtained in similar manner (except that the side sensitivity feature was considered):

1. Specify the values of n, μ_0, σ, δ, k and L_{ssg}.
2. Compute the lower and upper control limits (LCL and UCL) of the $\bar{X}$ sub-chart.
3. Set CRLU = 0, CRLL = 0 and $p = 0$.
4. Set $i = 1$.
5. For $j = 1$ to n, generate X from a normal distribution with mean $\mu_{0+}\sigma\delta$ and variance σ^2 then take the sample average as $\bar{X} = \frac{\sum_{j=1}^{n} X_j}{n}$. If $LCL < \bar{X} < UCL$, go to Step 6; otherwise, go to Step 7.
6. Set $a = 1$, CRLU = CRLU + 1, CRLL = CRLL + 1 and $i = i + 1$, then return to Step 5.
7. Set $p = p + 1$. If $\bar{X} > UCL$, go to Step 8, while if $\bar{X} > LCL$, go to Step 9.
8. If $a = 1$, set CRLU = CRLU + 1 and CRLUU (p) = CRLU; otherwise, if $a \neq 1$, set CRLUU (p) = CRLU. If $p = 1$, go to Step 10; otherwise, if $p \geq 3$, go to Step 11.
9. 9. If $a = 1$, set CRLL = CRLL + 1 and CRLLL (p) = CRLL; otherwise, if $a \neq 1$, set CRLLL (p) = CRLL. If $p = 1$, go to Step 12; otherwise, if $p \geq 3$, go to Step 13.
10. If CRLUU (p) $\leq L_{ssg}$, ATS = $i \times n$; otherwise, $i = i + 1$ and return to Step 5.
11. If CRLUU (p -1) $\leq L_{ssg}$ and CRLUU (p) $\leq L_{ssg}$, ATS = $i \times n$; otherwise, $i = i + 1$ and return to Step 5.
12. If CRLLL (p) $\leq L_{ssg}$, ATS = $i \times n$; otherwise, $i = i + 1$ and return to Step 5.
13. If CRLLL (p - 1) $\leq L_{ssg}$ and CRLLL (p)$\leq L_{ssg}$, ATS = $i \times n$; otherwise, $i = i + 1$ and return to Step 5.

Repeat Steps 3 to 13 for 10,000 times. The ATS is the average value of all the ATS values computed from the 10,000 simulation trials.

To compare the GR and SSGR charts, the following combinations of input parameters were selected:

n : 3 5 7
δ_{opt} : 0.2 0.5 1.0
ARL_0 : 370 500

Here, δ_{opt} denotes the size of a mean shift for which a quick detection is desired and ARL_0 is the in-control average run length. All the 18 possible combinations of the input parameters (n, δ_{opt}, ARL_0) are considered in this paper. These combinations of input parameters are selected so that practitioners can study the performances of the GR and SSGR charts for small sample sizes and small shift sizes. Small sample sizes are preferred in industrial applications, while the performance of the chart in detecting small shift sizes is important as large shift sizes are usually easily detected. Besides that, two different constraints in ARL_0 are used so that the effects of the constraints on the ATS can be studied. Practitioners can also choose other combinations of the input parameters according to their needs. The process is then monitored.

These input parameters (n, δ_{opt}, ARL_0) were used to obtain the optimal values, (k, L_g) and (k, L_{ssg}) of the SSGR and GR charts, respectively. The optimal control chart parameters are shown in Table 1. These optimal parameters are computed using the procedure described in the last two sections.

TABLE 1 : Optimal and Values of the GR Chart and SSGR Chart, Respectively

(n, δ_{opt}, ARL_0)	GR		SSGR	
	k	L_g	k	L_{ssg}
(3, 0.2, 370)	2.57	70	2.41	44
(3, 0.5, 370)	2.30	20	2.16	15
(3, 1.0, 370)	1.95	5	1.87	5
(5, 0.2, 370)	2.52	55	2.36	35
(5, 0.5, 370)	2.18	12	2.05	10
(5, 1.0, 370)	1.81	3	1.72	3
(7, 0.2, 370)	2.47	44	2.32	29
(7, 0.5, 370)	2.10	9	1.96	7
(7, 1.0, 370)	1.81	3	1.6	2
(3, 0.2, 500)	2.65	84	2.49	52
(3, 0.5, 500)	2.37	23	2.23	17
(3, 1.0, 500)	2.05	6	1.91	5
(5, 0.2, 500)	2.60	65	2.44	41
(5, 0.5, 500)	2.26	14	2.12	11
(5, 1.0, 500)	1.86	3	1.77	3
(7, 0.2, 500)	2.55	52	2.4	34
(7, 0.5, 500)	2.17	10	2.04	8
(7, 1.0, 500)	1.86	3	1.64	2

The optimal combinations (k, L_g) and (k, L_{ssg}) in Table 1 were used to compute the corresponding ATS(δ) for the GR and SSGR charts, which are shown in Tables 2 to 4. The ATS_G and ATS_{SSG} in Tables 2 to 4 represent the ATS values for the GR and SSGR charts, respectively. The in-control ATS for the two charts is equal to $ATS_0 = n \times ARL_0$. Table 5 shows the percentage of improvement in the ATSs of the SSGR chart as compared to the GR chart. For $\delta > 0$, the ATSs of the GR chart were larger than that of the SSGR chart, except for larger shifts where the ATSs of the GR chart were similar to that of the SSGR chart (see Tables 2 to 4). Thus, the SSGR chart had a higher detection speed of the out-of-control condition compared to the GR chart. However, the ATS_G and $ATSS_{SG}$ values were almost the same when the shifts were large ($\delta \geq 2.0$), which show that the GR and SSGR charts gave equal performance for large shifts. Table 5 shows that the percentage of improvement was larger for smaller shifts, especially for $\delta \leq 1.0$. In general, it is concluded that the SSGR chart is more sensitive than the GR chart in detecting process changes.

TABLE 2 : ATS Values of the GR and SSGR Charts when n = 3

(n, δ_{opt}, ARL_0)

δ	(3, 0.2, 370)		(3, 0.5, 370)		(3, 1.0, 370)		(3, 0.2, 500)		(3, 0.5, 500)		(3, 1.0, 500)	
	ATS_G	ATS_{SSG}	ATS_G	ATS_{SSG}	ATS_G	ATS_{SSG}	ATS_G	ATS_{SSG}	ATS_G	ATS_{SSG}	ATS_G	ATS_{SSG}
0.2	479.27	375.81	502.00	409.84	561.05	471.60	601.64	480.44	621.68	508.53	764.39	575.81
0.4	124.95	93.45	117.58	90.61	146.37	107.01	149.98	113.01	139.20	106.77	180.04	127.92
0.6	48.92	36.88	36.76	29.53	40.35	31.63	57.12	42.77	40.86	33.05	45.53	35.70
0.8	25.48	19.67	17.12	14.45	15.72	13.26	29.21	22.38	19.14	15.80	17.37	14.50
1.0	14.96	12.03	10.64	9.06	8.53	7.58	16.63	13.40	11.53	9.81	9.19	8.01
1.5	5.89	5.24	4.85	4.49	4.04	3.91	6.32	5.55	5.09	4.67	4.23	3.98
2.0	3.67	3.50	3.41	3.31	3.21	3.18	3.78	3.58	3.47	3.36	3.26	3.20
2.5	3.13	3.08	3.06	3.04	3.03	3.02	3.15	3.10	3.07	3.05	3.03	3.02
3.0	3.01	3.01	3.00	3.00	3.00	3.00	3.02	3.01	3.01	3.00	3.00	3.00

TABLE 3 : ATS Values of the GR and SSGR Charts when n = 5

(n, δ_{opt}, ARL_0)

δ	(5, 0.2, 370)		(5, 0.5, 370)		(5, 1.0, 370)		(5, 0.2, 500)		(5, 0.5, 500)		(5, 1.0, 500)	
	ATS_G	ATS_{SSG}	ATS_G	ATS_{SSG}	ATS_G	ATS_{SSG}	ATS_G	ATS_{SSG}	ATS_G	ATS_{SSG}	ATS_G	ATS_{SSG}
0.2	514.76	403.36	582.71	436.04	712.84	549.33	653.45	502.50	725.79	541.13	938.65	703.48
0.4	106.60	80.30	94.37	73.02	131.99	96.40	126.32	94.36	109.12	84.29	160.41	115.73
0.6	41.74	32.60	28.66	23.87	32.99	26.80	48.10	36.98	31.61	26.48	37.59	30.12
0.8	21.57	17.51	14.45	12.73	13.35	11.83	24.11	19.38	15.70	13.64	14.45	12.60
1.0	12.85	11.09	9.59	8.76	8.15	7.60	13.91	11.90	10.20	9.21	8.50	7.91
1.5	6.25	5.95	5.71	5.56	5.35	5.30	6.44	6.10	5.79	5.64	5.39	5.33
2.0	5.13	5.08	5.05	5.03	5.01	5.01	5.16	5.10	5.06	5.04	5.02	5.01
2.5	5.00	5.00	5.00	5.00	5.00	5.00	5.00	5.00	5.00	5.00	5.00	5.00
3.0	5.00	5.00	5.00	5.00	5.00	5.00	5.00	5.00	5.00	5.00	5.00	5.00

TABLE 4 : ATS Values of the GR and SSGR Charts when $n = 7$

δ	$(n, \delta_{opt}, \text{ARL}_0)$											
	(7, 0.2, 370)		(7, 0.5, 370)		(7, 1.0, 370)		(7, 0.5, 500)		(7, 1.0, 500)		(7, 1.0, 500)	
	ATS_G	ATS_{SSG}	ATS_G	ATS_{SSG}	ATS_G	ATS_{SSG}	ATS_G	ATS_{SSG}	ATS_G	ATS_{SSG}	ATS_G	ATS_{SSG}
0.2	502.38	405.46	578.10	460.36	740.46	609.92	629.02	494.90	717.41	561.10	971.45	729.34
0.4	93.10	72.69	80.16	65.40	103.67	91.44	107.79	82.93	90.59	74.66	123.86	103.67
0.6	37.44	30.34	24.98	21.87	26.64	25.54	41.88	33.74	27.00	23.68	29.50	27.54
0.8	19.35	16.67	13.82	12.50	12.47	12.08	21.14	17.99	14.65	13.22	13.12	12.53
1.0	12.27	11.09	9.90	9.33	8.98	8.62	12.97	11.66	10.24	9.66	9.17	8.79
1.5	7.51	7.35	7.22	7.15	7.10	7.06	7.60	7.43	7.25	7.19	7.11	7.07
2.0	7.01	7.01	7.00	7.00	7.00	7.00	7.02	7.01	7.00	7.00	7.00	7.00
2.5	7.00	7.00	7.00	7.00	7.00	7.00	7.00	7.00	7.00	7.00	7.00	7.00
3.0	7.00	7.00	7.00	7.00	7.00	7.00	7.00	7.00	7.00	7.00	7.00	7.00

TABLE 5 : Percentage of Improvement of the SSGR Chart Compared to the GR Chart for $n \in \{3, 5, 7\}$

δ	$(\delta_{opt}, \text{ARL}_0)$																	
	(0.2, 370)			(0.5, 370)			(1.0, 370)			(0.2, 500)			(0.5, 500)			(1.0, 500)		
	n = 3	n = 5	n = 7	n = 3	n = 5	n = 7	n = 3	n = 5	n = 7	n = 3	n = 5	n = 7	n = 3	n = 5	n = 7	n = 3	n = 5	n = 7
0.2	21.59%	21.64%	19.29%	18.36%	25.17%	20.37%	15.94%	22.94%	17.63%	20.14%	23.10%	21.32%	18.20%	25.44%	21.79%	24.67%	25.05%	24.92%
0.4	25.21%	24.67%	21.92%	22.94%	22.62%	18.41%	26.89%	26.96%	11.80%	24.65%	25.30%	23.06%	23.30%	22.75%	17.58%	28.95%	27.85%	16.30%
0.6	24.61%	21.90%	18.96%	19.67%	16.71%	12.45%	21.61%	18.76%	4.13%	25.12%	23.12%	19.44%	19.11%	16.23%	12.30%	21.59%	19.87%	6.64%
0.8	22.80%	18.82%	13.85%	15.60%	11.90%	9.55%	15.65%	11.39%	3.13%	23.38%	19.62%	14.90%	17.45%	13.12%	9.76%	16.52%	12.80%	4.50%
1.0	19.59%	13.70%	9.62%	14.85%	8.65%	5.76%	11.14%	6.75%	4.01%	19.42%	14.45%	10.10%	14.92%	9.71%	5.66%	12.84%	6.94%	4.14%
1.5	11.04%	4.80%	2.13%	7.42%	2.63%	0.97%	3.22%	0.93%	0.56%	12.18%	5.28%	2.24%	8.25%	2.59%	0.83%	5.91%	1.11%	0.56%
2.0	4.63%	0.97%	0.00%	2.93%	0.40%	0.00%	0.93%	0.00%	0.00%	5.29%	1.16%	0.14%	3.17%	0.40%	0.00%	1.84%	0.20%	0.00%
2.5	1.60%	0.00%	0.00%	0.65%	0.00%	0.00%	0.33%	0.00%	0.00%	1.59%	0.00%	0.00%	0.65%	0.00%	0.00%	0.33%	0.00%	0.00%
3.0	0.00%	0.00%	0.00%	0.00%	0.00%	0.00%	0.00%	0.00%	0.00%	0.33%	0.00%	0.00%	0.33%	0.00%	0.00%	0.00%	0.00%	0.00%

AN ILLUSTRATIVE EXAMPLE

To show the implementation and application of the GR and SSGR control charts, a set of real data from Wild and Seber (2000) was adopted. Consider a dry powder filling process, where the weight of content in each can is the quality characteristic of interest. In a canning plant, dry powder is packed into cans with a nominal weight of 2000 grams. Cans are filled at a four-head filler fed by a hopper, with each head filling about 25 cans every two minutes.

The process is controlled by a computer programme that calculates very crude adjustments to fill-times based on the filled weight recorded at a check weigher. A sub-group of 5 cans is a natural sub-group size for studying the process. The powder density is expected to change often. This is because of the settling effect in the bins where it was stored prior to canning. Therefore, automatic adjustment is needed.

The weights were recorded for 5 successive cans every two minutes, for 60 minutes, to see how the process was performing. Hence, the data consisted of 30 sub-groups, each of size n = 5. These weights, expressed as deviations from 1984 grams, are given in Table 6. The mean $\bar{X}_i$ and range R_i of each of these subgroups are also given in Table 6.

TABLE 6 : Canning Plant Data

Subgroup	Weight-1984 (grams)					Mean	Range
1	32.3	31.6	13.3	14.3	16.6	21.62	19.0
2	23.2	32.9	30.1	34.8	29.9	30.18	11.6
3	8.1	17.5	11.9	11.4	12.5	12.28	9.4
4	19.6	26.2	27.8	27.4	17.1	23.62	10.7
5	31.4	35.7	29.2	29.7	26.9	30.58	8.8
6	37.5	22.6	8.1	12.9	14.5	19.12	29.4
7	20.0	18.0	23.6	9.0	16.1	17.34	14.6
8	7.9	4.4	4.4	3.9	3.7	4.86	4.2
9	17.8	17.1	18.4	24.9	21.5	19.94	7.8
10	25.4	26.9	27.3	21.6	29.2	26.08	7.6
11	35.9	42.8	41.1	37.4	24.8	36.40	18.0
12	26.6	33.4	27.9	25.1	29.9	28.58	8.3
13	13.7	11.8	20.6	6.2	14.2	13.30	14.4
14	32.3	23.1	17.7	22.1	12.1	21.46	20.2
15	27.4	26.0	29.4	29.5	32.5	28.96	6.5
16	36.5	42.4	30.7	27.0	23.3	31.98	19.1
17	24.0	36.8	31.5	22.5	25.6	28.08	14.3
18	26.2	18.0	14.4	6.8	11.3	15.34	19.4
19	25.7	26.3	23.2	17.8	18.1	22.22	8.5
20	16.4	44.1	33.4	29.7	32.2	31.16	27.7
21	13.2	23.3	23.7	21.0	16.7	19.58	10.5
22	24.5	32.8	24.4	29.2	22.0	26.58	10.8
23	16.7	24.9	27.8	29.3	31.4	26.02	14.7

TABLE 6 : (Continued)

24	34.2	25.6	11.5	8.5	2.6	16.48	31.6
25	33.6	17.4	17.5	18.4	15.6	20.50	18.0
26	27.2	37.2	27.4	28.2	21.2	28.24	16.0
27	29.6	39.0	35.7	32.5	29.3	33.22	9.7
28	18.9	54.3	40.4	35.3	28.3	35.44	35.4
29	19.1	28.6	23.8	29.9	27.1	25.70	10.8
30	29.9	29.4	30.8	30.3	38.5	31.78	9.1

Firstly, the optimal values of (k, L_g) for the GR chart and (k, L_{ssg}) for the SSGR chart were obtained based on (n = 5, δ_{opt} = 1, ATS_0 = 2000). We used the optimal values (k, L_g) = (1.82, 3), as given in Gadre and Rattihalli (2004) for the GR chart, while optimal values of (k, L_{SSG}) = (1.74, 3) as given in Gadre and Rattihalli (2007), were adopted for the SSGR chart.

Next, the $\bar{X}$ sub chart was set up to declare whether a sub-group of data was conforming or non-conforming. The centre line was computed as $\hat{\mu}_0 = \frac{\sum_{i=1}^{m} \bar{X}_i}{m} = 24.22$, where m = 30 is the number of subgroups. Since there were five observations in each subgroup i.e. n = 5, the range method was used to estimate the standard deviation σ for this $\bar{X}$ sub chart. The average sample range was calculated as $\bar{R} = \frac{\sum_{i=1}^{m} R_i}{m} = 14.9$. Thus, the standard deviation for the $\bar{X}$ sub chart was estimated as $\hat{\sigma} = \frac{\bar{R}}{d_2} = \frac{14.9}{2.326} = 6.41$.

Therefore, with $\hat{\mu}_0 = 24.22$ and $\hat{\sigma} = 6.41$, the lower and upper control limits of the $\bar{X}$ sub chart could be computed. For the GR chart, the lower and upper control limits of the sub chart were $L_{\bar{X}|S} = 19.0027$ and $U_{\bar{X}|S} = 29.4373$, while for the SSGR chart, the lower and upper control limits of the $\bar{X}$ sub chart were $L_{\bar{X}|S}$ = 19.232 and $U_{\bar{X}|S}$ = 29.208. Hence, the $\bar{X}$ sub chart for the weights of dry powder in cans could be constructed as given in Fig.1 and Fig.2 for the GR and SSGR charts, respectively.

The dots in Fig.1 and Fig.2 are the non-conforming groups of canning plant data as those group means fell outside the lower and upper limits of the $\bar{X}$ sub chart. Let Y_r be the *rth* group-based CRL, for r ∈ { 1, 2, 3,.. }. Recall that the GR chart indicates an out-of-control signal if either $Y_1 \le L_g$ or two successive Y_r and Y_{r+1} (for r = 2, 3, …) are less than or equal to L_g for the first time, while for the SSGR chart, a process indicates an out-of-control signal if either $Y_1 \le L_{ssg}$ or two successive Y_r and Y_{r+1} (for r = 2, 3, …) are less than or equal to L_{ssg} for the first time, provided that the two successive $\bar{X}$ samples corresponding to the two successive group-based CRLs fall on the same side of the target value μ_0. From Fig.1 and Fig.2, we know that Y_1 = 2 , which is less than $L_G = L_{SSG}$ = 3. Therefore, the process was declared as being out-of-control by both the GR and SSGR control charts.

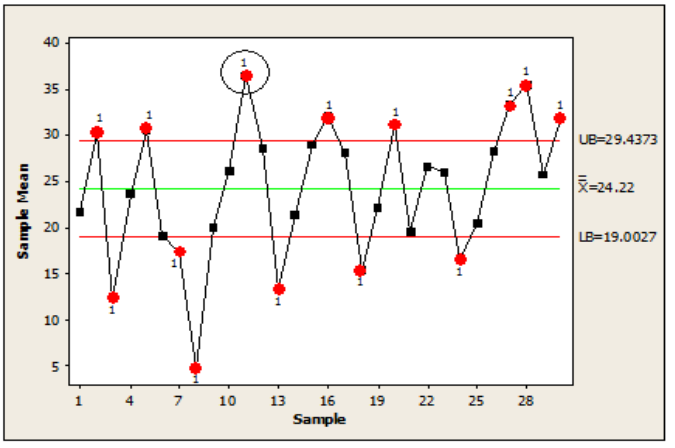

Fig.1: $\bar{X}$ sub chart for the weights of dry powder in cans (GR chart).

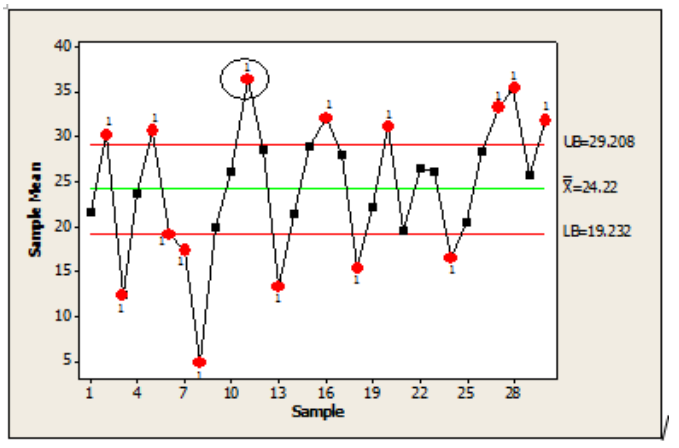

Fig.2: $\bar{X}$ sub chart for the weights of dry powder in cans (SSGR chart).

However, if we assume that all of the subgroups before the 11th (in circle) subgroup were conforming groups i.e. the first 10 subgroups have points plotting within the $L_{\bar{X}|S}$ and $U_{\bar{X}|S}$ limits, then $Y_1 = 11$, $Y_2 = 2$ and $Y_3 = 3$. Thus, for the GR chart, the process was declared as being out-of-control at the 16th sub-group as both Y_2 and Y_3 were less than or equal to L_g. However, the SSGR chart would not declare the process as being out-of-control after observing the third non-conforming group although both Y_2 and Y_3 were less than or equal to L_{ssg} . This is because the group means for Y_2 and Y_3 fell on the opposite side of the target value $\bar{X}$. The SSGR chart would only declare the dry powder filling process as out-of-control after plotting Y_8, as both $Y_7 = 3$ and $Y_8 = 1$ are not greater than L_{SSG} and both group means fall on the same side of the $\bar{X}$ sub chart. Thus, when the SSGR chart was adopted, the process was declared as being out-of-control at the 28th sub-group.

CONCLUSION

This study assumed that the underlying distribution followed an independent and identically distributed normal distribution. In this study, the ATSs of the GR and SSGR charts were compared for different sizes of mean shifts. When the in-control ATS of the charts under comparison was fixed at the same value, the chart having the smallest out-of-control ATS among all the competing charts was preferable. Since the ATS values of the SSGR chart were significantly less than the ATS values of the GR chart, the SSGR chart surpassed the GR chart for any sizes of shifts in the process mean.

Future research can be done to compare the performance of the GR and SSGR charts with estimated process parameters. Besides that, a comparative study of the performance of the GR and SSGR charts for skewed and heavy-tailed distributions can also be explored in future research.

ACKNOWLEDGEMENTS

This research was supported by the Universiti Sains Malaysia, Research University Grant no. 1001/PMATHS/811263 and Fundamental Research Grant Scheme, number FRGS/2/2014/SG04/UTAR/02/1.

REFERENCES

Ali, S., & Riaz, M. (2014). Cumulative quality control chart for the mixture of inverse Rayleigh process. *Computers & Industrial Engineering, 73,* 11-20.

Bourke, P. D. (1991). Detecting a shift in fraction nonconforming using run-length control charts with 100% inspection. *Journal of Quality Technology, 23*(2), 225-238.

Chong, Z. L., Khoo, M. B. C., & Castagliola, P. (2014). Synthetic double sampling np control chart for attributes. *Computers & Industrial Engineering, 75,* 157-169.

Costa, A. F. B., & Machado, M. A. G. (2015). The steady-state behavior of the synthetic and side-sensitive synthetic double sampling charts. *Quality and Reliability Engineering International, 31*(2), 297-303.

Costantino, F., Gravio, G.D., Shaban, A., & Tronci, M. (2015). SPC forecasting system to mitigate the bullwhip effect and inventory variance in supply chains. *Expert Systems with Applications, 42*(3), 1773-1787.

Davis, R. B., & Woodall, W. H. (2002). Evaluating and improving the synthetic control chart. *Journal of Quality Technology, 34*(2), 200-208.

Gadre, M. P. (2014). A multivariate group runs control chart for process dispersion. *Communications in Statistics - Simulation and Computation, 43*(4), 813-837.

Gadre, M. P., Joshi, K. A., & Rattihalli, R. N. (2010). A side sensitive modified group runs control chart to detect shifts in the process mean. *Journal of Applied Statistics, 37*(12), 2073-2087.

Gadre, M. P., & Rattihalli, R. N. (2004). A group runs control chart for detecting shifts in the process mean. *Economy Quality Control, 19*(1), 29-43.

Gadre, M. P., & Rattihalli, R. N. (2007). A side sensitive group runs control chart for detecting shifts in the process mean. *Statistical Methods and Applications, 16*(1), 27-37.

Haq, A., Brown, J., Moltchanova, E., & Al-Omari, A. (2015). Improved exponentially weighted moving average control charts for monitoring process mean and dispersion. *Quality and Reliability Engineering International, 31*(2), 217-237.

Moraes, D. A. O., Oliveira, F. L. P., Quinino, R. C., & Duczmal, L. H. (2014). Self-oriented control charts for efficient monitoring of mean vectors. *Computers & Industrial Engineering, 75,* 102-115.

Page, E. S. (1954). Continuous inspection schemes. Biometrics, 41, 100-115.

Roberts, S. W. (1959). Control chart tests based on geometric moving averages. *Technometrics, 42*(1), 97-102.

Teoh, W. L., Khoo, M. B. C., Castagliola, P., & Chakraboti, S. (2014). Optimal design of the double sampling chart with estimated parameters based on median run length. C*omputers & Industrial Engineering, 67,* 104-115.

Wild, C. J., & Seber, G. A. (2000). *Chance encounters: A first course in data analysis and inference*. New York: John Wiley & Sons.

Wu, Z., & Spedding, T. A. (2000). A synthetic control chart for detecting small shifts in the process mean. *Journal of Quality Technology, 32*(1), 32-38.

Pertanika J. Sci. & Technol. 24 (1): 191 - 203 (2016)

PERTANIKA JOURNALS

SCIENCE & TECHNOLOGY

Journal homepage: http://www.pertanika.upm.edu.my/

Analysis of Bit-Plane Images by using Principal Component on Face and Palmprint Database

Therry Z. Lee* **and David B. L. Bong**

Faculty of Engineering, Universiti Malaysia Sarawak, 94300, Kota Samarahan, Sarawak, Malaysia

ABSTRACT

The bit-plane feature extraction approach has lately been introduced for face and palm-print recognition. This approach decomposes an 8-bit grey level image into eight groups of bit layers. The assumption of this approach is that the highest order of a bit-plane decomposition, which has the most significant bits of all pixels, contains the most biometric features. Nonetheless, most research has identified bit-plane images illustratively. Hence, in order to endorse the assumption, we performed an analysis on face and palm-print images to identify the bit-plane that contributes most significantly to the recognition performance. Analysis was done based on Principal Component Analysis (PCA). The first principal component was applied as it is defined for the largest possible variance of the data. Next, Euclidean distance was calculated for matching performance. It was observed that bit-plane 6 and 7 contributed significantly to recognition performance.

Keywords: Bit-plane, Principal Component Analysis, face recognition, palm-print recognition

INTRODUCTION

Nowadays, biometric technologies are vital for personal authentication. This technology is able to provide security and privacy for identification because of the unique physical attribute that only an individual can present. Generally, biometrics such as face, finger, voice, iris, eye and palm-print are widely applied. There are two modes of the biometric system i.e. verification and identification, depending on the application (Matyáš & Říha, 2002). Verification is where the identity of an individual is verified as who he claims to be. On the other hand, identification is where the system will identify the unknown person. In order to verify or identify a biometric, significant information has to be extracted. In this relation, feature extraction is very crucial throughout the process of biometric recognition because it is where the distinct interest and significant characteristic of an individual are captured.

Many algorithms have been proposed for feature extraction techniques. In general, there are four basic approaches: geometry, colour

Article history:
Received: 12 March 2015
Accepted: 5 October 2015

E-mail addresses:
therry0608@hotmail.com (Therry Z. Lee),
bbldavid@unimas.my (David B. L. Bong)
*Corresponding author

ISSN: 0128-7680

segmentation, appearance and template-based techniques. One example of the geometry-based method is the Gabor wavelets transform approach (Lee, 1996; Lee & Wang, 1999; Lim *et al*., 2009; Bereta *et al*., 2013; Kong *et al*., 2003; Slavkovic *et al*., 2013; Shahamat & Pouyan, 2014) which is applied in face, palm-print and fingerprint recognition. In addition, the edge detection approach is also used on fingerprint and palm-print recognition (Bong *et al*., 2010). Colour-based feature extraction is mostly applied to face recognition where skin region or certain arrays of colour pixels is obtained (Seow *et al*., 2003; Singh *et al*., 2003). It is found to be used on palm-print in Sang, Ma and Huang (2013), where the authors utilised skin-colour thresholding to extract features and also on eye detection (Bong & Lim, 2007; Bong & Lim, 2009). Other than that, Bhoi and Mohanty (2010) used template-based feature extraction by detecting the eyes. Another approach that is commonly applied is the appearance-based technique that is mostly on Principal Component Analysis (PCA) and Independent Component Analysis (ICA). This method has been a favourite of researchers for either face, palm-print or fingerprint detection (Lu *et al*., 2003; Eleyan & Demirel, 2005; Lin, 2010; Ebied, 2012; Mohammadi *et al*., 2014).

In recent years, a new feature extraction technique based on bit-plane has been proposed. The bit-plane approach was recently introduced by several researchers. Most works have been applied for face and palm-print recognition (Lee & Bong, 2013). In (Hoque & Fairhurst, 2000), bit-plane decomposition was applied in face recognition based on the moving window method where every bit level was evaluated for its performance in recognition. This research was further evaluated in Li and Wang (2009) using the same method but emphasised the improvement of diversity of component classifiers, where several mathematical rules were applied for performance evaluation. Also in some works (Ting *et al*., 2008; Bong *et al*., 2009; Ting *et al*., 2013), the authors performed face recognition on single and combined bit planes using feed-forward neural network. Research was also carried out in the work by Ramlan *et al*. (2012) using neural network for thumbprint recognition. The bit-plane extraction approach in face recognition was also proposed by applying PCA (Wang *et al*., 2006; Srinivas *et al*., 2013). In these works, after the bit-plane decomposition, bit-planes were selected visually.

Most of the bit-plane-based biometric recognitions assume that the highest order of a bit-plane decomposition contains the most biometric features. This assumption is supported visually by looking at the decomposed bit planes. Generally, the higher order bit-planes contain binary images that have visual resemblance to the original grey images, whereas the lower order bit-planes do not seem to provide this resemblance. Thus far, not much research has been done to scientifically analyse bit-planes to validate the assumption.

Furthermore, PCA is an established technique for its multivariate analysis. It is used to find patterns in data of high dimension, while expressing data by highlighting their differences and similarities. Other than that, it is commonly applied in pattern recognition such as face recognition and also used for image compression (Jolliffe, 1986). PCA can effectively reduce the image's dimensionality, yet conserve the key identifying information (Turk & Pentland, 1991). It is done by obtaining the principal components that retain the highest variance of the original variables. Since the variance of the principal component indicates the amount of expressed information, bit-plane is analysed with PCA to observe the amount of information in each bit-plane. This is to justify the contribution of each bit-plane in recognition. Hence,

in this paper, we used PCA as a model to validate this assumption for face and palm-print recognition. This is different from the technique used by Srinivas *et al*. (2013) and Wang *et al*. (2006), who mainly focused on applying fusion on bit-planes with PCA for feature extraction to enhance recognition rate.

The paper is organised as follows: In Section 2, the idea of bit-plane decomposition is introduced. This is followed by a brief presentation of the PCA algorithm and a description of the database. The experimental results on Yale (Georghiades, 1997), ORL (AT&T Laboratories Cambridge, 1994) and PolyU Palm-print Databases (The Hong Kong Polytechnic University, n.d.) are presented in Section 3. Finally, Section 4 presents the conclusion.

MATERIALS AND METHODS

Bit-Plane Extraction

Schwartz and Barker (1966) presented an idea of decomposing an image from grey-scale to a collection of binary images, and called this the bit-plane decomposition technique. It is based on the conversion of decimal to binary for each pixel. An eight-bit grey level image has pixel values ranging from 0 to 225. Therefore, it can be decomposed into eight layers or bit-planes, whereby the first bit-plane (bit-plane 0) consists of the least significant bits while the last bit-plane (bit-plane 7) comprises the most significant bits.

The general derivation for bit-plane feature extraction is summarised as:

$$f(x,y)=\begin{bmatrix} f(0,0) & f(0,1) & \dots & f(0,N-1) \\ f(1,0) & f(1,1) & \dots & f(1,N-1) \\ \vdots & \vdots & \dots & \vdots \\ f(M-1,0) & f(M-1,1) & \dots & f(M-1,N-1) \end{bmatrix} \quad [1]$$

To convert to binary, the original image, *f(x,y)* , has to be divided by 2 in order to obtain the remainder, R, which represents the feature of a specific bit-plane. Mathematically, it can be written as in Equation [2]:

$$f_{bpi}(x,y) = \begin{bmatrix} R\left(\frac{floor\left(\frac{f(0,0)}{2}\right)}{2}\right) & R\left(\frac{floor\left(\frac{f(0,1)}{2}\right)}{2}\right) & \cdots & R\left(\frac{floor\left(\frac{f(0,N-1)}{2}\right)}{2}\right) \\ R\left(\frac{floor\left(\frac{f(1,0)}{2}\right)}{2}\right) & R\left(\frac{floor\left(\frac{f(1,1)}{2}\right)}{2}\right) & \cdots & R\left(\frac{floor\left(\frac{f(1,N-1)}{2}\right)}{2}\right) \\ \vdots & \vdots & \cdots & \vdots \\ R\left(\frac{floor\left(\frac{f(M-1,0)}{2}\right)}{2}\right) & R\left(\frac{floor\left(\frac{f(M-1,1)}{2}\right)}{2}\right) & \cdots & R\left(\frac{floor\left(\frac{f(M-1,N-1)}{2}\right)}{2}\right) \end{bmatrix}$$

$$= R\left[\frac{1}{2}floor\left(\frac{1}{2^i}[f(x,y)]\right)\right] \quad ; \text{i=0, 1, 2…7} \quad [2]$$

where *f(x,y)* is the original image, $f_{bp}(x,y)$ is the bit-plane information, *R* is the remainder, and *floor(x)* rounds the elements to *x* nearest integers less than or equal to *x* (Ting *et al*., 2008; Bong *et al*., 2009; Ting *et al*., 2013).

Fig.1 and Fig.2 show the decomposition of grey images into bit-planes for face and palm-print images. The first row represents the original image, while the second row shows the image of each bit-plane without image enhancement, starting from the least significant plane to most significant plane, and from left to right. From the visual observation in Fig.1, certain bit-planes are shown to have a distinguished face image. The visible face images indicate that the majority of the significant information is present in bit-planes 5, 6 and 7. In contrast, face images that cannot be distinguished indicate the minority of the significant information is present at bit-planes 0, 1, 2, 3 and 4. As for the palm-print image, the palm feature is also observable visually, especially the last bit-plane presented in Fig.2.

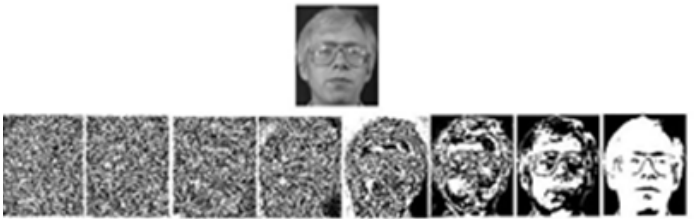

Fig.1: Illustration of an original face image and its 8 bit-planes.

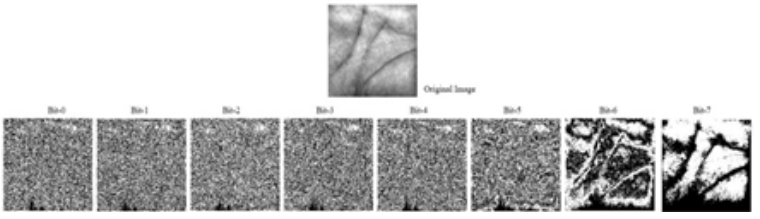

Fig.2: Illustration of a palm-print image and its 8 bit-plane.

Principal Component Analysis

The main idea of PCA is significant information of the data can be represented well by utilising only the first few principal components. The principal components are the new set of uncorrelated variables transformed from the original interrelated variables of the original image. In each principal component, the amount of information is presented as the variance. The 'first principal component' has the highest variance, which also means it consists of most information of an image (Jolliffe, 1986). In this work, first principal components for each bit-plane were obtained so as to compare their eigen values. The latter part was proceeded with recognition by using Euclidean distance. The performance shown thereby indicates the amount of information contributed by each bit-plane.

In PCA, the basic algorithm is that, firstl, a digital image can be represented as a matrix with the size of *x* row and *y* column. Let an image be denoted as *f(x,y)* or in short, as *f.* The training set is $f_1, f_2, f_3, \ldots f_M$ where M is the total number of images. Before computing the covariance matrix or eigen vectors, the average of the image set has to be determined. It is defined by:

$$\phi = \frac{1}{M}\sum_{n=1}^{M} f_n \qquad [3]$$

The mean-centred image, which is the difference between each image in the dataset from the average image, is:

$$w_i = f_i - \phi \qquad [4]$$

In order to obtain the largest possible principal component, the *k*th vector, uk, is selected on condition that Equation [5] fulfils the maximum of orthonormality constraint of Equation [6].

$$\tau_k = \frac{1}{M}\sum_{n=1}^{M} (u_k^T w_n)^2 \qquad [5]$$

$$u_l^T u_k = \delta_{lk} = \begin{cases} 1, if(l=k) \\ 0, otherwise \end{cases} \qquad [6]$$

This results as the vectors u_k, which are the eigen vector, and the scalars τk, which are the eigen values of the covariance matrix, and is defined by:

$$C = \frac{1}{M}\sum_{n=1}^{M} w_n^T w_n = AA^T \qquad [7]$$

where A=[w_1 w_2 w_3…. w_M].

Each image in the training set is now represented as an eigen vector. This means the number of eigen vectors produced is equal to the number of training images presented. Next, the eigen vectors are sorted from high to low corresponding to the eigen values. Let *M'* be the selected number of eigen vectors to be used. The *M'* numbers of the largest eigen vectors are then selected as the components of the eigen feature. After that, each of the mean-centred images is projected into an eigen space by using:

$$w_k = u_k^T (f - \phi)\,;\ k=1,2..M'; \qquad [8]$$

Hence, all the training images are now transferred into the eigen space. For recognition purposes, the equivalent process is applied to the testing images. The testing images are to be mean-centred first before being projected into the same eigen space as training images. This enables comparison between the projected testing images with the projected training images in the eigen space. The comparison is done using a Euclidean distance classifier as explained earlier. The matching images would be defined by the closest distance between the training and testing image.

DATABASES

The evaluation was performed using two categories of database: face and palm-print. The specifications of each database are presented below.

Face Databases

For face, Yale and ORL (Olivetti Research Laboratory) face databases were applied. Yale database consists of a total of 165 images from 15 subjects; each subject has 11 images including altered expressions and illumination conditions. The resolution for each image is 100x100pixels (Georghiades, 1997).

The ORL database consists of 400 images from 40 individual subjects; 10 images for each individual in varied poses. In the database, every subject is in an upright, frontal position with facial expression; there are some variations in lighting, facial details etc. The resolution of each image is 112×92 pixels, with 256 grey levels per pixel (AT&T Laboratories Cambridge, 1994).

Palmprint Database

PolyU Palm-print Database was also used for this research. It contains 7,752 greyscale images corresponding to 386 different palms in bitmap format. Approximately 20 samples were collected in two sessions for each palm. The number of the samples is uneven for each set. Around 10 of those samples were captured in the first session and the second session correspondingly. The average interval between the first and the second collections was two months. The original image size was 384 x 284 pixels. In this research, in order to extract the centre of the palm as the region of interest, the images were cropped manually to189 x 182pixels. The samples from the first session were used. Also, in the experiment of the current study, left palm and right palm were treated as two different databases. Some sets of data were filtered and eliminated due to insufficient number of samples or distorted images. Therefore, a total of 3,840 images from 192 subjects were used, with 10 sample images each from the left and right palms (The Hong Kong Polytechnic University, n.d.).

Recognition and Performance Metric

After applying PCA, analysis was continued by evaluating the recognition performance of the bit-planes. Firstly, in order to cluster the features in eigen space, Euclidean distance was applied. Classification was done by measuring the distance between the projection vectors of training images with projection vectors of testing images in the eigen space. The smaller the distance between the images, the more the similarity increased. The shortest distance thereby indicated the subject to be recognised. The mathematical expression for Euclidean distance d_k is:

$$d_k = \sum_{i=1}^{M} \frac{(f(i) - f_k(i))^2}{(s_k)^2} \qquad [9]$$

where f is the feature vector of testing set, f_k and s_k is the kth feature vector and its standard deviation and M denotes the number of eigen vectors.

Next, to observe the performance of recognition for bit-plane, accuracy was computed. Accuracy indicates the percentage of correctly accepted enrolment by the system, which is defined by:

$$Accuracy = \left(\frac{total\ correctly\ classified\ data}{total\ testing\ data}\right) \text{ x100} \qquad [10]$$

RESULTS AND DISCUSSION

In our experiments, the data were categorised into training set and testing set. The training set consisted of the first five images of each subject. The testing set, on the other hand, was obtained from the remaining images of database.

Two experiments were carried out. Firstly, the analysis was done by extracting the eigen values from the first principal component of each bit-plane to observe the performance of each bit-plane in all the databases. The assumption of bit-planes is that the highest order of bit-plane decomposition contains the most biometric features while the lower order of the bit-plane consists of less information regarding the biometric. Hence, the first experiment was to validate this assumption on face and palm-print; this is further explained below. Furthermore, in order to verify the assumption of bit-planes, analysis of eigenspace for recognition was done.

Principal Components

For our analysis, the first principal components of the bit-planes from all the databases were extracted for comparison. This is because the first principal component is known for the highest variance of the original image. In other words, from the first principal component, the contributed amount of information in each bit-plane can be observed.

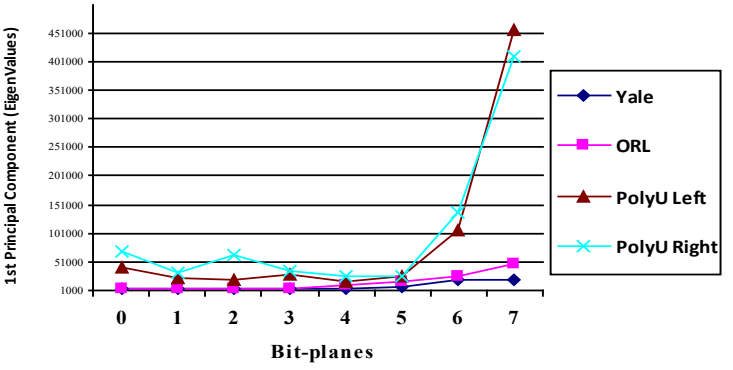

Fig.3: Comparison of eigenvalues of the first principal component for all databases.

Fig.3 shows the comparison of eigen values of the first principal component for all databases. Face and palm-print databases clearly show that the variance has significantly increased starting from bit-plane 5 in the first principal component, and bit-planes 6 and 7 have the most variances compared to others.

Since the first principal component accounts for the largest proportion of the total variance, it also represents the most information of data (Jolliffe, 1986). Hence, although Fig.3 shows stable eigen values from bit-plane 0 to bit-plane 4, the information it provides is insufficient to present data as shown in Fig.1 and Fig.2, where no visible face or palm images can be observed. On the other hand, bit-plane 5 to 7 with increasing variance, show a more discernable face and palm figure as illustrated in Fig.1 and Fig.2. Therefore, the characteristic of the first principal component in each bit-plane corresponds with the bit-plane presented through visualisation where more information is observed at bit-planes 6 and 7 that can contribute to recognition. In order to further verify the contribution of bit-planes, recognition was then continued using the Euclidean distance method.

Face and Palm-Print Recognitions

The bit-planes were then trained using the selected number of principal components. They were then tested for recognition using Euclidean distance. Here, the optimum number of the principal component was selected using the trial-and-error method. To evaluate the recognition performance, Euclidean distance was applied using Equation [9].

Face Database

The experiment was done on two face databases. For both databases, the first five images for each subject were selected in the training set. Therefore, the number of the training images for Yale was 75 (=15x5). The remaining images were then used for the testing set. This gave a total of 90 (=15x6) images for the testing set.

Through the trial and test with 12 eigen vectors, the matching performance showed higher rates for the last two most significant bit (MSB) bit-planes. Fig.4 shows that the last two MSB bit-planes can achieve approximately 86% recognition for bit-plane 6 and 81% for bit-plane 7. The remaining bit-planes showed recognition performance below 50%. It was observed that the lower order bit-planes required more principal components to achieve higher performance rate. Consequently, it was shown that the lower order bit-planes contained less variance than the higher order bit-planes, and thus, contributed less information for the recognition.

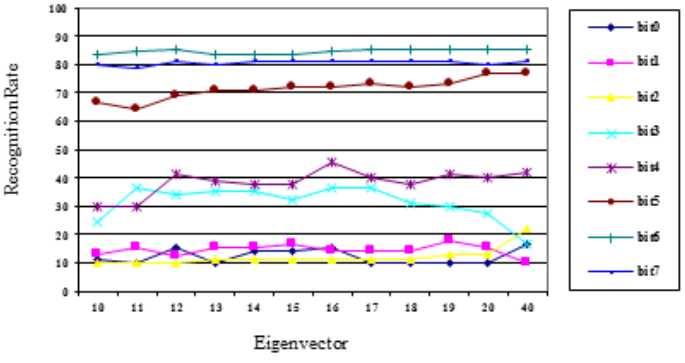

Fig.4: Recognition rate on Yale database.

As for ORL, 35 eigen vectors were selected as the optimum threshold in this study since the bit-planes could achieve 80% of the performance. The results presented in Fig.5 showed that only bit-planes 6 and 7 achieved the matching rate more than 80% while the rest showed higher error rates.

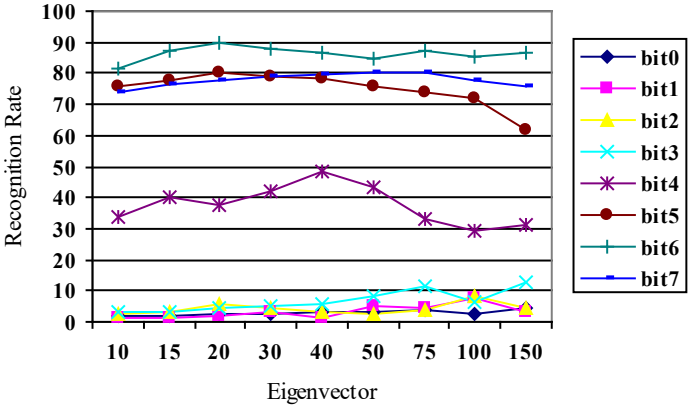

Fig.5: Recognition rate on ORL database.

Palm-print Database

The PolyU palm-print database, which used left and right palms, showed two different orientations, and were separately divided as two distinct databases. For each side of the palm, there were 192 samples with 10 images from each subject. In the experiment, the first five images were used per subject for training while the remaining images were used for testing. This also means that the number of training and testing samples was 960 (=192x5) each.

For the left palms, the experimental results clearly showed that the last two MSB bit-planes provided higher recognition rates than the other bit levels (see Fig.6). Similar to the face database, lower-order bit-planes need more principal components so as to increase the recognition rate. It is clearly shown in Fig.6 and Fig.7, especially for bit-plane 5, that the matching rate increased as more eigen vectors (principal components) were presented. This shows that the lower-order bit-planes consisted of lower variance as compared to the higher-order bit-planes. Hence, less information of the data was presented in the lower-order bit-planes to assist the recognition performance.

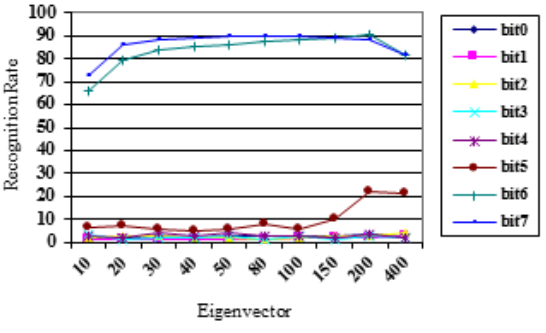

Fig.6: Recognition rate on PolyU left palm database.

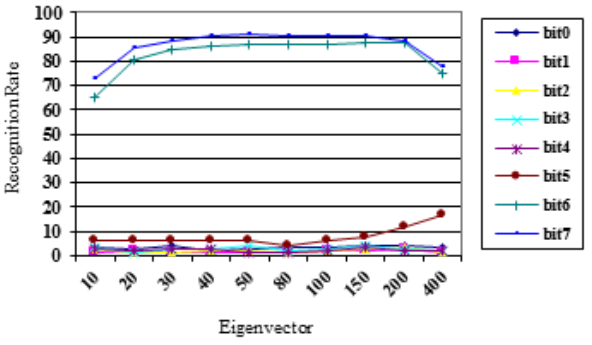

Fig.7: Recognition rate on PolyU right palm database.

BENEFITS OF STUDY

The analyses carried out in this study confirmed that the last two bit-planes, which were bit-plane 6 and bit-plane 7, were able to provide adequate information for feature extraction. No analysis of bit-planes from the perspective of PCA has been done before. PCA as an established technique is thereby eligible to confirm and prove the contribution of each bit-plane for biometric recognition. This analysis also concludes that bit-plane is able to contribute sufficient information for feature extraction in biometric recognition. Furthermore, it is able to overcome database storage limitation and reduce computation time because only the last two bit-planes are needed for biometric recognition.

CONCLUSION

In this paper, the performance of each bit-plane was justified using the PCA approach so as to verify its usefulness in recognition. Experiment was done on two types of biometric: face and palm-print. They were applied on the first principal component with the highest variance, which also showed the amount of information presented. It resulted in the highest variance shown by bit-plane 6 and 7. All the databases were then proceeded for recognition and showed a low matching rate for lower-order bit-planes (0-5), while the last two MSB bit-planes (6 and 7) provided rates above 80%. These verified that more information can be contributed for recognition at bit-planes 6 and 7. In conclusion, for face and palm-print recognition, the bit-plane extraction approach works effectively, as proven by above 80% for face and 90% for palm-print. This further validates the application of bit-planes for biometric recognition.

ACKNOWLEDGEMENTS

The authors would like to acknowledge the Ministry of Education, Malaysia for the provision of research grant FRGS/03(03)/771/2010(52) and the Faculty of Engineering, Universiti Malaysia Sarawak for the provision of research facilities.

REFERENCES

AT&T Laboratories Cambridge. (1994). *The database of faces, formerly ORL face database.* Retrieved from www.cl.cam.ac.uk/research/dtg/attarchive/facedatabase.html

Bereta, M., Pedrycz, W., & Reformat, M. (2013). Local descriptors and similarity measures for frontal face recognition: A comparative analysis. J*ournal of Visual Communication and Image Representation, 24*(8), 1213-1231.

Bhoi, N., & Mohanty, M. N. (2010). Template matching based eye detection in facial image. *International Journal of Computer Applications, 12*(5), 15-18.

Bong, D. B. L., & Lim, K. H. (2007). Non-intrusive eye gaze direction tracking using color segmentation and Hough transform. *2007 International Symposium on Communications and Information Technologies*, pp.602-607.

Bong, D. B. L., & Lim, K. H. (2009). Application of fixed-radius hough transform in eye detection. *International Journal of Intelligent Information Technology Application, 2*(3), 121-127.

Bong, D. B. L., Ting, K. C., & Wang, Y. C. (2009). Novel Face recognition approach using bit-level information and dummy blank images in feedforward neural network. *Applications of Soft Computing*, pp. 483-490. Springer.

Bong, D. B. L., Tingang, R. N., & Joseph, A. (2010). Palm print verification system. *Proc. of the World Congress on Engineering*, pp.667-670.

Ebied, H. M. (2012). Feature extraction using PCA and Kernel-PCA for face recognition. *2012 8th International Conference on Informatics and Systems (INFOS),* MM72-MM77.

Eleyan, A., & Demirel, H. (2005). Face recognition system based on PCA and feedforward neural networks. In *Computational Intelligence and Bioinspired Systems* (pp. 935-942). Springer Berlin Heidelberg.

Georghiades, A. (1997). *Yale Face database*. Retrieved from http://cvc.yale.edu/projects/yalefaces/yalefaces.html

Hoque, M. S., & Fairhurst, M. C. (2000). Face recognition using the moving window classifier. BMVC,*British Machine Vision Conference*, pp.1-10.

Jolliffe, I. T. (1986). *Principal component analysis*. Springer Verlag.

Kong, W. K., Zhang, D., & Li, W. (2003). Palmprint feature extraction using 2-D Gabor filters. *Pattern Recognition, 36*(10), 2339-2347.

Lee, C.-J., & Wang, S.-D. (1999). Fingerprint feature extraction using Gabor filters. *Electronics Letters, 35*(4), 288-290.

Lee, T. S. (1996). Image Representation using 2D Gabor wavelets. IEEE Trans. *Pattern Analysis & Machine Intelligence, 18*(10), 959-971.

Lee, T. Z., & Bong, D. B. L. (2013). Palmprint Recognition based on bit-plane extraction. *12th WSEAS International Conference on Applied Computer and Applied Computational Science*, 182-186.

Li, K., & Wang, L. (2009). Ensemble methods of face recognition based on bit-plane decomposition. *International Conference on Computational Intelligence and Natural Computing, CINC '09*, 1, 194-197.

Lim, J., Kim, Y., & Paik, J. (2009). Comparative analysis of wavelet-based scale-invariant feature extraction using different wavelet bases. *International Journal of Signal Processing, Image Processing and Pattern Recognition, 2*(4), 297-303.

Lin, L. (2010). Palmprint identification using PCA algorithm and hierarchical neural network. In *Life System Modeling and Intelligent Computing* (pp. 618-625). Springer Berlin Heidelberg.

Lu, G., Zhang, D., & Wang, K. (2003). Palmprint recognition using eigenpalms features. *Pattern Recognition Letters, 24*(9-10), 1463-1467.

Matyáš, V., & Říha, Z. (2002). Biometric authentication—security and usability. In *Advanced Communications and Multimedia Security* (pp. 227-239). Springer US.

Mohammadi, M. R., Fatemizadeh, E., & Mahoor, M. H. (2014). PCA-based dictionary building for accurate facial expression recognition via sparse representation. *Journal of Visual Communication and Image Representation, 25*(5), 1082-1092.

Ramlan, M. R., Bong, D. B. L., & Lee, T. Z. (2012). Analysis of Thumbprint recognition in different bit levels. *International Conference on Advanced Computer Science Applications and Technologies (ACSAT)* pp.192-196.

Sang, H., Ma, Y., & Huang, J. (2013). Robust palmprint recognition base on touch-less color palmprint images acquired. *Journal of Signal & Information Processing, 4*(2), 134-139.

Schwartz, J. W., & Barker, R. C. (1966). Bit-plane encoding: A technique for source encoding. IEEE *Transactions on Aerospace and Electronic Systems, AES-2*(4), 385-392.

Seow, M.-J., Valaparla, D., & Asari, V. K. (2003). Neural network based skin color model for face detection. *Proceedings of 32nd Applied Imagery Pattern Recognition Workshop,* pp.141-145.

Shahamat, H., & Pouyan, A. A. (2014). Face recognition under large illumination variations using homomorphic filtering in spatial domain. *Journal of Visual Communication and Image Representation, 25*(5), 970-977.

Singh, S. K., Chauhan, D. S., Vatsa, M., & Singh, R. (2003). A robust skin color based face detection algorithm. *Tamkang Journal of Science and Engineering, 6*(4), 227-234.

Slavkovic, M., Reljin, B., Gavrovska, A., & Milivojevic, M. (2013, July). Face recognition using Gabor filters, PCA and neural networks. In *Systems, Signals and Image Processing (IWSSIP), 2013 20th International Conference* (pp. 35-38). IEEE.

Srinivas, T., Mohan, P. S., Shankar, R. S., Reddy, C. S., & Naganjaneyulu, P. V. (2013, January). Face Recognition Using PCA and Bit-Plane Slicing. In *Proceedings of the Third International Conference on Trends in Information, Telecommunication and Computing* (pp. 515-523). Springer New York.

The Hong Kong Polytechnic University. (n.d.). *PolyU palmprint database*. Retrieved from http://www.comp.polyu.edu.hk/biometrics

Ting, K. C., Bong, D. B. L., & Wang, Y. C. (2008). Performance analysis of single and combined bit-planes feature extraction for recognition in face expression database. *International Conference on Computer and Communication Engineering, (ICCCE 2008)*, 792-795.

Ting, K. C., Tan, J. Y. B., Lee, T. Z., & Bong, D. B. L. (2013). Face recognition by neural network using bit-planes extracted from an image. *Journal of Information and Computational Science, 10*(16), 5253-5261.

Turk, M., & Pentland, A. (1991). Eigenfaces for recognition. *Journal of Cognitive Neuroscience, 3*(1), 71-86.

Wang, H., Leng, Y., Wang, Z., & Wu, X. (2006, January). Generalized PCA face recognition by image correction and bit feature fusion. In *Neural Information Processing* (pp. 227-235). Springer Berlin Heidelberg.

Pertanika J. Sci. & Technol. 24 (1): 205 - 211 (2016)

SCIENCE & TECHNOLOGY

Journal homepage: http://www.pertanika.upm.edu.my/

Classification Using the General Bayesian Network

Sau Loong Ang*, Hong Choon Ong and Heng Chin Low

School of Mathematical Sciences, Universiti Sains Malaysia, 11800 USM, Pulau Pinang, Malaysia

ABSTRACT

Naive Bayes (NB) is a simple but powerful tool for data classification. It is widely used in classification due to the simplicity of its structure and its capability to produce surprisingly good results for classification. However, the independence assumption among the features is not practical in real datasets. Attempts have been made to improve the Naive Bayes by introducing links or dependent relationships between the features such as the Tree Augmented Naive Bayes (TAN). In this study, we show the accuracy of a General Bayesian Network (GBN) used with the Hill-Climbing learning method, which does not impose any restrictions on the structure and better represents the dataset. We also show that it gives equivalent performances or even outperforms Naive Bayes and TAN in most of the data classification.

Keywords: Naive Bayes, classification, Tree Augmented Naive Bayes, General Bayesian Network

INTRODUCTION

Classification is the organisation of patterns that require the construction of a classifier, which is a function that does grouping based on shared attributes (Madden, 2009; Ahmed *et al*., 2014). Classification problems can be found in various fields ranging from medical, information technology to chemistry (Mishra *et al*., 2011; Chung *et al*., 2013; Ahmed *et al*., 2014). There are many approaches to solve various classification problems, including decision trees, decision lists, neural networks and decision graphs (Friedman *et al*., 1997). However, the focus here is on the improvement of Naive Bayes and TAN classification to achieve accuracy and reliability of structure.

The Bayesian Network has become one of the most effective classifiers (Elgammal *et al*., 2003; Lerner, 2004; Madden, 2009). The Bayesian Network is a directed graphical model that expresses the joint distribution between multiple interacting nodes of interest based on their probabilistic relationship (Pearl, 1998; Neopolitan, 2004). By applying Markov Chain-Rule, the joint probability distribution of the nodes in Bayesian Network can be decomposed as shown in Equation [1] (Pham & Ruz, 2009).

Article history:
Received: 3 June 2015
Accepted: 10 July 2015

E-mail addresses:
dellphin1223@gmail.com (Sau Loong Ang),
hcong@.usm.my (Hong Choon Ong),
hclow@.usm.my (Heng Chin Low)
*Corresponding author

ISSN: 0128-7680

$$P_B(X_1,\ldots,X_n) = \prod_{i=1}^{n} P(X_i \mid Pa_i) \qquad [1]$$

where $P_B(X_1,\ldots,X_n)$ is the joint probability distribution over a set of n random variables $X = \{X_1,\ldots,X_n\}$ and Pa_i is the parent of X_i in a Bayesian Network. With the representation of joint distributions as a product of conditional distributions, the dependency relationship between the nodes in Bayesian Network can be identified (Pham & Ruz, 2009).

In practice, we can compute the conditional probability of one node, given the values assigned to other nodes (Cheng and Greiner, 2001). Therefore, a Bayesian Network can be used as a classifier that gives the posterior probability distribution of the class node given the conditional probability of other attributes from the training data (Friedman *et al*., 1997; Cheng & Greiner, 2001). The classification is performed based on the highest posterior probability distribution that we obtain in the class node. Therefore, Bayesian Networks are used in classification as it allows a fast and intuitive understanding among the interactive nodes (Friedman *et al*., 1997; Madden, 2009).

BAYESIAN NETWORKS CLASSIFIERS

Naive Bayes

A Naive Bayes Network is a simple probabilistic model to classify data into specific classes based on different data features (Friedman *et al*., 1997; Ong, 2011). Naive Bayes has become a core method used in classification for a variety of data ranging from medical, computer network and text recognition due to its simplicity, effectiveness and capability in capturing the data reasoning in a graphical model as shown in Fig.1 (Abraham *et al*., 2009; Zhan & Gao, 2011; Mukherjee & Sharmaa, 2012). The arcs are linked to the nodes based on the conditional probability of class C given the attributes ($X_1,\ldots,X_n$).

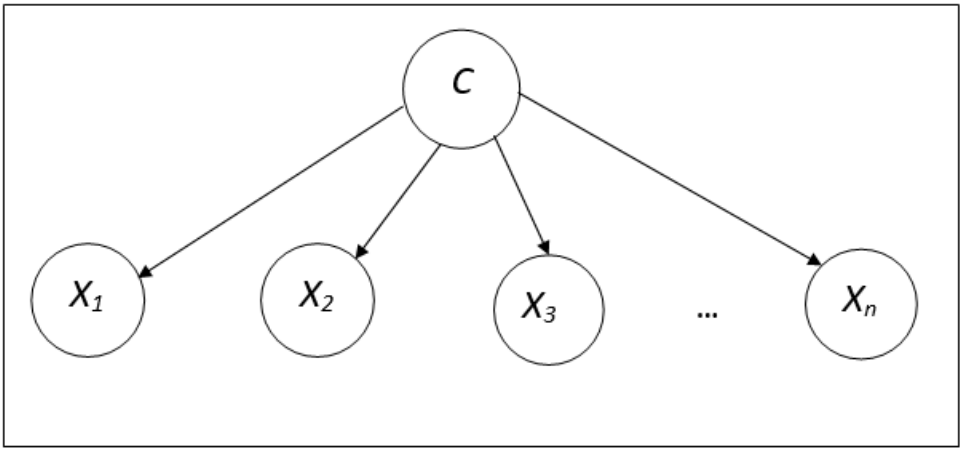

Fig.1: Graphical model of Naive Bayes.

In Naive Bayes, the classifier is set up by the assumption where the relationships between the variables ($X_1, X_2,...,X_n$) are independent given the class name C (Friedman *et al*., 1997). Under the independence assumption, the cost of the joint probability factorisation is reduced to the simplest form as shown in Equation [2] (Liew & Ji, 2009).

$$P(C \mid X) \ \alpha \ P(C)\prod_{i=1}^{n} p(X_i \mid Pa_i) \qquad [2]$$

where $p(X_i \mid Pa_i)$ is the probability of X_i given its parent Pa_i . In general, Bayesian Networks classification is based on a process to obtain the maximum value of the posterior probability of $P(C \mid X)$ as given in Equation [3].

$$P(C \mid X) = \arg_{\max} KP(C)\prod_{i=1}^{n} p(X_i \mid Pa_i) \qquad [3]$$

where K is a normalising constant.

Despite the high accuracy of classification and simplicity in data representation, Naive Bayes suffers from lack of sensitivity in showing the real relationship between the variables, which may not be totally independent (Friedman *et al*., 1997). Questions arise from researchers as to whether a modification in the strong independence assumptions can produce better results compared to Naive Bayes. One of the ways to fix the issue in the Naive Bayes is with added relationship as suggested by Ong (2011). The structure with added relationship is almost similar to Naive Bayes except for the condition where extra arcs are allowed between the variables. Extra arcs that link the dependent variables increase the validity of the graphical model in representing the data. This not only increases the reliability of the structure, but also contributes to higher accuracy of the classification as compared to Naive Bayes.

Tree Augmented Naive Bayes (TAN)

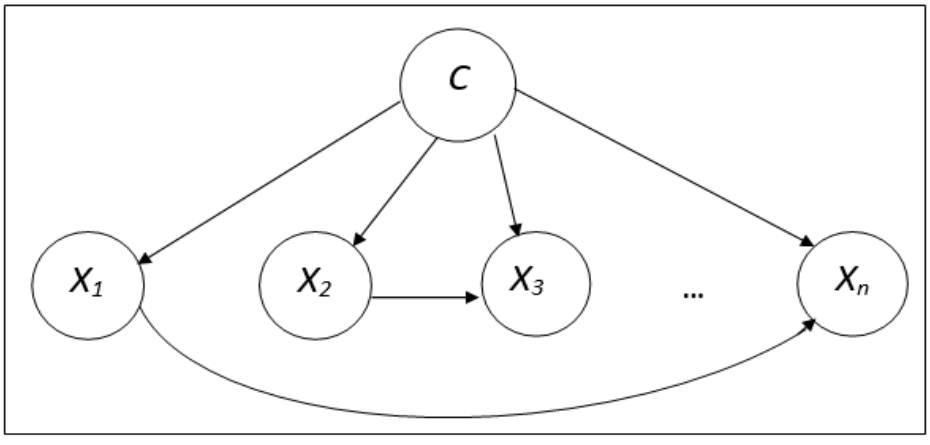

Fig.2: Graphical model of TAN.

Another prominent finding to enhance Naive Bayes is the Tree Augmented Naive Bayes (TAN) by Friedman *et al*. (1997). The structure of the Tree Augmented Naive Bayes is almost similar to the Naive Bayesian Network except for the condition where extra arcs are allowed between the variables to reduce the influence of the strong independence assumption that is made in Naive Bayes. Extra arcs that link the dependent variables increase the validity of the graphical model in representing the data as shown in Fig.2.

However, those models suffer from the aspect of reasoning and relationship between variables whereas in real datasets, the connections of the variables can be complicated and are not restricted. Even with good performance in classification, neither Naive Bayes nor TAN with added relationships is capable of capturing the topology of the Bayesian Network for classification.

General Bayesian Network in Classification

Contrary to the Naive Bayes and Tree Augmented Naive Bayes, the General Bayesian Network (GBN) offers more flexibility in forming the structure with a classifier. Firstly, there is no restriction in setting all the nodes $X_1, X_2,...,X_n$ to be the child of the parent, which is the class C. Secondly, the number of parents can be more than one. With the advantage of being flexible, the relationship between all nodes including the class nodes can be captured in the structure of GBN as shown in Fig.3. However, the searching space and the parameter learning can grow exponentially if the number of parents is not controlled. Thus, the number of parents is restricted to five in order to run the classification without overloading the Bayesian Network. We apply Hill Climbing, which is a score-based structural learning method to search for the structure of the GBN. Setting the initial structure to be random, Hill Climbing adds and deletes the arc until an optimum Bayes score is achieved (Hall *et al*., 2009). To estimate the conditional probability from the learnt structure, we use the Simple Estimator in Weka (Bouckaert, 2004). GBN is a better way to perform classification since having the unrestricted way to link the variables and the class, the structure learning tends to form a Bayesian Network, which is closer to the model required by expert knowledge.

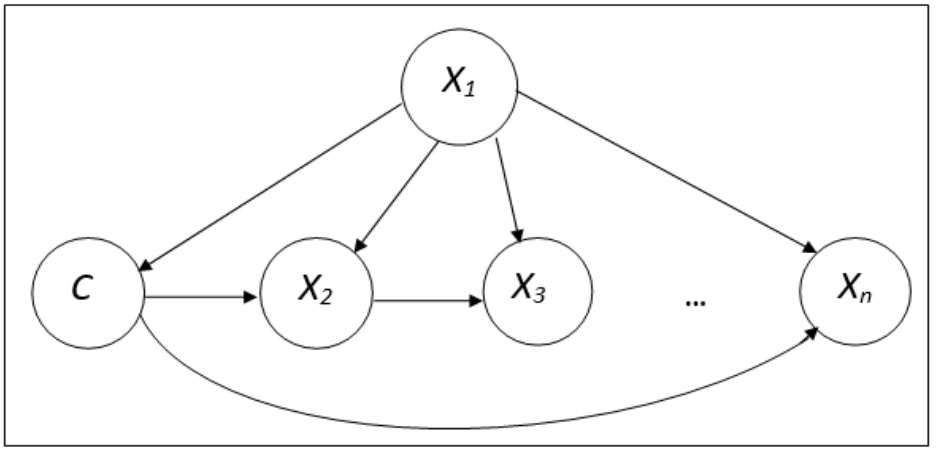

Fig.3: Graphical model of GBN.

This research is extended to various Bayesian Networks to meet different objectives based on the sizes of the dataset, accuracy, computational cost and level of simplicity in the structure (Cheng & Greiner, 1999).

RESULTS AND DISCUSSION

To measure the performance of GBN against the Naive Bayes and TAN, we used seven nominal datasets with the absence of missing values for comparative purposes. These nomimal datasets were taken from the UCI Machine Learning Repository (Lichman, 2013) and they were fed into the Naive Bayes, TAN and GBN for classification with ten-fold cross validation in WEKA software. We purposely selected seven datasets that differed in the size of the rows and number of attributes to determine the stability of Naive Bayes, TAN and GBN in classification. To show our findings, we tabulated the size of datasets, accuracy and time needed for classification for each classifier in Table 1.

TABLE 1: The Results of Naive Bayes, TAN and GBN

No.	Dataset	No. of Rows	No.of Attributes	Accuracy			Time		
				NB (%)	TAN (%)	GBN (%)	NB (s)	TAN (s)	GBN (s)
1	Vote	435	17	90.12	94.94	95.17	0	0.01	0.14
2	Breast Cancer	286	10	71.68	69.58	74.47	0	0.02	0.05
3	Fitting Contact Lenses	14	5	70.83	66.67	83.33	0	0	0
4	Chess	3196	37	87.89	92.05	94.39	0.02	0.32	2.37
5	Nurse	12960	9	90.36	94.26	94.71	0.05	0.13	0.47
6	Mushroom	8124	23	95.83	100	100	0.04	0.37	5.24
7	Balance	625	5	91.36	86.56	91.36	0.01	0	0.02

Table 1 shows the accuracy achieved by different models of the Bayesian networks, which are the Naive Bayes (NB), TAN and GBN. The time taken by those models in producing the outputs of classification is stated respectively based on the number of rows and the number attributes of the datasets.

In the first five datasets, GBN recorded the highest accuracy as compared to NB and TAN. For the remaining two datasets, which were Mushroom and Balance, GBN performed equal or better than the other two Bayesian Networks. GBN allows the nodes and the target class to form a structure without restriction as compared to NB and TAN. This gives an advantage in accuracy of the classification and also the representation in causal relationship. However, we can see that the time used to form the structure of the GBN was the longest among the Bayesian Network variants in Table 1 for all datasets except for the fitting contact lenses dataset. This is due to the structure of NB, TAN and GBN, which are almost the same for this study case. GBN consumes more time in giving results due to the complexity of the datasets especially for those

that have a higher number of rows or number of attributes or both. Even with the obstacles, the eligibility and usability of GBN were still better than Naive Bayes and TAN as the effect of time consumption was minimum. We summarised the advantages and disadvantages of the three Bayesian Networks in Table 2.

TABLE 2 : Brief Comparison of Naive Bayes, TAN and GBN

Type of Bayesian Classifier	Advantages	Disadvantages
NB	-Simple in structure -Moderately stable in classifying different sizes of training datasets and producing moderately good results of classification -Fastest in producing classification results	-Not practical to represent the causal relationships of the training datasets due to the fact that assumption of independence of features can be false.
TAN	-Better connectivity among the nodes -Better classification accuracy when the training datasets are relatively large	-Restricted structure, which limits the real representation of the training datasets -Not stable if the training datasets are small
GBN	-Less restriction set in forming the structure. Good graphical structure representation of datasets. -Stable and consistently good performance to classify large and small training datasets.	-Time consuming -Stability of classification reduced when handling small training datasets

CONCLUSION

In this study, GBN was proposed as a better option compared to Naive Bayes and TAN in terms of accuracy and the reasoning of node topology in its structure. The results showed GBN capability in dealing with different ranges of complexities of the datasets in providing high accuracy of classification consistently. The learning structure of the GBN can also be applied using different learning structure methods that can be constraint-based or score-based. A full structure of GBN with all the nodes linking to each other may also increase the chance of scoring better classification results.

REFERENCES

Abraham, R., Simha, J. B., & Iyengar, S. S. (2009). Effective discretization and hybrid feature selection using Naive Bayesian Classifier for medical data mining. *International Journal of Computational Intelligence Research, 5*(2), 116-129.

Ahmed, I., Guan, D., & Chung, T. C. (2014). SMS classification based on Naïve Bayes classifier and apriori algorithm frequent itemset. *International Journal of Machine Learning and Computing, 4*(2), 183-187.

Bouckaert, R. R. (2004). *Bayesian network classifiers in Weka*. Hamilton, New Zealand: University of Waikato.

Cheng, J., & Greiner, R. (1999). Comparing bayesian classifiers. *Proceedings of the Fifteenth Conference on Uncertainty in Artificial Intelligence*, pp.101-108.

Cheng, J., & Greiner, R. (2001). Learning Bayesian belief network classifiers: Algorithms and system. *AI '01 Proceedings of the 14th Biennial Conference of the Canadian Society on Computational Studies of Intelligence: Advances in Artificial Intelligence*, pp.141-151.

Chung, D., Lee, K. C., & Seong, S. C. (2013). General Bayesian network approach to health informatics prediction: Emphasis on performance comparison. *Procedia- Social and Behavioral Sciences, 81*, 465-468.

Elgammal, A., Duraiswami, R., & Davis, L. S. (2003). Efficient kernel density estimation using the Fast Gauss Transform with applications to color modeling and tracking. *IEEE Transactions on Pattern Analysis and Machine Intelligence, 25*(11), 1499-1504.

Friedman, N., Geiger, D., & Goldszmidt, M. (1997). Bayesian network classifiers, *Machine Learning, 29*(2-3), 131-163.

Hall, M., Frank, E., Holmes, G., Pfahringer, B., Reutemann, P., & Witten, I. H. (2009). The WEKA data mining software: An update. *SIGKDD Explorations, 11*(1), 10-18.

Lerner, B. (2004). Bayesian fluorescence in-situ hybridization signal classification. *Artificial Intelligence in Medicine, 30*(3), 301-316.

Lichman, M. (2013). *UCI machine learning repository*. Irvine, CA: University of California, School of Information and Computer Science. Retrieved from http://archive.ics.uci.edu/ml

Liew, W., & Ji, Q. (2009). Learning Bayesian network parameters under incomplete data with domain knowledge. *Pattern Recognition, 42*(11), 3046-3056.

Madden, M. G. (2009). On the classification performance of TAN and General Bayesian Networks. *Knowledge-Based Systems, 22*(7), 489-295.

Mishra, M., Potetz, B., & Huan, J. (2011). Bayesian classifiers for chemical toxicity prediction. *Proceedings of IEEE International Conference on Bioinformatics and Biomedicine,* pp.595-599.

Mukherjee, S., & Sharmaa, N. (2012). Intrusion detection using Naive Bayes Classifier with feature reduction. *Procedia Technology, 4*, 119-128.

Neapolitan, R. E. (2004). *Learning Bayesian networks.* Upper Saddle River, New Jersey, United States of America: Prentice Hall.

Ong, H. C. (2011). Improved classification in Bayesian networks using structural learning. *World Academy of Science, Engineering and Technology, 5*(3), 1073-1077.

Pearl, J. (1998). *Probabilistic reasoning in intelligent systems: Networks for plausible inference.* San Francisco: Morgan Kaufman.

Pham, D. T., & Ruz, G. A. (2009). Unsupervised training of Bayesian networks for data clustering. *Proceedings of the Royal Society A-Mathematical Physical and Engineering Sciences, 5*, 2927-2948.

Zhan, W., & Gao, F. (2011). An improvement to Naive Bayes for text classification. *Procedia Engineering, 15,* 2160-2164.

Pertanika J. Sci. & Technol. 24 (1): 213 - 224 (2016)

SCIENCE & TECHNOLOGY

Journal homepage: http://www.pertanika.upm.edu.my/

Potential Impacts of Climate Change on Precipitation and Temperature at Jor Dam Lake

Aida Tayebiyan[1*], Thamer Ahmad Mohammad[1], Abdul Halim Ghazali[1], M. A. Malek[2] and Syamsiah Mashohor[3]

[1]Department of Civil Engineering, Faculty of Engineering, Universiti Putra Malaysia, 43400 UPM Serdang, Selangor, Malaysia

[2]Institute of Energy, Policy and Research (IERRe), University Tenaga Nasional Malaysia, J alan IKRAM-UNITEN, 43000 Kajang, Selangor, Malaysia

[3]Department of Computer and Communication Systems Engineering, Faculty of Engineering, Universiti Putra Malaysia, 43400 UPM Serdang, Selangor, Malaysia

ABSTRACT

Rising global temperatures have threatened the operating conditions of Batang Padang hydropower reservoir system, Malaysia. It is therefore crucial to analyze how such changes in temperature and precipitation will affect water availability in the reservoir in the coming decades. Thus, to predict future climate data, including daily precipitation, and minimum and maximum temperature, a statistical weather generator (LARS-WG) is used as a downscaling model. Observed climate data (1984-2012) were employed to calibrate and validate the model, and to predict future climate data based on SRES A1B, A2, and B1 scenarios simulated by the General Circulation Model's (GCMs) outputs in 50 years. The results show that minimum and maximum temperatures will increase around 0.3-0.7 ºC. Moreover, it is expected that precipitation will be lower in most months. These parameters greatly influence water availability and elevation in the reservoir, which are key factors in hydropower generation potential. In the absence of a suitable strategy for the operation of the hydropower reservoir, which does not consider the effects of climate change, this research could help managers to modify their operation strategy and mitigate such effects.

Keywords: Climate change, precipitation, temperature, global climate models, weather generator, statistical downscaling, LARS-WG

Article history:
Received: 19 June 2015
Accepted: 9 September 2015

E-mail addresses:
ida_tayebiyan@yahoo.com (Aida Tayebiyan),
thamer@upm.edu.my (Thamer Ahmad Mohammad),
abdhalim@upm.edu.my (Abdul Halim Ghazali),
marlinda@uniten.edu.my (M. A. Malek),
syamsiah@upm.edu.my (Syamsiah Mashohor)
*Corresponding author

INTRODUCTION

Climate change is defined as a disruption in the statistical distribution of weather patterns that lasts for decades to millions of years. Climate change could involve a change in mean weather conditions or in the time and length of weather variation (i.e. more or fewer

ISSN: 0128-7680

extreme weather conditions such as floods and droughts). Since the industrial revolution, human activities, especially the burning of fossil fuels for energy production, heating processes and also agricultural activities, deforestation, and changing land uses have been identified as the main sources of climate change and global warming (Carnesale & Chameides, 2011).

In order to investigate past and future climatic conditions, researchers usually use observations and theoretical models. General Circulation Models (GCMs) based on the physical sciences are the most reliable theoretical methods. GCMs use observed data to project future climate models in large scale, and describe the causes and effects of climate change. GCMs have been used by many researchers to predict changes in climate parameters (Biasutti & Giannini, 2006; Hashmi *et al*., 2011). However, these studies have shown that there is a high level of uncertainty in rainfall projection among different GCMs and scenarios. Another significant weakness of GCMs is that their outputs lack sufficient detail to be usable in hydrological models. In order to overcome this limitation, it is essential to transform the country-level predictions of GCMs to the required regional-level information for precipitation and temperature. These methods, which transform the GCM outputs into fine-resolution climate parameters, are called 'downscaling' techniques (Seguí *et al*., 2010; Goyal & Ojha, 2012).

There are different types of downscaling methods, which can be categorised into two main groups: statistical and dynamic downscaling methods. Of the available statistical downscaling techniques, LARS-WG (Long Ashton Research Station Weather Generator) is preferred as it can generate future climate models with less data (Racsko *et al*., 1991; Semenov & Barrow, 1997; Semenov *et al*., 1998). LARS-WG simulates the time series of climate parameters in a daily scale at a single site based on as little as a single year of historical data. This is a well-regarded method that can be used in data-scarce regions like Malaysia. It has therefore been extensively employed in assessing the climate change impact on hydrology, water resources and environmental issues (Vicuña *et al*., 2008; Hashmi *et al*., 2011; Chen *et al*., 2013a). Another advantage of using LARS-WG is that the outputs of 15 GCMs with various emission scenarios could be incorporated into the model to cope with the GCMs uncertainties.

Dibike and Coulibaly (2005) have conducted a comparative study of downscaling models. They found that the LARS-WG method generates a growing trend in mean monthly minimum and maximum temperatures and a small decrement in the variation of temperature for most months. The results also showed that there was no significant change in mean monthly precipitation, or wet and dry spell lengths and the model performance was found to be acceptable. Thus, in this paper, LARS-WG is selected as the downscaling technique.

There is a need to test and evaluate the capability of LARS-WG in downscaling climate parameters like precipitation and temperature in tropical regions like Malaysia. Since these variables are the key weather parameters that directly affect the availability of water in the reservoir, estimating these parameters in the future could help managers and operators predict the potential of the system in generating hydropower and mitigating the effects of climate change by revising the reservoir operation strategy.

As a conclusion, LARS-WG is used as a downscaling model in this study and in order to overcome the uncertainties concerning GCMs, various scenarios are employed to predict the climate parameters under different conditions. Fortunately, simulation of climate change in the 20th century under the special reports on emission's scenario (SRES) is available for

most of the sub-models in GCMs (Alexander & Arblaster, 2009). The SRES comprises various storylines that portray the economic, demographic and technology changes in the future. The most common scenarios are namely A1B, A2 and B1, which are used in the present study. A1B portrays a rapid economic and population growth in the future world. New technologies bring out a combination of non-fossil and fossil fuels as greenhouse-gas emissions. The SRES A2 scenario describes a highly heterogeneous world. As a result, economical growth and technological change per capita are slower than in other storylines. SRES B1 scenario depicts a world with a global population growth that peaks mid-century and decreases afterwards. As a result of globalisation, rapid changes in economic structure are projected to occur. This scenario has a positive view for the future, which shows the world with declined material consumption and usage of clean source of technologies.

The main objective of this research is to predict and analyse the changes in future precipitation and temperature using the LARS-WG downscaling model at Jor Reservoir (part of the Batang Padang hydropower system) under SRES B1A, A2 and B1 scenarios generated by one of GCMs model. The results could be a valuable source of information in future water resource planning and management.

RESEARCH METHOD

Study Area and Data Collection

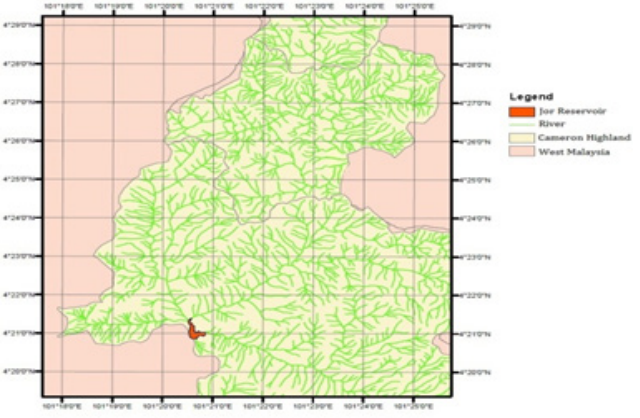

Fig.1: Location of Jor Reservoir in the State of Perak, Malaysia.

This research took place at Jor Reservoir, which is situated in the Tapah Hills Forest Reserve in the state of Perak, Malaysia (Fig.1). Jor Reservoir is part of the Batang Padang hydroelectric scheme (BPHS). The BPHS will impound the discharge from the Sultan Yussuf Power Station together with the waters of the Jor River, Sekam River and Batang Padang River within the Jor Reservoir. From Jor Reservoir, the water will flow 14.5 km through Menglang Tunnel, generating power in the Sultan Idris II underground power station with an installed capacity of 150 KW. The availability of water in the reservoir will, therefore, directly affect power production in the hydropower reservoir system (BPHS). Meanwhile, rising global temperatures and greater climatic variations are significantly influencing water availability. Thus, it is

essential to predict and analyse future temperature and precipitation at the Jor Reservoir, as these climate parameters will directly affect water resources. The nearest rainfall and temperature stations in the Jor Reservoir were selected to provide the LARS-WG input for future climate projections in this area (Table 1).

TABLE 1 : Weather Data Used as LARS-WG Input

Station	Climate parameters	Longitude	Latitude	Altitude	Range of data	Source
Empangan Jor	Daily precipitation	101° 20' E	4° 20' N	519.9	1984-2012	Tenaga Nasional Berhad
Cameron Highlands	Daily min and max temperatures	101° 22' E	4° 28' N	1545	1984-2012	Meteorological Department

Procedure of Downscaling by LARS-WG Model

The LARS-WG method was developed by Semenov and Barrow (1997). LARS-WG is extensively used to simulate daily weather data at a single site under present and future conditions (Racsko *et al*.,1991; Semenov & Stratonovitch, 2010). The first step in the weather generation process involves analysing observed daily weather data to calibrate the model. During calibration, LARS-WG analyses observed weather data to determine its statistical characteristics and generate site-specific cumulative probability distributions (*CPDs*) for the climate parameters. LARS-WG employs precipitation, minimum (*Tmin*) and maximum (*Tmax*) temperatures, and solar radiation (or sunshine hours). The process of data analysis involves applying semi-empirical distributions, such as frequency distributions based on the observed data for wet and dry spell lengths, daily precipitation and solar radiation. A Fourier series is used for the maximum and minimum temperatures. The site-specific file is then used in the generation process. Afterwards, the probability distributions of climate variables are used to generate synthetic weather time series of arbitrary lengths by randomly selecting values from the suitable distributions (Chen *et al*., 2013b). LARS-WG applies a semi-empirical distribution (*SED*), which is specified as the cumulative probability distribution's function (*CPF*), to approximate the probability distribution of dry and wet series of daily precipitation, *Tmin* and *Tmax*. *SED* is divided into 23 intervals for each climate variable. Each climate variable (v) corresponds to the probability of occurrence (P), which is defined as:

$$v_0 = min\ \{v = P(v_{obs} < v)\}\ i = 0, \ldots, n \quad (1)$$

$$P_0 = 0,\ corresponds\ to\ v_0 = min\ (v_{obs}) \quad (2)$$

$$P_n = 0,\ corresponds\ to\ v_n = max\ (v_{obs}) \quad (3)$$

where, P defines the probability of accordance corresponding to (v_{obs}), P_0 and P_n are denoted as 0 and 1 for the climate variable of v_0 and v_n, respectively. To assign the extreme values of climate variables, extremely low values are assigned P values close to 0 and extremely high values are assigned P values close to 1. The other values of P_i are distributed evenly on the probability scale. Since the occurrence probability of low daily precipitation (<1 mm) is high

and this low precipitation has no significant effect on the climate model output, Semenov and Stratonovitch (2010) recommended using v_1=0.5 mm and v_2=1 mm for precipitation within the interval [0, 1] with the corresponding probability, which is written as:

$$P_i = P\ (v_{obs} < v) \quad i=1, 2 \tag{4}$$

In the model, extremely long time series of dry and wet data are considered with two values close to 1, with P_{n-1}=0.99 and P_{n-2}=0.98 in *SEDs*. In addition, in the case of minimum and maximum temperature, two values close to 0 and 1 are assigned for extremely low and high temperatures. For instance P_2=0.01, P_3=0.02, P_{n-1}=0.99, P_{n-2}=0.98 (Hassan *et al*., 2014).

The overall process of generating synthetic weather data by the LARS-WG method can be divided into three steps: calibration, validation and generation of synthetic weather data.

Model calibration. LARS-WG calculates the statistical parameters for each climate variable based on the observed historical data. Once LARS-WG has been calibrated, a series of daily synthetic weather data is generated. A random number generator chooses climate variables from the *CPDs* and as a result, the synthetic weather has the same statistical characteristics as the observed dataset. The generation process requires selecting the number of years to be simulated, as well as a random seed, which controls the stochastic component of the weather generation. Different random seeds generate the same weather statistics, while variables differ on a day-to-day basis (Semenov & Barrow, 2002). In this study, the number of years was taken as 50 and the random seed was chosen as 541.

Model validation. The statistical parameters that were derived from the calibration process were then employed to generate synthetic climate variables with the same statistical characteristics as the original observed weather data. Model validation involved analysing and comparing the statistical characteristics of the observed and synthetic weather data to test the capability of LARS-WG to simulate the precipitation, *Tmax* and *Tmin* at the selected site in order to determine whether or not it is suitable for use. LARS-WG facilitated the validation procedure by employing the *Q*-test option to determine how well it simulated the observed data. LARS-WG, therefore, uses a number of statistical tests such as the Kolmogorov Smirnov, student's *t* test and the *F* test to determine whether the distributions, mean values and standard deviations of the synthetic data were significantly different from the observed data set.

Generation of synthetic weather data. LARS-WG then generated synthetic weather data by synthesising the statistical parameter files derived from the observed weather data in the calibration process with a scenario file containing information about changes in the amount of precipitation, wet and dry series duration, mean temperature, temperature variability and solar radiation. LARS-WG was used to generate daily data based on a particular scenario simulated by GCMs. The scenario file contained the appropriate monthly changes.

Generation of Climate Scenarios

By perturbing the parameters of distributions for a specific site with the predicted climate changes derived from global or regional climate models, a daily climate scenario for the selected site could be generated. In order to generate climate scenarios for a certain future

period and an emission scenario at Jor site, the baseline parameters, which were calculated from the observed dataset from 1984-2012, were adjusted by the Δ-changes for the future period based on emission scenarios, which were predicted by the GCM sub-model for each climatic variable. In this research, the local-scale climate scenarios were based on the A1B, A2 and B1 scenarios simulated by one of the GCMs sub-models, which is called the Hadley GCM3 (HadCM3). HadCM3 was proposed by the UK Meteorological Office's research centre. This model is the most popular and mature of the GCMs, which uses 360 days per annum, where each month is 30 days and has a spatial grid with dimensions 2.5° latitude × 3.75° longitude (Toews & Allen, 2009). It is similar to a coupled atmosphere-ocean general circulation model (AOGCM), which used the coupled model to generate the transient projections. HadCM3 has been applied in many studies (Houghton *et al*., 2001; Qian *et al*., 2004; King *et al*., 2009). This model is unique among GCMs models because it does not need flux adjustments to produce a realistic scenario (Collins *et al*., 2001).

Overall, the future weather data in this study are generated by using LARS-WG [V 5.5] for the time periods of 2011-2030 to predict the future precipitation and minimum and maximum temperature change at Jor Reservoir.

RESULTS AND DISCUSSION

Evaluation of LARS-WG Performance for Prediction of Climate Variables at Jor Reservoir Using Statistical Tests

Before running simulations of future climate parameters, the performance of LARS-WG must be evaluated for the selected site (Jor Reservoir). The main purpose of any weather generator is to simulate climate with the same statistical characteristics as the observed data. In this step, the statistical characteristics of the observed data are compared with the generated data. LARS-WG simplifies this procedure by providing the *Q*-test option to determine the equivalence of the generated data with the observed data in terms of the distributions, mean values and standard deviations, using statistical tests such as Kolmogorov Smirnov test, student's *t* test, and *F* test, respectively.

In this study, the observed historical data from 1984-2012 was used to validate the model for the Jor site. In order to discover the capability of LARS-WG, the Kolmogorov Smirnov (*KS*) test was used to evaluate the equivalence of the seasonal distributions of wet and dry series (*W/D*), distributions of the maximum (*D/Tmax*) and minimum daily temperatures (*D/Tmin*) and distributions of daily rainfall *(D/Rain*) between observed historical data and synthetic data. The t test was performed to test the equivalence of the monthly mean rainfall (*M/Rain*) and the monthly means of maximum (*M/Tmax*) and minimum (*M/Tmin*) temperatures. The F test is applied to testing the equivalence of monthly variances of rainfall (MV/Rain) calculated from observed data and synthetic data. The statistical test result is presented in Table 2, where the numbers show how many tests give significant different results at the 5% significance level out of the total number of tests (four wet and four dry seasonally scaled) or 12 (monthly scaled). A large number reveals a poor performance modelling in the generated synthetic data. The KS test results show that LARS-WG perfectly simulated the distributions of (*W/D*), (*D/Tmax*), (*D/Tmin*) and (*D/Rain*) for this site. The number zero reveals the most desired performance outcome

in generating the synthetic data. Mean monthly minimum and maximum temperatures are two out of 12, which means there are significant differences between observed and simulated data in two months of the year, while in the majority of months (10 out of 12 months), the model can perfectly simulate the minimum and maximum temperatures. The result was, therefore, acceptable.

TABLE 2 : Statistical Results of Comparing the Equality of Observed and Simulated Data Generated

Site	*W/D* series	*D/Rain*	*D/Tmax*	*D/Tmin*	*M/Rain*	*M/Tmax*	*M/Tmin*	*MV/ Rain*
	KS test					*t* test		*F* test
Jor	0	0	0	0	0	2	2	4
Total tests	8	12	12	12	12	12	12	12

The rainfall results show that although there was a dramatic change in mean monthly rainfall in the tropical region, the LARS-WG could perfectly simulate the monthly mean rainfall (0/12), while it had some difficulty in simulating monthly variances of rainfall (4/12). Thus in four months of the year, there was a significant difference between the variance of observed and simulated data. The months were May, June, July and October, which are months affected by the Southwest monsoon in Malaysia that starts in May. This monsoon causes the drier weather and sporadic rainfall, which significantly affects rainfall variance.

Visual comparison of monthly mean and standard deviation of observed and synthetic rainfall is shown in Fig.2 and Fig.3, respectively. While there were good matches between the monthly means of the observed and simulated rainfall, the performance of the standard deviation was not as good a match; however, the results were still acceptable. The outputs of the model in simulating the monthly mean maximum and minimum temperatures are illustrated in Fig.4 and Fig.5, respectively. It is evident that the model could simulate these parameters extremely well and the synthetic data match very well with the observed historical data in all months.

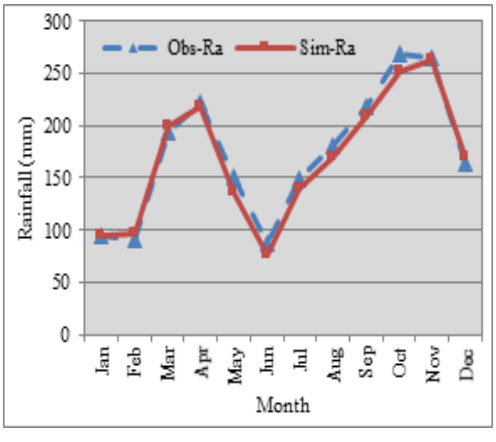

Fig.2: Comparing monthly means of observed and simulated rainfall, 1984-2012

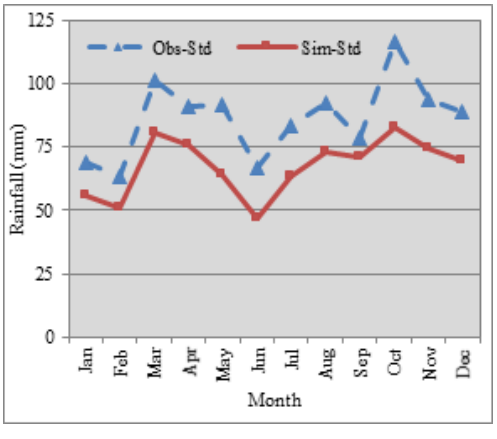

Fig.3: Comparing monthly standard deviations of observed and simulated rainfall, 1984-2012.

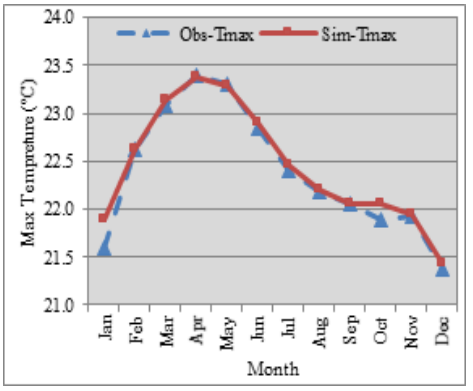

Fig.4: Comparing monthly means of observed and simulated maximum temperatures, 1984-2012.

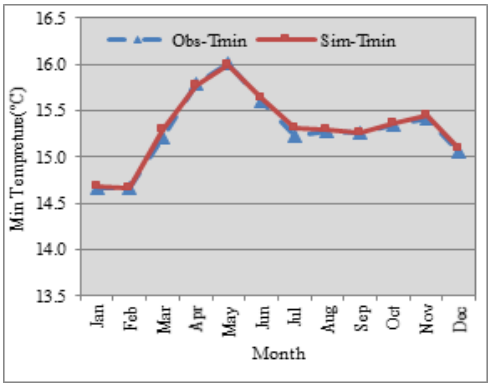

Fig.5: Comparing monthly means of observed and simulated minimum temperatures, 1984-2012.

Change in Temperature

The monthly minimum temperatures in the baseline and future periods are shown in Fig.6. The simulated data were developed for A1B, A2, and B1 scenarios for the 2020s. All scenarios predicted an increment in minimum temperature of around 0.3-0.7 ºC in the next 50 years. The monthly future trends of temperature follow a uniform shape like an observed data trend. The greatest and lowest discrepancies between observed and synthetic data were predicted for March by A1B and September by A2, respectively (Fig.7).

The discrepancy of maximum temperatures in the baseline and future periods is shown in Fig.8, which varies from 21-24 ºC. The maximum temperature will increase by around 0.3 to 0.7ºC in the 2020s (Fig.9). It is evident that the future outputs are highly variable. The greatest discrepancy between future and baseline values will occur in January and March (around 0.7 ºC increments), while the lowest difference will be in September. From the given results, it can be concluded that both *Tmin* and *Tmax* parameters will increase by around 0.3 to 0.7 ºC in the next 50 years. These parameters directly increase the surface evaporation in the reservoir and reduce the available storage at the Jor Lake, which is the key factor in determining hydropower generation. In addition, rising temperatures cause extreme events like droughts or floods, both of which are harmful to power generation. During droughts, the reservoir cannot satisfy the hydropower demand, and during floods, the safety of the reservoir system is threatened.

It is remarkable to note that the main reason for increasing temperature in this area is deforestation. Cameron Highlands is one of the few highland areas with a cool climatic regime that has undergone phenomenal pressures for unplanned development over the last few decades. Development pressures cause more areas to be deforested and cleared. Deforestation is one of the key factors resulting in negative environmental effects, including local climate change. Deforestation is among the human activities that contribute to the spread of carbon dioxide in Cameron Highlands. Deforestation and land-clearing activity for tourism, urbanisation, infrastructure development and agriculture is a major reason for climate change and temperature increment. Deforestation is not the only reason for climate change in this area, but is the major factor of climate change in Cameron Highlands (Hamdan *et al*., 2014).

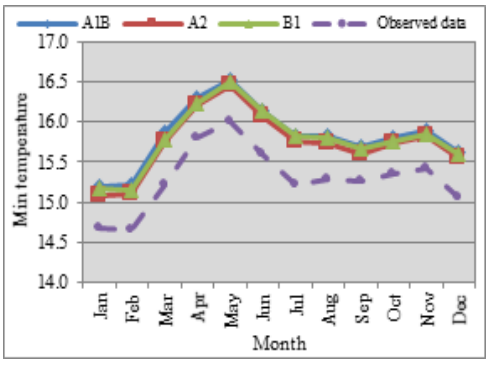

Fig.6: Comparing monthly minimum temperatures between present data and simulated data by A1B, A2, and B1.

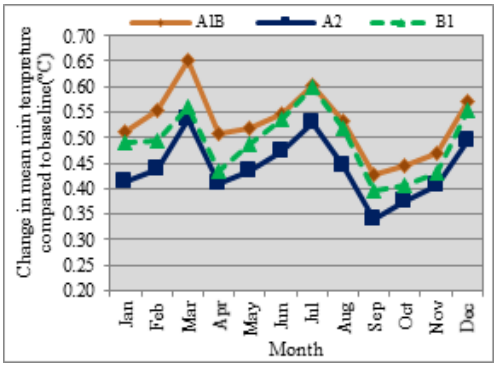

Fig.7: Change in average of monthly minimum temperature.

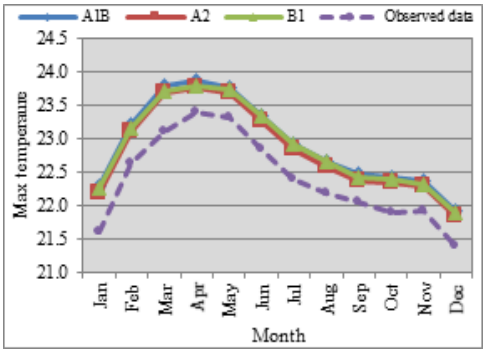

Fig.8: Comparing monthly maximum temperatures between present data and simulated data by A1B, A2, and B1.

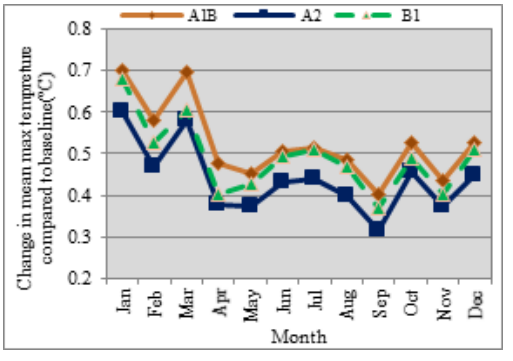

Fig.9: Change in average of monthly maximum temperature.

Change in Precipitation

The monthly amount of observed and simulated rainfall is shown in Fig.10. The given results indicate that in most months, the monthly rainfall will decrease due to global warming in this area. The percentage changes between the simulated and observed values of monthly rainfall were plotted in Fig.11 in 50 years. A positive value indicates an increment and a negative value indicates a decrement in total monthly rainfall. The greatest differences between baseline and future rainfall values among these months are found in February, March and October, which have more than ± 20% variation. Most of the months show a decrement in rainfall, which directly affects the amount of stream flow, water availability and the potential of the reservoir system in producing hydropower. Accordingly, it can be predicted that the potential of hydropower generation will decrease in the future.

The main reason for erratic rainfall in Cameron Highlands is climate change. Climate change is caused by an emission of carbon dioxide in the atmosphere. Greenhouse gases trap electromagnetic radiation form the sun and reflect them back into space. This is the main reason for overall global warming and irregular weather. Besides the negative effects of deforestation

in Cameron Highlands, another factor that brings out the greenhouse gas is the installation of rain shelters for some crops, which causes the emission of greenhouse gases. The heat from the sun is supposed to be fully absorbed into the earth; however, by installation of rain shelters in Cameron Highlands, the heat is reflected into space. As a result, more extreme events will occur and the rainfall pattern will change.

In summary, climate change threatens the socio-economic welfare of farmers, the ecology and the environment and also affects the sustainability of agriculture in Cameron Highlands. Since agriculture is a sector that is highly vulnerable to climate change and its production activity considerably depends on natural resources (Alam *et al*., 2012), farmers are also affected by these changes. Among these changes, three principal factors are the rising temperature, deforestation and the considerable numbers of rain shelters that produce uncontrolled greenhouse gases. These changes have negative effects on the two main industries in Cameron Highlands i.e. agriculture and tourism. A number of factors have been distinguished as significant reasons for such changes. The higher cost of living has put pressure on Cameron Highlands' farmers. This is the main factor driving farmers to increase their income somehow. Land clearing is a solution for doubling their productivity and income (Siwar *et al*., 2013). However, it causes a negative effect on the agriculture sector and increases temperature. In addition, the rising trend in temperature will influence the tourism industry as the coolness of Cameron Highlands has always been the principal attraction for tourists. It can be concluded that the Malaysian government needs to develop policies to protect the environment and ecosystem in Cameron Highlands.

CONCLUSION

This research investigates the effects of global warming on key climate parameters such as precipitation and minimum and maximum temperatures in the Batang Padang hydropower reservoir system, Malaysia. These parameters greatly influence the available water in the reservoir, which is the key element of hydropower generation potential. Therefore, the observed climate data on precipitation and minimum and maximum temperatures for 29 years (1984-2012) were employed to prepare the weather generator model and estimate future climate data. In this research, LARS-WG was chosen as a downscaling technique to generate the time series of daily temperature and precipitation under the three climate scenarios of A1B, A2 and B1, simulated by one General Circulation Model's outputs for 50 years in the future. The results indicated that LARS-WG demonstrates good performance in simulating the statistical properties of daily climate data to forecast future climate change. It is estimated that global warming will cause an increase in minimum and maximum temperatures of 0.3-0.7 ºC, which will greatly intensify reservoir surface evaporation. In addition, the overall results demonstrated that the amount of precipitation will experience a decrement in most months under selected scenarios. However, it is expected that the percentage change in mean monthly precipitation will be an increase of +20% or more in February and October. The aforementioned parameters highly influence the availability of water in the reservoir, and thereby, the potential of hydropower generation. This research offers valuable information to managers and operators and implies the need to modify the reservoir system operation in order to mitigate the effects of climate change.

REFERENCES

Alam, M. M., Siwar, C., Talib, B., Mokhtar, M., & Toriman, M. E. (2012). Climate change adaptation policy in Malaysia: Issues for agricultural sector. *African Journal of Agricultural Research, 7*(9), 1368-1373.

Alexander, L. V., & Arblaster, J. M. (2009). Assessing trends in observed and modelled climate extremes over Australia in relation to future projections. *International Journal of Climatology, 29*(3), 417-435.

Brissette, F., Leconte, R., Minville, M., & Roy, R. (2006). *Can we adequately quantify the increase/ decrease of flooding due to climate change?* Paper presented at the EIC Climate Change Technology, 2006 IEEE.

Carnesale, A., & Chameides, W. (2011). *America's climate choices.* NRC/NAS USA Committee on America's Climate Choices. Retrieved from http://download. nap. edu/cart/deliver. cgi.

Chen, H., Guo, J., Zhang, Z., & Xu, C.-Yu. (2013). Prediction of temperature and precipitation in Sudan and South Sudan by using LARS-WG in future. *Theoretical and Applied Climatology, 113*(3-4), 363-375.

Collins, M., Tett, S. F. B., & Cooper, C. (2001). The internal climate variability of HadCM3, a version of the Hadley Centre coupled model without flux adjustments. *Climate Dynamics, 17*(1), 61-81.

Dibike, Y. B., & Coulibaly, P. (2005). Hydrologic impact of climate change in the Saguenay watershed: Comparison of downscaling methods and hydrologic models. *Journal of hydrology, 307*(1), 145-163.

Goyal, M. K., & Ojha, C. S. P. (2012). Downscaling of surface temperature for lake catchment in an arid region in India using linear multiple regression and neural networks. *International Journal of Climatology, 32*(4), 552-566.

Hamdan, M. E., Man, N., Yassin S. M. D., D`Silva, J. L., & Shaffril, H. A. M. (2014). Farmers sensitivity towards the changing climate in the Cameron Highlands. *Agricultural Journal, 9*(2), 120-126.

Hashmi, M. Z., Shamseldin, A. Y., & Melville, B. W. (2011). Comparison of SDSM and LARS-WG for simulation and downscaling of extreme precipitation events in a watershed. *Stochastic Environmental Research and Risk Assessment, 25(*4), 475-484.

Hassan, Z., Shamsudin, S., & Harun, S. (2014). Application of SDSM and LARS-WG for simulating and downscaling of rainfall and temperature. *Theoretical and applied climatology, 116*(1-2), 243-257.

Houghton, J. T., Ding, Y. D. J. G., Griggs, D. J., Noguer, M., van der Linden, P. J., Dai, Xiaosu, . . . Johnson, C. A. (2001). *Climate change 2001: The scientific basis* (Vol. 881): Cambridge university press Cambridge.

King, L., Solaiman, T., & Simonovic, S. P. (2009). *Assessment of climatic vulnerability in the Upper Thames River Basin*: Department of Civil and Environmental Engineering, The University of Western Ontario.

Qian, B., Hayhoe, H., & Gameda, S. (2004). Evaluation of the stochastic weather generators LARS-WG and AAFC-WG for climate change impact studies. *Climate Research, 29*(1), 3.

Racsko, P., Szeidl, L., & Semenov, M. (1991). A serial approach to local stochastic weather models. *Ecological modelling, 57*(1), 27-41.

Seguí, P. Q., Ribes, A., Martin, E., Habets, F., & Boé, J. (2010). Comparison of three downscaling methods in simulating the impact of climate change on the hydrology of Mediterranean basins. *Journal of Hydrology, 383*(1), 111-124.

Semenov, M. A, & Barrow, E. M. (2002). *LARS-WG: A stochastic weather generator for use in climate impact studies: User manual.* Harpenden: Rothamsted Research.

Semenov, M. A., & Barrow, E. M. (1997). Use of a stochastic weather generator in the development of climate change scenarios. *Climatic change, 35*(4), 397-414.

Semenov, M. A., Brooks, R. J., Barrow, E. M., & Richardson, C. W. (1998). Comparison of the WGEN and LARS-WG stochastic weather generators for diverse climates. *Climate research, 10*(2), 95-107.

Semenov, M. A., & Stratonovitch, P. (2010). Use of multi-model ensembles from global climate models for assessment of climate change impacts. *Climate research (Open Access for articles 4 years old and older), 41*(1) 1.

Siwar, C., Ahmed, F., & Begum, R. A. (2013). Climate change, agriculture and food security issues: Malaysian perspective. *Journal: Food, Agriculture and Environment, 11*(2), 1118-1123.

Toews, M. W., & Allen, D. M. (2009). Evaluating different GCMs for predicting spatial recharge in an irrigated arid region. *Journal of Hydrology, 374*(3), 265-281.

Vicuña, S., Leonardson, R., Hanemann, M. W, Dale, L. L., & Dracup, J. A. (2008). Climate change impacts on high elevation hydropower generation in California's Sierra Nevada: A case study in the Upper American River. *Climatic Change, 87*(1), 123-137.

Pertanika J. Sci. & Technol. 24 (1): 225 - 230 (2016)

PERTANIKA JOURNALS

SCIENCE & TECHNOLOGY

Journal homepage: http://www.pertanika.upm.edu.my/

Case Study

Parotid Oncocytoma in Birt-Hogg-Dubé Syndrome: A New Pitfall in ^{18}F-Fluorodeoxyglucose Positron Emission Tomography/Computed Tomography Imaging Study

Sethu Thakachy Subha[1*], Abdul Jalil Nordin[2], Norhafizah Mohtarrudin[3] and Fathinul Fikri Ahmad Saad[2]

[1]Department of Surgery/ENT, Faculty of Medicine Health Sciences, Universiti Putra Malaysia, 43400 UPM Serdang , Selangor, Malaysia

[2]Centre for Diagnostic Nuclear Imaging, Universiti Putra Malaysia, 43400 UPM Serdang, Selangor, Malaysia

[3]Faculty of Medicine Health Sciences, Universiti Putra Malaysia, 43400 UPM Serdang, Selangor, Malaysia

ABSTRACT

Oncocytomas are rare head and neck neoplasms that occur most commonly in the parotid salivary gland. Birt-Hogg-Dubé syndrome is a rare inherited genodermatosis manifested by a group of cutaneous lesions, in association with several renal and lung pathology, parotid oncocytoma, thyroid and colonic tumours. Here we report on the case of a patient who presented with parotid oncocytoma in association with skin lesions, multinodular goitre and uterine leiomyoma. This array of lesions suggested the possibility of Birt-Hogg-Dubé syndrome. ^{18}F-Fluorodeoxyglucose Positron Emission Tomography/Computed Tomography (^{18}F FDG PET/CT) was used to evaluate head and neck malignancies, including salivary gland tumours. In this report, we highlight a case of bilateral parotid oncocytoma with suspected Birt-Hogg-Dubé syndrome that showed increased FDG uptake in a PET-CT study. This marked FDG avidity in a benign parotid oncocytoma, adding to the list of common pitfalls related to the parotid glands during a FDG PET-CT study.

Keywords: Oncocytoma, parotid gland, ^{18}F FDG PET CT (^{18}F-Fluorodeoxyglucose Positron Emission Tomography/Computed Tomography), BHD (Birt-Hogg-Dubé Syndrome)

Article history:
Received: 8 January 2015
Accepted: 2 June 2015

E-mail addresses:
subhast2@yahoo.com (Sethu Thakachy Subha),
drimaging@yahoo.com (Abdul Jalil Nordin),
norhafizahm@upm.edu.my (Norhafizah Mohtarrudin),
ainurff@gmail.com (Fathinul Fikri Ahmad Saad)
*Corresponding author

INTRODUCTION

Oncocytomas of the salivary glands are rare benign epithelial tumours that comprise less than 1% of salivary gland tumours. The parotid gland is the most commonly affected salivary gland, accounting for 78-84% of

ISSN: 0128-7680

salivary gland oncocytoma, while bilateral presentation is reported to be extremely rare (Tana *et al*., 2010; Uzunkulaoglu *et al*., 2012). Birt-Hogg- Dubé syndrome is a rare autosomal dominant condition characterised by a group of cutaneous lesions, in association with several renal and lung pathology, parotid oncocytoma, thyroid and colonic tumours (Liu *et al*., 2000; Adley *et al*., 2006; López *et al*., 2012).

18F FDG PET CT is an integrated imaging modality that has been vastly utilised in investigation and management of head and neck tumours. This multimodality diagnostic imaging positron emission tomography computed tomography (PET-CT) is a known improved method for oncology staging in comparison to conventional modalities. The use of 2-[fluorine-18]-fluoro-2-deoxy-D-glucose, a glucose analogue in PET-CT study as a biomarker, facilitates the identification of abnormal tissues with high glycolytic activity, albeit the fact that biological response cannot separate an active benign lesion from malignancy, leading to pitfalls and false positive interpretations of the study.

CASE REPORT

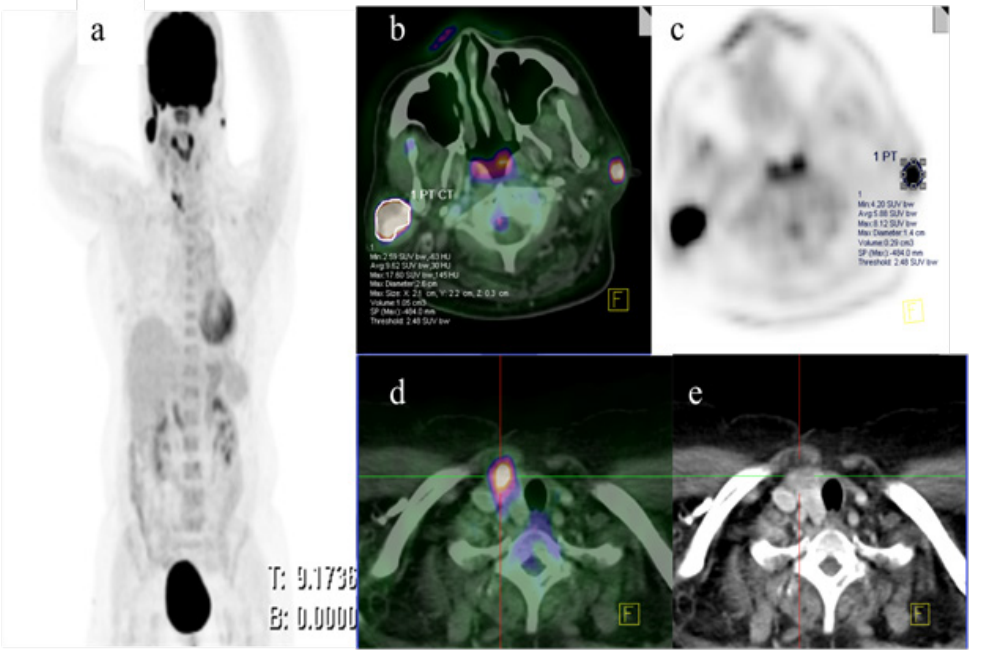

Fig.1: MIP (image a) demonstrate abnormal foci of high FDG uptake in the region of the neck and right upper chest. Integrated fused PET and CT images in the axial plane at the level of the post nasal space (image b) demonstrate increased FDG uptake in both parotids with SUV_{max} 17.6 and 8.1 (image c) in the right and left, respectively. In addition to this finding, there is a foci of high FDG uptake seen in the remnant of the right thyroid lobe (image d), which was reported as normal on initial CT. The corresponding contrasted CT (image e) demonstrates a poorly enhanced low attenuation lesion within the right lobe.

The subject was a 60-year-old woman who had been diagnosed with a progressively increasing right parotid swelling for six months prior to the study. The non-tender swelling was without any other significant clinical signs or symptoms. Her past medical and surgical history revealed that she had skin lesions over the anterior part of the neck many years ago that were excised and informed to be benign lesions. She also underwent a left hemithyroidetomy for multinodular goiter and a hysterectomy for uterine leiomyoma. Meanwhile, an ENT examination showed non-tender firm mass (3 x 4 cm) in the right parotid region. A CT scan demonstrated enhancing lesions in both parotid glands. The right parotid gland was found to be bigger than the left. The right thyroid lobe looked normal.

Further investigation was also carried out on the patient using FDG PET-CT so as to exclude malignancy, mainly lymphoma. The study was conducted following standard protocol. The images were analysed by two nuclear radiologists in a systematic manner at 1 mm reconstruction in axial, coronal and sagittal planes. The imaging results from the PET study were interpreted qualitatively to look for abnormally high FDG uptake lesions and quantitatively using an automated maximum standardised uptake value (SUVmax) derived from the region of interest (ROI) drawn over FDG avid lesions. The CT images were analysed for any abnormal morphology and enhancing patterns. Eventually, both the PET and CT images were fused and interpreted together. The study showed ill-defined enhancing mass lesions arising from both parotid glands. Both the parotid lesions demonstrated high FDG uptake. The metabolism of the lesions was semi-quantified through the region of interest drawn over the lesions and represented as 17.6 and 8.2 in the right and left, respectively. In addition, there was a focus of high FDG uptake in the remnant of the right thyroid lobe without morphological change with the maximum standardised uptake value (SUVmax) of 14.8. The lesion enhanced well and homogenously following intravenous contrast administration. The morphological changes found at imaging, in combination with high metabolic activity, aroused suspicions for malignancy within the glands; thus, a fine needle aspiration procedure was conducted for the parotids and thyroid lesions. Meanwhile, a cytological smear from the parotid lesions demonstrated clusters of round to polygonal shaped cells, with small monomorphic nuclei and coarse granular cytoplasm on Diff Quick stain (see Fig.2). These features are highly suggestive of parotid oncocytoma. Ultrasound guided FNA of the right thyroid showed granulomatous thyroiditis. There were no lesions found in the lung parenchyma and both kidneys by PET-CT imaging. It is important to note that the patient refused any further surgical intervention.

DISCUSSION

Oncocytomas are rare head and neck neoplasms that occur most commonly in parotid salivary gland. Oncocytoma, which is also known as oxyphilic adenoma, is a benign neoplasm that clinically presents as solid, well circumscribed nodules. These tumours are usually seen in the elderly and affect the parotid gland in 80% of related cases (Tana *et al*., 2010; Uzunkulaoglu *et al*., 2012). Birt-Hogg- Dubé syndrome is a rare autosomal dominant condition that consists of fibrofolliculomas, trichodiscomas and acrochordons. It is also associated with several non-cutaneous tumours. Various reports have revealed that these constellations of cutaneous lesions are associated with parotid oncocytoma, multinodular goiter and lipoma, as well as

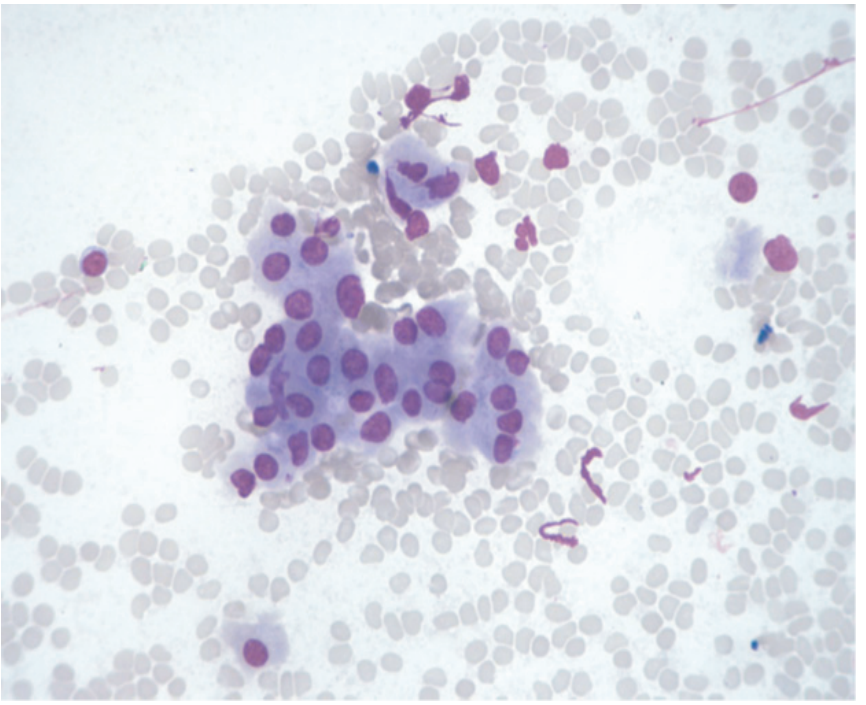

Fig.2: Oncocytoma. The neoplastic oncocytic epithelium is arranged in clusters. The cells are round to oval monomorphic nuclei with abundant densely granular cytoplasm. (Diff Quick. Original magnification ×400).

several renal and lung pathology (Liu *et al*., 2000; Adley *et al*., 2006; Menko *et al*., 2009). However, the actual incidence of Birt-Hogg-Dubé syndrome is unknown, and it is most likely under-diagnosed. In this study, we reported a patient with parotid oncocytoma associated with multinodular goitre, uterine leiomyoma and history of skin lesions. The possibility of the Birt-Hogg-Dubé syndrome was considered in view of constellation of these lesions. CT scan is a well-established first line imaging modality that has been widely used in diagnoses of salivary gland tumours. The common CT findings of parotid oncocytoma described in the literature are that it is a well-defined mass with homogenous enhancement (Shellenberger *et al.*, 2008; Tana *et al*., 2010). The important differential diagnoses for well-defined enhancing parotid lesions detected in CT include Warthin's tumour and basal cell adenomas. Pleomorphic adenoma, the most common parotid neoplasm, demonstrates minimal or no enhancement. Hence, it is less likely to be the differential diagnosis in this case. A low-grade parotid malignancy is an important differential diagnosis and a major diagnostic pitfall in the imaging assessment of a well-defined enhancing parotid tumour. MR imaging allows markedly improved soft tissue delineation and thus, helps to characterise parotid gland mass lesions. Oncocytomas appear hypointense and well demarcated on T1 but are isointense to the native parotid gland on fat-saturated T2 and T1 post contrast imaging (Patel *et al*., 2011). 18F FDG PET CT has been shown to be superior to conventional imaging in evaluating patients with head and neck tumours. However, non-specificity of FDG uptake in benign lesion has led to false positive findings in the interpretation of the results, as in this case (Shah *et al*., 2007; Uzunkulaoglu *et al*., 2012)

Fine Needle Aspiration (FNA) is an investigation of choice for making a diagnosis in the majority of cases (Vlachaki *et al.*, 2009; Uzunkulaoglu *et al.*, 2012). Likewise, in this case, the aspirates confirmed the diagnosis of oncocytoma. The smears showed oncocytes with no evidence of atypia. The presence of marked atypical oncocytes suggests the possibility of an oncocytic carcinoma. However, oncocytic carcinoma cannot be distinguished reliably from oncocytoma on FNA because diagnosis of malignancy is based on either local invasion or metastasis. Oncocytoma generally presents as a solid, well circumscribed mass characterised as having a tan colour. Microscopically, it is composed of large cells with round nuclei and abundant granular acidophilic cytoplasm (Vlachaki *et al*., 2009). Mitotic figures are absent. The malignant counterpart of oncocytoma is oncocytic carcinoma. It is characterised by cellular atypia, increased mitotic activity and infiltrative growth (Shah *et al*., 2007; Menko *et al*., 2009). Ki-67 immunostaining has been used to differentiate benign from malignant oncocytoma. The treatment of choice for these tumours is mainly surgical. It is mandatory to identify the extent and nature of tumours prior to any definitive surgical treatment (Vlachaki *et al.*, 2009; Tana *et al.*, 2010; Uzunkulaoglu *et al*., 2012).

CONCLUSION

Oncocytic neoplasms should be considered as a possible diagnosis in elderly patients with parotid enlargement. It is important to conduct a histological investigation before finalising any diagnosis of FDG avid lesion within parotid glands since FDG is a non-specific tracer.

REFERENCES

Adley, B. P., Smith, N. D., Nayar, R., & Yang, X. J. (2006). Birt-Hogg-Dubé Syndrome. Clinicopathologic findings and genetic alterations. *Archives of Pathology and Laboratory Medicine, 130,* 1865-1870.

Kunogi, M., Kurihara, M., Ikegami, T. S., Kobayashi, T., Shindo, N., Kumasaka, T., ... & Seyama, K. (2010). Clinical and genetic spectrum of Birt–Hogg–Dubé syndrome patients in whom pneumothorax and/or multiple lung cysts are the presenting feature. *Journal of medical genetics, 47*(4), 281-287.

Liu, V., Kwan, T., & Page, E. H. (2000). Parotid oncocytoma in the Birt-Hogg-Dubé syndrome. *Journal of the American Academy of Dermatology, 43*(6), 1120-1122.

López, V., Jordá, E., & Monteagudo, C. (2012). Birt–Hogg–Dubé Syndrome: An Update. *Actas Dermo-Sifiliográficas (English Edition), 103*(3), 198-206.

Maffe, A., Toschi, B., Circo, G., Giachino, D., Giglio, S., Rizzo, A., ... & Genuardi, M. A. U. R. I. Z. I. O. (2011). Constitutional FLCN mutations in patients with suspected Birt–Hogg–Dubé syndrome ascertained for non-cutaneous manifestations. *Clinical Genetics, 79*(4), 345-354.

Menko, F. H., van Steensel, M. A., Giraud, S., Friis-Hansen, L., Richard, S., Ungari, S., ... & European BHD Consortium. (2009). Birt-Hogg-Dubé syndrome: diagnosis and management. *The Lancet Oncology, 10*(12), 1199-1206.

Mukunyadzi, P. (2002). Review of fine-needle aspiration cytology of salivary gland neoplasms, with emphasis on differential diagnosis. American Journal of Clinical Pathology. *Pathology Patterns Reviews, 118*(Suppl 1), S100-S115.

Patel, N. D., van Zante, A., Eisele, D. W., Harnsberger, H. R., & Glastonbury, C. M. (2011). Oncocytoma: the vanishing parotid mass. *American Journal of Neuroradiology, 32*(9), 1703-1706.

Shah, V. N., & Branstetter IV, B. F. (2007). Oncocytoma of the parotid gland: a potential false-positive finding on ^{18}F-FDG PET. *American Journal of Roentgenology, 189*(4), W212-W214.

Shellenberger, T. D., Williams, M. D., Clayman, G. L., & Kumar, A. J. (2008). Parotid gland oncocytosis: CT findings with histopathologic correlation. *American Journal of Neuroradiology, 29*(4), 734-736.

Tana, T. J., & Tana, T. Y., (2010). CT features of parotid oncocytomas: A case study of 10 cases and literature review. *American Journal of Neuroradiology, 31*, 1413-1417.

Uzunkulaoglu, H., Yazici, H., Can, I. H., Dogan, S., & Uzunkulaoglu, T. (2012). Bilateral oncocytoma in the parotid gland. *The Journal of Craniofacial Surgery, 23*(3), e246-e247.

Vlachaki, E., Tsapas, A., Dimitrakopoulos, K., Kontzoglou,G., & Klonizakis, I. (2009). Parotid oncocytoma: A case report. *Cases Journal, 2,* 6423.

REFEREES FOR THE PERTANIKA
JOURNAL OF SCIENCE AND TECHNOLOGY

VOL. 24(1) JAN. 2016

The Editorial Board of the Journal of Science and Technology wishes to thank the following for acting as referees for manuscripts published in this issue of JST.

Abdul Aziz Abdul Raman
(UM, Malaysia)

Abdul Talib Bon
(UTHM, Malaysia)

Ahmad Taufek Abdul Rahman
(UiTM, Malaysia)

Aissa Boudjella
(Al Khawarizmi International College, UAE)

Bassim H. Hameed
(USM, Malaysia)

Biswa Mohan Biswal
(KPJ Ipoh Specialist Hospital, Malaysia)

Che Fauziah Ishak
(UPM, Malaysia)

Chonticha Kaewanuchit
(Phranakhon Si Ayutthaya Rajabhat University, Thailand)

Chung-Ho Chen
(Southern Taiwan University of Science and Technology, Taiwan)

Farzad Ismail
(USM, Malaysia)

Hasliza Abu Hassim
(UPM, Malaysia)

Idawaty Ahmad
(UPM, Malaysia)

Loganathan Muruganandam
(VIT University, India)

Md Sabri Mohd Yusoff
(UPM, Malaysia)

Micah Osilike
(University of Nigeria, Nigeria)

Michael Khoo Boon Chong
(USM, Malaysia)

Mohammed Alias Yusof
(UTHM, Malaysia)

Mohd Fadzil Hassan
(UTP, Malaysia)

Muhammad Ekhlasur Rahman
(Curtin University Sarawak, Malaysia)

Ng Choung Min
(UM, Malaysia)

Ngoh Gek Cheng
(UM, Malaysia)

Noorjahan Banu Alitheen
(UPM, Malaysia)

Nor Fazlida Mohd Sani
(UPM, Malaysia)

Pah Rokiah Syed Hussain
(UUM, Malaysia)

Prakash Chandra Srivastava
(G.B. Pant University of Agriculture and Technology, India)

Ramasamy Kandasamy
(UTHM, Malaysia)

Rattihalli R. N.
(University of Hyderabad, India)

Ravi Prakash
(Amity University, India)

Said Salah Eldin Elnashaie
(UPM, Malaysia)

Saratha Sathasivam
(USM, Malaysia)

Subapriya Suppiah
(UPM, Malaysia)

Syazrah Mohd Razi
(UMK, Malaysia)

Wan Ainun Mior Othman
(UM, Malaysia)

Wong Voon Hee
(UTAR, Malaysia)

UPM - Universiti Putra Malaysia
USM - Universiti Sains Malaysia
UM - Universiti Malaya
UiTM - Universiti Teknologi MARA Malaysia
UTP - Universiti Teknologi PETRONAS
UUM - Universiti Utara Malaysia
UTHM - Universiti Tun Hussein Onn Malaysia
UMK - Universiti Malaysia Kelantan
UTAR - Universiti Tunku Abdul Rahman

While every effort has been made to include a complete list of referees for the period stated above, however if any name(s) have been omitted unintentionally or spelt incorrectly, please notify the Chief Executive Editor, *Pertanika* Journals at nayan@upm.my.

Any inclusion or exclusion of name(s) on this page does not commit the *Pertanika* Editorial Office, nor the UPM Press or the University to provide any liability for whatsoever reason.

Pertanika Journals

Our goal is to bring high quality research to the widest possible audience

INSTRUCTIONS TO AUTHORS

(Manuscript Preparation & Submission Guidelines)

Revised: August 2015

We aim for excellence, sustained by a responsible and professional approach to journal publishing.
We value and support our authors in the research community.

Please read the Pertanika guidelines and follow these instructions carefully. Manuscripts not adhering to the instructions will be returned for revision without review. The Chief Executive Editor reserves the right to return manuscripts that are not prepared in accordance with these guidelines.

MANUSCRIPT PREPARATION

Manuscript Types

Pertanika accepts submission of mainly **four** types of manuscripts for peer-review.

1. **Regular article**

Regular articles are full-length original empirical investigations, consisting of introduction, materials and methods, results and discussion, conclusions. Original work must provide references and an explanation on research findings that contain new and significant findings.

Size: Generally, these are expected to be between 6 and 12 journal pages (excluding the abstract, references, tables and/or figures), a maximum of 80 references, and an abstract of 100–200 words.

2. **Review article**

These report critical evaluation of materials about current research that has already been published by organizing, integrating, and evaluating previously published materials. It summarizes the status of knowledge and outline future directions of research within the journal scope. Review articles should aim to provide systemic overviews, evaluations and interpretations of research in a given field. Re-analyses as meta-analysis and systemic reviews are encouraged. The manuscript title must start with "Review Article:".

Size: These articles do not have an expected page limit or maximum number of references, should include appropriate figures and/or tables, and an abstract of 100–200 words. Ideally, a review article should be of 7 to 8 printed pages.

3. **Short communications**

They are timely, peer-reviewed and brief. These are suitable for the publication of significant technical advances and may be used to:

(a) report new developments, significant advances and novel aspects of experimental and theoretical methods and techniques which are relevant for scientific investigations within the journal scope;

(b) report/discuss on significant matters of policy and perspective related to the science of the journal, including 'personal' commentary;

(c) disseminate information and data on topical events of significant scientific and/or social interest within the scope of the journal.

The manuscript title must start with "*Brief Communication*:".

Size: These are usually between 2 and 4 journal pages and have a maximum of three figures and/or tables, from 8 to 20 references, and an abstract length not exceeding 100 words. Information must be in short but complete form and it is not intended to publish preliminary results or to be a reduced version of Regular or Rapid Papers.

4. **Others**

Brief reports, case studies, comments, concept papers, Letters to the Editor, and replies on previously published articles may be considered.

PLEASE NOTE: NO EXCEPTIONS WILL BE MADE FOR PAGE LENGTH.

Language Accuracy

Pertanika **emphasizes** on the linguistic accuracy of every manuscript published. Articles must be in **English** and they must be competently written and argued in clear and concise grammatical English. Contributors are strongly advised to have the manuscript checked by a colleague with ample experience in writing English manuscripts or a competent English language editor.

Author(s) **must provide a certificate** confirming that their manuscripts have been adequately edited. A proof from a recognised editing service should be submitted together with the cover letter at the time of submitting a manuscript to Pertanika**. All editing costs must be borne by the author(s)**. This step, taken by authors before submission, will greatly facilitate reviewing, and thus publication if the content is acceptable.

Linguistically hopeless manuscripts will be rejected straightaway (e.g., when the language is so poor that one cannot be sure of what the authors really mean). This process, taken by authors before submission, will greatly facilitate reviewing, and thus publication if the content is acceptable.

MANUSCRIPT FORMAT

The paper should be submitted in one column format with at least 4cm margins and 1.5 line spacing throughout. Authors are advised to use Times New Roman 12-point font and *MS Word* format.

1. Manuscript Structure

Manuscripts in general should be organised in the following order:

Page 1: *Running title*

This page should **only** contain the running title of your paper. The running title is an abbreviated title used as the running head on every page of the manuscript. The running title should not exceed 60 characters, counting letters and spaces.

Page 2: *Author(s) and Corresponding author information.*

This page should contain the **full title** of your paper not exceeding 25 words, with name(s) of all the authors, institutions and corresponding author's name, institution and full address (Street address, telephone number (including extension), hand phone number, and e-mail address) for editorial correspondence. First and corresponding authors must be clearly indicated.

The names of the authors may be abbreviated following the international naming convention. e.g. Salleh, A.B.[1], Tan, S.G[2*]., and Sapuan, S.M[3].

Authors' addresses. Multiple authors with different addresses must indicate their respective addresses separately by superscript numbers:

George Swan[1] and Nayan Kanwal[2]
[1]Department of Biology, Faculty of Science, Duke University, Durham, North Carolina, USA.,
[2]Office of the Deputy Vice Chancellor (R&I), Universiti Putra Malaysia, Serdang, Malaysia.

A **list** of number of **black and white / colour figures and tables** should also be indicated on this page**.** Figures submitted in color will be printed in colour. See *"5. Figures & Photographs"* for details.

Page 3: *Abstract*

This page should **repeat** the **full title** of your paper with only the **Abstract** (the abstract should be less than 250 words for a Regular Paper and up to 100 words for a Short Communication), and **Keywords**.

Keywords: Not more than eight keywords in alphabetical order must be provided to describe the contents of the manuscript.

Page 4: *Introduction*
This page should begin with the **Introduction** of your article and followed by the rest of your paper.

2. *Text*

Regular Papers should be prepared with the headings *Introduction, Materials and Methods, Results and Discussion*, *Conclusions, Acknowledgements, References, and Supplementary data* (if avavailble) in this order.

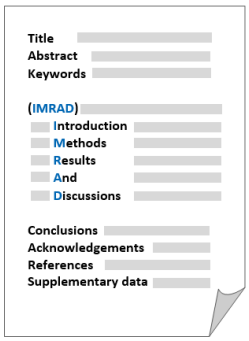

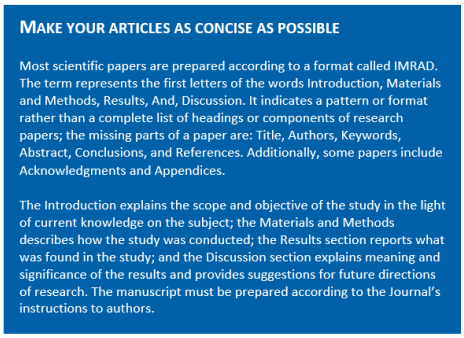

3. *Equations and Formulae*

These must be set up clearly and should be typed double spaced. Numbers identifying equations should be in square brackets and placed on the right margin of the text.

4. *Tables*

All tables should be prepared in a form consistent with recent issues of Pertanika and should be numbered consecutively with Roman numerals. Explanatory material should be given in the table legends and footnotes. Each table should be prepared on a new page, embedded in the manuscript.

When a manuscript is submitted for publication, tables must also be submitted separately as data - .doc, .rtf, Excel or PowerPoint files- because tables submitted as image data cannot be edited for publication and are usually in low-resolution.

5. *Figures & Photographs*

Submit an **original** figure or photograph. Line drawings must be clear, with high black and white contrast. Each figure or photograph should be prepared on a new page, embedded in the manuscript for reviewing to keep the file of the manuscript under 5 MB. These should be numbered consecutively with Roman numerals.

Figures or photographs must also be submitted separately as TIFF, JPEG, or Excel files- because figures or photographs submitted in low-resolution embedded in the manuscript cannot be accepted for publication. For electronic figures, create your figures using applications that are capable of preparing high resolution TIFF files. In general, we require **300 dpi** or higher resolution for **coloured and half-tone artwork**, and **1200 dpi or higher** for **line drawings** are required.

Failure to comply with these specifications will require new figures and delay in publication. **NOTE**: Illustrations may be produced in colour at no extra cost at the discretion of the Publisher; the author could be charged Malaysian Ringgit 50 for each colour page.

6. *References*

References begin on their own page and are listed in alphabetical order by the first author's last name. Only references cited within the text should be included. All references should be in 12-point font and double-spaced.

NOTE: When formatting your references, please follow the **APA reference style** (6th Edition). Ensure that the references are strictly in the journal's prescribed style, failing which your article will **not be accepted for peer-review**. You may refer to the *Publication Manual of the American Psychological Association* for further details (http://www.apastyle.org/).

7. *General Guidelines*

Abbreviations: Define alphabetically, other than abbreviations that can be used without definition. Words or phrases that are abbreviated in the introduction and following text should be written out in full the first time that they appear in the text, with each abbreviated form in parenthesis. Include the common name or scientific name, or both, of animal and plant materials.

Acknowledgements: Individuals and entities that have provided essential support such as research grants and fellowships and other sources of funding should be acknowledged. Contributions that do not involve researching (clerical assistance or personal acknowledgements) should **not** appear in acknowledgements.

Authors' Affiliation: The primary affiliation for each author should be the institution where the majority of their work was done. If an author has subsequently moved to another institution, the current address may also be stated in the footer.

Co-Authors: The commonly accepted guideline for authorship is that one must have substantially contributed to the development of the paper and share accountability for the results. Researchers should decide who will be an author and what order they will be listed depending upon their order of importance to the study. Other contributions should be cited in the manuscript's Acknowledgements.

Copyright Permissions: Authors should seek necessary permissions for quotations, artwork, boxes or tables taken from other publications or from other freely available sources on the Internet before submission to Pertanika. Acknowledgement must be given to the original source in the illustration legend, in a table footnote, or at the end of the quotation.

Footnotes: Current addresses of authors if different from heading may be inserted here.

Page Numbering: Every page of the manuscript, including the title page, references, tables, etc. should be numbered.

Spelling: The journal uses American or British spelling and authors may follow the latest edition of the Oxford Advanced Learner's Dictionary for British spellings.

SUBMISSION OF MANUSCRIPTS

Owing to the volume of manuscripts we receive, we must insist that all submissions be made electronically using the **online submission system ScholarOne™**, a web-based portal by Thomson Reuters. For more information, go to our web page and click "**Online Submission**".

Submission Checklist

1. **MANUSCRIPT**: Ensure your MS has followed the Pertanika style particularly the first four pages as explained earlier. The article should be written in a good academic style and provide an accurate and succinct description of the contents ensuring that grammar and spelling errors have been corrected before submission. It should also not exceed the suggested length.

2. **COVER LETTER**: All submissions must be accompanied by a cover letter detailing what you are submitting. Papers are accepted for publication in the journal on the understanding that the article is **original** and the content has **not been published** or **submitted for publication elsewhere**. This must be stated in the cover letter. Submission of your manuscript will not be

accepted until a signed cover letter *(original pen-to-paper signature)* has been received. The cover letter must also contain an acknowledgement that all authors have contributed significantly, and that all authors are in agreement with the content of the manuscript. The cover letter of the paper should contain (i) the title; (ii) the full names of the authors; (iii) the addresses of the institutions at which the work was carried out together with (iv) the full postal and email address, plus telephone numbers and emails of all the authors. The current address of any author, if different from that where the work was carried out, should be supplied in a footnote.

3. **COPYRIGHT**: Authors publishing the Journal will be asked to sign a copyright form. In signing the form, it is assumed that authors have obtained permission to use any copyrighted or previously published material. All authors must read and agree to the conditions outlined in the form, and must sign the form or agree that the corresponding author can sign on their behalf. Articles cannot be published until a signed form *(original pen-to-paper signature)* has been received.

Please do **not** submit manuscripts to the editor-in-chief or to any other office directly. Any queries must be directed to the **Chief Executive Editor's** office via email to nayan@upm.my.

Visit our Journal's website for more details at http://www.pertanika.upm.edu.my/home.php.

HARDCOPIES OF THE JOURNALS AND OFF PRINTS

Under the Journal's open access initiative, authors can choose to download free material (via PDF link) from any of the journal issues from Pertanika's website. Under "**Browse Journals**" you will see a link, "*Current Issues*" or "*Archives*". Here you will get access to all current and back-issues from 1978 onwards.

The **corresponding author** for all articles will receive one complimentary hardcopy of the journal in which his/her articles is published. In addition, 20 off prints of the full text of their article will also be provided. Additional copies of the journals may be purchased by writing to the Chief Executive Editor.

Why should you publish in *Pertanika*?

BENEFITS TO AUTHORS

PROFILE: Our journals are circulated in large numbers all over Malaysia, and beyond in Southeast Asia. Our circulation covers other overseas countries as well. We ensure that your work reaches the widest possible audience in print and online, through our wide publicity campaigns held frequently, and through our constantly developing electronic initiatives such as Web of Science Author Connect backed by Thomson Reuters.

QUALITY: Our journals' reputation for quality is unsurpassed ensuring that the originality, authority and accuracy of your work is fully recognised. Each manuscript submitted to Pertanika undergoes a rigid originality check. Our double-blind peer refereeing procedures are fair and open, and we aim to help authors develop and improve their scientific work. Pertanika is now over 35 years old; this accumulated knowledge has resulted in our journals being indexed in SCOPUS (Elsevier), Thomson (ISI) Web of Knowledge [BIOSIS & CAB Abstracts], EBSCO, DOAJ, Google Scholar, AGRICOLA, ERA, ISC, Citefactor, Rubriq and MyAIS.

AUTHOR SERVICES: We provide a rapid response service to all our authors, with dedicated support staff for each journal, and a point of contact throughout the refereeing and production processes. Our aim is to ensure that the production process is as smooth as possible, is borne out by the high number of authors who prefer to publish with us.

CODE OF ETHICS: Our Journal has adopted a Code of Ethics to ensure that its commitment to integrity is recognized and adhered to by contributors, editors and reviewers. It warns against plagiarism and self-plagiarism, and provides guidelines on authorship, copyright and submission, among others.

PRESS RELEASES: Landmark academic papers that are published in Pertanika journals are converted into press releases as a unique strategy for increasing visibility of the journal as well as to make major findings accessible to non-specialist readers. These press releases are then featured in the university's UK-based research portal, ResearchSEA, for the perusal of journalists all over the world.

LAG TIME: The elapsed time from submission to publication for the articles averages 4 to 5 months. A decision on acceptance of a manuscript is reached in 3 to 4 months (average 14 weeks).


KEMENTERIAN PENDIDIKAN TINGGI
MINISTRY OF HIGHER EDUCATION

Sijil Pengiktirafan

Dengan ini adalah diperakui bahawa
Pertanika Journal of Social Sciences & Humanities
Penerbit Universiti Putra Malaysia
Telah memenuhi syarat-syarat pengiktirafan sebagai penerima
Skim Galakan Penerbitan Program Pemberian Taraf CREAM* 2015
bagi
Kategori Jurnal dalam Scopus
Bidang
Seni, Sains Sosial dan Kemanusiaan

CREAM

Dato' Seri Idris bin Jusoh
Menteri Pendidikan Tinggi
Kementerian Pendidikan Tinggi
3 September 2015

Pertanika Granted **CREAM Status** by MOHE
—SEPTEMBER 2015

About the Journal

Pertanika is an international multidisciplinary peer-reviewed leading journal in Malaysia which began publication in 1978. The journal publishes in three different areas — Journal of Tropical Agricultural Science (JTAS); Journal of Science and Technology (JST); and Journal of Social Sciences and Humanities (JSSH).

JTAS is devoted to the publication of original papers that serves as a forum for practical approaches to improving quality in issues pertaining to **tropical agricultural research-** or related fields of study. It is published four times a year in **February**, **May**, **August** and **November**.

JST caters for **science and engineering research-** or related fields of study. It is published twice a year in **January** and **July**.

JSSH deals in **research or theories in social sciences and humanities research**. It aims to develop as a flagship journal with a focus on emerging issues pertaining to the social and behavioural sciences as well as the humanities, particularly in the Asia Pacific region. It is published four times a year in **March**, **June**, **September** and **December**.

PERTANIKA JOURNALS

Call for Papers 2016-17

now accepting submmissions...

Pertanika invites you to explore frontiers from all key areas of **agriculture**, **science and technology** to **social sciences and humanities**.

Original research and review articles are invited from scholars, scientists, professors, post-docs, and university students who are seeking publishing opportunities for their research papers through the Journal's three titles; JTAS, JST & JSSH. Preference is given to the work on leading and innovative research approaches.

Pertanika is a fast track peer-reviewed and open-access academic journal published by **Universiti Putra Malaysia**. To date, Pertanika Journals have been indexed by many important databases. Authors may contribute their scientific work by publishing in UPM's hallmark SCOPUS & ISI indexed journals.

Our journals are open access - international journals. Researchers worldwide will have full access to all the articles published online and be able to download them with **zero subscription fee**.

Pertanika uses online article submission, review and tracking system for quality and quick review processing backed by Thomson Reuter's ScholarOne™. Journals provide rapid publication of research articles through this system.

For details on the Guide to Online Submissions, visit
http://www.pertanika.upm.edu.my/guide_online_submission.php

Questions regarding submissions should only be directed to the **Chief Executive Editor**, Pertanika Journals.

Remember, ***Pertanika*** is the resource to support you in strengthening research and research management capacity.

Address your submissions to:
The Chief Executive Editor
Tel: +603 8947 1622
nayan@upm.my

Journal's profile: www.pertanika.upm.edu.my

Pertanika Journal of Science & Technology
Vol. 24 (1) Jan. 2016

Contents

Pertanika Editorial Office, Journal Division
Office of the Deputy Vice Chancellor (R&I),
1st Floor, IDEA Tower II,
UPM-MTDC Technology Centre
Universiti Putra Malaysia
43400 UPM Serdang
Selangor Darul Ehsan
Malaysia

http://www.pertanika.upm.edu.my/
E-mail: executive_editor.pertanika@upm.my
Tel: +603 8947 1622/1620

PENERBIT UPM PRESS
http://penerbit.upm.edu.my
E-mail : penerbit@putra.upm.edu.my
Tel : +603 8946 8855/8854
Fax : +603 8941 6172

ISSN 0128-7680
01 >
9 770128 768083